Thin-film calorimetric gas sensors for hydrogen peroxide monitoring in aseptic food processes

Dissertation
zur
Erlangung des Doktorgrades
der Naturwissenschaften
(Dr. rer. nat.)

dem
Fachbereich Pharmazie
der Philipps-Universität Marburg
vorgelegt von
Patrick Kirchner
aus Bad Neustadt a.d. Saale

Marburg/Lahn 2013

Vom Fachbereich Pharmazie
der Philipps-Universität Marburg als Dissertation am
_____ angenommen.

Erstgutachter Prof. Dr. M.J. Schöning
Zweitgutachter Prof. Dr. M. Keusgen
Tag der mündlichen Prüfung am 24. Juni 2013

Erklärung

Ich versichere, dass ich meine Dissertation

"Thin-film calorimetric gas sensors for hydrogen peroxide monitoring in aseptic food processes"

selbständig ohne unerlaubte Hilfe angefertigt und mich dabei keiner anderen als der von mir ausdrücklich bezeichneten Quellen bedient habe.

Die Dissertation wurde in der jetzigen oder einer ähnlichen Form noch bei keiner anderen Hochschule eingereicht und hat noch keinen sonstigen Prüfungszwecken gedient.

Marburg, den 22. April 2013

Abstract

The sterilisation of the packaging material is the essential step in aseptic food processes to ensure safely packed products, which are microbiologically stable throughout their shelf life. Today, gaseous hydrogen peroxide (H_2O_2) in the range of several volume percent and at elevated temperature is the preferred sterilant due to its strong microbicidal efficiency and its decomposition in environment-friendly products, namely water vapour and oxygen. In order to obtain a high degree of sterility, the initial H_2O_2 concentration has to be high enough and uniformly distributed over the package's inner surface. To ensure that the packaging surface is thoroughly treated by H_2O_2, a gas sensor is required that detects the present H_2O_2 concentration on selected locations of the package's surface while it is sterilised.

The present thesis describes the realisation and characterisation of thin-film gas sensors based on an "on chip" differential set-up for monitoring the H_2O_2 gas concentration during the sterilisation of the packaging material. The differential set-up contains a catalytically active sensor segment, where H_2O_2 decomposes in an exothermic reaction causing a temperature increase towards a passive sensor segment, where a surface reaction is inhibited. In a first sensor arrangement, thin-film thermopiles have been fabricated on a single silicon chip, respectively, and their response behaviour has been characterised in H_2O_2 atmosphere. In a further arrangement, thin-film resistances have been built up as temperature-sensitive transducer platform on a silicon chip. On this platform, different catalytically active materials – platinum black, palladium and manganese oxide – have been tested with regard to their response against H_2O_2, wherein all of them showed a linear response characteristic, but manganese oxide posseses the highest sensitivity. Furthermore, three temperature-stable polymeric materials – fluorinated ethylene propylene, perfluoralkoxy and epoxy-based SU-8 photoresist – have been tested for the encapsulation of the sensor surface in terms of their chemical inertness against H_2O_2. Therein, all of them have shown a high resistivity against H_2O_2 underlining their suitability for sensor passivation.

Within the frame of this work, the sensor set-up has further been realised on a thin polyimide foil because of its high temperature endurance, its chemical stability and particularly, its low thermal conductivity allowing an improved thermal separation of the active and passive sensor segment. As a result, the sensitivity of the polyimide-based

sensor was strongly increased compared to the concentration-dependent response of the silicon-based sensors.

Microbiological experiments with bacterial spores of *Bacillus atrophaeus* have demonstrated that the microbicidal effectiveness of the sterilisation process depends on the present H_2O_2 concentration in first order as well as on the contact time between the item that has to be sterilised and the gaseous H_2O_2. By means of sensor measurements conducted at the same time, a correlation model between the microbial inactivation kinetics and the sensor response was established that allows to use the sensor not only for concentration measurements, but also for the quantification and control of the degree of the package's sterility.

In order to determine the present H_2O_2 concentration spatially resolved over the package surface during the short sterilisation cycle, a wireless sensor electronic based on the industrial ZigBee standard was developed. The sensor electronic contains a remote unit, which is connected to one of the calorimetric gas sensors fixed on a test package, and an external base unit connected to a laptop computer. For real-time measurements, a novel sensor read-out strategy was established, wherein the sensor response is measured within the short sterilisation time and correlated with both the present H_2O_2 concentration as well as the microbicidal effectiveness. As a result, this kind of "intelligent" package represents a novel instrumentation to monitor the package sterilisation in aseptic food processes under real-time conditions.

Contents

1 Introduction

Parts of this chapter (from section 1.1 to section 1.3 and section 1.4.2) are in preparation for publication as book article:

Hydrogen peroxide monitoring in aseptic food processes by means of calorimetric gas sensors

KIRCHNER, P., Reisert, S., and Schöning, M. J.

In *Springer series on chemical sensors and biosensors: Gas sensing fundamentals*, C.-D. Kohl and T. Wagner, Eds. Springer, Berlin, 2013, *submitted*.

1.1 Calorimetric gas sensors

Gas sensors based on calorimetry can generally be divided into three different types: catalytic gas sensors, adsorbent-based gas sensors and thermal conductivity gas sensors. All of them detect a change in temperature induced by either a chemical reaction on the sensor surface with a gas species or a change of thermal conductivity of the sensor's surrounding gas atmosphere. The elementary sensing element is based on the conversion of temperature in an electrical signal, which is one of the most important physical transduction principles with well-known sensitivity and accuracy for each temperature detector [1]. In general, temperature-resistance detectors, monolithic thermopiles or even pyroelectric sensors are embedded as temperature detectors in calorimetric sensing devices [2]. Therein, the choice of which temperature detector to use depends on the operational conditions – the range of temperature change that has to be detected, the scope of application, the gas concentration as well as the calorimetric sensor type itself.

1.1.1 Catalytic gas sensors

At the beginning of the twentieth century, several oil and gasoline tanker ship-wrecks occurred, which were caused by gas explosions in the storage tanks. Consequently, the Standard Oil Company of California sponsored the investigation of detectors for explosive gases [3]. With the financial support of the oil company, Oliver W. Johnson developed the first portable gas detector in 1927, whose sensing principle relies on the catalytic combustion of flammable gases on a heated platinum filament generating a temperature rise in reference to an enclosed compensation filament [3, 4]. The portable detector was applied to prevent fuel explosions in storage tanks of oil and gasoline tankers. This became the birth of the catalytic gas sensors. In the 1950's, the catalytic detection principle was broadened to quantitatively monitor methane concentrations as critical combustible gas in coal mines. The resulting hazard alert-tool enabled miners to protect them from gas explosions and to replace unspecific flame-safety lamps most frequently deployed before [5]. Even today, catalytic gas sensors are used for monitoring the presence of combustible gases such as hydrogen and hydrocarbons (e.g., methane) in concentration levels up to their respective lower explosive limit (LEL) [6]. The LEL is defined as lowest concentration of the combustible gas in air, which is sufficiently large enough to result in an explosion initiated through an ignition source [7]. For example, the LEL of methane amounts to be 4.6% v/v [8]. The detected gas concentration of the sensing device is often expressed in percentage of LEL [7].

Current catalytic gas sensors are still also derived from the detection principle firstly introduced by Johnson, and applied in diversified industrial sectors (oil and gas industry, mining, chemical plants). They are simply made up of two coils of platinum wires, where

both of them are embedded in identical porous ceramic beads (in most instances, alumina beads). One of the ceramic beads is additionally impregnated with an active catalyst made up of platinum, palladium, rhodium or iridium [9], whilst a corresponding bared bead serves as in reference (s. Fig. 1.1). This sensor arrangement is called pellistor (or catalytic bead sensor) and was first named by A. Baker [10].

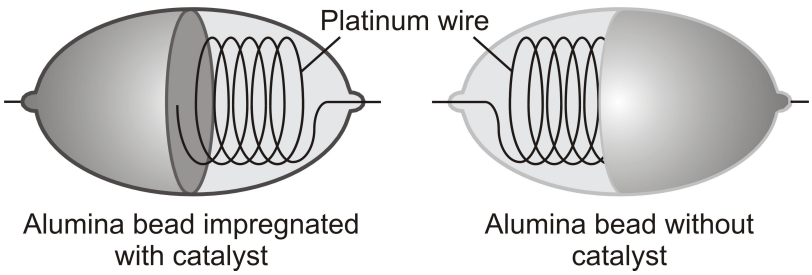

Figure 1.1: Schematic view of an "active" pellistor element with platinum wire embedded in an alumina bead that is impregnated with a catalyst (left) and a reference pellistor element without catalyst (right) (modified from [11]).

The sensor arrangement detects the reaction heat evolved during the catalytic combustion of a flammable gas component on the heated "active" pellistor element in form of a temperature rise leading to a resistance change of the platinum wire, whereas the corresponding reference pellistor element compensates effects occurring in form of altering temperature of the surrounding gas atmosphere [12]. The combustion induced on the hot catalyst surface proceeds in form of an exothermic reaction between a flammable gas and an oxidant of ambient air accompanied by the liberation of heat. In an exothermic reaction, the total energy required for breaking the bonds of a chemical substance is less than the total energy released, while the chemical bonds of the products are formed [1]. Thus, the resulting excess of energy is liberated from the chemical reaction known as reaction enthalpy. The reaction enthalpy ($\Delta_\mathrm{R}H^\Theta$) can be described by Hess's law [13]:

$$\Delta_\mathrm{R}H^\Theta = \sum n_\mathrm{i} \cdot \Delta_\mathrm{F}H^\Theta_\mathrm{prod,i} + \sum n_\mathrm{j} \cdot \Delta_\mathrm{F}H^\Theta_\mathrm{react,j} \tag{1.1}$$

Here, n_i and n_j are the number of moles, and $\Delta_\mathrm{F}H^\Theta_\mathrm{prod,i}$ and $\Delta_\mathrm{F}H^\Theta_\mathrm{react,j}$ are the heat of formation of the products and reactants at standard conditions.

For example, the combustion of hydrocarbons (here, methane) with oxygen of ambient air occurs in the following net reaction:

$$\mathrm{CH_4} + 2\mathrm{O_2} \rightarrow \mathrm{CO_2} + 2\mathrm{H_2O} + \Delta_\mathrm{R}H \tag{1.2}$$

where $\Delta_\mathrm{R}H$ is the reaction enthalpy and in case of methane amounts to 890.8 kJ/mol at standard conditions [14].

In absence of a catalyst, combustion of a flammable gas is only initiated and sustained, if the gas temperature reaches the ignition temperature of the gas species (autoignition) or if an external ignition source (e.g., a spark) is present in order to yield enough kinetic energy of the reactants above the required activation energy of the chemical reaction (s. Fig. 1.2) [15, 16]. Consequently, the reaction rate rises with increasing temperature considerably. This fact is expressed by the Arrhenius equation, which defines the rate constant of the reaction (k) as a function of temperature (T) and activation energy (E_a) [16]:

$$k = A \cdot \mathrm{e}^{-\frac{E_\mathrm{a}}{R \cdot T}} \tag{1.3}$$

with A as pre-exponential factor and R as gas constant.

Moreover, in absence of a catalyst, the concentration range of the flammable gas has to be at a specific level between the lower explosive limit (LEL) – lowest concentration level – and the upper explosive limit (UEL) – highest concentration level – so that combustion can proceed [7].

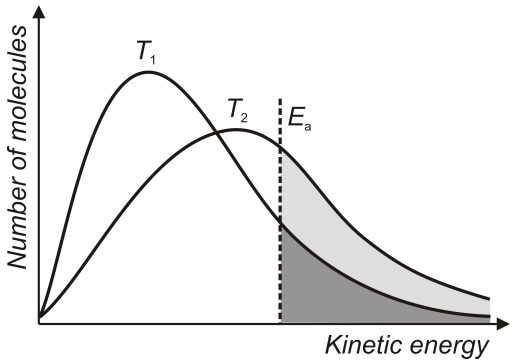

Figure 1.2: Distribution (according to Boltzmann) of the molecules' kinetic energy for two different temperatures T_1<T_2 in relation to the activation energy (E_a) (modified from [17]).

In contrast to that, the presence of a solid catalyst enables combustion at a temperature much lower than the ignition temperature and even in a concentration range of the flammable gas below its LEL [18]. The catalytic gas sensor is electrically heated through the platinum coil to reach a temperature usually of about 500 °C, so that catalytic combustion readily occurs on the "active" pellistor element [9, 19]. The chemical reaction between the reactants, flammable gas and oxygen, is accomplished in contact with the catalyst surface forming the combustion products, whereby the catalyst itself is not consumed. Therefore, the catalyst provides an alternative reaction pathway, wherein lower activation energy is required for the reaction process, and as a consequence the rate of the combustion reaction is enhanced according to the Arrhenius equation (s. Eq. 1.3). The catalytically promoted reaction pathway can be divided into a sequence

of several intermediate steps (s. Fig. 1.3) referring to [20]. In a first step, the reactants, the flammable gas and oxygen, are adsorbed on the catalytic surface, which is in most cases an exothermic process by liberation heat of adsorption. Here, the adsorption predominantly occurs in form of chemisorption, wherein the electronic states of the catalyst and adsorbates are strongly perturbed. The heat of adsorption of the reactants must be low enough to reduce the activation energy for oxidation, but high enough to ensure an almost complete surface coverage of the adsorbed reactants [9]. If the catalyst is made up of a transition metal such as platinum or palladium, known as good catalysts for flammable gases with variable oxidation states and with partially filled *d*-orbitals leading to a surface with unsatisfied valencies, the reactants become adsorbed by an electron exchange with the catalyst surface [2]. In a following step, the adsorbates react with each other resulting in an intermediate transition complex as precursor to form the final products, which are first adsorbed on the catalytic surface and finally, desorb from the surface.

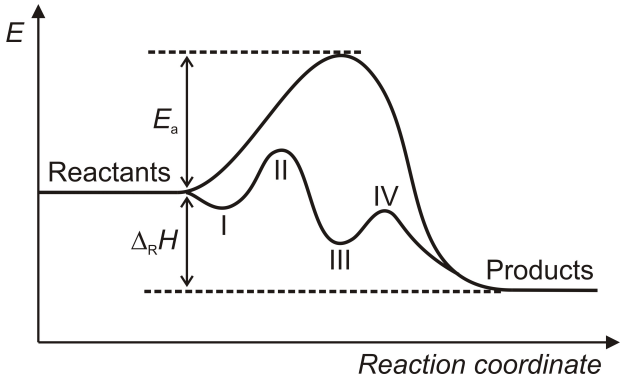

Figure 1.3: Energy profile of a homogeneous exothermic reaction without catalyst (upper curve) and of a heterogeneous catalysis (lower curve) with the intermediate steps: adsorption of the reactants (I), reaction of the adsorbates (II), adsorbed products (III) and desorption of the products (IV) (modified from [20]).

For sensor operation, the catalytic gas sensor is electrically connected in a Wheatstone-bridge circuit, wherein the two pellistor elements are wired into opposing arms of it (s. Fig. 1.4) [9, 21]. The pellistor elements are heated to their operating temperature through a constant power supply in form of an applied constant bias voltage or bias current. When the sensor is operated in air free of flammable gas components, the two pellistor elements are balanced and a stable baseline voltage is generated across the bridge. However, the presence of combustible gas components in air causes a change of the resistance of the "active" pellistor element due to the exothermic reaction on the catalyst that generates an out-of-balance voltage across the Wheatstone bridge [9, 22]. The out-of-balance voltage constitutes directly as sensor-output signal, which increases almost linearly with rising

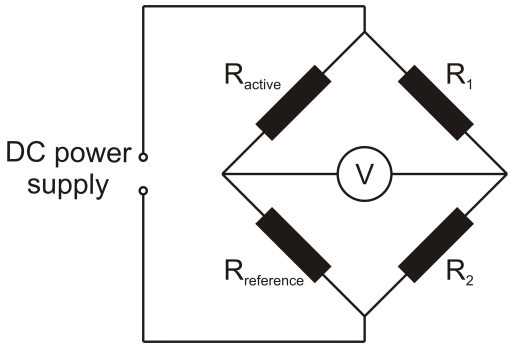

Figure 1.4: Wheatstone-bridge configuration of a catalytic gas sensor with "active" pellistor element and reference pellistor element situated in opposing arms of the bridge circuit (modified from [11]).

gas concentration of the flammable gas component in air [22].

Conventional catalytic gas sensors designed as pellistors feature a high response with low susceptibility to environmental changes and high durability due to the fact that they are rugged even in harsh environments [6]. Furthermore, they are easy to fabricate and afford sensor operation with low complexity in circuit design. But pellistors have also a few drawbacks such as non-specific response to various combustible gases, limited for concentration measurements up to the LEL and high power consumption between 300 and 700 mW [23]. The latter could be overcome by using micro-machined catalytic gas sensors, which are based on micro-hotplates, resulting in a low power consumption, in most cases below 100 mW [19, 23, 24]. This makes micro-machined catalytic gas sensors especially attractive for usage in portable gas detectors, wherein the sensors are driven by battery. Krawczyk & Namiesnik introduced also a new method to detect hydrogen concentrations above the LEL and up to the UEL by driving the catalytic gas sensor with an altered bias voltage [25]. In further studies, the selectivity of catalytic gas sensors was improved. Instead of using a catalyst made up of a noble metal and an insulation layer or dielectric ceramic pellet, the platinum heating wire is covered by a semiconducting metal oxide of SnO_2 or In_2O_3 enabling a gas-specific detection through selective adsorption of the gas species [6, 26]. This extraordinary kind of catalytic gas sensor is also called one-electrode semiconductor gas sensor or semistor.

1.1.2 Gas sensors based on adsorption effects

The detection mechanism of a further type of calorimetric gas sensor relies on the liberation or the abstraction of heat, since a gas species adsorbs on a selective organic compound. Although, the heat of adsorption is rather low, especially for physical adsorption compared to the reaction heat of combustible gases detected by catalytic gas sensors, the adsorption of gas molecules on a corresponding adsorbent in form of an in-

clusion reaction between a gas species and an adsorbent on the sensor surface is highly selective. To measure the change in temperature resulting from the adsorption process with an accurate resolution in the sub-Kelvin range, monolithic thin-film thermopiles with enlarged Seebeck coefficient are used. On top of the "hot" junctions of a thermopile, a gas-selective polymeric membrane as host compound is applied [27]. This type of calorimetric gas sensors has been used in gas-sensing microsystems to seek out volatile compounds in unknown gas atmosphere [28, 29]. At present time, however, gas sensors based on adsorption effects are still subject of current research.

1.1.3 Thermal conductivity gas sensors

The detection mechanisms of the two calorimetric sensor types described above rely on the chemical reaction between the sensor surface and gas species that is to be detected. The sensor based on thermal conductivity, however, exploits the heat transfer from a heated sensing element to the surrounding gas influenced by the thermal conductivity of the gas as a quantitative measurement principle without any chemical interaction [2]. The thermal conductivity sensor, also called katharometer or hot-wire detector, is one of the oldest gas sensors that was first mentioned by the Siemens & Halske Company in 1913 for the detection of methane in binary gas mixtures [30]. Today, thermal conductivity sensors are mainly applied as non-selective or low-selective but reliable detectors in gas chromatography [2, 31] and as monitoring devices for combustible gases even at high gas concentrations implicating the concentration range above the LEL, wherein they are often used in complementary combination with catalytic gas sensors [9, 32, 33].

The thermal conductivity sensor consists of two platinum or tungsten filaments, which are electrically heated up to an operating temperature of about 300 °C and both are situated in a Wheatstone bridge. One of the filaments is exposed to the surrounding gas acting as "active" filament and the other one is either enclosed in a sealed housing for compensating temperature changes of the surrounding gas or exposed to a reference gas [21, 34]. If the sensor is exposed to a gas mixture with air as carrier gas and wherein the thermal conductivity of present gas compounds is higher than the conductivity of air, then heat is dissipated from the "active" heated filament. The dissipation of heating power (P) of the "active" filament can be described by [21]:

$$P = \alpha_{\mathrm{T}} \cdot k_{\mathrm{g}} \cdot \Delta T \tag{1.4}$$

Here, α_{T} is a constant defined by the geometry of the heated filament of the sensor, k_{g} is the thermal conductivity of the surrounding gas and ΔT is the temperature difference between the filament and surrounding gas.

The power dissipation causes a change in the resistance of the filament that can be

measured then by generating an out-of-balance voltage in the Wheatstone bridge. For an adequate sensor operation, the heated filaments must be protected from contact with water vapour, since the thermal conductivity of water vapour could strongly interfere with the thermal conductivity of the gas mixture [21]. Even though, the detection mechanism seems to be trivial, a precise calculation of the thermal conductivity of an unknown gas mixture depends on temperature and does not end up in a linear function of the mole fraction of the gas components, as considered for ideal binary gas mixtures. A precise description of the thermal conductivity of a non-binary gas mixture is given by an empirical equation from Wassiljewa [35, 36]:

$$k_{\mathrm{g}}(x_{\mathrm{i}}, T) = \sum_{i=1}^{n} \frac{x_{\mathrm{i}} \cdot k_{\mathrm{i}}(T)}{\sum_{j=1}^{n} x_{\mathrm{j}} \cdot \Phi_{\mathrm{ij}}(T)} \tag{1.5}$$

wherein x_{i} and x_{j} are the mole fractions of the gas components i and j, k_{i} is the thermal conductivity of the component i and $\Phi_{\mathrm{ij}}(T)$ is a correction factor depending on the viscosity of each gas component according to Mason and Saxena [37]:

$$\Phi_{\mathrm{ij}}(T) = \frac{\left(1 + \sqrt{\mu_{\mathrm{i}}(T)/\mu_{\mathrm{j}}(T)}\,\sqrt[4]{M_{\mathrm{j}}/M_{\mathrm{i}}}\right)^2}{\sqrt{8 \cdot (1 + M_{\mathrm{i}}/M_{\mathrm{j}})}} \tag{1.6}$$

Here, μ_{i} and μ_{j} are the viscosities of the gas compound i and j, and M_{i} and M_{i} are the molecular weights of the compounds i and j.

1.2 Hydrogen peroxide

Hydrogen peroxide (H_2O_2) was discovered for the first time by L. J. Thénard in 1818. He produced it by a reaction of diluted nitric acid with barium peroxide (BaO_2) and named it first oxygenated water [38]. After the discovery of H_2O_2, the production of aqueous H_2O_2 solutions with concentrations up to 50% w/w was performed by slightly improved processes of the reaction described by Thénard. During this time, it was thought that pure H_2O_2 must be unstable due to the fact that H_2O_2 gradually decomposed resulting from traces of metallic and organic impurities of the aqueous solutions [39]. In 1894, R. Wolffenstein gained almost pure H_2O_2 (99% w/w) by vacuum distillation for the first time and demonstrated its stability under cleanest conditions [40]. Until the end of the nineteenth century, different formulas of H_2O_2 have been proposed, where finally, P. Melikishvili and L. Pizarjevski determined that the correct formula of H_2O_2 must be H-O-O-H [41].

H_2O_2 (CAS No.: 7722-84-1) is a clear, colourless liquid, which is weakly acid and has a moderately pungent odour [42]. It has strong oxidising properties and is very reactive under certain circumstances, which makes it attractive for many applications,

wherein reactive oxidants are required. In comparison to water, H_2O_2 is heavier as well as slightly more viscous. It is miscible with water in any proportion, even though they do not form an azeotropic mixture, so that H_2O_2 could be fully separated by distillation [43]. In Tab. 1.1, the main physical properties of H_2O_2 and the corresponding properties of water are summarised. A comprehensive overview of the physical and chemical properties of H_2O_2 over a wide temperature range is given elsewhere [44].

Table 1.1: Physical properties of H_2O_2 and water (adapted from [45]).

Property	Hydrogen peroxide	Water
Molar mass (g/mol)	34.016	18.015
Melting point (°C)	-0.43	0.0
Boiling point (°C)	150.2	100
Heat of melting (J/g)	368	334
Heat of vaporisation at 25 °C (J/(g · K))	1519	2445
Specific heat at 25 °C (J/(g · K))	2.629	4.182
Critical temperature (°C)	457	374
Critical pressure (MPa)	20.99	21.44
Relative density at 25 °C (g/m^3)	1.4425	0.9971
Viscosity at 20 °C (mPa · s)	1.249	1.002
Refractive index	1.4084	1.3330

H_2O_2 occurs as a ubiquitous substance in the environment. It naturally exists in surface water, wherein it is mainly produced by a photochemical process of ultraviolet light and dissolved organic compounds [46]. In atmosphere, H_2O_2 is produced by photolysis of ozone or aldehydes [47]. It can be found in living cells as a by-product of aerobic cell metabolism [48]. Exhale breath of humans contains also small amounts of endogenously formed H_2O_2 [49]. Furthermore, a special insect with regard to H_2O_2 is the bombardier beetle, which produces concentrated amounts of H_2O_2 up to 25% w/w for defence purposes [50].

Even though the industrial production of H_2O_2 could be carried out by various wet chemical, electrochemical and organic oxidation processes as shown in [45], almost the total amount of hydrogen peroxide is gained by the organic autoxidation process with anthraquinone today. Therein, 2-alkyl-anthraquinone reacts with hydrogen in the presence of a catalyst (e.g., palladium) to form 2-alkyl-anthrahydroquinone in a first step. After removing the catalyst, the hydroquinone is oxidised usually in ambient air under the formation of hydrogen peroxide, which is extracted in water and the process begins

anew [51]. The organic autoxidation process enables large-scale production of H_2O_2 and permits its widely usage in a variety of industrial, medical and environmental application fields. Today, hydrogen peroxide is commercially available as aqueous solutions up to 90% w/w. Due to the fact that hydrogen peroxide could easily decompose on traces of impurities, the solutions are generally stabilised by added weak organic acids [52].

In 2008, the global production of H_2O_2 amounted to be 3 million tons [53]. According to a new market report from Global Industry Analysts, a H_2O_2 world market of 4.3 million tons is forecast for 2015 [54]. The paper and pulp industry represents the main field of application of estimated 50% of the total H_2O_2 production, wherein it is used for bleaching and delignification [53, 55, 56]. The textile industry deploys H_2O_2 as bleaching agent as well [57]. In metallurgy and mining, it is applied for leaching processes and for the detoxification and destruction of cyanides [58, 59]. Highly concentrated H_2O_2 up to 90% is used as rocket propellant in space technology [60]. Today, it is increasingly applied for environmental protection in industrial plants, especially to detoxify industrial effluents and exhaust gases [45]. The chemical industry uses H_2O_2 for the production of other chemicals such as peroxide compounds, for epoxidation as well as for etching and cleaning processes during the fabrication of micro-machined/semiconductor devices [51]. Last but not least, H_2O_2 at low concentrations of 3% w/w is a highly efficient disinfectant for medical applications, and at high concentrations up to 35% w/w it is used as sterilant in the food and the pharmaceutical industry as well [61, 62].

1.3 Aseptic food processing

1.3.1 Introduction

Packaging is a key element in food processing in order to ensure a high safety standard and quality assurance of a packed product by avoiding any physical, chemical as well as microbiological interaction between the product and environment within its shelf life [63]. Today, aseptic food processing is one of the most important food-packaging methods, which allows to keep up with the great demand of the food industry for long-term preservation of food products at ambient temperature [64]. It is defined as the filling and hermetic sealing of microbiologically stable products (e.g., ultra-high temperature-processed (UHT) milk) into pre-sterilised packages under sterile conditions in an aseptic zone so that microbiological recontamination is prevented [65]. A schematic flow diagram of an aseptic food process is depicted in Fig. 1.5.

The result of aseptic processing is a safe, packed product with long shelf-life that does not require preservatives or refrigeration during storage. Thus, aseptically packed products offer beneficial attitudes to the consumer, the food manufacturer and to the

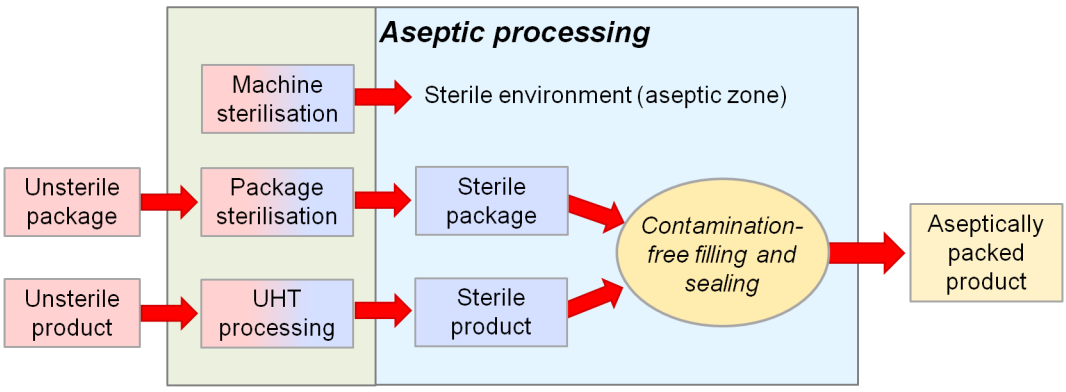

Figure 1.5: Schematic flow diagram of aseptic food processing (modified from [66]).

distributor compared to conventionally canned products: the product retains most of its natural nutrients and of the original sensory characteristics (flavour, texture and colour); and it enables high savings on logistics (no cold chain is required) and on packaging material (do not need to be long-term stable at high temperature and pressure such as cans) [67, 68].

1.3.2 Package sterilisation

A decisive step within aseptic food processing is the sterilisation[1] of the packaging material prior to the food filling due to the fact that the material could get contaminated by operational staff, surrounding air or even by recontaminated machine components [71, 72]. According to Ansari & Datta, the sterilisation of the packaging material must fulfil the following requirements [61]:

- rapid, reliable and economical microbicidal effectiveness;
- compatibility to the packaging material;
- almost complete removal of residues of the sterilisation agent;
- harmlessness for the consumer at highest possible residue level;
- no adverse effect on product at highest possible residue level;
- compatibility to environment.

[1] According to Wallhäußer, sterility is defined as the total absence of viable microorganisms and transferable genetic material [69]. Besides this general definition, "commercial sterility" is an established term in the food industry. It is defined as "the absence of microorganisms capable of growing in food at normal non-refrigerated conditions at which the food is likely to be held during manufacture, distribution and storage" [70]. In this work, sterilisation stands always for "commercial sterilisation" except where noted otherwise.

The sterilisation of the packaging material could be carried out by various physical methods in form of heat and irradiation or chemical sterilants such as ethylene oxide, formaldehyde, peracetic acid or hydrogen peroxide [61, 73, 74]. However, some of the mentioned chemicals are unsuitable for package sterilisation. While ethylene oxide and formaldehyde show strong microbicidal effectiveness, they could not be used in food processing because they are toxic, carcinogenic and potentially explosive leading to a careful handling [75]. Peracetic acid possesses a rapid microbicidal effectiveness even at low concentration levels. However, it decomposes to water and acetic acid, which could generate an off-flavour of the food product and moreover, its vapour is very pungent [61, 65].

1.3.3 Hydrogen peroxide as sterilant

Today, hydrogen peroxide (H_2O_2) is the most frequently used sterilant for package-sterilisation processes. Amongst its benefits, it is non-toxic at residual concentrations and it decomposes to environment-friendly products, namely water vapour and oxygen, in a net reaction [76]. Due to the fact that H_2O_2 has merely a low microbicidal effect at room temperature, in most instances, a combination of hydrogen peroxide and heat or even irradiation is applied, in order to increase its microbicidal effectiveness [61, 74, 77]. In general, the microbicidal effectiveness of sterilisation processes with H_2O_2 depends in particular on the H_2O_2 concentration besides other process parameters, like temperature, humidity and gas velocity [78, 79]. Furthermore, the effectiveness is significantly enhanced through the usage of gaseous H_2O_2 [62, 80]. In this case, H_2O_2 is active against a broad spectrum of microorganisms: bacteria, yeasts, fungi, viruses and spores [75, 81]. It acts as an oxidant that affords inactivation most likely through formation of free hydroxyl radicals as intermediate products induced by heat, irradiation or even by transition-metal ions contained in microorganisms [62, 82]. The hydroxyl radicals serve as electrophilic surfactants with high reactivity, which could damage essential cell components such as DNA, proteins, lipids and carbohydrates very site-specific [83–87]. The decisive inactivation step for viable microorganisms during H_2O_2 treatment relies on the DNA damage through strand breaks caused by the formed radicals [82, 88, 89]. However, numerous studies have been conducted, wherein various inactivation mechanisms of bacterial spores through H_2O_2 treatment are supposed. Bacterial spores offer a much higher resistance towards oxidants, like hydrogen peroxide, than their vegetative counterparts due to their thick, proteinaceous spore coats [84], the low water content of the spore core [90, 91], the high impermeability of the inner spore membrane [92] and the protection of the DNA encased by special proteins of spores, the so-called small, acid-soluble spore proteins (SASP) [89, 93, 94]. The latter one blocking DNA damage

occurring by viable bacteria through free radicals [94]. Shin et *al.* and King & Gould found out that H_2O_2 at elevated concentrations causes dissolution of the outer and inner spore coat as well as lysis of the cortex, which could end up in degradation of the spore core or protoplast structures [95, 96]. However, at lower lethal concentrations, treated spores remain fully their shape, so that dissolution of spore coats seems not to be the initial step of the spores' lethality [95, 97]. Further studies have shown that possible targets of H_2O_2 are enzymes within spores, which are important for the bacterial metabolism after the germination, or enzymes, which are involved in germination (e.g., hydrolysis of the cortex) [89, 97]. Whereas Cortezzo et *al.* found out that H_2O_2 attacks the spore's inner membrane by creating pores or channels, so that the membrane become leaky for substances of the spore core [98]. Nevertheless, the decisive inactivation process, which is of major significance in order to understand the inactivation mechanism of spores by H_2O_2, is not effectually identified at present time.

1.3.4 Inactivation kinetics

To determine the sterilisation effectiveness, the reduction of the most resistant bacterial spores for the used chemical sterilant has to be considered. For sterilisation processes, wherein hydrogen peroxide is deployed, spores of *Bacillus atrophaeus* (ATCC 9372) or *Bacillus subtilis* SA 22 are typically used as test organisms [99]. The microbial inactivation kinetic is expected to follow a first-order reaction [100]:

$$\frac{dN}{dt} = -k \cdot N \tag{1.7}$$

Here, N is the number of spores and k is the inactivation rate constant.

By integration of Eq. 1.7, one can obtain a more familiar expression for the microbial reduction:

$$\ln\frac{N_\mathrm{t}}{N_0} = -k \cdot t \tag{1.8}$$

where N_t and N_0 are the survived spore number at time t and the initial spore number, respectively.

A general parameter to evaluate the microbicidal effectiveness is the D-value, which is calculated from the survivor curves (survived spores *versus* time). The D-value represents an exposure time (Δt) at a constant temperature setting that results in 90% reduction of the initial spore number:

$$D = \frac{\Delta t}{\lg N_0 - \lg N_{90\%}} = \frac{2.303}{k} \tag{1.9}$$

However, for chemical sterilisation agents, the microbicidal effectiveness is often merely

determined by the logarithmic cycle reduction (LCR). This is expressed mathematically as follows [101]:

$$LCR = \lg \frac{N_0}{N_t} \tag{1.10}$$

1.4 Aim and scope of the work

1.4.1 Initial situation

In current research there exists the necessity to develop a gas sensor for monitoring the H_2O_2 concentration during the package sterilisation in aseptic filling machineries. In sterilisation processes with gaseous H_2O_2, the gas concentration must be sufficiently high enough to ensure the sterility of the packaging material. Furthermore, a homogeneous distribution of the gaseous H_2O_2 must be maintained within the short contact time between the H_2O_2 and packaging material. Due to the fact that the H_2O_2 concentration seems to be the decisive factor for a sufficient sterilisation effect, the sensor should conduce to verify an effectual sterility of the packages treated by H_2O_2 through sporadic control measurements in aseptic filling machineries. Therefore, the sensor should be applied to examine the homogeneity of the overall distribution of gaseous H_2O_2 on the package's inner surface as well as to detect the local H_2O_2 concentration on folding edges and curved areas of the packaging material, which are the most critical spots to sterilise. As a consequence, the sensor could contribute to the control and to the optimisation of the package sterilisation process with regard to finding out the relevant parameter settings for the gas flow, H_2O_2 dosage as well as contact time between the packaging material and gaseous H_2O_2.

For industrial application, the sensor must fulfil certain requirements. It has to operate reliably under harsh environmental conditions of the sterilisation process. This means that the sensor has to be suitable and approved for elevated gas temperatures, strong gas flows and H_2O_2 concentrations up to the percentage range. For an accurate measurement of the H_2O_2 concentration, the sensor's concentration-dependent signal should not be interfered by altering the gas temperature, gas velocity as well as the humidity in the ambient gas atmosphere. Furthermore, the sensor must detect the present H_2O_2 concentration in a package within its short contact time with gaseous H_2O_2 during the sterilisation process. For placing the sensor directly on the package surface, the sensor has to have a flat design as well as a small lateral dimension to situate it even on folding edges. Due to the fact that the measurements must be carried out in a dynamic process, wherein the packages are moved by a chain, a specific electronic unit for reading out the signal is required.

1.4.2 H_2O_2 monitoring in gas phase – state of the art

During the last two decades, intensive efforts have been focused on detecting gaseous or vaporised H_2O_2 by diversified strategies such as infrared spectroscopy, colorimetry, mass spectroscopy, chemiluminescence as well as amperometric methods. Even though, most of this detecting principles could merely be used for low concentrations, or are not suitable either for harsh environmental conditions or for measurement applications inside of a package, a brief introduction to this methods is given below.

For detecting H_2O_2 by IR spectroscopy, the strong absorbance band of H_2O_2 at 1420 nm serves as indication peak, whose intensity is used for determining the H_2O_2 concentration. However, water vapour shows also a strong absorbance in this wavelength range and interferes with the H_2O_2 band. Therefore, a correction must be done by identifying at first the amount of water vapour at a further peak (i.e., at 1360 nm) and by following determining the ratio of water vapour and H_2O_2 at the absorbance band of 1420 nm [102–104].

In a further sensor approach, colorimetric indicators are described, which are based on a colour change, after they have been exposed to H_2O_2. For instance, Xu et *al.* described paper-based vapour detection of H_2O_2, wherein a cellulose substrate has been impregnated by Ti(IV) oxo complexes for binding and reacting with H_2O_2 and generating a yellow colour formation [105].

For monitoring H_2O_2 in workplace atmosphere, amperometric sensors are particularly suited [106–108]. In its easiest form, such a sensor consists of a two-electrodes arrangement (working and counter electrode), and between both electrodes a solid electrolyte (e.g., Nafion) is situated as ion-exchange material. At an appropriate potential of the working electrode (in general, at 600 mV), hydrogen peroxide becomes oxidised by an anodic reaction, and released hydrogen ions trapped in the membrane are reduced at the counter electrode by a cathodic reaction. As a result a current is generated, which depends on the present H_2O_2 concentration.

A further H_2O_2-detection principle is described in [109], which is based on chemiluminescence. Therein, a reaction between a peroxalate compound and vapour-phase H_2O_2 can generate a high-energy intermediate (dioxetanedione) that quickly decomposes producing carbon dioxide and photons, which could further chemically excite a fluorescent dye resulting in an efficient luminescence. This detection principle has been established to selectively detect H_2O_2 at low concentrations.

In [110], a mass-spectrometric method for the detection of gaseous H_2O_2 using a chemical ionisation source is introduced. Therein, oxygen ions are produced from the ionisation of ambient air, which react with H_2O_2 to form stable, ionised clusters of H_2O_2 and oxygen, whose specific mass-to-charge ratio was detected by a time-of-flight mass

spectrometer. The intensity of the mass-to-charge ratio can be used to determine the present H_2O_2 gas concentration.

In a further work, Reisert et *al.* presented the usage of metal-oxide gas sensors even for the detection of high H_2O_2 concentrations up to the percentage range and at elevated temperatures [111]. Therein, the concentration was measured by a change of the resistance of the semiconducting material (in this case, SnO_2 showing a drop of the resistance in the presence of H_2O_2). Even though, this sensor seems to be suitable for detecting high concentrations under harsh environmental conditions, for an accurate operation, the sensor must be heated by an additional voltage source, which makes it complicated to drive it directly in a package during the sterilisation process.

Nevertheless, all of the above described sensing techniques for gaseous H_2O_2 are not suitable for monitoring H_2O_2 inside the package or package surface in real-time during the sterilisation process.

1.4.3 Content of the work

In a preceded work, a gas sensor for on-line monitoring H_2O_2 concentrations in sterilisation processes was established by Näther [112, 113], which relies on a catalytic detection mechanism. The sensor was built on top of a conventional transistor-outline (TO) socket (s. Fig. 1.6). As temperature-sensing elements, two commercial resistance temperature detectors are situated in opposing positions on the TO socket and are soldered on the socket's contact pins. One of the temperature-sensing elements was treated by a catalytically active material, whereas the second element was covered by a thick layer of a passive coating. The basic sensing principle is based on the exothermic reaction of H_2O_2 on the catalyst leading to a temperature rise on one of the sensing elements. Such a sensor could be used for detecting the overall H_2O_2 concentration at a gas pipe in the

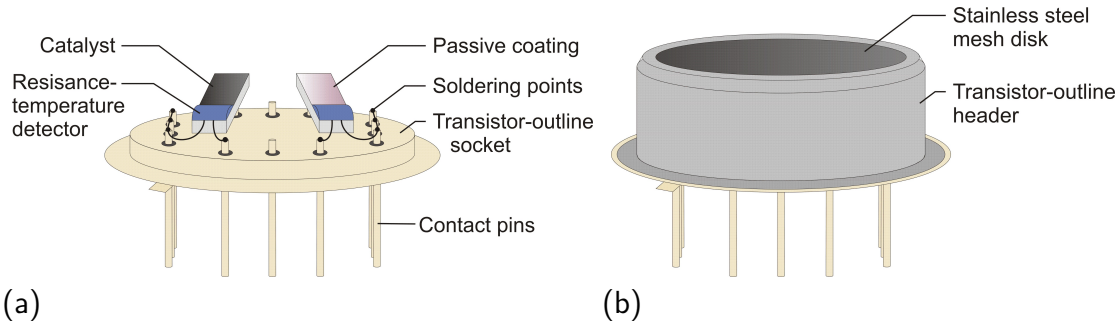

Figure 1.6: Schematic view of the sensor arrangement for continuous H_2O_2 monitoring; a) calorimetric differential set-up on transistor-outline (TO) socket and b) sensor shielded by a TO header and a stainless steel mesh disk.

sterilisation process in aseptic filling machineries. Based on the developed macroscopic sensor set-up in the prior work of Näther, the objective of this thesis was to realise calorimetric thin-film gas sensors, which are suitable for measuring H_2O_2 concentrations in packages, while they are being sterilised. Moreover, a sensor read-out electronic should be designed, which allows the concentration monitoring during package sterilisation in real-time.

To attain such an ambitious goal, the content of this thesis was split into explicitly defined scopes corresponding to the number of publications, referring to chapter 2 to chapter 8:

Chapter 2 describes the investigation of calorimetric gas sensors based on monolithic thin-film thermopiles, which have been realised for H_2O_2 detection. Therein, the main focus was to investigate the influencing factor of chosen material pairs as thermocouple, which can be deposited by means of thin-film technology, on the sensor response. The influence of the geometrical arrangement of the thermopile on the sensor signal was studied as well. Furthermore, two catalytically active materials have been compared with each other in terms of their sensitivities. A second focus of this chapter was to extensively validate the sensor-response behaviour of the sensor arrangement with largest sensitivity in an experimental H_2O_2 test rig under varied process conditions.

In **chapter 3**, a calorimetric H_2O_2 gas sensor that consists of thin-film resistances as temperature-sensing elements on a single silicon chip is introduced. First of all, potential catalysts were studied on a sensor-chip platform with regard to their effect on the overall response behaviour of the calorimetric gas sensor. In addition, the sensor response was examined in H_2O_2 atmosphere under altered process conditions according to the sensor validation in chapter 2.

Chapter 4 deals with an intensified study of the passive coating of the calorimetric gas sensor against H_2O_2. Here, polymeric materials have been used with enlarged thermal endurance as well as high chemical inertness. In order to realise coatings with thin but homogeneous thicknesses, the materials have been deposited by thin-film technique on equal sensor platforms and subsequently tested in H_2O_2 atmosphere with respect to their suitability as passivation of calorimetric gas sensors. The chapter is additionally supported by thermal characterisation of the polymeric materials as well as by studying possible degradation effects of the coatings, after they are treated by H_2O_2.

In **chapter 5**, an optimisation of the thin-film calorimetric gas sensors introduced in the chapters before was performed, wherein their response behaviour against H_2O_2 was strongly improved. The sensor was fabricated on a novel basic substrate made up of a polyimide foil instead of conventional silicon, whereon the sensor's transducer structures were fabricated in the same manner as before. Besides a subsequent characterisation of the sensor in H_2O_2 atmosphere, a thermal model was designed to evaluate the thermal

response behaviour of the novel sensor set-up. Moreover, a possible mechanism of the catalytic surface reaction is given in this chapter that is confirmed by a supplementary material inspection of the catalytic surface. As additional information, a theoretical consideration of the sensor's sensitivity is devised for a better understanding of the sensor-response behaviour.

In a continuing study presented in **chapter 6**, the calorimetric sensor arrangement built on top of the polyimide foil was further on miniaturised and extensively characterised in H_2O_2 atmosphere under diversified process conditions. In addition, material investigations have been conducted to evaluate the thermal properties of polyimide as well as its chemical consistency in gaseous H_2O_2.

To demonstrate the necessity for monitoring the H_2O_2 concentration in sterilisation processes, the microbicidal effectiveness of gaseous H_2O_2 was determined by microbiological test series with bacterial spores carried out in a wide range of parameter settings. At the same time, sensor measurements have been conducted at corresponding process parameters. From the results of both, the microbiological inspection and the sensor measurements, a correlation model was established, whereby the sensor signal was directly related to the microbicidal effectiveness of gaseous H_2O_2. This study is the main content of **chapter 7**.

In **chapter 8**, a novel wireless sensor system comprising one of the thin-film calorimetric gas sensors introduced in the previous chapters and a specially designed electronic unit that enables real-time monitoring of gaseous H_2O_2 during the package sterilisation in aseptic filling machineries is presented. For a rapid concentration measurement in such a dynamic process, a novel read-out strategy of the sensors was established. The chapter ends with an exemplary H_2O_2 measurement with the wireless sensors system that was accomplished in an industrial aseptic filling machinery for demonstrating its suitability as monitoring device for sterilisation processes.

Chapter 9 closes the current thesis with a final summary of the results, new experiences gained throughout this work and an outlook including potential ongoing strategies.

References

[1] Bársony, I., Dücso, C., and Fürjes, P. Thermometric gas sensing. In *Solid state gas sensing*, E. Comini, G. Faglia, and G. Sberveglieri, Eds. Springer, New York, 2009.

[2] Walsh, P. T., and Jones, T. A. Calorimetric chemical sensors. In *Sensors – a comprehensive survey*, W. Göpel, J. Hesse, and J. N. Zemel, Eds., vol. 2. Wiley-VCH, Weinheim, 1991.

[3] Henderson, R. E. Portable gas detectors used in confined space and other industrial atmospheric monitoring programs. Technical report, PK Safety, 2002.

[4] Kleven, B. A summary of gas detection. Technical report, Advanced Calibration Designs, 2001.

[5] Unwin, I. D. Mine monitoring for safety and health. Monograph, The Coalmining History Resource Centre, 2007.

[6] Korotcenkov, G. Practical aspects in design of one-electrode semiconductor gas sensors: Status report. *Sensors and Actuators B: Chemical 121*, 2 (2007), 664–678.

[7] Erickson, P. A., Ed. *Practical guide to occupational health and safety.* Academic Press, San Diego, 1996.

[8] De Smedt, G., de Corte, F., Notelé, R., and Berghmans, J. Comparison of two standard test methods for determining explosion limits of gases at atmospheric conditions. *Journal of Hazardous Materials 70*, 3 (1999), 105–113.

[9] Jones, T. A., and Walsh, P. T. Flammable gas detection. *Platinum Metals Review 32*, 2 (1988), 50–60.

[10] Baker, A. Patent UK 892530 (Improvements in or relating to electrically beatable filaments), 1962.

[11] Chou, J., Ed. *Hazardous gas monitors – a practical guide to selection, operation and applications.* McGraw-Hill, New York, 2000.

[12] Jones, E. The pellistor catalytic gas sensor. In *Solid state gas sensors*, P. Moseley and B. Tofield, Eds. Adam Hilger, Bristol, 1987.

[13] Glassman, I., Ed. *Combustion*, 3 ed. Academic Press, San Diego, 1996.

[14] Haynes, W. M., Ed. *Handbook of chemistry and physics*, 93 ed. CRC Press, Colorado, 2012.

[15] McAllister, S., Chen, J.-Y., and Fernandez-Pello, A. C., Eds. *Fundamentals of combustion processes.* Mechanical engineering series. Springer, New York, 2011.

[16] Liberman, M. A., Ed. *Introduction to physics and chemistry of combustion.* Springer, Berlin, 2008.

[17] Terao, K., Ed. *Irreversible Phenomena – ignition, combustion and detonation waves.* Springer, Berlin, 2007.

[18] Cottilard, S. A., Ed. *Catalytic combustion*. Chemical engineering methods and technology. Nova Science Publisher, New York, 2011.

[19] Moseley, P. Solid state gas sensors. *Measurement Science and Technology 8*, 3 (1997), 223–237.

[20] Gentry, S., and Jones, T. The role of catalysis in solid-state gas sensors. *Sensors and Actuators 10*, 1–2 (1986), 141–163.

[21] Korotcenkov, G., Ed. *Chemical sensors: Fundamentals of sensing materials*, vol. 1 of *Sensor technology series*. Momentum Press, New York, 2010.

[22] Firth, J., Jones, A., and Jones, T. The principles of the detection of flammable atmospheres by catalytic devices. *Combustion and Flame 20*, 3 (1973), 303–311.

[23] Krebs, P., and Grisel, A. A low power integrated catalytic gas sensor. *Sensors and Actuators B: Chemical 13*, 1–3 (1993), 155–158.

[24] Vauchier, C., Charlot, D., Delapierre, G., and Accorsi, A. Thin-film gas catalytic microsensor. *Sensors and Actuators B: Chemical 5*, 1–4 (1991), 33–36.

[25] Krawczyk, M., and Namiesnik, J. Application of a catalytic combustion sensor (pellistor) for the monitoring of the explosiveness of a hydrogen-air mixture in the upper explosive limit range. *Journal of Automated Methods and Management in Chemistry 25*, 5 (2003), 115–122.

[26] Williams, G., and Coles, G. S. The semistor: a new concept in selective methane detection. *Sensors and Actuators B: Chemical 57*, 1–3 (Sept. 1999), 108–114.

[27] Lerchner, J., Seidel, J., Wolf, G., and Weber, E. Calorimetric detection of organic vapours using inclusion reactions with organic coating materials. *Sensors and Actuators B: Chemical 32*, 1 (1996), 71–75.

[28] Lerchner, J., Caspary, D., and Wolf, G. Calorimetric detection of volatile organic compounds. *Sensors and Actuators B: Chemical 70*, 1–3 (2000), 57–66.

[29] Hagleitner, C., Hierlemann, A., Lange, D., Kummer, A., Kerness, N., Brand, O., and Baltes, H. Smart single-chip gas sensor microsystem. *Nature 414*, 6861 (2001), 293–296.

[30] Company, S. H. Patent DRP 283677 (Verfahren und Einrichtung zum Anzeigen von Gasbeimengungen in der Luft, insbesondere von Grubengasen), 1913.

[31] McNair, H. M., and Miller, J. M., Eds. *Basic gas chromatography*, 2 ed. John Wiley & Sons, Hoboken, 2009.

[32] Accorsi, A., Delapierre, G., Vauchier, C., and Charlot, D. A new microsensor for environmental measurements. *Sensors and Actuators B: Chemical 4*, 3–4 (1991), 539–543.

[33] Simon, I., and Arndt, M. Thermal and gas-sensing properties of a micromachined thermal conductivity sensor for the detection of hydrogen in automotive applications. *Sensors and Actuators A: Physical 97–98* (2002), 104–108.

[34] Brown, J. E., and Lipták, B. G. Thermal conductivity detectors. In *Instrument engineers' handbook: Process measurement and analysis*, B. G. Lipták, Ed., vol. 1. CRC Press, Boca Raton, 1995.

[35] Poling, B. E., Prausnitz, J. M., and O'Connell, J. P., Eds. *The properties of gases and liquids*, 5 ed. McGraw-Hill, New York, 2001.

[36] Wassiljewa, A. Wärmeleitung in Gasgemischen. *Physikalische Zeitschrift 5*, 22 (1904), 737–742.

[37] Mason, E. A., and Saxena, S. C. Approximate formula for the thermal conductivity of gas mixtures. *Physics of Fluids 1*, 5 (1958), 361–369.

[38] Thénard, L. J. Observations sur des nouvelles combinaisons entre l'oxigène et divers acides. *Annales de Chimie et de Physique 8* (1818), 306–312.

[39] Schumb, W. C., Satterfield, C. N., and L., W. R., Eds. *Hydrogen peroxide*. Reinhold Publishing Corporation, New York, 1955.

[40] Wolffenstein, R. Concentration und Destillation von Wasserstoffsuperoxyd. *Berichte der Deutschen Chemischen Gesellschaft 27*, 3 (1894), 3307–3312.

[41] Pokhodenko, V. D. Life and work of academician L. V. Pisarzhevskii (on the 120th anniversary of his birth). *Theoretical and Experimental Chemistry 29*, 6 (1994), 313–319.

[42] Ayling, G. W. Waste treatment with hydrogen peroxide. *Chemical Engineering 88*, 24 (1981), 79–82.

[43] Eul, W., Moeller, A., and Steiner, N. Hydrogen peroxide. In *Kirk-Othmer Encyclopedia of Chemical Technology*. John Wiley & Sons, Hoboken, 2000.

[44] Yaws, C., and Setty, H. Water and hydrogen peroxide. *Chemical Engineering 81*, 27 (1974), 67–74.

[45] Jones, C. W., and Clark, J. H., Eds. *Applications of hydrogen peroxide and its derivatives*. The Royal Society of Chemistry, Cambridge, 1999.

[46] Cooper, W. J., Zika, R. G., Petasne, R. G., and Plane, J. M. C. Photochemical formation of hydrogen peroxide in natural waters exposed to sunlight. *Environmental Science & Technology 22*, 10 (1988), 1156–1160.

[47] Calvert, J. G., and Stockwell, W. R. Acid generation in the troposphere by gas-phase chemistry. *Environmental Science & Technology 17*, 9 (1983), 428–443.

[48] Armogida, M., Nisticó, R., and Mercuri, N. B. Therapeutic potential of targeting hydrogen peroxide metabolism in the treatment of brain ischaemia. *British Journal of Pharmacology 166*, 4 (2012), 1211–1224.

[49] Halliwell, B., Clement, M. V., and Long, L. H. Hydrogen peroxide in the human body. *FEBS Letters 486*, 1 (2000), 10–13.

[50] Schildknecht, H., and Holoubek, K. Die Bombardierkäfer und ihre Explosionschemie V. Mitteilung über Insektenabwehrstoffe. *Angewandte Chemie 73*, 1 (1961), 1–7.

[51] Goor, G., Glenneberg, J., and Jacobi, S. Hydrogen peroxide. In *Ullmann's Encyclopedia of Industrial Chemistry*. Wiley-VCH Verlag, Weinheim, 2000.

[52] Nederhoff, E. Hydrogen peroxide for cleaning irrigation system. *The Commercial Grower 55*, 10 (2000), 32–34.

[53] KEMI – Swedish Chemicals Agency. Information on substances – hydrogen peroxide. Technical report, 2010.

[54] Global Industry Analysts, Inc. Hydrogen peroxide – a global strategic business report. Document, 2012.

[55] Hage, R., and Lienke, A. Anwendung von Übergangsmetallkomplexen zum Bleichen von Textilien und Holzpulpe. *Angewandte Chemie 118*, 2 (2006), 212–229.

[56] Miro, S., and S., A. D. Catalysis and activation of oxygen and peroxide delignification of chemical pulps: a review. In *ACS Symposium Series*, vol. 785. American Chemical Society, 2001, pp. 2–43.

[57] Spiro, M., and Griffith, W. P. The mechanism of hydrogen peroxide bleaching. *Textile Chemist and Colorist 29*, 11 (1997), 12–13.

[58] Antonijevic, M., Dimitrijevic, M., and Jankovic, Z. Leaching of pyrite with hydrogen peroxide in sulphuric acid. *Hydrometallurgy 46*, 1–2 (1997), 71–83.

[59] Kitis, M., Akcil, A., Karakaya, E., and Yigit, N. Destruction of cyanide by hydrogen peroxide in tailings slurries from low bearing sulphidic gold ores. *Minerals Engineering 18*, 3 (2005), 353–362.

[60] Wernimont, E., Ventura, M., Garboden, G., and Mullens, P. Past and present uses of rocket grade hydrogen peroxide. Technical report, General Kinetics, LLC, 1999.

[61] Ansari, I., and Datta, A. An overview of sterilization methods for packaging materials used in aseptic packaging systems. *Food and Bioproducts Processing 81*, 1 (2003), 57–65.

[62] McDonnell, G., and Russell, A. D. Antiseptics and disinfectants: activity, action, and resistance. *Clinical Microbiology Reviews 12*, 1 (1999), 147–179.

[63] Muranyi, P. *Einsatz eines Atmosphärendruckplasmas zur Entkeimung von lebensmittelrelevanten Verpackungen aus Kunststoff*. Dissertation, Technische Universität München, 2008.

[64] Wu, J. S. B., Hsu, H.-Y., and Yang, B.-H. B. Aseptic processing and packaging. In *Handbook of fruits and fruit processing*. Wiley-Blackwell, 2012, pp. 175–187.

[65] von Bockelmann, B. A. H., and von Bockelmann, I. L. I. Aseptic packaging of liquid food products: a literature review. *Journal of Agricultural and Food Chemistry 34*, 3 (1986), 384–392.

[66] Muranyi, P., Wunderlich, J., and Dobosz, M. Sterilisation von Abfüllmaschinen: Standardisierung von Bioindikatoren, Untersuchungsmethoden und Validierungsverfahren. *Chemie Ingenieur Technik 78*, 11 (2006), 1667–1673.

[67] Buchner, N., Ed. *Verpackung von Lebensmitteln*, 1 ed. Springer, Berlin, 1999.

[68] David, J. R. D., Graves, R. H., and Carlson, V. R., Eds. *Aseptic processing and packaging of food: a food industry perspective*. CRC Press, New York, 1996.

[69] Wallhäusser, K. H., Ed. *Praxis der Sterilisation, Desinfektion, Antiseptik und Konservierung – Keimidentifizierung-Betriebshygiene*, 4 ed. Thieme, Stuttgart, 1988.

[70] Codex Alimentarius Commission Code of hygienic practice for aseptically processed and packaged low-acid food. Technical Report CAC/RCP 40, 1993.

[71] Cerny, G. Packstoffsterilisation beim aseptischen Abpacken. *Internationale Zeitschrift für Lebensmittel-Technik, Marketing, Verpackung und Analytik 41*, 1–2 (1990), 54–58.

[72] Gould, G. W. Methods for preservation and extension of shelf life. *International Journal of Food Microbiology 33*, 1 (1996), 51–64.

[73] Russell, A. D. Bacterial spores and chemical sporicidal agents. *Clinical Microbiology Reviews 3*, 2 (1990), 99–119.

[74] Reuter, H. Aseptisches Verpacken von Lebensmitteln - Grundlagen und Stand der Technik. *Chemie Ingenieur Technik 58*, 10 (1986), 785–793.

[75] Heckert, R. A., Best, M., Jordan, L. T., Dulac, G. C., Eddington, D. L., and Sterritt, W. G. Efficacy of vaporized hydrogen peroxide against exotic animal viruses. *Applied And Environmental Microbiology 63*, 10 (1997), 3916–3918.

[76] Cardoso, C. F., Faria, J. d. A. F., and Miranda Walter, E. H. Modeling of sporicidal effect of hydrogen peroxide in the sterilization of low density polyethylene film inoculated with <i>bacillus subtilis<ı> spores. *Food Control 22*, 10 (2011), 1559–1564.

[77] Bayliss, C. E., and Waites, W. M. Effect of simultaneous high intensity ultraviolet irradiation and hydrogen peroxide on bacterial spores. *International Journal of Food Science & Technology 17*, 4 (1982), 467–470.

[78] Engelhard, P., and Kulozik, U. Packstoffentkeimung mittels Wasserstoffperoxid - Methoden und Kombinationsverfahren. *Chemie Ingenieur Technik 78*, 11 (2006), 1717–1722.

[79] Unger-Bimczok, B., Kottke, V., Hertel, C., and Rauschnabel, J. The influence of humidity, hydrogen peroxide concentration, and condensation on the inactivation of *Geobacillus stearothermophilus* spores with hydrogen peroxide vapor. *Journal of Pharmaceutical Innovation 3*, 2 (2008), 123–133.

[80] Engelhard, P. *Inaktivieren von Mikroorganismen auf festen Oberflächen mittels Atmosphären aus feuchter Luft/Wasserstoffperoxid und IR-Behandlung.* Dissertation, Technische Universität München, 2005.

[81] Block, S. S., Ed. *Desinfection, sterilization and preservation.* Lea & Febiger, Philadelphia, 1991.

[82] Imlay, J. A., and Linn, S. DNA damage and oxygen radical toxicity. *Science 240*, 4857 (1988), 1302–1309.

[83] Mohan, A., Dunn, J., Hunt, M. C., and Sizer, C. E. Inactivation of *Bacillus atrophaeus* spores with surface-active peracids and characterization of formed free radicals using electron spin resonance spectroscopy. *Journal of Food Science 74*, 7 (2009), M411–M417.

[84] Riesenman, P. J., and Nicholson, W. L. Role of the spore coat layers in *Bacillus subtilis* spore resistance to hydrogen peroxide, artificial UV-C, UV-B, and solar UV radiation. *Applied and Environmental Microbiology 66*, 2 (2000), 620–626.

[85] Imlay, J. A. Pathways of oxidative damage. *Annual Review of Microbiology 57*, 1 (2003), 395–418.

[86] Baldry, M. The bactericidal, fungicidal and sporicidal properties of hydrogen peroxide and peracetic acid. *Journal of Applied Microbiology 54*, 3 (1983), 417–423.

[87] Setlow, B., Setlow, C. A., and Setlow, P. Killing bacterial spores by organic hydroperoxides. *Journal of Industrial Microbiology and Biotechnology 18*, 6 (1997), 384–388.

[88] Linley, E., Denyer, S. P., McDonnell, G., Simons, C., and Maillard, J.-Y. Use of hydrogen peroxide as a biocide: new consideration of its mechanisms of biocidal action. *Journal of Antimicrobial Chemotherapy 67*, 7 (2012), 1589–1596.

[89] Melly, E., Cowan, A., and Setlow, P. Studies on the mechanism of killing of *Bacillus subtilis* spores by hydrogen peroxide. *Journal of Applied Microbiology 93*, 2 (2002), 316–325.

[90] Popham, D. L., Sengupta, S., and Setlow, P. Heat, hydrogen peroxide, and UV resistance of *Bacillus subtilis* spores with increased core water content and with or without major DNA-binding proteins. *Applied and Environmental Microbiology 61*, 10 (1995), 3633–3638.

[91] Gilmore, M. E., Bandyopadhyay, D., Dean, A. M., Linnstaedt, S. D., and Popham, D. L. Production of muramic δ-lactam in *Bacillus subtilis* spore peptidoglycan. *Journal of Bacteriology 186*, 1 (2004), 80–89.

[92] Setlow, P. Spores of *Bacillus subtilis*: their resistance to and killing by radiation, heat and chemicals. *Journal of Applied Microbiology 101*, 3 (2006), 514–525.

[93] Setlow, B., and Setlow, P. Binding of small, acid-soluble spore proteins to DNA plays a significant role in the resistance of *Bacillus subtilis* spores to hydrogen peroxide. *Applied and Environmental Microbiology 59*, 10 (1993), 3418–3423.

[94] Setlow, P. Mechanisms for the prevention of damage to DNA in spores of *Bacillus* species. *Annual Review of Microbiology 49*, 1 (1995), 29–54.

[95] Shin, S.-Y., Calvisi, E. G., Beaman, T. C., Pankratz, H. S., Gerhardt, P., and Marquis, R. E. Microscopic and thermal characterization of hydrogen peroxide killing and lysis of spores and protection by transition metal ions, chelators, and antioxidants. *Applied and Environmental Microbiology 60*, 9 (1994), 3192–3197.

[96] King, W. L., and Gould, G. W. Lysis of bacterial spores with hydrogen peroxide. *Journal of Applied Microbiology 32*, 4 (1969), 481–490.

[97] Palop, A., Rutherford, G. C., and Marquis, R. E. Hydroperoxide inactivation of enzymes within spores of *Bacillus megaterium* ATCC19213. *FEMS Microbiology Letters 142*, 2–3 (1996), 283–287.

[98] Cortezzo, D., Koziol-Dube, K., Setlow, B., and Setlow, P. Treatment with oxidizing agents damages the inner membrane of spores of *Bacillus subtilis* and sensitizes spores to subsequent stress. *Journal of Applied Microbiology 97*, 4 (2004), 838–852.

[99] Verband Deutscher Maschinen- und Anlagenbauer (VDMA). Filling machines of VDMA hygiene class V: testing the effectiveness of packaging sterilization devices. Code of practice 6, 2008.

[100] Bazin, M. J., and Prosser, J. I., Eds. *Physiological models in microbiology*, vol. 2. CRC Press, Boca Raton, 1988.

[101] Institute For Thermal Processing Specialists (IFTIPS). Guidelines for microbiological validation of the sterilization of aseptic filling machines and packages, including containers and closures. Document G.005.V1, 2011.

[102] Adams, D., Brown, G. P., Fritz, C., and Todd, T. R. Calibration of a near-infrared (NIR) H_2O_2 vapor monitor. *Pharmaceutical Engineering 18*, 4 (1998), 66–85.

[103] Corveleyn, S., Vandenbossche, G. M. R., and Remon, J. P. Near-infrared (NIR) monitoring of H_2O_2 vapor concentration during vapor hydrogen peroxide (vhp) sterilisation. *Pharmaceutical Research 14*, 3 (1997), 294–298.

[104] Haney, R. L. *Principal component analysis for enhancement of infrared spectra monitoring*. Ph.D. thesis, Auburn University, 2011.

[105] Xu, M., Bunes, B. R., and Zang, L. Paper-based vapor detection of hydrogen peroxide: colorimetric sensing with tunable interface. *ACS Applied Materials & Interfaces 3*, 3 (2011), 642–647.

[106] Toniolo, R., Geatti, P., Bontempelli, G., and Schiavon, G. Amperometric monitoring of hydrogen peroxide in workplace atmospheres by electrodes supported on ion-exchange membranes. *Journal of Electroanalytical Chemistry 514*, 1–2 (2001), 123–128.

[107] Kuwata, S., and Sadaoka, Y. Detection of gaseous hydrogen peroxide using planar-type amperometric cell at room temperature. *Sensors and Actuators B: Chemical 65*, 1–3 (2000), 325–326.

[108] Huang, H., Dasgupta, P. K., Genfa, Z., and Wang, J. A pulse amperometric sensor for the measurement of atmospheric hydrogen peroxide. *Analytical Chemistry 68*, 13 (1996), 2062–2066.

[109] Zheng, J. Y., Yan, Y., Wang, X., Shi, W., Ma, H., Zhao, Y. S., and Yao, J. Hydrogen peroxide vapor sensing with organic core/sheath nanowire optical waveguides. *Advanced Materials 24*, 35 (2012), 194–199.

[110] Chen, L. C., Yu, Z., and Hiraoka, K. Vapor phase detection of hydrogen peroxide with ambient sampling chemi/chemical ionization mass spectrometry. *Analytical Methods 2*, 7 (2010), 897–900.

[111] Reisert, S., Geissler, H., Flörke, R., Näther, N., Wagner, P., and Schöning, M. J. Towards a multi-sensor system for the evaluation of aseptic processes employing hydrogen peroxide vapour (H_2O_2). *Physica Status Solidi A 208*, 6 (2011), 1351–1356.

[112] Näther, N., Henkel, H., Schneider, A., and Schöning, M. J. Investigation of different catalytically active and passive materials for realising a hydrogen peroxide gas sensor. *Physica Status Solidi A 206*, 3 (2009), 449–454.

[113] NÄTHER, N. *Entwicklung eines H_2O_2-Messverfahrens für die Überwachung der mikrobioziden Wirksamkeit bei der Sterilisation aseptischer Verpackungen.* Dissertation, Philipps-Universität Marburg, 2009.

2 Gas sensor investigation based on a catalytically activated thin-film thermopile for H_2O_2 detection

KIRCHNER, P., Ng, Y. A., Spelthahn, H., Schneider, A., Henkel, H., Friedrich, P., Kolstad, J., Berger, J., Keusgen, M., and Schöning, M. J.

Physica Status Solidi A 207, 4 (2010), 787–792.

2.1 Abstract

In aseptic filling systems, hydrogen peroxide vapour is commonly used for the reduction of microbial contaminations in carton packages. In this process, the germicidal efficiency of the vapour depends especially on the H_2O_2 concentration. To monitor the H_2O_2 concentration, a calorimetric H_2O_2 gas sensor based on a catalytically activated thin-film thermopile is investigated. Two different sensor layouts, namely a circular and a linear form, as well as two various material pairs such as tungsten/nickel and gold/nickel, have been examined for the realisation of a thin-film thermopile. Additionally, manganese oxide and palladium particles have been compared as responsive catalysts towards H_2O_2. The thin-film sensors have been investigated at various H_2O_2 concentrations, gas temperatures and flow rates.

2.2 Introduction

In recent years, the packaging material in aseptic filling processes has become more and more important, especially to assure high quality of the shelf life of food and beverages, because the material was found to represent a significant source for microbial contaminations of the filled products [1–4]. Obviating this contamination, hence, the packages have to be antimicrobially pre-treated before the products are filled into it. In aseptic filling processes, one of the mostly used sterilisation agents for carton packages is hydrogen peroxide vapour (HPV) besides to other chemicals, like formaldehyde and ozone. This is caused by the oxidising effect and the decomposition of HPV in water vapour and oxygen [4–7]. In such an aseptic filling process, the carton packages are firstly pre-heated, subsequently microbially reduced by HPV and finally filled with the food products or beverages. During the reduction of microbial contaminations, an H_2O_2 solution (35% w/w) is evaporated and afterwards streamed together with compressed air into the pre-heated package at a temperature of nearly 250 °C and a flow rate of about 10 m^3/h. The H_2O_2 concentration of the gas mixture, varying between 4 and 10% v/v, correlates thereby with the germicidal efficiency and should be monitored in this process. Hence, a sensor system is needed, which can detect the H_2O_2 concentration in an aseptic filling process and consequently controls the reduction of microbial contaminations in carton packages.

In the last years, various types of sensors for the detection of hydrogen peroxide have been introduced. Mainly, these sensors are electrochemical sensors [8–12]. However, electrochemical sensors cannot be applied either at the required elevated temperatures or be used for determination of H_2O_2 concentrations up to 10% v/v in a gas mixture, like in the introduced aseptic filling process. Other sensors, being presented, are calorimetric sensors for the detection of volatile and combustible gases which could be used for the monitoring of HPV [13–19]. But those sensors are highly unspecific and they could also be responsive to other components of the gas mixture of the HPV process. In this work, a novel calorimetric H_2O_2 gas sensor based on a thin-film thermopile is investigated. The calorimetric sensor device relies on a differential set-up of a catalytically activated and a passivated segment that was introduced in former works [20–22]. In HPV atmosphere, the hydrogen peroxide decomposes on the catalyst and exothermic heat can be determined by a thin-film thermopile in the form of a temperature increase. Therefore, different layouts and material pairs for the thermopile and catalyst have been examined.

2.3 Experimental

2.3.1 Sensor design and fabrication

For the realisation of the calorimetric H_2O_2 gas sensor a thin-film thermopile as temperature-sensing element that relies on the Seebeck effect was designed. The temperature gradient of a thermopile between the two segments containing the respective junctions of the material pair can be determined by the thermoelectric voltage:

$$\Delta U_{\mathrm{Th}} = \sum_{n=1}^{N} (\alpha_{\mathrm{A/B}} \cdot \Delta T) \tag{2.1}$$

with the Seebeck coefficient $\alpha_{\mathrm{A/B}}$ for the material pair A/B and N as the number of junctions.

As substrate for the thin-film thermopile, silicon with an insulation layer of 500 nm SiO_2 has been used. The thin-film thermopile was designed in a circular and linear form, both of them consisting of eight junctions of the material pair shown in Fig. 2.1.

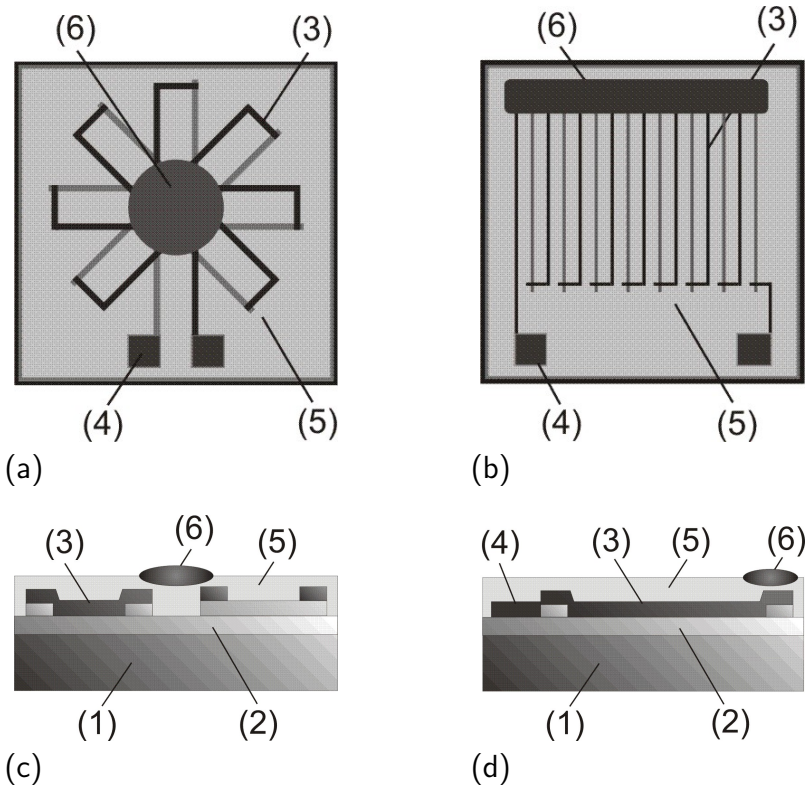

Figure 2.1: Schematic top-view of the calorimetric H_2O_2 gas sensor based on a thin-film thermopile with (a) circular and (b) linear layout of the material pair with a chip size of 10 x 10 mm^2; cross-section scheme of the sensor with (c) circular and (d) linear thin-film thermopile. (1) Si substrate, (2) SiO_2 layer, (3) thin-film thermopile, (4) contact pads, (5) passivation layer and (6) catalyst.

Two different material pairs, tungsten/nickel and gold/nickel, which have a relatively high Seebeck coefficient, have been investigated for the thin-film thermopile. The theoretical characteristics of the thermoelectric voltage of W/Ni and Au/Ni thermocouples at various temperature differences are shown in Fig. 2.2. The materials for the thin-film thermopile have been separately deposited via physical vapour deposition and patterned by conventional photolithography. The layer thickness of the first deposited material, tungsten as well as gold, is 200 nm and of the subsequently deposited material, nickel, 300 nm, so that an overlapping of the material pairs at the junctions is assured.

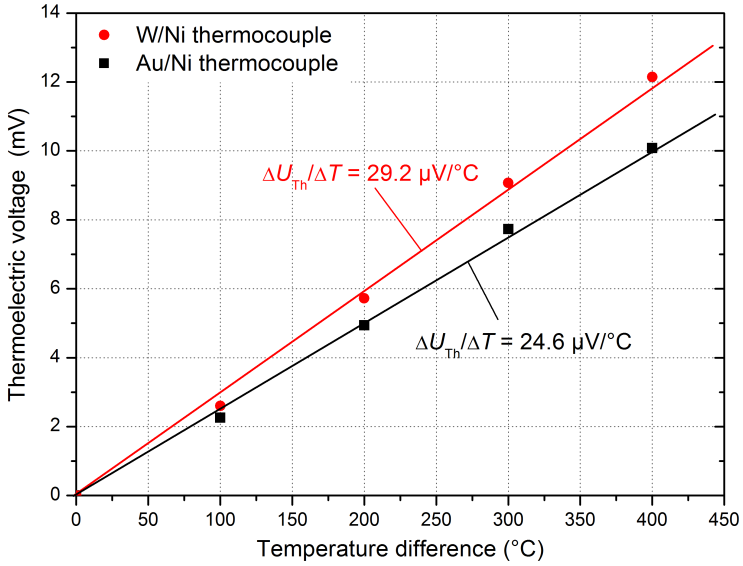

Figure 2.2: Theoretical characteristics of the thermoelectric voltage of tungsten/nickel and gold/nickel thermocouples at various temperature differences between the junctions (data adapted from [23]).

Afterwards, the thin-film thermopile was passivated with SU-8 photoresist because of its chemical and thermal stability. The resist was deposited by spin-coating to achieve a homogenous layer with a thickness of 1.5 μm. In a final step, the thin-film thermopile was activated by a catalyst, which is highly selective to H_2O_2. As catalytically active materials, manganese oxide and palladium have been investigated. Therefore, the thin-film thermopile was deposited with either a dispersion of MnO_2 particles or Pd particles via drop-coating and heat-treated at 360 °C for 30 min. Particles are chosen to achieve a high sensitivity towards H_2O_2 due to their large contact area. The grain size of the MnO_2 amounts to be 10 μm and of Pd particles is up to 500 nm (s. Fig. 2.3).

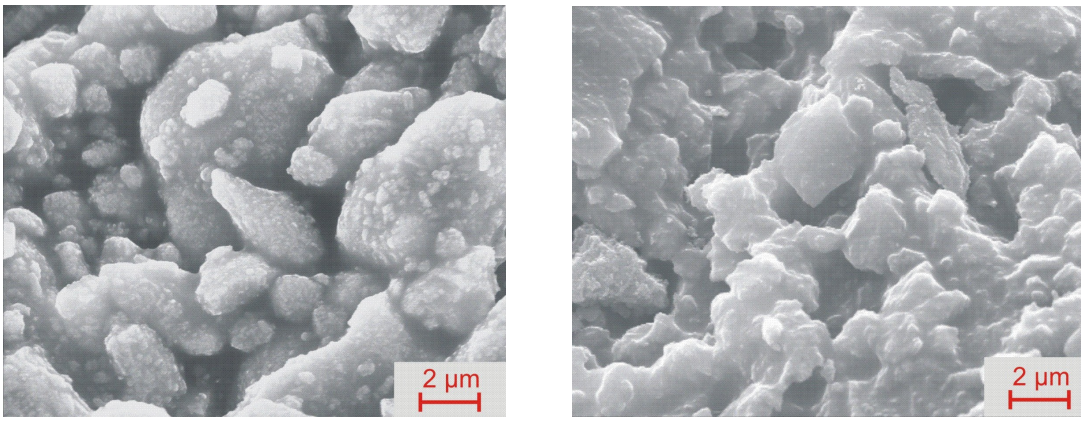

Figure 2.3: Scanning electron microscopic pictures of the catalytically active materials: (a) MnO_2 particles and (b) Pd particles.

In HPV atmosphere, a temperature difference between the catalytically active and passive segment can be detected in the form of a thermoelectric voltage caused by the released reaction enthalpy of the exothermal decomposition of H_2O_2 on the MnO_2 or Pd particles. Therein, the reaction enthalpy correlates linearly with the H_2O_2 concentration of the gas mixture and the resulting temperature difference can be approximately calculated as in Ref. [24].

2.3.2 Experimental set-up

For the characterisation of the calorimetric H_2O_2 gas sensor, an experimental set-up was developed, where the HPV process of aseptic filling systems can be reproduced. The set-up contains two reservoirs for H_2O_2 solution (35% w/w) and deionised water as well as a dosing system with a flow-control unit and a dosing pump for each reservoir to realise various concentrations and flow rates. Compressed air is used as carrier gas for the H_2O_2 solution and the deionised water. Before the aerosol of air and H_2O_2 solution or deionised water is streamed into the measuring chamber, it is vaporised in a heater of the evaporation unit, which also contains a control system to regulate the gas temperature. A diagram of the experimental set-up is shown in Fig. 2.4.

The control and regulation of the experimental set-up are accomplished via a data acquisition system and a LabVIEW program that is also used for reading out the sensor signal during the measurement.

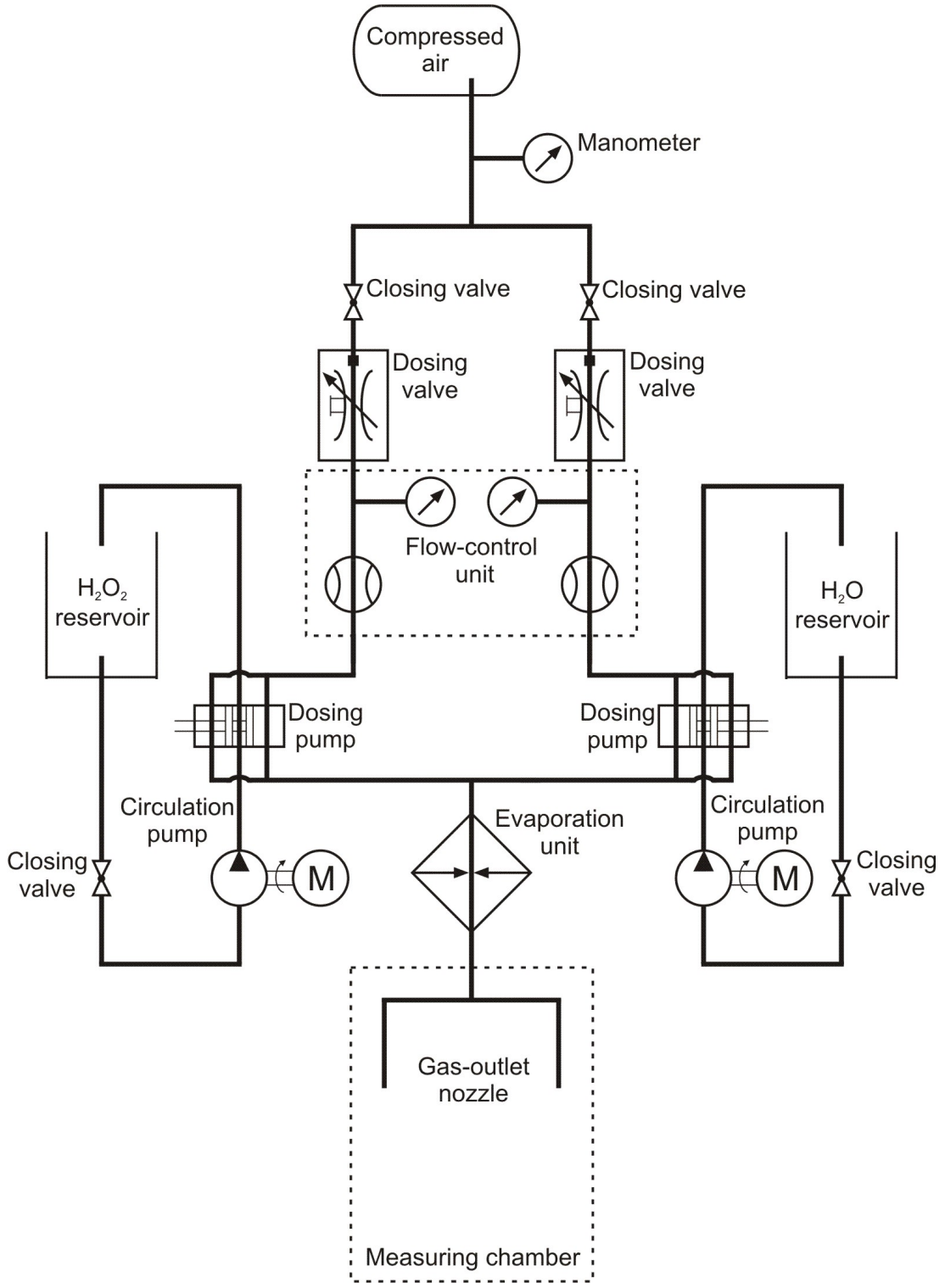

Figure 2.4: Diagram of the experimental set-up with measuring chamber for the sensor characterisation.

2.4 Results and discussion

2.4.1 Material characterisation

In the experimental set-up the two different sensor layouts, circular and linear, for both material pairs, tungsten/nickel and gold/nickel, with MnO_2 particles as catalyst have been characterised firstly. Therefore, the combined materials and different layouts have been examined at various gas concentrations with regard to their sensitivity against H_2O_2. In Tab. 2.1, the sensitivities of these compositions are summarised.

Table 2.1: Sensitivities to H_2O_2 of the sensors as a function of the sensor's scheme and the junction's material pair with MnO_2 catalyst.

Material pair	Sensitivity (μV/(% v/v))	
	Circular thermopile	Linear thermopile
Tungsten/nickel	22.0	103
Gold/nickel	22.3	111

The gas sensor based on a circular thermopile of W/Ni as well as Au/Ni provides a relatively low sensitivity of 22 μV/(% v/v), whereas the sensor based on a linear thermopile possesses a sensitivity above 100 μV/(% v/v) against H_2O_2. This effect relies on the shorter distance between the catalytically activated and passivated junctions of the circular thermopile that causes an increase in temperature on the passive segment during the exothermal decomposition of H_2O_2 on the active segment and reduces the temperature difference between both segments. Additionally, the sensor based on the Au/Ni thermopile offers a higher response as the W/Ni-based sensor in spite of the higher theoretical Seebeck coefficient of W/Ni. This behaviour probably relies on the large resistance of tungsten, which causes a voltage drop during the measurement. The resistance of the tungsten layer is about 2.5 times higher than the resistance of the gold layer.

As a result, the calorimetric gas sensor based on a linear Au/Ni thermopile has been used for the investigation of the two different catalysts, namely manganese oxide and palladium. The Pd particles are more catalytically active against H_2O_2 than the MnO_2 particles that may be caused by the rougher and thus larger surface to volume ratio of the Pd particles. As a consequence of this, the calorimetric H_2O_2 gas sensor based on a linear Au/Ni thermopile with Pd particles as catalyst has been used for further sensor investigations. The sensor signal in the form of a thermoelectric voltage for all of the combined materials and layouts at various H_2O_2 concentrations is presented in Fig. 2.5.

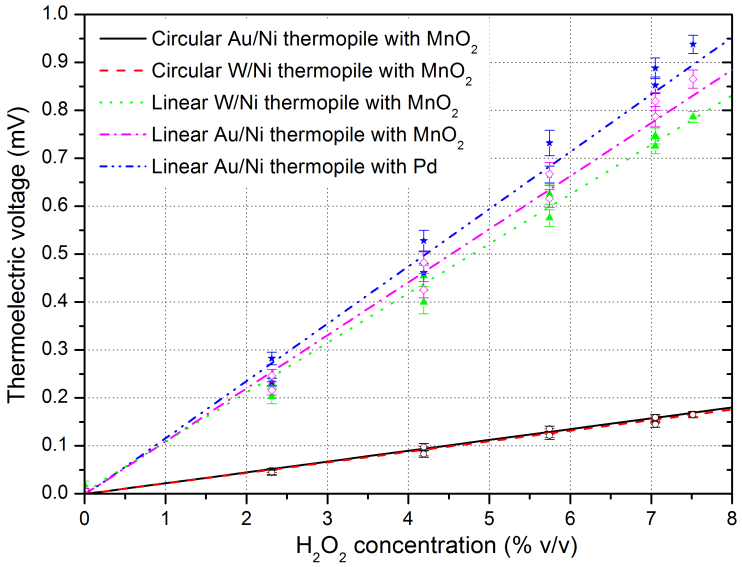

Figure 2.5: Thermoelectric voltage of the different combined materials and sensor layouts at various H_2O_2 concentrations (off-set corrected).

2.4.2 Sensor validation

After the material characterisation, the calorimetric H_2O_2 gas sensor based on a linear Au/Ni thermopile with Pd particles as catalyst is studied in the experimental set-up. Therefore, the sensor signal was detected at various H_2O_2 concentrations from 0 to 8% v/v at a constant gas temperature of 270 °C and a flow rate of 10 m^3/h to determine the sensor characteristics and the hysteresis. In Fig. 2.6(a), the sensor signal in the form of a thermoelectric voltage is presented for various H_2O_2 concentrations. The calorimetric gas sensor shows a linear characteristic against H_2O_2 and has a maximum hysteresis of 67 μV in this measurement. The response time of this sensor was 2.5 s to achieve 90% of the stable sensor signal for each concentration. The calibration plot of the calorimetric H_2O_2 gas sensor is shown in Fig. 2.6(b). The sensor possesses a sensitivity of 166 μV/(% v/v) in the concentration range of 0-8% v/v H_2O_2 and has an off-set of 120 μV that results from a nonuniform temperature distribution in the measuring chamber.

Afterwards, the influence of the gas temperature on the sensor signal has been investigated in the experimental set-up. Various gas temperatures reaching from 180 to 300 °C were adjusted in the set-up and the sensor signal has been determined for these temperatures at a constant H_2O_2 concentration of 4.2% v/v and a flow rate of 10 m^3/h.

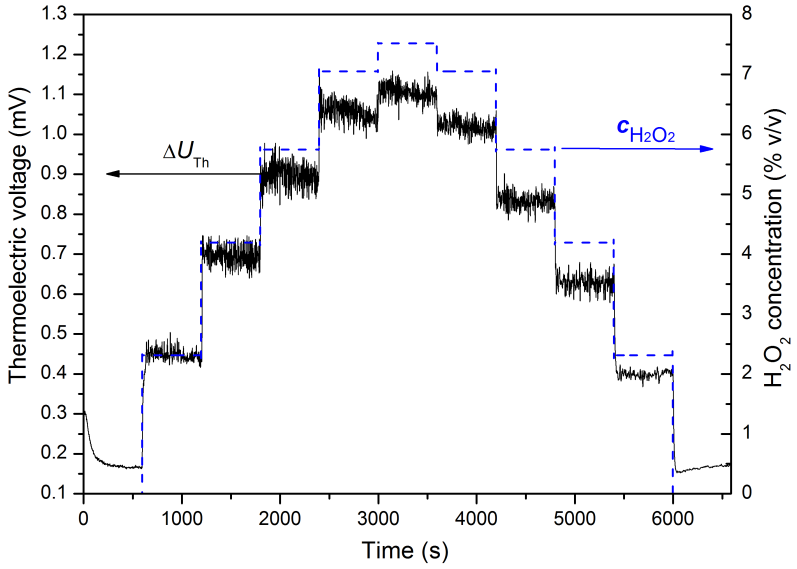

(a)

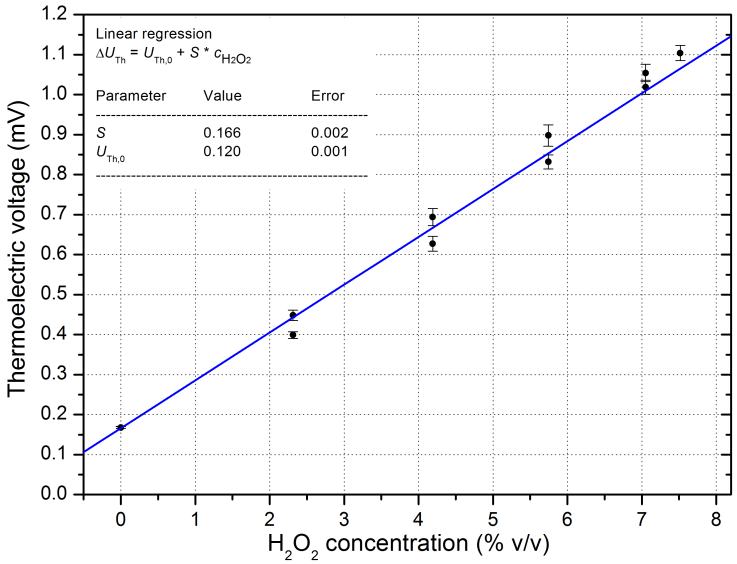

(b)

Figure 2.6: (a) Thermoelectric voltage of the calorimetric gas sensor based on a linear Au/Ni thermopile with Pd as catalyst at various H_2O_2 concentrations (gas temperature: 270 °C, flow rate: 10 m^3/h); and (b) resulting calibration plot.

In Fig. 2.7, the small influence of the gas temperature on the sensor signal is depicted. At a low gas temperature, close to 180 °C, the sensor exhibits a slightly lower thermoelectric voltage of 16% compared to the sensor signals between 210 and 300 °C, which are nearly equal. The decreasing sensor signal at lower temperatures can be explained by means of the Arrhenius equation:

$$k = A \cdot \mathrm{e}^{-E_\mathrm{A}/(R \cdot T)} \tag{2.2}$$

Therein, k is the reaction rate, A is the pre-exponential factor, E_A is the activation energy, R is the gas constant and T is the temperature.

If the gas temperature is reduced, the reaction rate for the exothermal decomposition of H_2O_2 on the catalyst decreases and a lower thermoelectric voltage is detected.

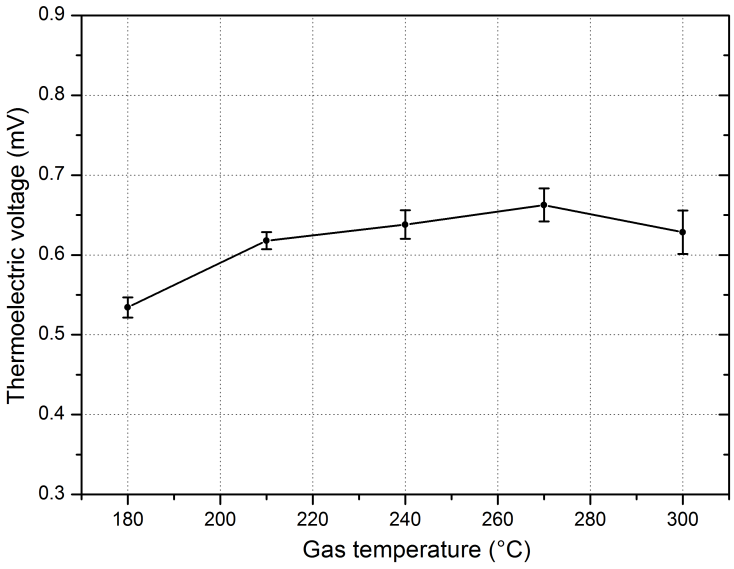

Figure 2.7: Temperature influence on the sensor signal at a constant H_2O_2 concentration of 4.2% v/v and a flow rate of 10 m^3/h.

In the final measurement series, shown in Fig. 2.8, the influence of the gas-flow rate on the thermoelectric voltage of the calorimetric gas sensor has been determined at a constant H_2O_2 concentration of 4.2% v/v and a temperature of 270 °C. Here, the gas-flow rate was varied from 7.5 to 15 m^3/h. The sensor shows an almost constant thermoelectric voltage at the various gas-flow rates from 7.5 to 15 m^3/h. At higher flow rates the sensor signal slightly increases up to about 8.8% at the highest rate of 15 m^3/h towards the thermoelectric voltage at 10 m^3/h.

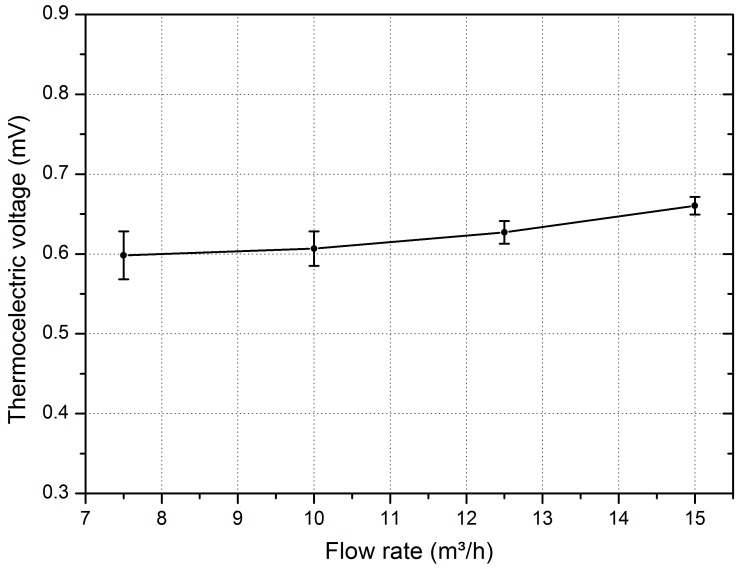

Figure 2.8: Influence of the gas-flow rate on the sensor signal at a constant H_2O_2 concentration of 4.2% v/v and a gas temperature of 270 °C.

2.5 Conclusions

A calorimetric gas sensor based on a catalytically activated thin-film thermopile for the H_2O_2 detection has been investigated. Therefore, an experimental set-up together with a data acquisition system to control and regulate the set-up and to read out the gas sensor has been developed. The sensor device relies on the Seebeck effect. In a first step, two different layouts, a circular and a linear thermopile of tungsten/nickel and gold/nickel have been examined as suitable temperature transducer. Therein, the linear thermopile has shown a higher sensor signal in the form of a thermoelectric voltage than the circular one. The material pair gold/nickel possesses a slightly higher sensitivity than tungsten/nickel. In a subsequent characterisation of the sensor device in the experimental set-up, the catalytical activity of manganese oxide and palladium particles towards H_2O_2 has been compared, in which palladium has shown a higher activity. As a consequence of the material characterisation, a calorimetric gas sensor based on a linear Au/Ni thermopile that is catalytically activated with Pd particles has been realised and further verified. The sensor device offers a sensitivity of 166 μV/(% v/v) against H_2O_2 in the concentration range from 0 to 8% v/v and a response time of 2.5 s. For a constant H_2O_2 concentration, the sensor shows a nearly steady sensor signal in a gas temperature range of 210-300 °C and at a gas-flow rate between 7.5 and 15 m^3/h.

In a next step, the verified calorimetric gas sensor will be coupled on an RFID transmission system for the in-line monitoring of the H_2O_2 concentration during the reduction of microbial contaminations in carton packages in aseptic filling systems.

Acknowledgements

The authors thank the Bundesministerium für Bildung und Forschung and VDI/VDE for financial support of this work, project "Intellipack", and N. Näther for valuable discussions.

References

[1] Lau, O.-W., and Wong, S.-K. Contamination in food from packaging material. *Journal of Chromatography A 882*, 1–2 (2000), 255–270.

[2] Cerny, G. Testing of aseptic machines for efficiency of sterilization of packaging materials by means of hydrogen peroxide. *Packaging Technology and Science 5*, 2 (1992), 77–81.

[3] Graumlich, T. R., Marcy, J. E., and Adams, J. P. Aseptically packaged orange juice and concentrate: a review of the influence of processing and packaging conditions on quality. *Journal of Agricultural and Food Chemistry 34*, 3 (1986), 402–405.

[4] von Bockelmann, B. A. H., and von Bockelmann, I. L. I. Aseptic packaging of liquid food products: a literature review. *Journal of Agricultural and Food Chemistry 34*, 3 (1986), 384–392.

[5] Yamamoto, M., Nishioka, M., and Sadakata, M. Sterilization by H_2O_2 droplets under corona discharge. *Journal of Electrostatics 55*, 2 (2002), 173–187.

[6] Johnston, M., Lawson, S., and Otter, J. Evaluation of hydrogen peroxide vapour as a method for the decontamination of surfaces contaminated with *Clostridium botulinum* spores. *Journal of Microbiological Methods 60*, 3 (2005), 403–411.

[7] Klapes, N. A., and Vesley, D. Vapor-phase hydrogen peroxide as a surface decontaminant and sterilant. *Applied and Environmental Microbiology 56*, 2 (1990), 503–506.

[8] Huang, H., Dasgupta, P. K., Genfa, Z., and Wang, J. A pulse amperometric sensor for the measurement of atmospheric hydrogen peroxide. *Analytical Chemistry 68*, 13 (July 1996), 2062–2066.

[9] Toniolo, R., Geatti, P., Bontempelli, G., and Schiavon, G. Amperometric monitoring of hydrogen peroxide in workplace atmospheres by electrodes supported on ion-exchange membranes. *Journal of Electroanalytical Chemistry 514*, 1–2 (2001), 123–128.

[10] Huang, H., and Dasgupta, P. K. Renewable liquid film-based electrochemical sensor for gaseous hydroperoxides. *Talanta 44*, 4 (1997), 605–615.

[11] Guwy, A., Hawkes, F., Martin, S., Hawkes, D., and Cunnah, P. A technique for monitoring hydrogen peroxide concentration off-line and on-line. *Water Research 34*, 8 (2000), 2191–2198.

[12] Mehta, A., Patil, S., Bang, H., Cho, H. J., and Seal, S. A novel multivalent nanomaterial based hydrogen peroxide sensor. *Sensors and Actuators A: Physical 134*, 1 (2007), 146–151.

[13] Chen, A., Luo, R., Tan, T.-C., and Liu, C.-C. A thick-film calormetric sensor for monitoring the concentration of combustible gases. *Sensors and Actuators 19*, 3 (1989), 237–248.

[14] Makovos, E. B., Montague, F. W., Dudik, L., and Liu, C.-C. A calorimetric combustible gas detector employing platinum film heaters. *Sensors and Actuators B: Chemical 12*, 2 (1993), 91–94.

[15] Vauchier, C., Charlot, D., Delapierre, G., and Accorsi, A. Thin-film gas catalytic microsensor. *Sensors and Actuators B: Chemical 5*, 1–4 (1991), 33–36.

[16] Lerchner, J., Caspary, D., and Wolf, G. Calorimetric detection of volatile organic compounds. *Sensors and Actuators B: Chemical 70*, 1–3 (2000), 57–66.

[17] Houlet, L. F., Shin, W., Tajima, K., Nishibori, M., Izu, N., Itoh, T., and Matsubara, I. Thermopile sensor-devices for the catalytic detection of hydrogen gas. *Sensors and Actuators B: Chemical 130*, 1 (2008), 200–206.

[18] Rettig, F., and Moos, R. Direct thermoelectric gas sensors: Design aspects and first gas sensors. *Sensors and Actuators B: Chemical 123*, 1 (2007), 413–419.

[19] Casey, V., Cleary, J., D'Arcy, G., and McMonagle, J. B. Calorimetric combustible gas sensor based on a planar thermopile array: fabrication, characterisation, and gas response. *Sensors and Actuators B: Chemical 96*, 1–2 (2003), 114–123.

[20] Näther, N., Juárez, L. M., Emmerich, R., Berger, J., Friedrich, P., and Schöning, M. J. Detection of hydrogen peroxide (H_2O_2) at exposed temperatures for industrial processes. *Sensors 6*, 4 (2006), 308–317.

[21] Näther, N., Emmerich, R., Berger, J., Friedrich, P., Henkel, H., Schneider, A., and Schöning, M. J. A novel gas-phase hydrogen peroxide sensor basing on a combined physical/chemical transduction mechanism. *Materials Research Society Symposium Proceedings 951* (2006), 0951–E12–03.

[22] Näther, N., Henkel, H., Schneider, A., and Schöning, M. J. Investigation of different catalytically active and passive materials for realising a hydrogen peroxide gas sensor. *Physica Status Solidi A 206*, 3 (2009), 449–454.

[23] Göpel, W., Hesse, J., and Zemel, J. N., Eds. *Sensors: Thermal sensors*, vol. 4. Wiley-VCH, Weinheim, 1990.

[24] McBride, J. R., Nietering, K. E., and Ellwood, K. R. Design considerations for optimizing the sensitivity of catalytic calorimetric gas sensors: modeling and experimental results. *Sensors and Actuators B: Chemical 73*, 2–3 (2001), 163–173.

2.6 Appendix

2.6.1 Additional measurement curves as support to material characterisation

In the following diagrams, the measurement curves of the calorimetric gas sensors with different layouts and material compositions of the thin-film thermopile are summarised as supporting material for section 2.4.1.

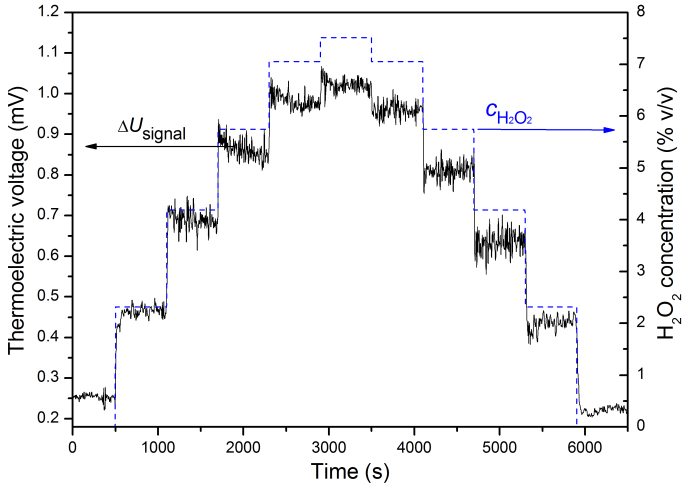

(a)

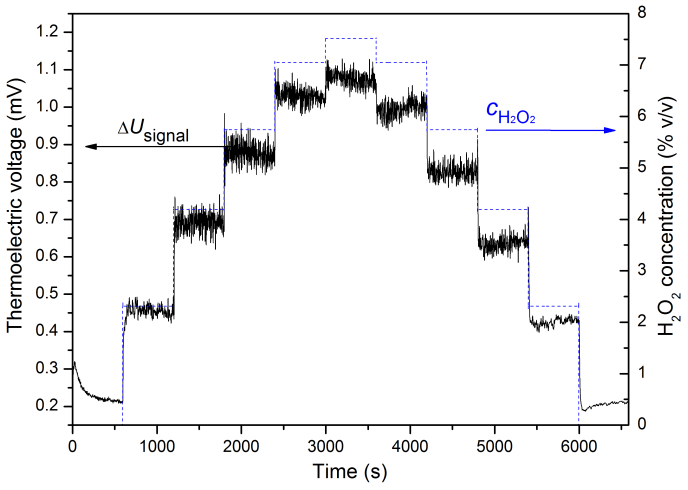

(b)

Figure 2.9: Measurement curves of the calorimetric gas sensors based (a) on a linear Au/Ni thermopile and (b) on a linear W/Ni thermopile, both with MnO_2 as catalyst at various H_2O_2 concentrations (gas temperature: 270 °C, flow rate: 10 m^3/h).

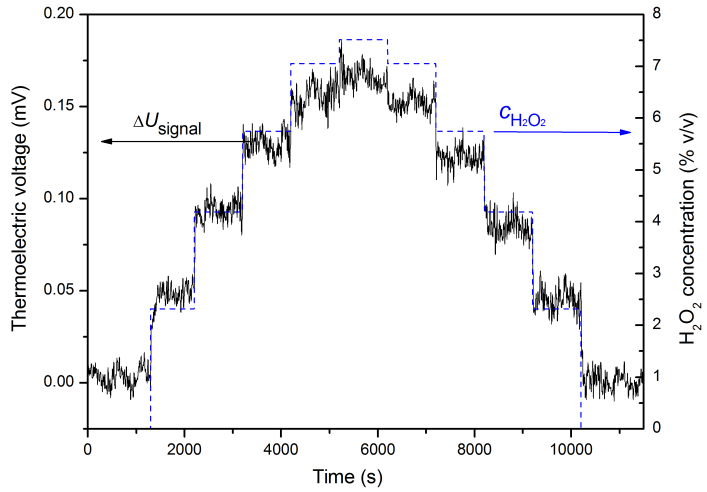

(a)

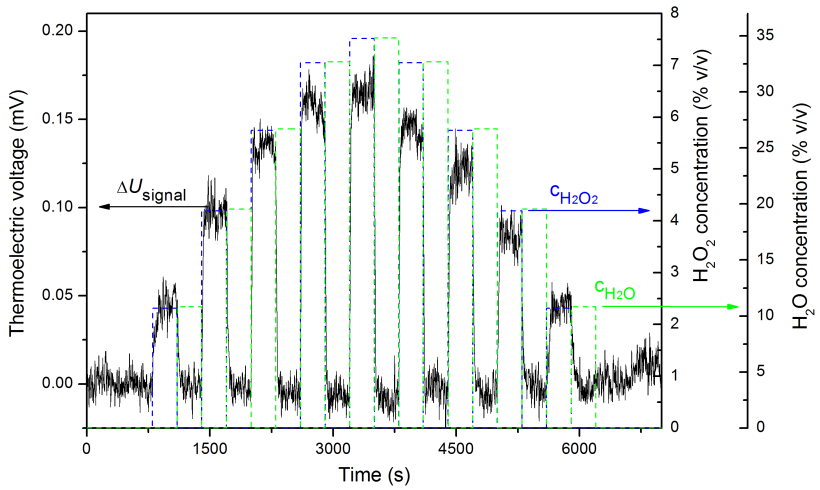

(b)

Figure 2.10: Measurement curves of the calorimetric gas sensors based (a) on a circular Au/Ni thermopile and (b) on a circular W/Ni thermopile, both with MnO_2 as catalyst at various H_2O_2 concentrations (gas temperature: 270 °C, flow rate: 10 m^3/h).

2.6.2 Additional measurement curves as support to sensor validation

Additional measurement curves of the calorimetric gas sensor with linear Au/Ni thermopile and Pd as catalyst are shown in the next diagrams as support to section 2.4.2.

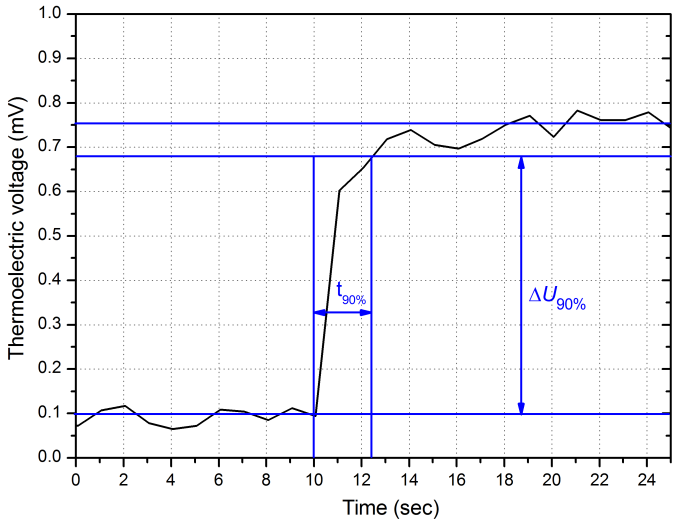

Figure 2.11: Response time of the calorimetric H_2O_2 gas sensor based on a linear Au/Ni thermopile with Pd as catalyst (H_2O_2 concentration: 4.2% v/v, gas temperature: 270 °C, flow rate: 10 m^3/h).

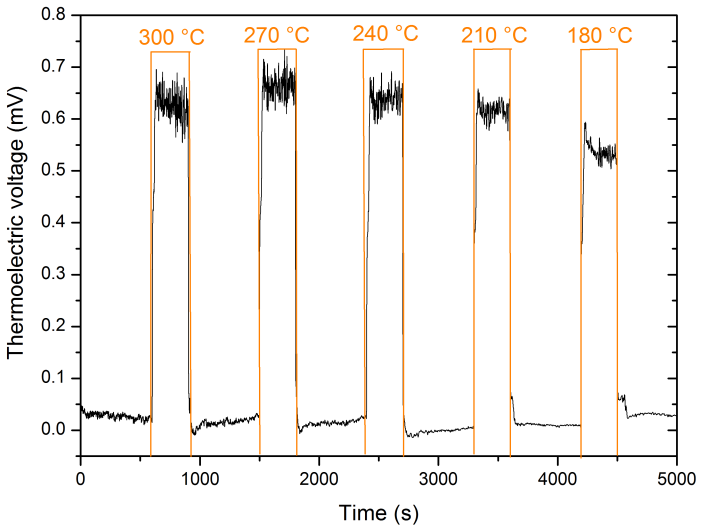

Figure 2.12: Measurement curve for the determination of the temperature influence on the sensor signal at a constant H_2O_2 concentration of 4.2% v/v and a flow rate of 10 m^3/h.

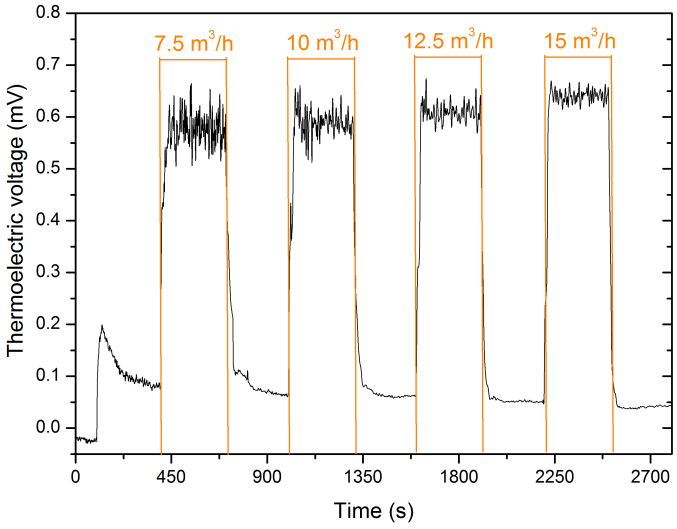

Figure 2.13: Measurement curve for the determination of the influence of the gas-flow rate on the sensor signal at a constant H_2O_2 concentration of 4.2% v/v and a gas temperature of 270 °C.

3 Thin-film calorimetric H_2O_2 gas sensor for the validation of germicidal effectivity in aseptic filling processes

KIRCHNER, P., Li, B., Spelthahn, H., Henkel, H., Schneider, A., Friedrich, P., Kolstad, J., Keusgen, M., and Schöning, M. J.

Sensors and Actuators B 154, 2 (2011), 257–263.

3.1 Abstract

In common aseptic filling processes, hydrogen peroxide vapour is a predominantly applied antimicrobial for the inactivation of microorganisms in packages. During this process, the germicidal effectivity of the antimicrobial treatment depends especially on the H_2O_2 concentration of the gas mixture. For the detection of H_2O_2 in aseptic filling processes, a novel thin-film calorimetric gas sensor based on a differential set-up of a catalytically activated and a passivated temperature-sensing element has been realised in the present work. The sensor device contains two meander-shaped platinum resistances as temperature-sensing elements; both have been passivated with spin-coated perfluoralkoxy. As catalytically active materials for the calorimetric gas sensor, palladium, platinum black and manganese oxide particles have been studied in the developed experimental set-up, wherein MnO_2 has shown the highest sensitivity of 0.565 °C/(% v/v) towards H_2O_2. Afterwards, the characteristic of the sensor device with MnO_2 particles as catalyst has been examined at various H_2O_2 concentrations and additionally, the influence of gas temperature and gas-flow rate on the sensor signal has been validated in the experimental set-up.

3.2 Introduction

At present time, the inactivation of microorganisms on the surface of packages for food and beverages plays an important role in pharmacy and food industry, especially to assure the shelf life and the hygienic standard of filled products [1–4]. For the inactivation of microorganisms, hence, the packages have to be pretreated by antimicrobials before filling them with food products or beverages [3–6]. Therefore, hydrogen peroxide vapour (HPV) has become a prevalent antimicrobial in aseptic filling processes compared to other chemicals, like formaldehyde, ethylene oxide and ozone, due to its strong oxidising effect and the decomposition in environment-friendly products, namely water vapour and oxygen [6–9]. In such an aseptic filling process, the carton packages are firstly pre-heated, afterwards antimicrobially treated by HPV and finally, filled with the food products or beverages. For the inactivation of microorganisms an aqueous solution with 35% w/w H_2O_2 is evaporated and subsequently streamed together with compressed air into the carton package at a temperature above 200 °C and a gas-flow rate of nearly 10 m^3/h. During this process, the H_2O_2 concentration of the gas mixture can be varied between 4 and 10% v/v and correlates thereby with the germicidal effectivity of the HPV treatment [8, 9]. To control the germicidal effectivity, a sensor system is required, which detects the H_2O_2 concentration of the gas mixture and ensures a sufficient HPV treatment.

Over the past years, different types of H_2O_2 sensors have been realised. In most cases, these sensors are electrochemical sensors [10–14] that can neither be applied at those elevated temperatures nor detect H_2O_2 concentrations up to 10% v/v. Furthermore, calorimetric sensors for the detection of several volatile and combustible gases have been introduced [15–20], which were considered for monitoring the HPV process. In [15, 16], thick-film calorimetric sensors of two platinum heater structures are presented, where one of them is catalytically activated and a second structure without catalyst serves as a compensating element. However, a significant disadvantage of these sensors for monitoring the H_2O_2 concentration in HPV processes is that they are not passivated, leading to a strong drift of the sensor signal due to the humidity of HPV. A microsensor of two platinum filaments for the detection of combustible gases has been introduced in [17], which could also be applied for H_2O_2 monitoring. The authors mentioned that this sensor is also responsive to changes in the gas-flow rate and temperature, so that the device is not suited in HPV processes. Thermopile-based sensors for the detection of hydrogen are presented in [18, 19]. The sensor devices offer a sensor signal depending on the gas-flow rate and they possess a long response time. In addition, a calorimetric sensor arrangement was developed for the detection of volatile organic compounds in [20]. As reported in this work, the catalytically active layers of the realised sensors are responsive to several compounds and they rely on a drift according to the gas flow.

Considering the different calorimetric sensor devices [15–20], a novel thin-film calorimetric gas sensor for the detection of H_2O_2 concentrations in aseptic filling processes has been investigated in this work. The sensor device is based on a differential set-up of a catalytically activated and a passivated temperature-sensing element, similar to the sensor set-up in [21–23]. An adequate passivation material has been selected, which is stable in the chemically aggressive atmosphere and at elevated temperatures. Additionally, various catalysts for H_2O_2 decomposition have been studied with regard to their sensitivity. The temperature-sensing elements of the sensor device are not actively heated, like for conventional calorimetric gas sensors. Instead of an active sensor heating, the gas temperature of the HPV process is exploited to obtain a sufficiently high sensor temperature. In order to monitor the H_2O_2 concentration in-line during the HPV treatment of packages, the calorimetric gas sensor shall be coupled on an RFID (radio frequency identification) circuit and embedded in a test package.

3.3 Experimental

3.3.1 Sensor design and fabrication

The calorimetric H_2O_2 gas sensor based on a differential set-up on chip level consists of two meander-shaped platinum structures as temperature-sensing elements (s. Fig. 3.1(a)). As bulk material a silicon substrate with an insulation layer of 500 nm SiO_2 has been used. A platinum layer of 200 nm together with an adhesion layer of 20 nm titanium was deposited on the bulk material via physical vapour deposition and patterned by conventional photolithography. The theoretical resistance value of the meander-shaped platinum structures is in the range of 1.5 kΩ at room temperature. Both structures have been covered with perfluoralkoxy (PFA) due to its stability at elevated temperatures of up to 300 °C as well as in reactive atmospheres and its hydrophobic property to avoid condensation on the sensor surface. The PFA resin was deposited via spin-coating at 750 rpm for 10 s to gain a homogeneous and closed passivation layer. Afterwards, the PFA resin was pre-heated at 160 °C for 5 min and finally, heat-treated at 360 °C for 25 min. As catalytically active materials, palladium, platinum black and manganese oxide particles have been investigated. Therefore, one of the passivated platinum structure was coated and heat-treated with a dispersion of either Pd, Pt black or MnO_2 particles, to achieve a large contact area. The catalytically active surface of each dispersion was inspected by a scanning electron microscope, Gemini 1550 from Zeiss (s. Fig. 3.2). From the images, large surface areas of the different catalysts can be assured, which imply a high sensitivity of each sensor. A photographic picture of the fabricated calorimetric H_2O_2 gas sensor is presented in Fig. 3.1(b).

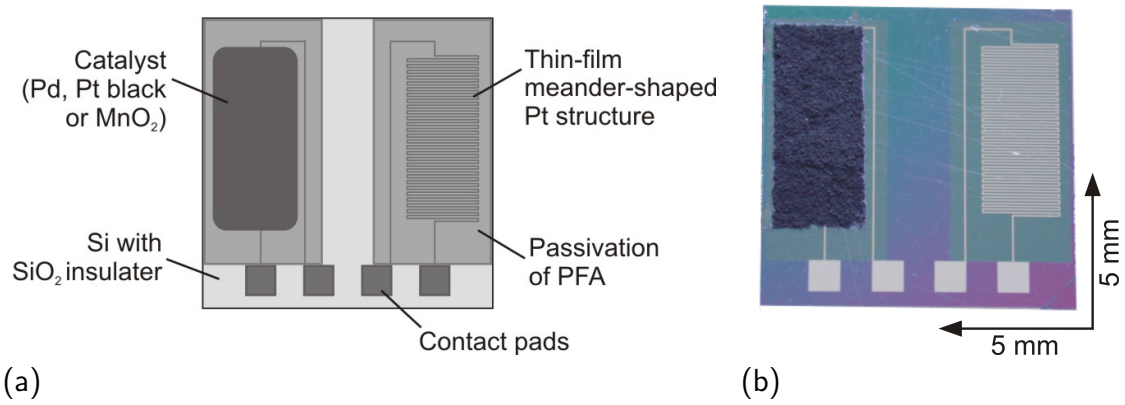

Figure 3.1: (a) Scheme of the calorimetric H_2O_2 gas sensor and (b) photographic picture of a fabricated sensor with two meander-shaped resistances covered with PFA and catalytically activated with MnO_2 particles (chip size: 10 x 10 mm^2).

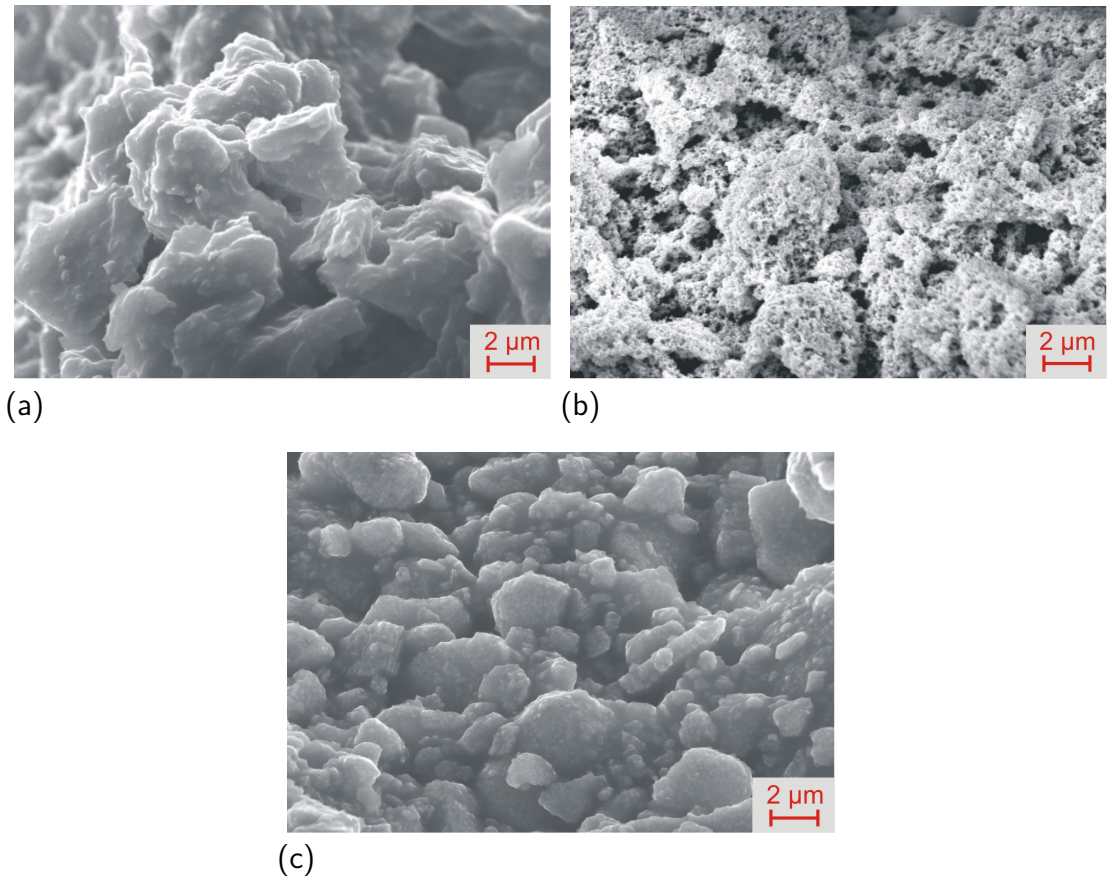

Figure 3.2: Scanning electron microscopic pictures of the catalytically active materials, (a) Pd particles, (b) Pt black particles and (c) MnO_2 particles.

If the calorimetric gas sensor is exposed in HPV atmosphere, a temperature difference between the activated and passivated temperature-sensing element can be detected that is caused by the exothermal decomposition of H_2O_2 on the catalytically active particles. The theoretical temperature difference can be calculated as follows:

$$\Delta T = \frac{H_R \cdot n}{C_p} \tag{3.1}$$

where H_R is the change of enthalpy during the exothermal decomposition of H_2O_2 on the catalyst, n as number of H_2O_2 and C_p is the heat capacity of the gas components.

3.3.2 Experimental set-up

For material characterisation and sensor validation an experimental test system has been developed, whereby the HPV process of aseptic filling systems can be simulated. The experimental set-up consists of two reservoirs for H_2O_2 solution (35% w/w) and deionised water, a dosing system for each reservoir, a flow-control and an evaporation unit as well as a measuring chamber, in which the sensor device can be investigated. In this set-up, compressed air is used as carrier gas for both reservoirs. With the dosing systems, various H_2O_2 concentrations of up to 10% v/v and gas-flow rates between 7.5 and 15 m^3/h can be adjusted. Additionally, the influence of humidity on the sensor device can be studied by dosing deionised water to the carrier gas. In the heater of the evaporation unit, the mixture is vaporised at a certain temperature and then, streamed into the measuring chamber.

In Fig. 3.3, a diagram of the experimental test system is shown. For regulation and control of the experimental set-up, a data acquisition system and a LabVIEW program were established, which have also been used for supplying the sensor device and reading out the sensor signal during the measurement.

3.4 Results and discussion

3.4.1 Material characterisation

In a first step, the various catalytically active materials such as palladium, platinum black and manganese oxide particles have been examined with regard to their sensitivity towards H_2O_2. Therefore, the signal of the calorimetric gas sensors as temperature difference between the catalytically activated and passivated temperature sensing element has been detected at various H_2O_2 concentrations from 0 to 8% v/v. All catalytically active materials have shown a linear response characteristic towards H_2O_2 in the investigated concentration range. In Fig. 3.4, the regression curves of the temperature

difference signal for the various catalytically active materials are depicted. The diagram shows that manganese oxide possesses the highest sensitivity of 0.565 °C/(% v/v) towards H_2O_2 compared to palladium with 0.261 °C/(% v/v) and platinum black with 0.229 °C/(%v/v). Nevertheless, the sensitivity of the sensor with MnO_2 particles is reduced to 12.2% in contrast to the sensor device reported in [23]. The reason for the lower

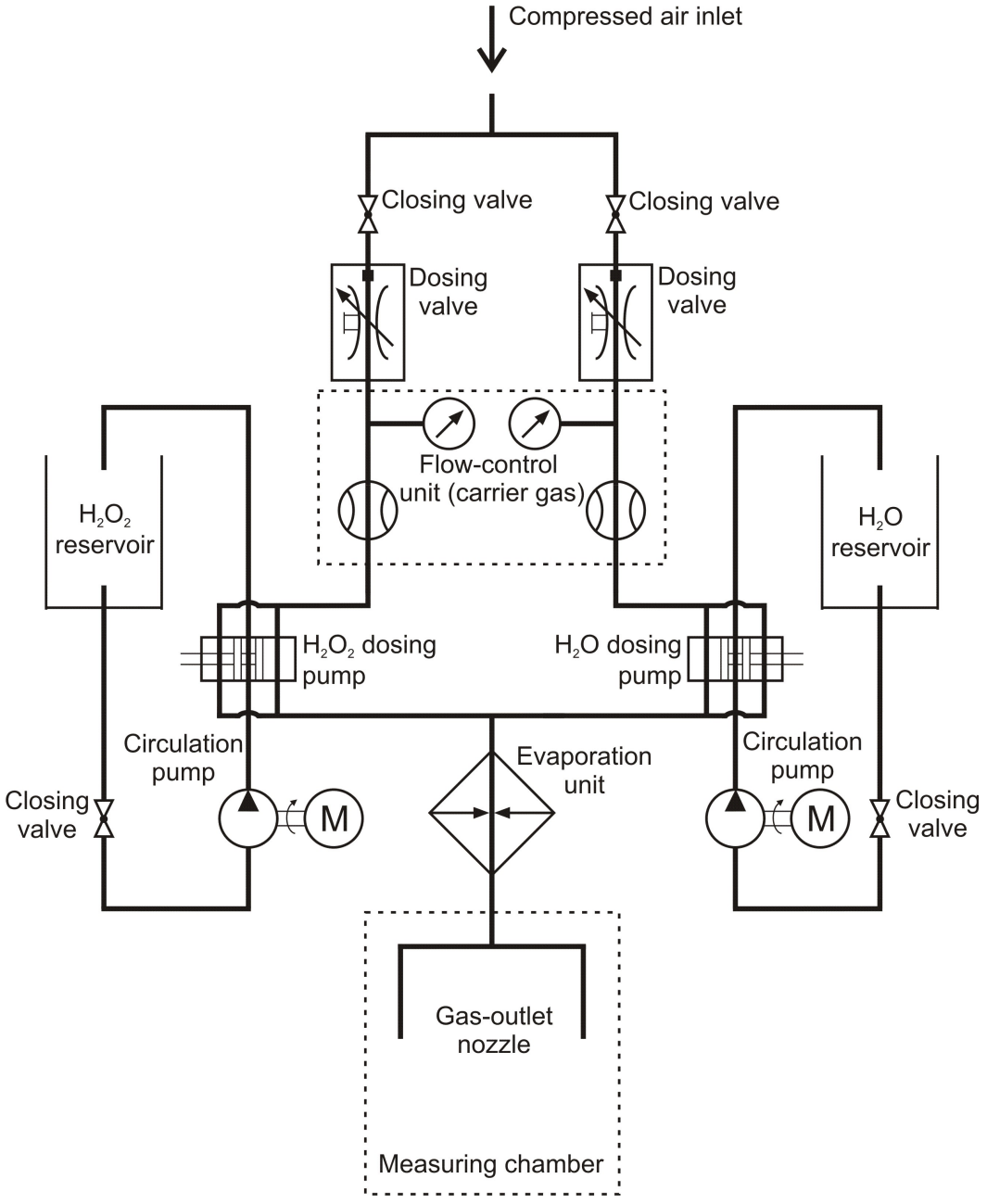

Figure 3.3: Diagram of the experimental test system with measuring chamber for material characterisation and sensor validation in HPV atmosphere.

sensitivity might be that the catalytically active surface area is smaller than the active area of the sensor in the former work. In addition, the whole differential set-up of catalytically activated and passivated sensor element is built-up on one single chip so that the increasing temperature on the catalyst due to the exothermal H_2O_2 decomposition has also an influence on the detected reference temperature of the passivated sensor element, which can result in a smaller temperature difference for each H_2O_2 concentration. The sensitivity values of the catalytically active materials, characterised in this work, are summarised in Tab. 3.1.

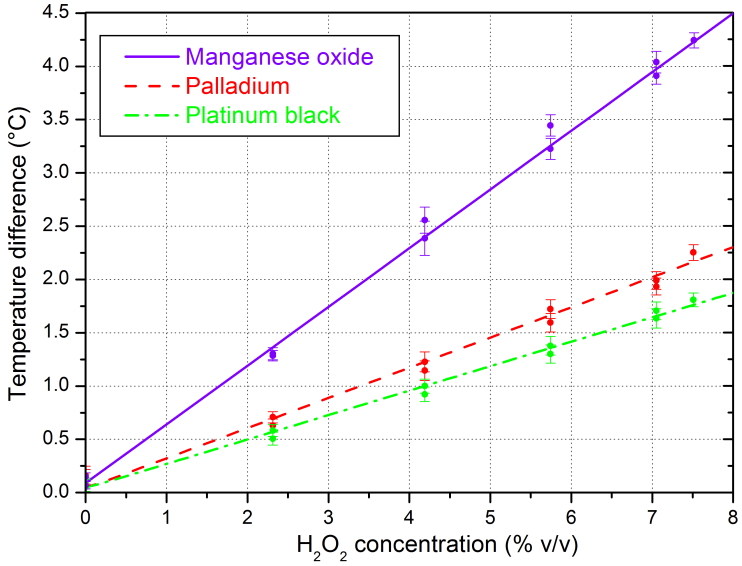

Figure 3.4: Temperature difference of the investigated calorimetric gas sensors activated by Pd, Pt black and MnO_2 particles at various H_2O_2 concentrations.

Table 3.1: Sensitivity of the different calorimetric gas sensors activated by Pd, Pt black and MnO_2 particles.

Catalyst	Sensitivity (°C/(% v/v))
Palladium	0.261 ± 0.010
Platinum black	0.229 ± 0.008
Manganese oxide	0.565 ± 0.007

For the subsequent sensor validation, the calorimetric H_2O_2 gas sensor with MnO_2 particles as catalytically active material has been used due to its high sensitivity towards H_2O_2.

3.4.2 Sensor validation

After characterisation of the different catalytically active materials, the thin-film calorimetric H_2O_2 gas sensor with MnO_2 particles has been validated in the experimental set-up. First, the sensor device has been examined at various H_2O_2 concentrations in the measuring chamber. Therefore, the sensor signal in form of a temperature difference between the catalytically activated and passivated temperature-sensing element has been detected towards higher and then, towards lower concentrations between 0 and 8% v/v H_2O_2 (s. Fig. 3.5(a)). Each concentration was adjusted for 1000 s during the measurement. Additionally, deionised water was dosed between the H_2O_2 concentrations. The resultant calibration plot of the calorimetric gas sensor is presented in Fig. 3.5(b). The sensor device has shown a sensitivity of 0.565 °C/(% v/v) towards H_2O_2 and an off-set of 0.120 °C. The origin of the off-set relies on the slight different positions of the catalytically activated and passivated sensor elements under the gas-outlet nozzle in the measuring chamber of the experimental set-up, which leads to a small difference in temperature of the two sensor elements. The hysteresis of the sensor amounts to be 0.178 °C. At a constant H_2O_2 concentration of 4.2% v/v, the response behaviour of the calorimetric gas sensor was determined (s. Fig. 3.6), where the response time is about 6.7 s (to achieve 90% of a stable sensor signal). Regarding the influence of humidity on the calorimetric gas sensor, no change in the sensor signal was observed when deionised water was dosed in the measuring chamber. The whole sensor characteristics are summarised in Tab. 3.2.

In addition, the influence of gas temperature on the calorimetric gas sensor has been studied in the experimental set-up. Therefore, the temperature of the gas mixture has been varied in steps of 30 °C between 180 and 330 °C, which is equivalent to a change in sensor temperature from above 80 to 180 °C, and at the same time the temperature difference signal of the sensor device has been detected at a constant H_2O_2 concentration of 4.2% v/v and a gas-flow rate of 10 m^3/h. The relative sensor signal for each gas temperature is shown in Fig. 3.7(a).

The diagram shows that the sensitivity of the calorimetric gas sensor decreases with lower gas temperatures. At a gas temperature of 180 °C the sensor signal was reduced by 30% compared to 330 °C. The dependence of the sensor signal on the gas temperature can be described by means of the Arrhenius equation:

$$k = A \cdot \mathrm{e}^{-E_\mathrm{A}/(R \cdot T)} \tag{3.2}$$

Therein, k is the reaction rate, A the pre-exponential factor, E_A the activation energy, R the gas constant and T is the temperature.

For decreased gas temperatures, the reaction rate of the exothermal decomposition of H_2O_2 on the catalyst of the calorimetric H_2O_2 gas sensor is reduced and consequently,

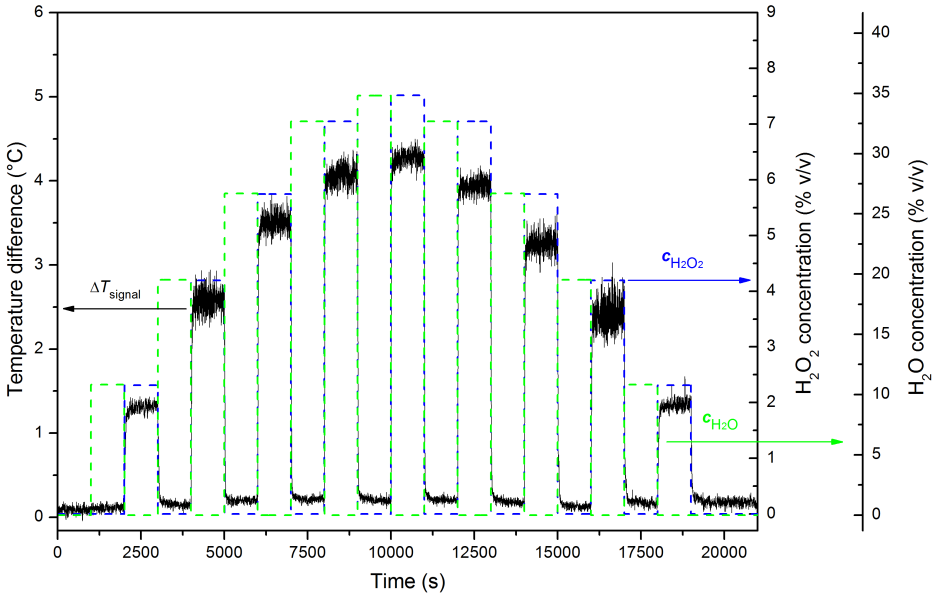

(a)

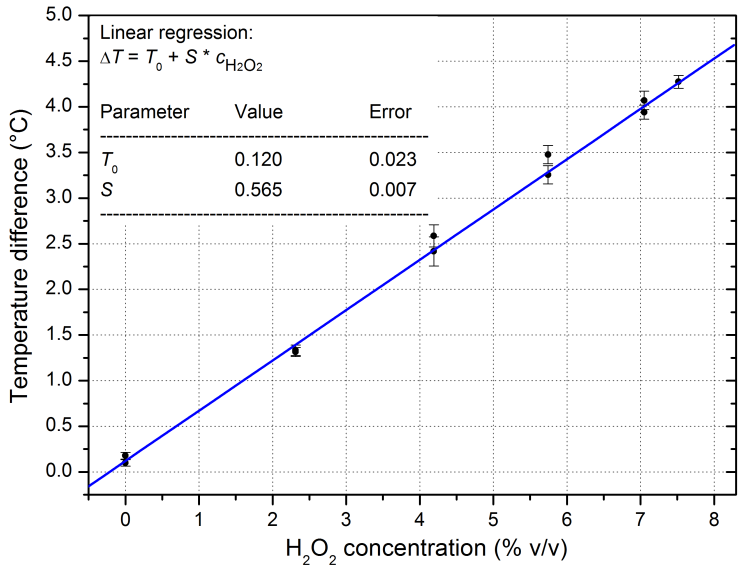

(b)

Figure 3.5: (a) Sensor signal of the thin-film calorimetric gas sensor based on a differential set-up with MnO_2 as catalyst at various H_2O_2 concentrations and H_2O concentrations and (b) calibration plot of the sensor device (gas temperature: 270 °C, gas-flow rate: 10 m^3/h).

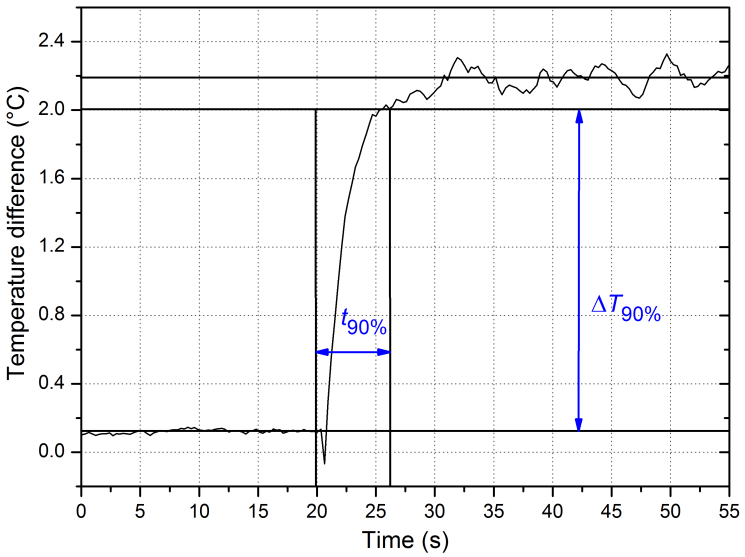

Figure 3.6: Response time of the calorimetric H_2O_2 gas sensor with MnO_2 as catalyst (H_2O_2 concentration: 4.2% v/v, gas temperature: 270 °C, gas-flow rate: 10 m^3/h).

leads to a lower temperature difference of the sensor device. For industrial sensor applications in aseptic filling processes, the gas temperature can be measured with the passivated temperature-sensing element of the calorimetric gas sensor additionally, so that the temperature-dependent behaviour can be compensated accordingly.

Finally, the impact of the gas-flow rate on the sensor signal has been investigated in the experimental set-up. During the measurement, the gas-flow rate has been changed from 7.5 to 15 m^3/h and the temperature difference of the calorimetric gas sensor has been detected at a constant H_2O_2 concentration of 4.2% v/v. The sensor signals in form

Table 3.2: Characteristics of the thin-film calorimetric H_2O_2 gas sensor with MnO_2 particles as catalytically active material.

Characteristics	
Sensitivity (°C/(% v/v))	0.565
Off-set (°C)	0.120
Response time (s)	6.7
Hysteresis (°C)	0.178
Accuracy (% v/v)	0.11
Stability (h)	>10
Influence of humidity	No

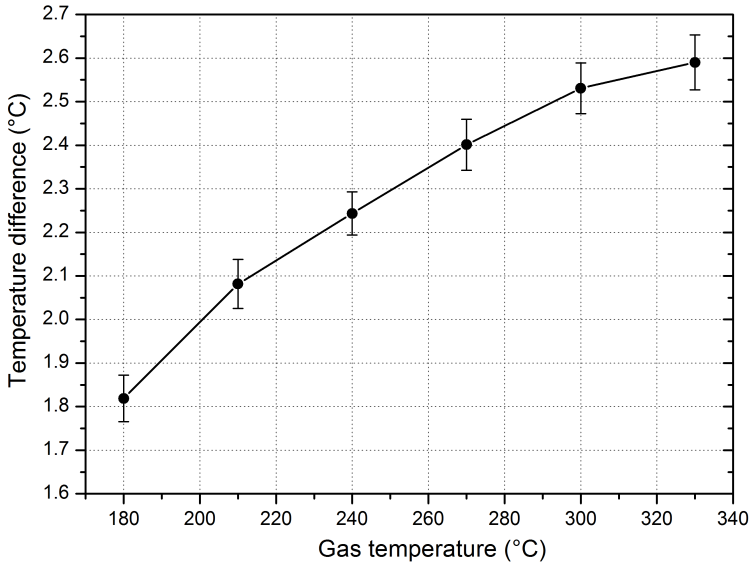

(a)

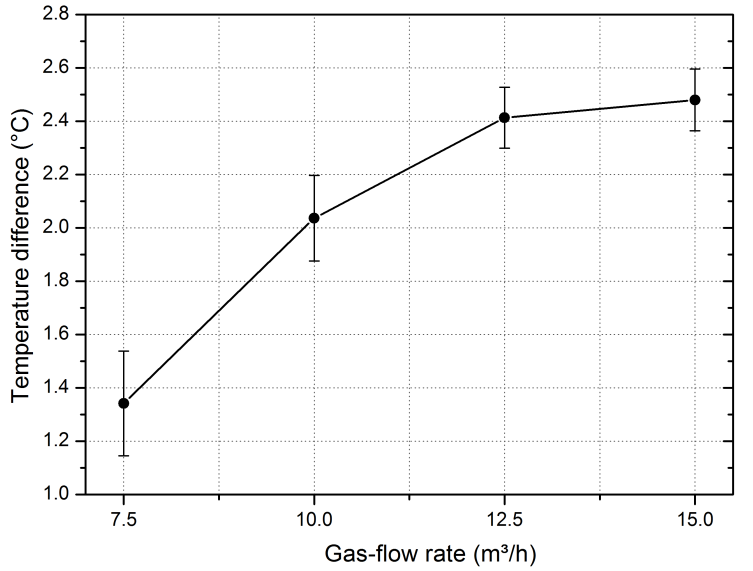

(b)

Figure 3.7: Influence of (a) gas temperature (gas-flow rate: 10 m^3/h) and (b) gas-flow rate (gas temperature: 270 °C) on the sensor signal of the calorimetric gas sensor with MnO_2 as catalyst at a constant H_2O_2 concentration of 4.2% v/v.

of temperature differences at the various gas-flow rates are shown in Fig. 3.7(b). The sensor device possesses nearly the same sensitivity at the higher flow rates of 12.5 and 15 m^3/h. At the lowest gas-flow rate of 7.5 m^3/h, the sensor signal decreased to 54% of its initial value of about 2.45 °C at 15 m^3/h. This behaviour can be explained due to the heat dissipation on the sensor surface, which correlates with the gas-flow rate. On the catalytically activated temperature-sensing element, H_2O_2 decomposes exothermically and consequently, reaction heat in form of an increase in temperature is released. At lower gas-flow rates, the reaction heat has also an influence on the passivated temperature-sensing element, because the ambient gas next to the catalytically active surface of the sensor device is heated up and a lower temperature difference between the catalytically activated and passivated temperature-sensing element of the calorimetric gas sensor is then detected. At gas-flow rates above 10 m^3/h, the heated gas on the sensor surface is completely dissipated by the gasflow and the reaction heat has no influence on the passivated temperature-sensing element. In industrial aseptic filling processes, the gas-flow rate is regulated with a flow-control unit and represents a fixed parameter during the treatment of packages. This means that the change in sensitivity with respect to the gas-flow rate has to be considered mainly before the sensor is established for the first time in an aseptic filling process.

3.5 Conclusions

A thin-film calorimetric H_2O_2 gas sensor for the validation of the germicidal effectivity in aseptic filling processes has been fabricated and characterised in the developed experimental set-up. The sensor device is based on an "on chip" differential set-up of a catalytically activated and a passivated temperature-sensing element, which consists of two meander-shaped platinum structures. Spin-coated perfluoralkoxy has been established as a suitable passivation layer for the calorimetric H_2O_2 gas sensor. As catalytically active materials towards H_2O_2, palladium, platinum black and manganese oxide particles have been examined in the experimental test system. Therein, MnO_2 particles have shown the highest sensitivity towards H_2O_2 and have subsequently been used for further sensor characterisation in the experimental set-up. The parameters of the calorimetric H_2O_2 gas sensor have firstly been determined at various H_2O_2 concentrations in the range of 0 to 8% v/v. The sensor device has shown a linear response behaviour with a sensitivity of 0.565 °C/(% v/v) and an accuracy of 0.11% v/v. The sensor response time ($t_{90\%}$) amounts to be 6.7 s. In addition, the calorimetric H_2O_2 gas sensor has been validated at various gas temperatures. Therefore, the sensor signal has been detected at a constant H_2O_2 concentration in a temperature range of 180-330 °C. If the gas temperature decreases, the sensor device possesses a lower sensitivity. While measuring the gas

temperature with the passivated temperature-sensing element, the influence of the gas temperature on the sensor signal can be compensated by means of the sensor electronic and read-out software. In a final step, the influence of the gas-flow rate on the sensor signal has been determined. It was observed that the sensitivity is decreased with lower gas-flow rates beneath 10 m^3/h. In aseptic filling processes, the gas-flow rate is adjusted at a constant value, so that the appropriate calibration parameters of the calorimetric H_2O_2 gas sensor have to be used.

In order to read out the sensor signal of the thin-film calorimetric H_2O_2 gas sensor in-line during the antimicrobial treatment of packages, an RFID transmission system is envisaged. The transmission system contains a passive RFID transponder that is inductively coupled to an RFID transceiver. The transponder is directly connected to the calorimetric gas sensor and shall be fabricated on chip level with an integrated low power circuit, which includes a microcontroller, receiver circuit with antenna and a capacitor bank for short energy storage. The RFID transceiver, placed outside of the aseptic filling system, is used for the power supply of the transponder and to read out the sensor signal in a pulsed mode at an evaluated frequency. In a final step, the calorimetric H_2O_2 gas sensor shall be embedded inside of the test package and the RFID transponder on the outer surface of this package, so that an in-line detection of the H_2O_2 concentration in aseptic filling systems is allowed.

Acknowledgements

The authors gratefully thank N. Näther for valuable discussions, H. P. Bochem for technical support and the Federal Ministry of Education and Research (Germany) and VDI/VDE, project “Intellipack”, for financial support.

References

[1] Graumlich, T. R., Marcy, J. E., and Adams, J. P. Aseptically packaged orange juice and concentrate: a review of the influence of processing and packaging conditions on quality. *Journal of Agricultural and Food Chemistry 34*, 3 (1986), 402–405.

[2] Lau, O.-W., and Wong, S.-K. Contamination in food from packaging material. *Journal of Chromatography A 882*, 1–2 (2000), 255–270.

[3] Appendini, P., and Hotchkiss, J. H. Review of antimicrobial food packaging. *Innovative Food Science & Emerging Technologies 3*, 2 (2002), 113–126.

[4] von Bockelmann, B. A. H., and von Bockelmann, I. L. I. Aseptic packaging of liquid food products: a literature review. *Journal of Agricultural and Food Chemistry 34*, 3 (1986), 384–392.

[5] Moruzzi, G., Garthright, W. E., and Floros, J. D. Aseptic packaging machine pre-sterilisation and package sterilisation: statistical aspects of microbiological validation. *Food Control 11*, 1 (2000), 57–66.

[6] Cerny, G. Testing of aseptic machines for efficiency of sterilization of packaging materials by means of hydrogen peroxide. *Packaging Technology and Science 5*, 2 (1992), 77–81.

[7] McDonnell, G., and Russell, A. D. Antiseptics and disinfectants: activity, action, and resistance. *Clinical Microbiology Reviews 12*, 1 (1999), 147–179.

[8] Johnston, M., Lawson, S., and Otter, J. Evaluation of hydrogen peroxide vapour as a method for the decontamination of surfaces contaminated with *Clostridium botulinum* spores. *Journal of Microbiological Methods 60*, 3 (2005), 403–411.

[9] Klapes, N. A., and Vesley, D. Vapor-phase hydrogen peroxide as a surface decontaminant and sterilant. *Applied and Environmental Microbiology 56*, 2 (1990), 503–506.

[10] Huang, H., Dasgupta, P. K., Genfa, Z., and Wang, J. A pulse amperometric sensor for the measurement of atmospheric hydrogen peroxide. *Analytical Chemistry 68*, 13 (July 1996), 2062–2066.

[11] Toniolo, R., Geatti, P., Bontempelli, G., and Schiavon, G. Amperometric monitoring of hydrogen peroxide in workplace atmospheres by electrodes supported on ion-exchange membranes. *Journal of Electroanalytical Chemistry 514*, 1–2 (2001), 123–128.

[12] Huang, H., and Dasgupta, P. K. Renewable liquid film-based electrochemical sensor for gaseous hydroperoxides. *Talanta 44*, 4 (1997), 605–615.

[13] Guwy, A., Hawkes, F., Martin, S., Hawkes, D., and Cunnah, P. A technique for monitoring hydrogen peroxide concentration off-line and on-line. *Water Research 34*, 8 (2000), 2191–2198.

[14] Mehta, A., Patil, S., Bang, H., Cho, H. J., and Seal, S. A novel multivalent nanomaterial based hydrogen peroxide sensor. *Sensors and Actuators A: Physical 134*, 1 (2007), 146–151.

[15] Chen, A., Luo, R., Tan, T.-C., and Liu, C.-C. A thick-film calormetric sensor for monitoring the concentration of combustible gases. *Sensors and Actuators 19*, 3 (1989), 237–248.

[16] Makovos, E. B., Montague, F. W., Dudik, L., and Liu, C.-C. A calorimetric combustible gas detector employing platinum film heaters. *Sensors and Actuators B: Chemical 12*, 2 (1993), 91–94.

[17] Accorsi, A., Delapierre, G., Vauchier, C., and Charlot, D. A new microsensor for environmental measurements. *Sensors and Actuators B: Chemical 4*, 3–4 (1991), 539–543.

[18] Houlet, L. F., Shin, W., Tajima, K., Nishibori, M., Izu, N., Itoh, T., and Matsubara, I. Thermopile sensor-devices for the catalytic detection of hydrogen gas. *Sensors and Actuators B: Chemical 130*, 1 (2008), 200–206.

[19] Casey, V., Cleary, J., D'Arcy, G., and McMonagle, J. B. Calorimetric combustible gas sensor based on a planar thermopile array: fabrication, characterisation, and gas response. *Sensors and Actuators B: Chemical 96*, 1–2 (2003), 114–123.

[20] Lerchner, J., Caspary, D., and Wolf, G. Calorimetric detection of volatile organic compounds. *Sensors and Actuators B: Chemical 70*, 1–3 (2000), 57–66.

[21] Näther, N., Juárez, L. M., Emmerich, R., Berger, J., Friedrich, P., and Schöning, M. J. Detection of hydrogen peroxide (H_2O_2) at exposed temperatures for industrial processes. *Sensors 6*, 4 (2006), 308–317.

[22] Näther, N., Emmerich, R., Berger, J., Friedrich, P., Henkel, H., Schneider, A., and Schöning, M. J. A novel gas-phase hydrogen peroxide sensor basing on a combined physical/chemical transduction mechanism. *Materials Research Society Symposium Proceedings 951* (2006), 0951–E12–03.

[23] Näther, N., Henkel, H., Schneider, A., and Schöning, M. J. Investigation of different catalytically active and passive materials for realising a hydrogen peroxide gas sensor. *Physica Status Solidi A 206*, 3 (2009), 449–454.

3.6 Appendix

3.6.1 Additional measurement curves as support to material characterisation

The measurement curves of the calorimetric gas sensors activated by different catalysts are shown in the following diagrams as support to section 3.4.1.

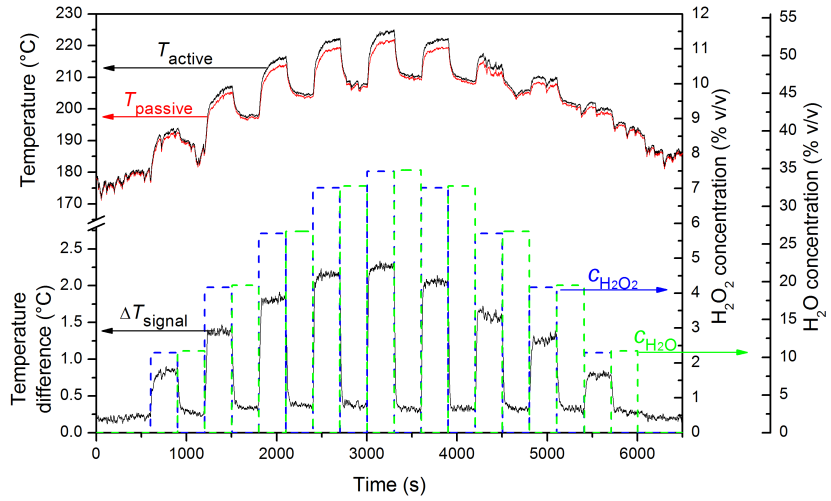

(a)

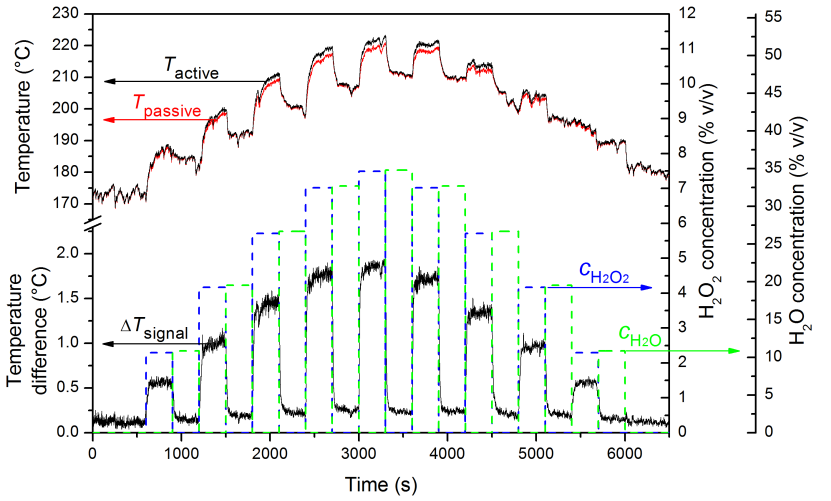

(b)

Figure 3.8: Temperature on activated and passivated temperature-sensing element (upper curves) and temperature difference (lower curve) of (a) the calorimetric gas sensor with Pd and (b) the calorimetric gas sensor with Pt black as catalyst at various H_2O_2 and H_2O concentrations (gas-flow rate: 10 m^3/h, gas temperatures 270 °C).

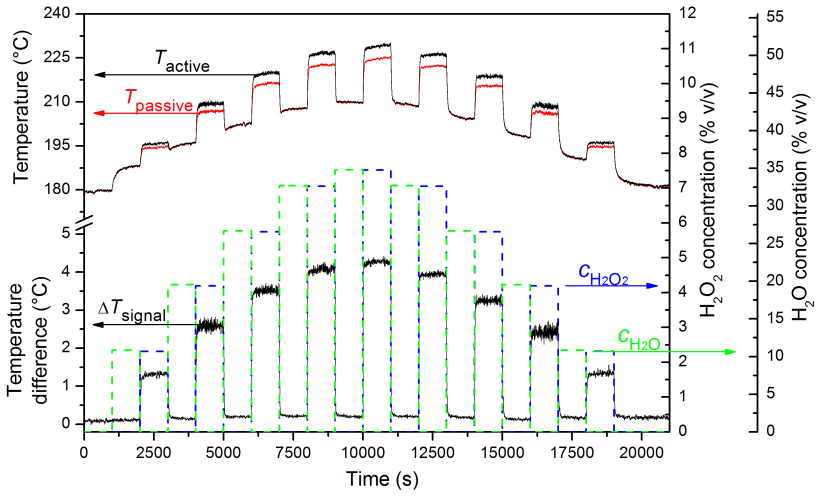

Figure 3.9: Temperature on activated and passivated temperature-sensing element (upper curves) and temperature difference (lower curve) of the thin-film calorimetric gas sensor based on a differential set-up with MnO_2 as catalyst at various H_2O_2 and H_2O concentrations (gas temperature: 270 °C, gas-flow rate: 10 m^3/h).

3.6.2 Additional measurement curves as support to sensor validation

In the following diagrams, the measurement curves of the calorimetric gas sensor activated by MnO_2 are shown as support to section 3.4.2.

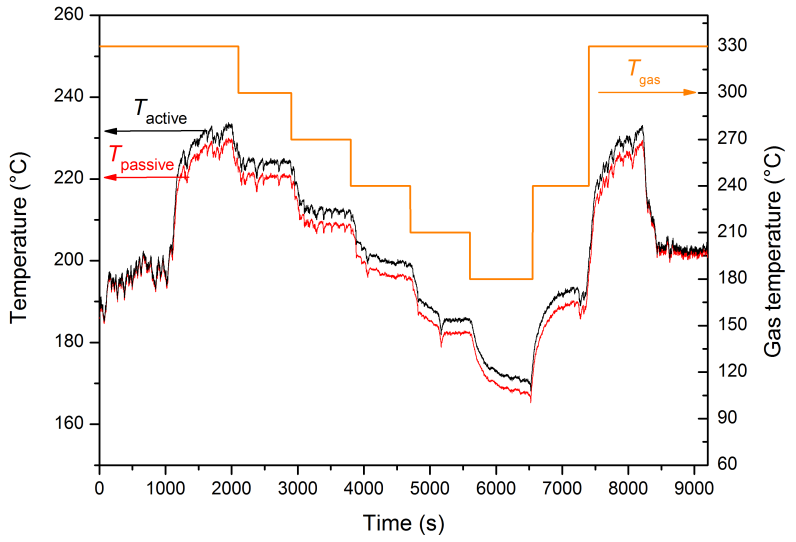

(a)

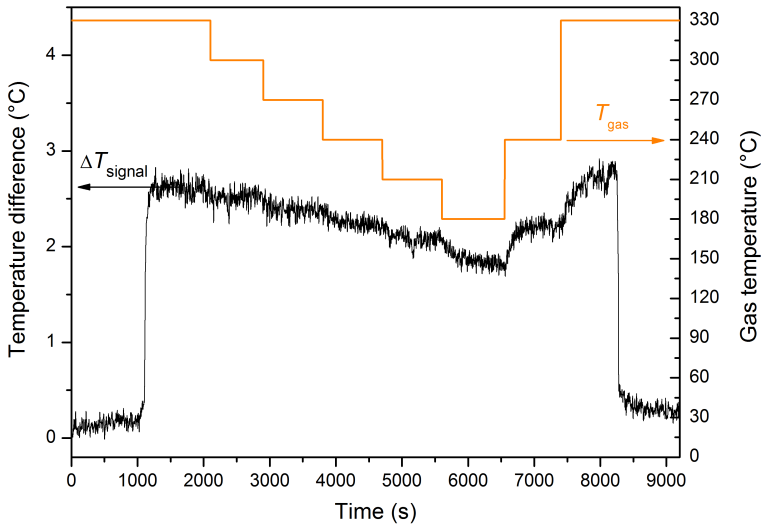

(b)

Figure 3.10: (a) Temperature on activated and passivated temperature-sensing element and (b) resulting temperature difference of the calorimetric gas sensor with MnO_2 as catalyst at different gas temperatures varied between 180 and 330 °C (gas-flow rate: 10 m^3/h, H_2O_2 concentration of 4.2% v/v).

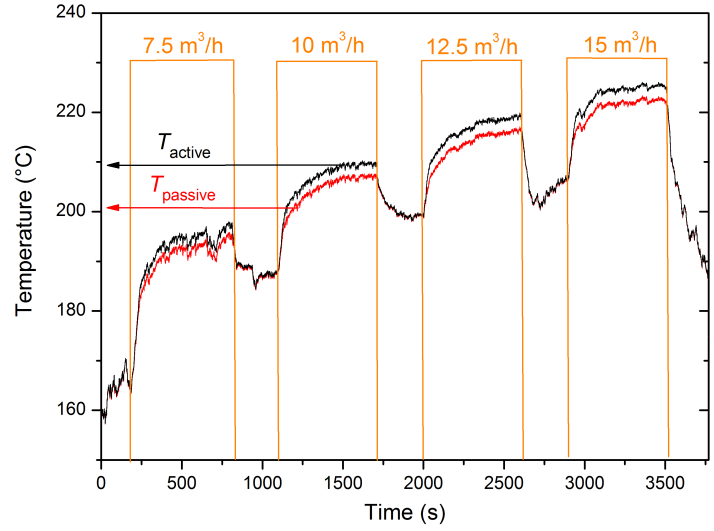

(a)

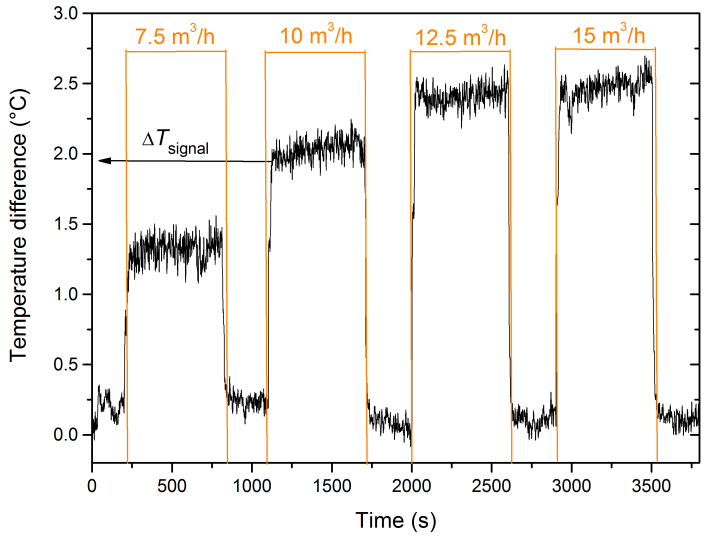

(b)

Figure 3.11: (a) Temperature on activated and passivated temperature-sensing element and (b) resulting temperature difference of the calorimetric gas sensor with MnO_2 as catalyst at different gas-flow rates varied between 7.5 and 15 m^3/h (gas temperature: 270 °C, H_2O_2 concentration of 4.2% v/v).

4 Characterisation of polymeric materials as passivation layer for calorimetric H_2O_2 gas sensors

KIRCHNER, P., Reisert, S., Pütz, P., Keusgen, M., and Schöning, M. J.

Physica Status Solidi A 209, 5 (2012), 859–863.

4.1 Abstract

Calorimetric gas sensors for monitoring the H_2O_2 concentration at elevated temperatures in industrial sterilisation processes have been presented in previous works. These sensors are built up in form of a differential set-up of a catalytically active and passive temperature-sensitive structure. Although, various types of catalytically active dispersions have been studied, the passivation layer has to be established and therefore, chemically as well as physically characterised. In the present work, fluorinated ethylene propylene (FEP), perfluoralkoxy (PFA) and epoxy-based SU-8 photoresist as temperature-stable polymeric materials have been investigated for sensor passivation in terms of their chemical inertness against H_2O_2, their hygroscopic properties as well as their morphology. The polymeric materials were deposited via spin-coating on the temperature-sensitive structure, wherein spin-coated FEP and PFA show slight agglomerates. However, they possess a low absorption of humidity due to their hydrophobic surface, whereas the SU-8 layer has a closed surface but shows a slightly higher absorption of water. All of them were inert against gaseous H_2O_2 during the characterisation in H_2O_2 atmosphere that demonstrates their suitability as passivation layer for calorimetric H_2O_2 gas sensors.

4.2 Introduction

Hydrogen peroxide is a weak acid and serves as a strong oxidising agent [1]. It is commercially available in form of aqueous solutions and has a wide spectrum of use in industry that ranges from bleaching agent to propulsion for rockets, reagent for organic peroxides, disinfection and sterilisation agent for medical devices and food packages [2–4]. In aseptic food industry, hydrogen peroxide has become the most significant sterilisation agent for carton packages within the last decades. Therein, one of the sterilisation methods employs gaseous hydrogen peroxide gained by the evaporation of a H_2O_2 solution at an elevated temperature of above 250 °C, which is streamed into the package for a short contact time prior to the food filling. In this sterilisation process, the microbicidal efficiency depends predominantly on the present H_2O_2 concentration that can attain 8% v/v inside the carton package.

For in-line monitoring the sterilisation process with gaseous hydrogen peroxide, a calorimetric gas sensor in form of a differential set-up of a catalytically activated and a passivated temperature-sensitive structure was established (s. Fig. 4.1). On the catalytically active area, hydrogen peroxide decomposes in a chain reaction, wherein free radicals are generated as intermediates and accelerate the exothermic H_2O_2 decomposition releasing water vapour and oxygen as final products [5, 6]. The exothermic reaction causes a local temperature increase that can be detected in form of a temperature difference between the activated and passivated temperature-sensitive structure, which correlates linearly with the present H_2O_2 concentration.

In a prior work [7], dispersions of palladium, platinum black and manganese oxide were studied as potential catalysts, wherein manganese oxide possessed the highest catalytic activity against hydrogen peroxide. As temperature-sensitive structures, thin-film resistances [7] and thin-film thermopiles [8] were realised on silicon substrates.

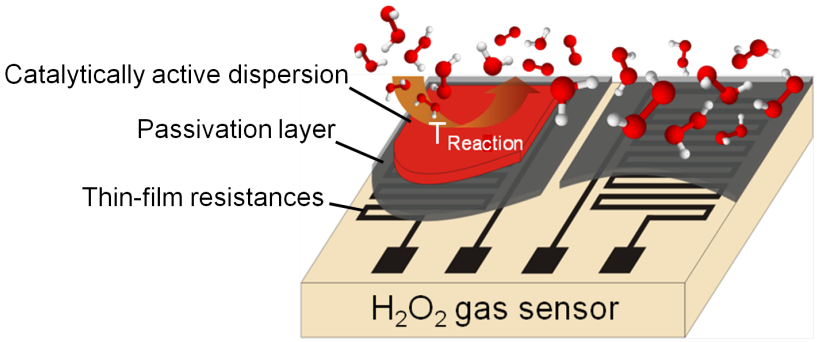

Figure 4.1: Schematic of the calorimetric gas sensor consisting of two thin-film resistances as temperature-sensitive structures, passivation layer and catalytically active dispersion.

In the present work, the passivation layer of the calorimetric gas sensor has been intensively studied. The passivation layer serves as an electrical insulation and protection film for avoiding corrosion of the temperature-sensitive structures. It should be temperature-stable up to 200-250 °C, chemically inert in H_2O_2 atmosphere and ideally water-resistant by a hydrophobic surface. Conventional insulation layers, like silicon oxide, alumina or other ceramics, catalytically react with hydrogen peroxide [9–13], so that they are unsuitable for this differential set-up. Hence, adequate encapsulating materials have to be found, which can be deposited on the sensor surface as passivation layer via thin-film technology, too.

4.3 Experimental

4.3.1 Materials

Three different polymers – epoxy-based photoresist (SU-8) as well as fluoropolymers (perfluoralkoxy (PFA) and fluorinated ethylene propylene (FEP) – have been studied as passivation layer for the calorimetric gas sensor. These polymers offer excellent chemical and thermal stability and the fluoropolymers additionally feature outstanding hydrophobicity (s. Tab. 4.1).

Table 4.1: Chemical and physical properties of SU-8 photoresist, PFA and FEP [14–17].

Polymer	Density (g/cm^3)	Max. service temperature (°C)	Thermal conductivity ($W°C^{-1}m^{-1}$)	Water absorption (%)
SU-8	1.075-1.238	300-315	0.2-0.3	0.55-0.65
PFA	2.150	260	0.195	<0.03
FEP	2.150	205	0.24	<0.01

The initial liquid of SU-8 (Nano SU-8 from Micro-Chem) is a negative photoresist that primarily consists of an epoxy resin including a photo-acid generator dissolved in an organic solvent [14, 15, 18]. The fluoropolymers are made of aqueous suspensions with dispersing agents either of PFA (DuPont PFA 857-110) or FEP (Dyneon FEP 6300G Z).

4.3.2 Polymer coating

The polymers were deposited onto a sensor substrate of silicon with an insulation layer of silicon oxide (500 nm) that contains meander-shaped resistance structures of platinum with a thickness of 200 nm together with an adhesion layer of 20 nm titanium as temperature-sensitive structures. For sensor tests in H_2O_2 atmosphere, one of the passivated resistance structures was additionally coated with a dispersion of manganese oxide

as catalyst. For obtaining a homogenous and stable coating, the polymers were deposited onto the sensor surface via spin-coating, which have been heat-treated afterwards.

The SU-8 photoresist was spin-coated with 500 rpm for 5 s and afterwards at 3000 rpm for 30 s. After the spin-coating process, the resist was soft-baked at 65 and 95 °C, in each case for 1 min to remove the organic solvent and improve the adhesion on the sensor surface. During the photolithographic cycle, the resist was exposed with UV radiation at a wavelength of 365 nm (i-line) leading to the formation of a strong acid that subsequently initiates the epoxy cross-linking during the post-exposure bake again at the two temperature steps of 65 and 95 °C for 1 min. In a final heat treatment, the SU-8 was hard-baked at 175 °C for 5 min to ensure a good adhesion of the coating even at an increased operating temperature. Such SU-8 coatings are chemically and mechanically stable and feature a highly thermal endurance.

The fluoropolymers (PFA as well as FEP) were also deposited via spin-coating on the sensor surface and were sintered by a following heat treatment. Both were spin-coated at 750 rpm for 20 s and at first heat-treated at 95 °C for 1 min and at 160 °C for 5 min to remove water and additives. Afterwards, the PFA coating was sintered at 360 °C for 30 min and the FEP coating at 340 °C for 25 min. After the spin-coating process, the polymers' surfaces have been characterised.

4.3.3 Polymer characterisation

For measuring the average film thickness of the polymer coatings, a surface profiler (Alpha Step IQ from KLA Tencor) was used and the surface texture of each coating was inspected by a scanning electron microscope (Gemini 1550 from Zeiss). The sessile drop method measuring the contact angle of a water droplet on a surface was applied to determine the hydrophobic properties of the resulting polymer coatings. A surface analyser (OCA 15 from Dataphysics) was used for the measurements. The samples were placed on a test stage and a deionised water droplet of 4 ml was placed onto the surface through a microsyringe and the steady-state contact angles were measured. At least, five different measurements were performed on different areas of each polymer coating at room temperature.

Finally, the inertness and stability of the passivation layers have been characterised in H_2O_2 atmosphere. Therefore, the gas sensors with passivation layers were set in an experimental test rig introduced in Refs. [7, 8] and various H_2O_2 concentration steps between 0 and 8% v/v were adjusted with a constant heating temperature of 270 °C and a constant gas flow of 10 m^3/h. For studying the influence of water vapour on the polymers, the sensors were additionally exposed to H_2O concentrations up to 35% v/v at same heating temperature and gas flow between the H_2O_2 concentration steps.

4.4 Results and discussion

4.4.1 Surface characterisation

The resultant thickness of the spin-coated SU-8 photoresist measured by the surface profiler is 1.7 μm in average. The average thickness of the PFA coating is 20.4 μm and the thickness of the FEP layer is 4.1 μm (listed in Tab. 4.2). All of them have a good adhesion on the sensor surface. However, from the SEM images (s. Fig. 4.2) the coatings of FEP and PFA show agglomerates in the range of 120 nm on the surface, whereas SU-8 depicts a homogenously enclosed surface. The reason for the agglomerates of the fluoropolymers could be explained by an incomplete sintering of the polymeric particles on the surface during the heat treatment. Nevertheless, due to the high thickness of the fluoropolymers, the coatings are completely dense.

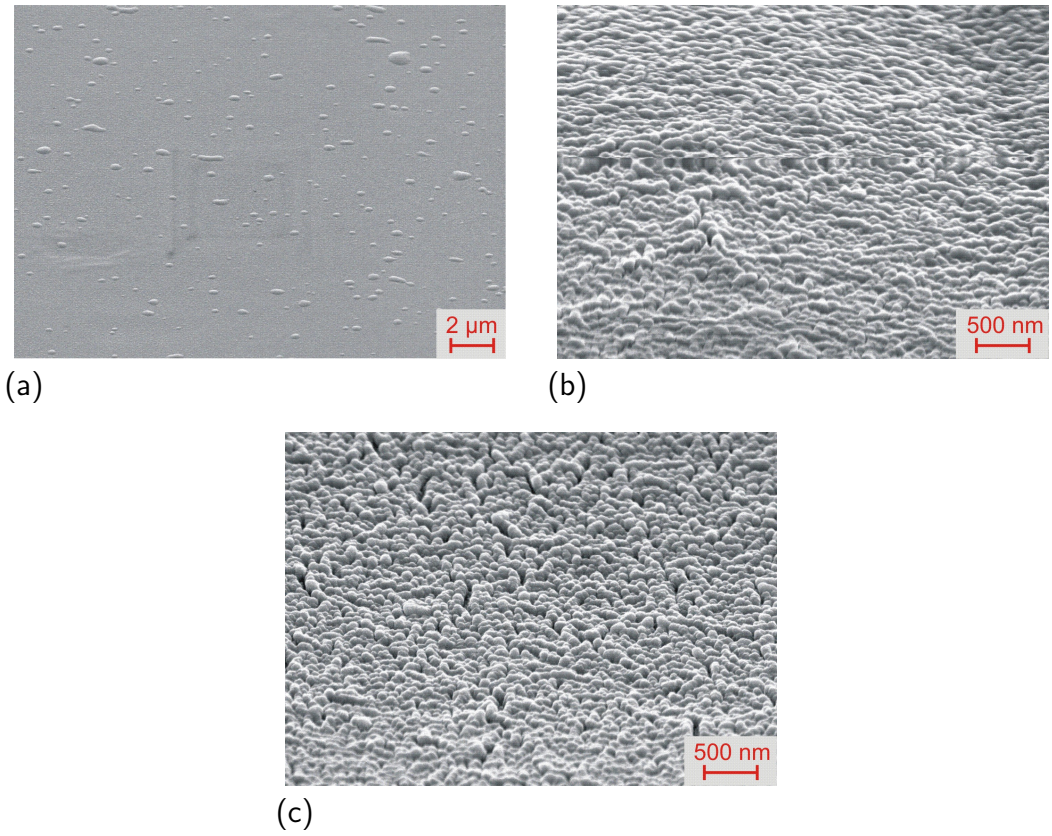

Figure 4.2: SEM images of (a) SU-8 photoresist, (b) PFA and (c) FEP passivation layer.

From the contact angle measurements (s. Fig. 4.3), the hydrophobictiy of the fluoropolymers can be inspected: the contact angle of the water droplet on PFA is 106.3° and the angle on FEP is 113.5° (see also Tab. 4.2). The contact angle of the water droplet on

Table 4.2: Contact angle and average film thickness of the spin-coated polymeric layers.

Polymer	Average contact angle	Average film thickness (μm)
SU-8	61.68°	1.7
PFA	106.3°	20.4
FEP	113.5°	4.1

the surface of the SU-8 photoresist amounts to be 61.68° indicating a more hydrophilic surface. For the measurements in H_2O_2 atmosphere, it can be expected that the heat transfer of the differential sensor set-up with an SU-8 layer is more influenced by water vapour due to its hydrophilic surface, which may lead to micro-condensation on it.

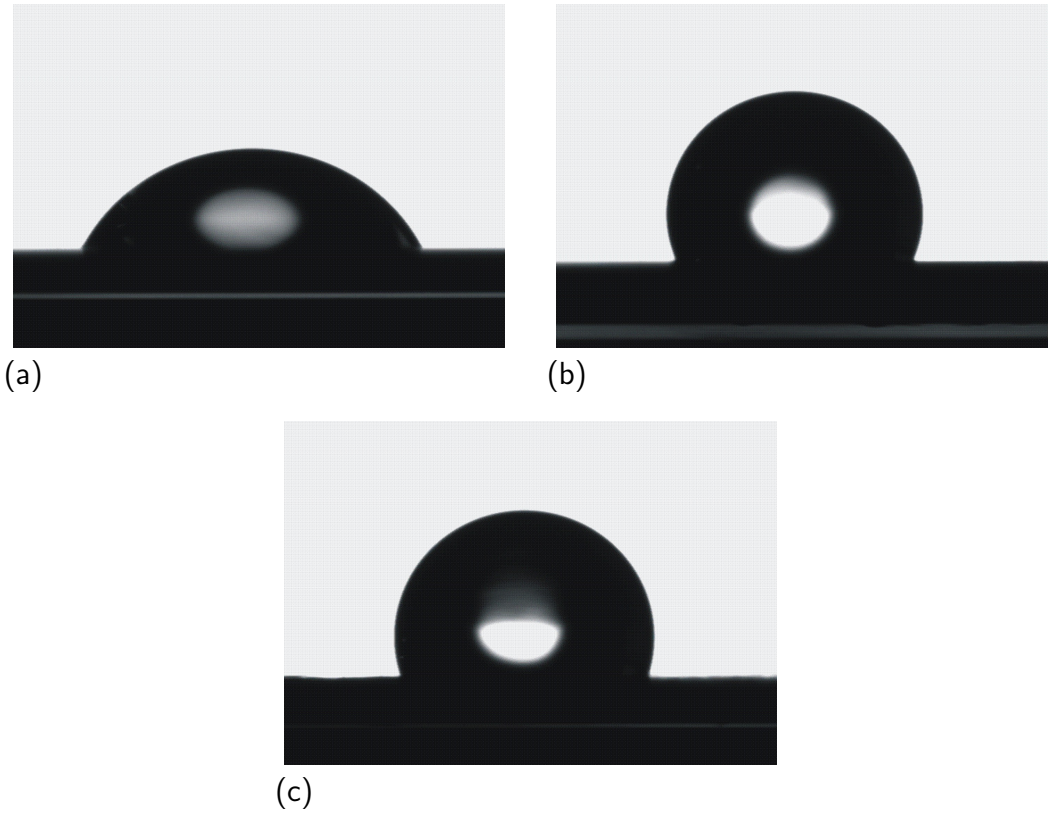

Figure 4.3: Contact angle measurements of a 4 ml water droplet on the polymer coatings; water droplet on (a) SU-8 photoresist, (b) PFA and (c) FEP layer.

4.4.2 Characteristics in H_2O_2 atmosphere

The three calorimetric types of gas sensors with different encapsulation materials have been exposed to H_2O_2 and H_2O atmosphere. Therefore, alternately different amounts of an aqueous hydrogen peroxide solution and water have been fed to a carrier gas stream at a temperature of 270 °C. This way, concentrations of H_2O_2 up to 8% v/v and concentrations of H_2O up to 35% v/v have been achieved in gaseous phase. Exemplarily, the results of a measurement with the SU-8-coated sensor will be shown here. Fig. 4.4(a) depicts the absolute temperatures of the passive and active temperature-sensitive structures as well as the temperature difference between them, plotted over time. As expected, the sensor responds with an increase of the temperature difference when exposed to H_2O_2, while the difference in temperature is rising with increasing H_2O_2 concentration. The exposure to H_2O does not affect the difference signal when compared to the value in dry air at the beginning and end of the measurement. Though, there is an off-set of the difference signal in hot air and when exposed to H_2O.

To compare the different polymeric encapsulation materials, the characteristics of each of the three sensors are overviewed in Fig. 4.4(b). Thereby, the measured temperature differences between the active and passive element are plotted against the hydrogen peroxide concentration in gaseous phase. Values at 0% v/v H_2O_2 correspond to the temperature differences obtained in dry air and during the exposure to water. The determined off-set values and sensitivities are listed in Tab. 4.3. The PFA-coated sensor exhibits the highest sensitivity and lowest off-set, while the off-set values of FEP- and SU-8-coated sensors are somewhat higher and sensitivities somewhat lower. However, it is not evident that the exposure to water causes any influence on the sensor signal. The catalytic component on the active element has been prepared the same way for each of the three sensors with different encapsulation materials. The fact that the sensors exhibit different sensitivities towards H_2O_2 may be explained by the thermal conductivity coefficient on the one hand (s. Tab. 4.1). On the other hand, the heat transfer from the active to passive temperature-sensitive structure will be influenced by the film thickness of the different polymers in test (s. Tab. 4.2). The thermal isolation between the active and passive temperature-sensitive structure is highest for PFA. It has the lowest thermal conductivity coefficient and highest film thickness, while the thermal conductivity is the highest and film thickness is lowest in case of the SU-8 photoresist, respectively. The heat transfer from the active to the passive element will cause a decrease in the temperature difference resulting in a lower sensitivity. This effect may be increased with the absorption of water into the passivation layer or micro-condensation on its surface, especially for hydrophilic surfaces, like that of SU-8. Physical damage of the encapsulation materials after the exposure to H_2O_2/H_2O could not be observed in any of the materials in test.

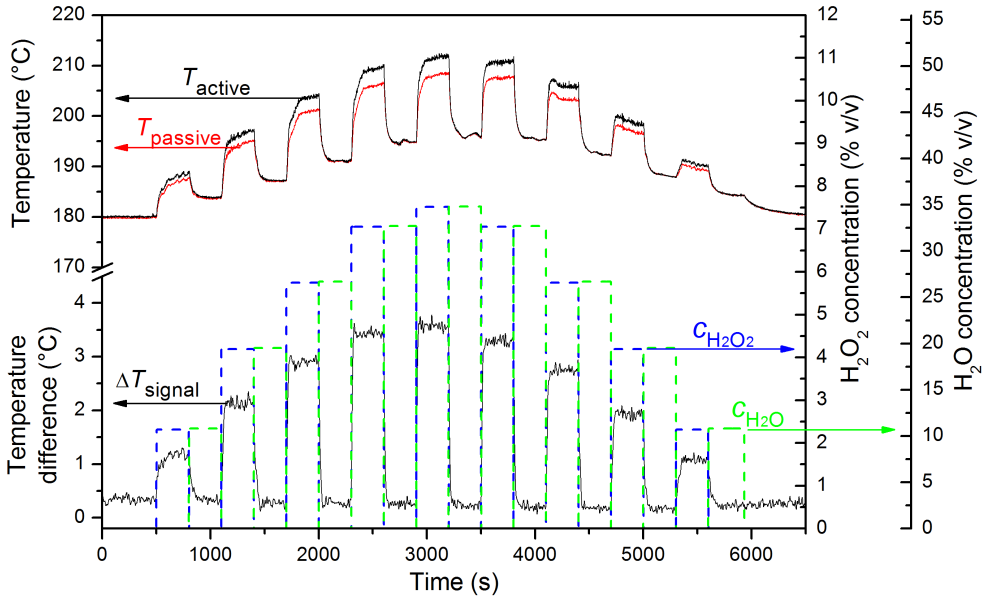

(a)

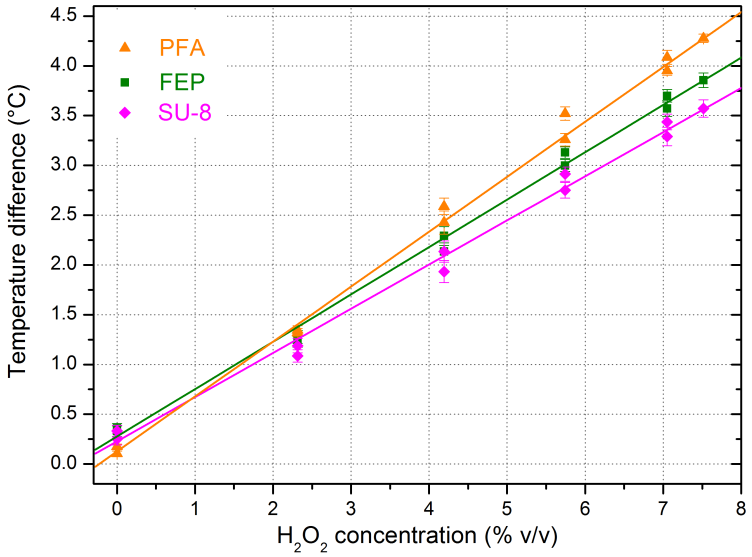

(b)

Figure 4.4: (a) Typical measurement protocol of a calorimetric gas sensor encapsulated by a polymer-coating as passivation layer (in this case, SU-8), and (b) resulting characteristics of the sensors with different polymer coatings (SU-8, FEP and PFA).

Table 4.3: Sensor characteristics of three calorimetric gas sensors with different polymeric encapsulation material in H_2O_2/H_2O atmosphere.

Polymer	Off-set (°C)	Sensitivity (°C/(% v/v))
SU-8	0.21	0.45
PFA	0.12	0.56
FEP	0.26	0.48

4.5 Conclusions

In the present work, polymeric materials, epoxy-based SU-8 photoresist, FEP and PFA, have been investigated as passivation layer for a calorimetric H_2O_2 gas sensor. The polymers have been deposited via spin-coating on the sensor surface. All polymers provide good adhesion on the sensor surface. The SU-8 resist has an enclosed surface, whereas the surfaces of the fluoropolymers (FEP and PFA) show slight agglomerates in the range of about 120 nm. All materials in test showed good insulation characteristics in the presence of H_2O_2 and H_2O. A possible explanation could be the absorption or micro-condensation of water on the hydrophilic surface of the photoresist SU-8 that may influence the heat transfer on the sensor. The highest thermal insulation was achieved by PFA.

Acknowledgements

The authors want to thank M. Raue from the Institute of Applied Polymer Chemistry (Jülich), for providing the contact angle measurements.

References

[1] Hess, W. T. Hydrogen peroxide. In *Kirk-Othmer encyclopedia of chemical technology*. John Wiley & Sons, Inc., 2000.

[2] Fraise, A. P., Lambert, P. A., and Maillard, J.-Y., Eds. *Russell, Hugo and Ayliffe's principles and practice of disinfection, preservation and sterilization*, 4 ed. Blackwell Publishing Ltd, Oxford, 2008.

[3] Hage, R., and Lienke, A. Anwendung von Übergangsmetallkomplexen zum Bleichen von Textilien und Holzpulpe. *Angewandte Chemie 118*, 2 (2006), 212–229.

[4] Bostwick, S. L. Determining hydrogen peroxide exposure of employees at company XYZ. Reserach paper, University of Wisconsin-Stout, 2002.

[5] Hart, A. B., McFadyen, J., and Ross, R. A. Solid-oxide-catalyzed decomposition of hydrogen peroxide vapour. *Transactions of the Faraday Society 59* (1963), 1458–1469.

[6] Haber, F., and Weiss, J. The catalytic decomposition of hydrogen peroxide by iron salts. *Proceedings of the Royal Society of London. Series A - Mathematical and Physical Sciences 147*, 861 (1934), 332–351.

[7] Kirchner, P., Li, B., Spelthahn, H., Henkel, H., Schneider, A., Friedrich, P., Kolstad, J., Keusgen, M., and Schöning, M. J. Thin-film calorimetric H_2O_2 gas sensor for the validation of germicidal effectivity in aseptic filling processes. *Sensors and Actuators B: Chemical 154*, 2 (2011), 257–263.

[8] Kirchner, P., Ng, Y. A., Spelthahn, H., Schneider, A., Henkel, H., Friedrich, P., Kolstad, J., Berger, J., Keusgen, M., and Schöning, M. J. Gas sensor investigation based on a catalytically activated thin-film thermopile for H_2O_2 detection. *Physica Status Solidi A 207*, 4 (2010), 787–792.

[9] Salem, I. A., El-Maazawi, M., and Zaki, A. B. Kinetics and mechanisms of decomposition reaction of hydrogen peroxide in presence of metal complexes. *International Journal of Chemical Kinetics 32*, 11 (2000), 643–666.

[10] Ono, Y., Matsumura, T., Kitajima, N., and Fukuzumi, S. Formation of superoxide ion during the decomposition of hydrogen peroxide on supported metals. *The Journal of Physical Chemistry 81*, 13 (1977), 1307–1311.

[11] Giamello, E., Rumori, P., Geobaldo, F., Fubini, B., and Paganini, M. The interaction between hydrogen peroxide and metal oxides: EPR investigations. *Applied Magnetic Resonance 10*, 1 (1996), 173–192.

[12] Anpo, M., Che, M., Fubini, B., Garrone, E., Giamello, E., and Paganini, M. Generation of superoxide ions at oxide surfaces. *Topics in Catalysis 8*, 3 (1999), 189–198.

[13] Salem, I. A., Elhag, R. I., and Khalil, K. M. S. Catalytic activity of a zirconium(IV) oxide surface supported with transition metal ions. *Transition Metal Chemistry 25*, 3 (2000), 260–264.

[14] Hassler, C., Boretius, T., and Stieglitz, T. Polymers for neural implants. *Journal of Polymer Science Part B: Polymer Physics 49*, 1 (2011), 18–33.

[15] del Campo, A., and Greiner, C. SU-8: a photoresist for high-aspect-ratio and 3D submicron lithography. *Journal of Micromechanics and Microengineering 17*, 6 (2007), R81–R95.

[16] Schmid, S., Kühne, S., and Hierold, C. Influence of air humidity on polymeric microresonators. *Journal of Micromechanics and Microengineering 19*, 6 (2009), 1–9.

[17] Leivo, E., Wilenius, T., Kinos, T., Vuoristo, P., and Mäntylä, T. Properties of thermally sprayed fluoropolymer PVDF, ECTFE, PFA and FEP coatings. *Progress in Organic Coatings 49*, 1 (2004), 69–73.

[18] Anhoj, T. A., Jorgensen, A. M., Zauner, D. A., and Hübner, J. The effect of soft bake temperature on the polymerization of SU-8 photoresist. *Journal of Micromechanics and Microengineering 16*, 9 (2006), 1819–1824.

[19] Gabbott, P., Ed. *Principles and applications of thermal analysis*. Blackwell Publishing Ltd, Oxford, 2008.

[20] Griffiths, P., and Haseth, J. A. D., Eds. *Fourier transform infrared spectrometry*, 2 ed. John Wiley & Sons, Hoboken, 2007.

[21] Cho, J.-D., Ju, H.-T., Park, Y.-S., and Hong, J.-W. Kinetics of cationic photopolymerizations of UV-curable epoxy-based SU-8-negative photoresists with and without silica nanoparticles. *Macromolecular Materials and Engineering 291*, 9 (2006), 1155–1163.

[22] Rath, S., Boey, F., and Abadie, M. Cationic electron-beam curing of a high-functionality epoxy: effect of post-curing on glass transition and conversion. *Polymer International 53*, 7 (2004), 857–862.

[23] Inayoshi, M., Ito, M., Hori, M., Goto, T., and Hiramatsu, M. Formation and micromachining of Teflon (fluorocarbon polymer) film by a completely dry process using synchrotron radiation. *Journal of Vacuum Science and Technology B: Microelectronics and Nanometer Structures 17*, 3 (1999), 949–956.

4.6 Supporting information[1]

4.6.1 Thermal characterisation

The spin-coated polymeric layers of the calorimetric gas sensors have been additionally characterised by differential scanning calorimetry (DSC) and thermogravimetric analysis (TGA) to demonstrate their elevated thermal endurance. A detailed description of DSC and TGA is given elsewhere [19].

Via DSC the melting points of the polymers have been detected, wherein the heat flow, which has been required to increase the temperature of the polymeric material against a reference probe, was measured as a function of temperature. The DSC characterisation of the polymers is depicted in Fig. 4.5. Therein, PFA shows a melting point at 309 °C, FEP at 268 °C and SU-8 does not have a melting point in the considered temperature range up to 325 °C.

By means of TGA, the weight loss of the polymers has been determined in relation to a temperature profile, whereby the initial degradation temperature of each polymeric material could be identified (s. Fig. 4.6). SU-8 started to thermally degrade at 393 °C, PFA at 516 °C and FEP at 485 °C.

Both thermal characterisation methods, differential scanning calorimetry and thermogravimetric analysis, underline the outstanding endurance of the spin-coated polymeric layers even at elevated temperatures that is necessary to be applied for the envisaged sterilisation process.

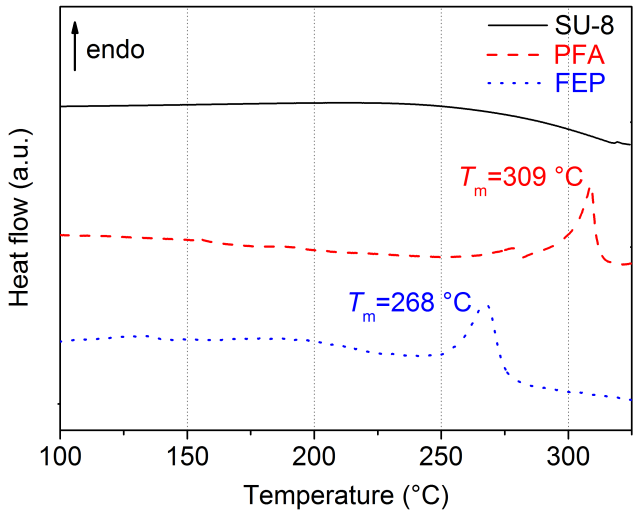

Figure 4.5: DSC diagram of spin-coated SU-8 photoresist, PFA and FEP.

[1]Note: Results of section 4.6.1 and section 4.6.2 are not part of the present article and will be published separately.

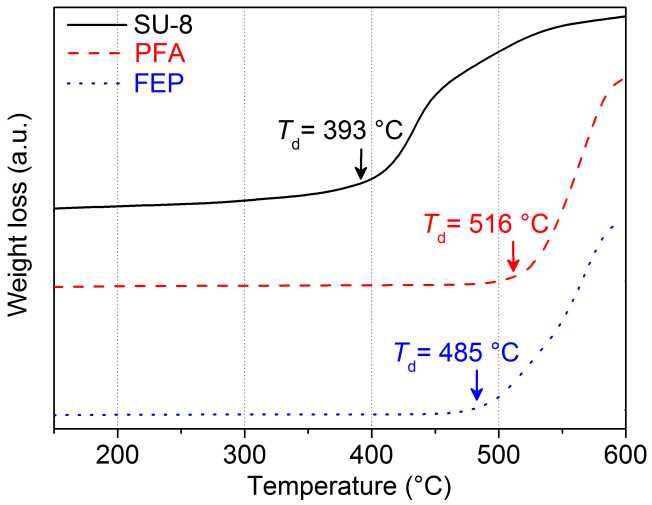

Figure 4.6: TGA of spin-coated SU-8 photoresist, PFA and FEP.

4.6.2 FTIR spectroscopy

Furthermore, the polymeric layers have been investigated by Fourier transform infrared spectroscopy (FTIR) in order to study their chemical composition before and after they were exposed to H_2O_2. In an IR spectrometer, IR radiation is passed through a material probe, where some of the radiation is absorbed by the atomic and molecular composition of the probe (atomic and molecular rotation, vibration and translational motion) and some of it is transmitted, whereby the resulting spectrum represents a molecular fingerprint of the material probe. With the help of an interferometer and the Fourier transform method, the total IR spectrum can be detected in a single moment. In this work, the FTIR spectrosopy has been carried out with attenuated total reflectance (ATR), wherein an evanescent wave is passed through the interface of a crystal and the polymeric layer. A detailed introduction to ATR-FTIR spectroscopy is given in [20].

By using the FTIR spectroscopy, the chemical structures of the polymers could be determined and hence, their chemical consistency after H_2O_2 treatment could be pointed out. For the investigation of the polymeric layers by FTIR spectroscopy, their structural formulas are given in Fig. 4.7. In Fig. 4.8, the ATR-FTIR spectra of spin-coated SU-8 before and after its exposition to H_2O_2 are shown. Therein, the strong band at 1508 cm^{-1} is caused by the aromatic C=C stretching mode. The peak at 830 cm^{-1} corresponds to the aromatic C-H compounds and the strong absorption bands at 1030 cm^{-1} as well as at 1250 cm^{-1} are due to the symmetrical stretching vibration of the epoxy group. The decisive peak for indicating the curing of the spin-coated SU-8 photoresist is presented by

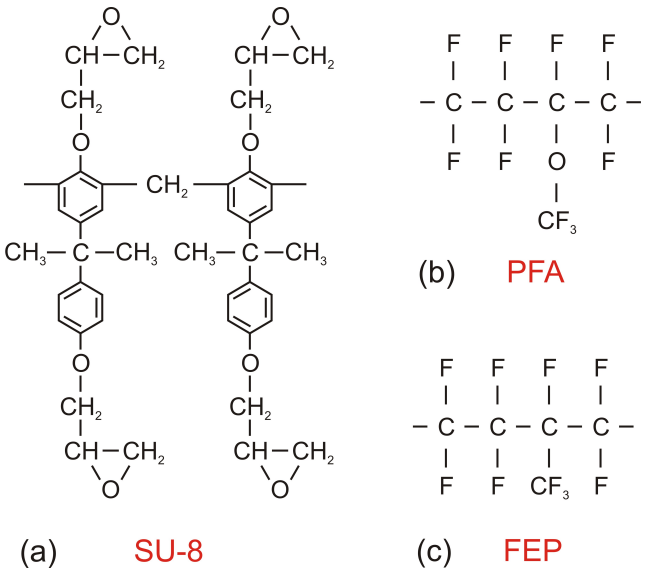

Figure 4.7: Structural formulas of (a) SU-8 photoresist, (b) PFA and (c)FEP (adopted from [22, 23]).

the absorption band at 912 cm^{-1} caused by the C-H asymmetrical stretching vibration of the epoxy group [21]. If the peak appeared, a perfectly cured SU-8 layer can be expected. The spectra of the SU-8 before and after exposure to H_2O_2 largely correspond to each other demonstrating the chemical inertness of the SU-8 photoresist. A distinction can merely be drawn at the absorption band at 912 cm^{-1}, where the peak disappeared after exposition to H_2O_2. This phenomenon results from a subsequent curing of the SU-8 photoresist at the elevated temperature of the H_2O_2 atmosphere.

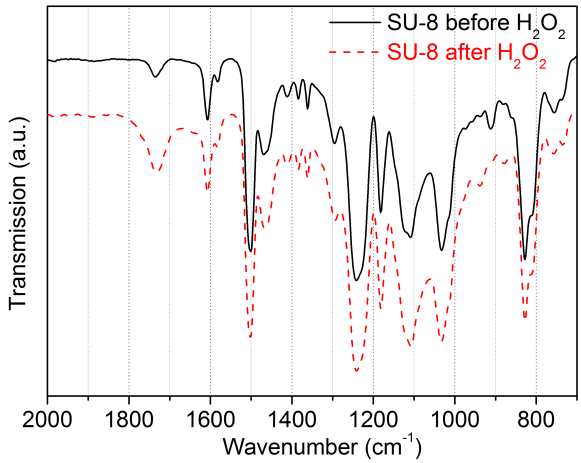

Figure 4.8: ATR-FTIR spectra of spin-coated SU-8, before and after it was exposed to various H_2O_2 concentrations (gas flow rate: 10 m^3/h, gas temperatures 270 °C).

The ATR-FTIR spectra of the spin-coated fluoropolymers (PFA and FEP), both before and after treated by H_2O_2, are presented in Fig. 4.9. For both materials, two absorption peaks at 1200 cm^{-1} and 1147 cm^{-1} correspond to the asymmetrical and symmetrical CF_2 stretching mode. A distinction between the fluoropolymers can be drawn by the small peak at 993 cm^{-1} for PFA and at 981 cm^{-1} for FEP, which are due their specific stretching mode of the CF_3 side group. Both materials show no difference in their ATR-FTIR spectra, before and after they have been treated by H_2O_2 demonstrating their chemical consistency.

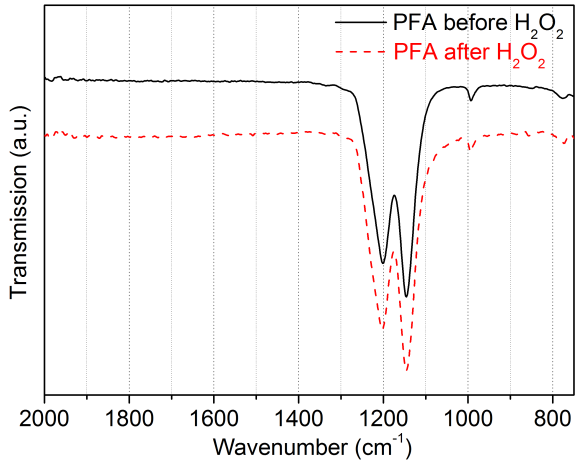

(a)

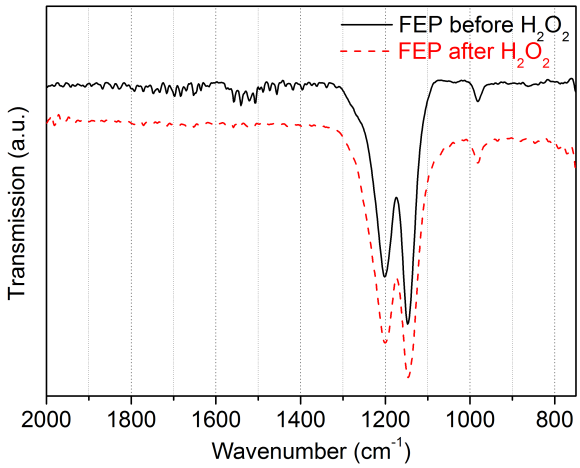

(b)

Figure 4.9: ATR-FTIR spectra of (a) spin-coated PFA and (b) FEP, before and after they were exposed to various H_2O_2 concentrations (gas flow rate: 10 m^3/h, gas temperatures 270 °C).

4.6.3 Elevation profiles of the passivation layers as support to surface characterisation

In the following diagram (Fig. 4.10), the elevation profiles of the passivation layers are depicted as supporting information for section 4.4.1.

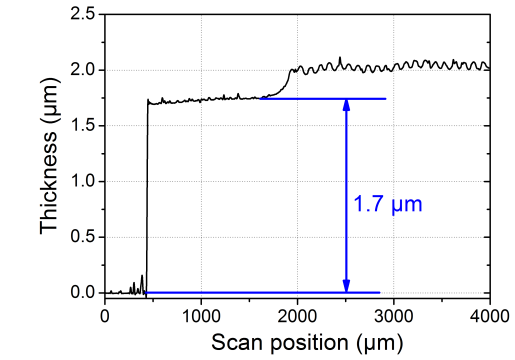

(a)

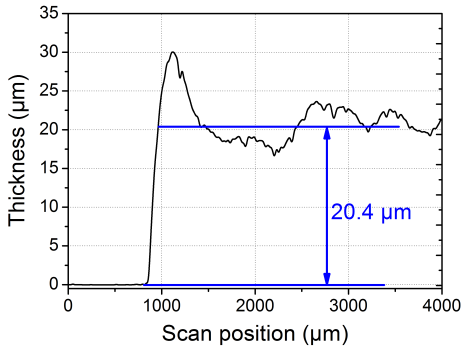

(b)

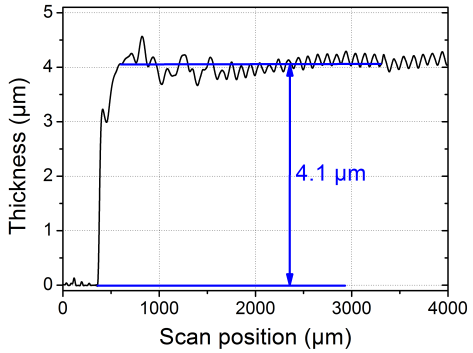

(c)

Figure 4.10: Elevation profiles of (a) spin-coated SU-8 photoresist, (b) perfluoralkoxy (PFA) and (c) fluorinated ethylene propylene (FEP) passivation layer.

4.6.4 Additional measurement curves

In the following diagram (Fig. 4.11), the measurement curves of the calorimetric gas sensors encapsulated by FEP and by PFA are overviewed, wherefrom the sensor characteristics, depicted in Fig. 4.4, results.

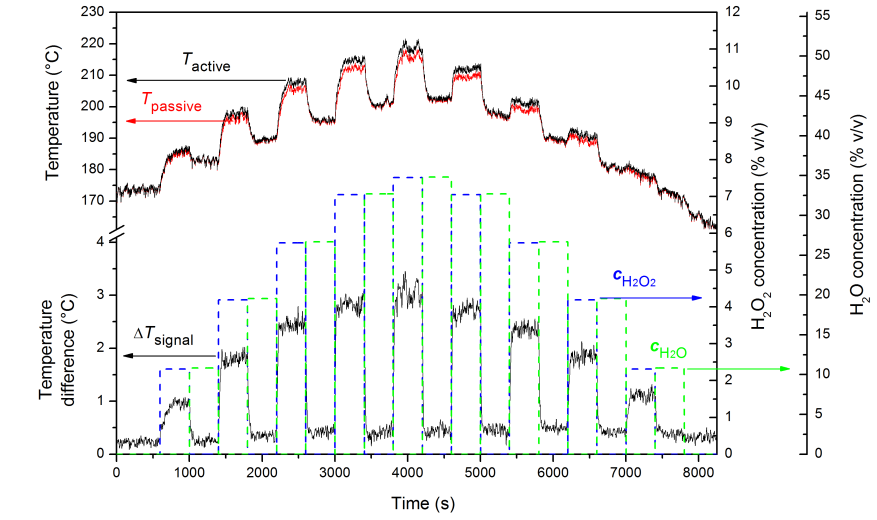

(a)

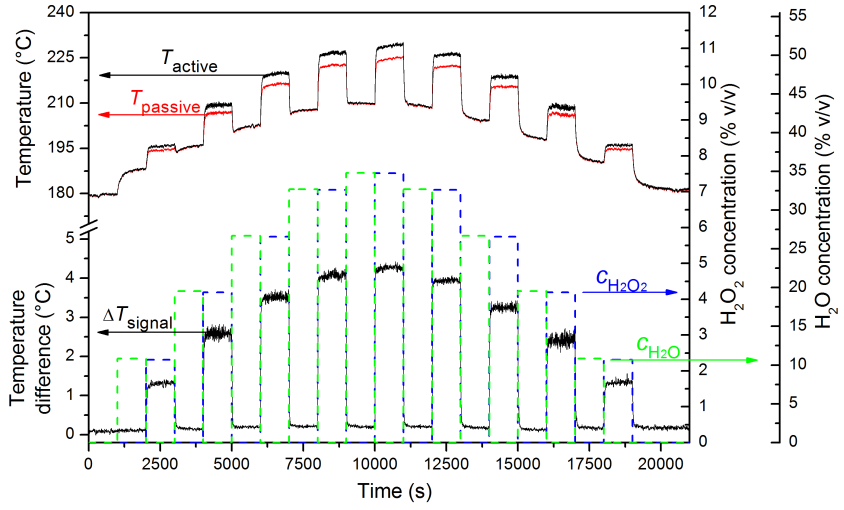

(b)

Figure 4.11: Measurement curves of (a) a calorimetric gas sensor encapsulated by FEP as passivation layer and (b) a calorimetric gas sensor encapsulated by PFA at various H_2O_2 and H_2O concentrations (gas flow rate: 10 m^3/h, gas temperatures 270 °C).

5 Optimisation and fabrication of a calorimetric gas sensor built up on a polyimide substrate for H_2O_2 monitoring

KIRCHNER, P., Oberländer, J., Friedrich, P., Berger, J., Suso, H.-P., Kupyna, A., Keusgen, M., and Schöning, M. J.

Physica Status Solidi A 208, 6 (2011), 1235–1240.

5.1 Abstract

A calorimetric gas sensor for the detection of vapourised H_2O_2 in aseptic filling processes was built up on a polyimide foil instead of silicon as substrate material in order to optimise the sensor-response behaviour. The sensor was catalytically activated with a dispersion of manganese(IV) oxide. The reaction mechanism of the exothermic H_2O_2 decomposition on the catalyst involves two pathways: an initial reaction with electron exchange between the catalyst surface and H_2O_2 creating free radicals, and a chain reaction of these radicals with H_2O_2, in which the final products, namely water and oxygen, are formed. The calorimetric gas sensor possesses a linear response behaviour with a sensitivity of 7.15 °C/(% v/v) in a H_2O_2 concentration range from 0 to 8% v/v.

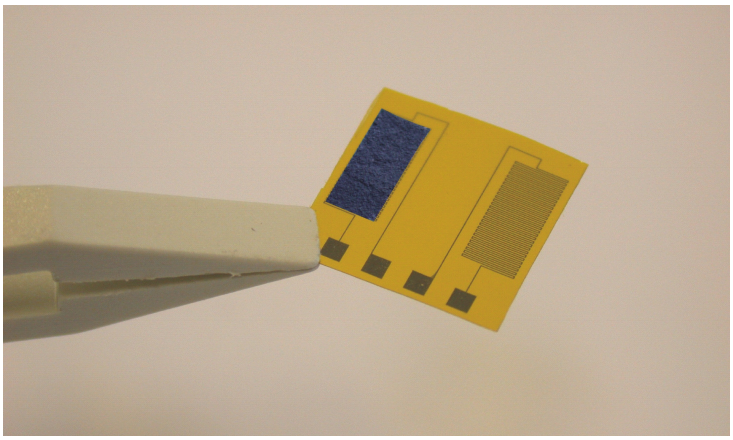

Figure 5.1: Calorimetric gas sensor on polyimide foil for H_2O_2 monitoring in sterilisation processes.

5.2 Introduction

In aseptic filling machineries, the sterilisation of packages for food, especially perishable food, like milk and fruit juice, is indispensable to assure a long shelf life of filled products and obviate the transmission of pathogenic microorganisms [1, 2]. For carton packages, hydrogen peroxide in combination with heat has become one of the most significant sterilisation agents [3]. Therein, a hydrogen peroxide solution vaporised at a temperature above 200 °C is shortly streamed into pre-heated food packages. The efficiency of the sterilisation process predominantly depends on the present H_2O_2 concentration on the inner surface of the packages.

For monitoring the sterilisation process directly on the inner surface of the carton packages, silicon-based calorimetric-type sensors were developed in prior works [4, 5]. These sensors are based on an "on-chip" differential set-up of a catalytically activated and a passivated temperature-sensitive segment and possess a temperature difference between both segments as sensor signal correlating with the H_2O_2 concentration. However, a disadvantage in using silicon substrates is due to the high thermal conductivity (156 $Wm^{-1}K^{-1}$ [6]). This leads to a heat transfer from the active to the passive sensor segment during the catalytic decomposition of H_2O_2 that is finally resulting in a low sensitivity.

In order to optimise the sensor characteristics, a flexible polyimide foil that offers a low thermal conductivity (0.147 $Wm^{-1}K^{-1}$ [7]) and a heat resistance of up to 400 °C was considered as sensor substrate in the present work. In addition to the thermal abilities, polyimide as an out-standing polymer features high mechanical stability and flexibility, electrical insulation as well as chemical inertness. Due to these superior properties, the application field of polyimide has generally been enlarged from printed circuit boards and electrical insulation layers in microelectronics to functional layers of humidity sensors [8–10], shielding layers for sensor surfaces [11] and novel platforms for thermal sensor devices, like bolometers [12, 13], temperature sensor arrays [14, 15] and micro-hotplates integrated in gas sensors [16–18]. The fabrication process with polyimide substrates is relatively simple and inexpensive by utilising conventional chip technology. Compared to rigid silicon substrates, the flexible sensor chips can also be applied on non-planar, curved surfaces.

In the following sections, we will demonstrate the feasibility of developing a calorimetric gas sensor on a flexible polyimide foil for in-line monitoring of vapour-phase H_2O_2 in sterilisation processes of food packages, which has to operate under harsh ambient conditions (H_2O_2 concentration up to 8% v/v, gas-flow rate of 10 m^3/h, gas temperature above 200 °C and elevated humidity of the gas stream).

5.3 Experimental

5.3.1 Sensor design and fabrication

The design of the calorimetric gas sensor is similar to the sensor devices, introduced in [5, 19, 20]. It is based on an "on-chip" differential set-up of two temperature-sensitive thin-film resistances (s. Fig. 5.2(a)), where one of them is catalytically activated and another one is passivated serving as a reference segment. Instead of an active heating element, the sensor utilises the elevated temperature of the vapour-phase hydrogen peroxide.

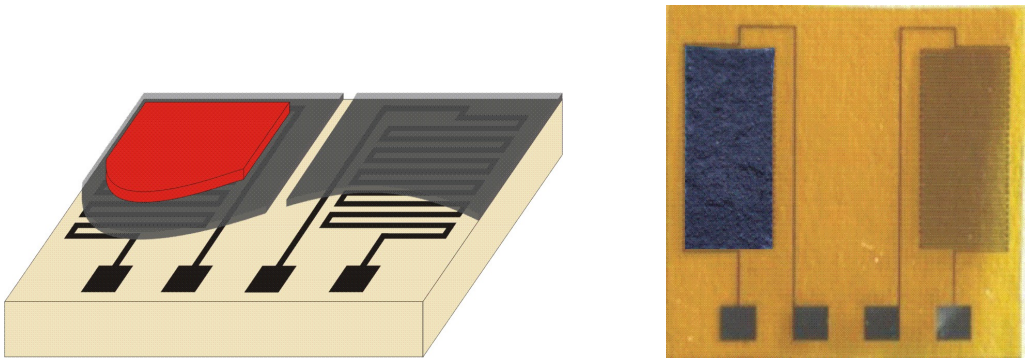

(a) (b)

Figure 5.2: (a) Schematic picture of the sensor set-up, and (b) calorimetric gas sensor on polyimide substrate (chip size: 10 x 10 mm^2).

The differential set-up was built-up on a flexible polyimide substrate instead of conventional silicon. Generally, two different fabrication methods with polyimide as flexible substrate were established in chip technology [14]: (*i*) a liquid polyimide film is deposited by spin-coating onto a silicon wafer with a release layer, which is completely removed at the end of the fabrication process, and (*ii*) a solid polyimide foil is temporarily attached to a silicon carrier wafer by an adhesive and separated after finishing the fabrication process on wafer level. In the present work, the second method has been utilised, wherein a flexible polyimide foil (Kapton® HN from DuPont) with a thickness of 25 μm serves as sensor substrate. Platinum with a thickness of 200 nm was deposited together with an adhesion layer of 20 nm titanium onto the polyimide substrate by physical vapour deposition and patterned as meander-shaped resistance structures by conventional photolithography. This results in a resistance of ca. 1.5 kΩ at 0 °C for each structure. Both resistances were covered by SU-8 photoresist, which was established as passivation material against hydrogen peroxide in [4]. The resist was spin-coated at 3000 rpm and subsequently heat-treated at 175 °C resulting in a layer thickness of 1.5 μm.

After the separation of the wafer-level polyimide foil in single sensor chips with an area

of 10 x 10 mm^2, each of them was catalytically activated by a drop-coated dispersion of manganese(IV) oxide (s. Fig. 5.3) in the same manner as in [4, 5]. The reason for using manganese oxide as catalyst relies on its high activity in exothermic decomposition of vapour-phase hydrogen peroxide even at elevated temperatures compared to other solid oxides, which was extensively studied by Hart et *al.* [21]. The final calorimetric gas sensor built-up on a flexible polyimide foil with two passivated thin-film resistances and catalyst is depicted in Fig. 5.2(b).

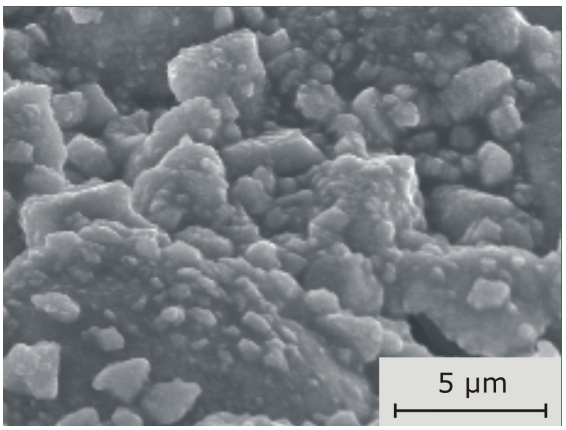

Figure 5.3: SEM picture of the dispersion of manganese(IV) oxide.

5.3.2 Catalytic surface reaction

During the heterogeneous decomposition of hydrogen peroxide on the manganese oxide surface, reaction enthalpy is released, which causes an increase in temperature on the catalytically activated thin-film resistance of the sensor. Over the last decades, various reaction mechanisms have been proposed for the heterogeneous decomposition of H_2O_2 over solid interfaces, like metal [22, 23], metal oxide [24–26] and especially, manganese oxide surfaces [21, 27–30]. However, most of them are based on the classical Haber-Weiss mechanism [31], which invokes a chain reaction with free radicals (e.g., OH and H_2O radicals) as intermediates during the catalytic decomposition of H_2O_2. The formation of free radicals is important for a rapid H_2O_2 decomposition, and the evidence for the participation of these intermediates has experimentally been adduced in several works [23–25, 32].

The decisive point for the chain reaction is the initial reaction step in formation of free radicals – the interaction of hydrogen peroxide with the catalyst surface. Therein, an electron exchange takes place either by donating an electron from the surface to the

vapour-phase H_2O_2 or *vice versa* [24, 29, 30]:

$$H_2O_2 + e^- \rightarrow OH^- + OH^\bullet \tag{5.1}$$

$$H_2O_2 + e^+ \rightarrow H^+ + HO_2^\bullet \tag{5.2}$$

Additionally, the decomposition can also be initiated by homolytic cleavage of the O-O bindings of H_2O_2 molecules without electron exchange, which occurs predominantly on metal oxides at elevated temperatures [24, 25, 32]:

$$H_2O_2 \rightarrow OH^\bullet + OH^\bullet \tag{5.3}$$

Once free radicals are formed, the further steps can be described by the following reactions:

$$OH^\bullet + H_2O_2 \rightarrow HO_2^\bullet + H_2O \tag{5.4}$$

$$HO_2^\bullet + H_2O_2 \rightarrow OH^\bullet + H_2O + O_2 \tag{5.5}$$

$$HO_2^\bullet + OH^\bullet \rightarrow H_2O + O_2 \tag{5.6}$$

The stoichiometric relationship of the exothermic decomposition of H_2O_2 on the catalyst surface can be summarised as Eq. 5.7.

$$2\ H_2O_2 \rightarrow 2\ H_2O + O_2 + \Delta_R H \tag{5.7}$$

Here, $\Delta_R H$ is the released reaction enthalpy.

The reaction kinetic follows a first-order decay and can be written as [20, 22, 31]:

$$\frac{-\mathrm{d}c_{H_2O_2}}{\mathrm{d}t} = k \cdot c_{H_2O_2} \tag{5.8}$$

Here, k is the decomposition rate coefficient, $c_{H_2O_2}$ is the H_2O_2 concentration and t is the resident time.

The temperature increase on the surface of the active sensor segment arising from the released reaction enthalpy during the catalytic decomposition of hydrogen peroxide can

be described by the following equation[1]:

$$\Delta T_{\mathrm{reaction}} = \frac{c_{\mathrm{H_2O_2}} \cdot \Delta_{\mathrm{R}} H}{C_{\mathrm{c}}} \tag{5.9}$$

with C_{c} as heat capacity of the ambient gas close to the sensor surface.

From Eq. 5.9, the resulting temperature increase on the sensor surface, which depends on the H_2O_2 concentration, was determined with a reaction enthalpy of 105.3 kJ/mol by Eq. 5.10:

$$\Delta T_{\mathrm{reaction}} = c_{\mathrm{H_2O_2}} \cdot 24.1\,^{\circ}\mathrm{C}/(\%\ \mathrm{v/v}) \tag{5.10}$$

5.3.3 Sensor modelling

In order to evaluate the thermal response behaviour of the calorimetric gas sensor, equivalent circuits have been developed, which are similar to electric circuits. Therein, the thermal quantities (heat resistance, heat capacitance, temperature) correspond to electrical quantities (electrical resistance, capacitance, voltage) as shown in [33, 34]. Two simplified equivalent circuits were considered, where one of them describes the thermal response behaviour of the sensor in terms of an increase of the ambient gas temperature (T_{gas}) and another one specifies the sensor-response behaviour due to the temperature increase (T_{reaction}) on the surface of the active sensor segment caused by the exothermic decomposition of hydrogen peroxide (s. Fig. 5.4). Both of them consist of a heat-transmission resistance R_α between the interface solid-fluid and an RC element – thermal resistance and thermal capacity – for each sensor layer (catalyst $R_{\mathrm{cat}}/C_{\mathrm{cat}}$, passivation layer $R_{\mathrm{pas}}/C_{\mathrm{pas}}$, resistance structure $R_{\mathrm{res}}/C_{\mathrm{res}}$ and substrate $R_{\mathrm{sub}}/C_{\mathrm{sub}}$), respectively, wherein the equivalent circuit for determining the sensor-response behaviour due to the exothermic H_2O_2 decomposition is only based on the local heating of the catalyst and passivation layer on the active sensor segment. The equivalent circuits were simulated with a SPICE program and the thermal response time has been determined (s. Fig. 5.5). Therein, the sensor takes 51.7 s until 90% of the increased gas temperature is achieved and 4.7 s to attain 90% of the temperature increase caused by the exothermic H_2O_2 decomposition.

5.4 Results and discussion

The characterisation of the polyimide-based calorimetric gas sensor was performed under a gas mixture with vapour-phase hydrogen peroxide – an evaporated aerosol of a carrier

[1] A detailed theoretical consideration of the sensor's sensitivity in form of calculation models for determining the concentration-dependent temperature increase is given in section 5.6.2.

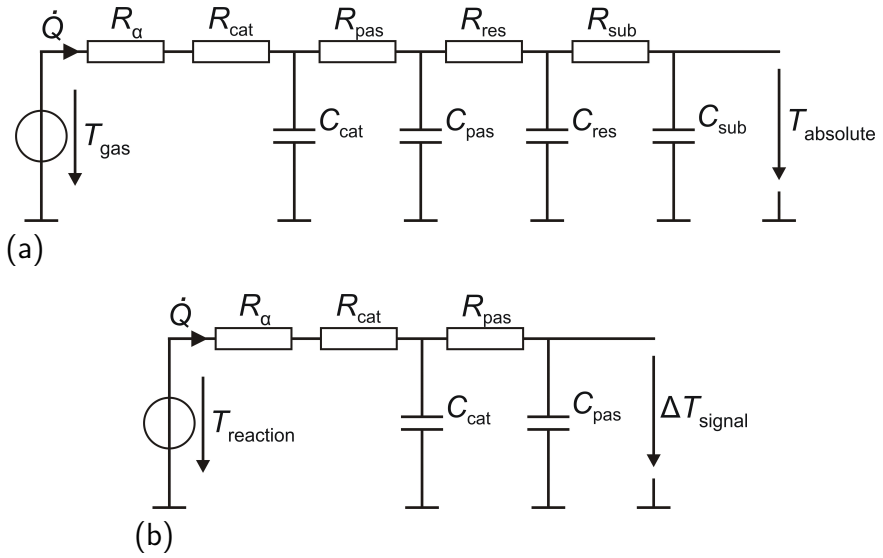

Figure 5.4: Equivalent circuits of the calorimetric gas sensor for evaluating the thermal response time (a) due to an increase of the ambient gas temperature (T_{gas}), and (b) in terms of temperature increase (T_{reaction}) caused by the catalytic H_2O_2 decomposition.

gas and a H_2O_2 solution (35% w/w) – in a measuring chamber of an experimental test rig, introduced in [4]. In a first step, the sensor response behaviour was determined at gradually increasing H_2O_2 concentrations from 0 to 8% v/v (at constant evaporation temperature of 270 °C and flow rate of 10 m^3/h) and *vice versa*. Therein, each concentration step was adjusted for 300 s, respectively. Between two H_2O_2 concentrations, water vapour 0-35% v/v was dosed also for 300 s to study the influence of humidity on the polyimide-based sensor. The regressions of the temperature on the active (T_{active}) and

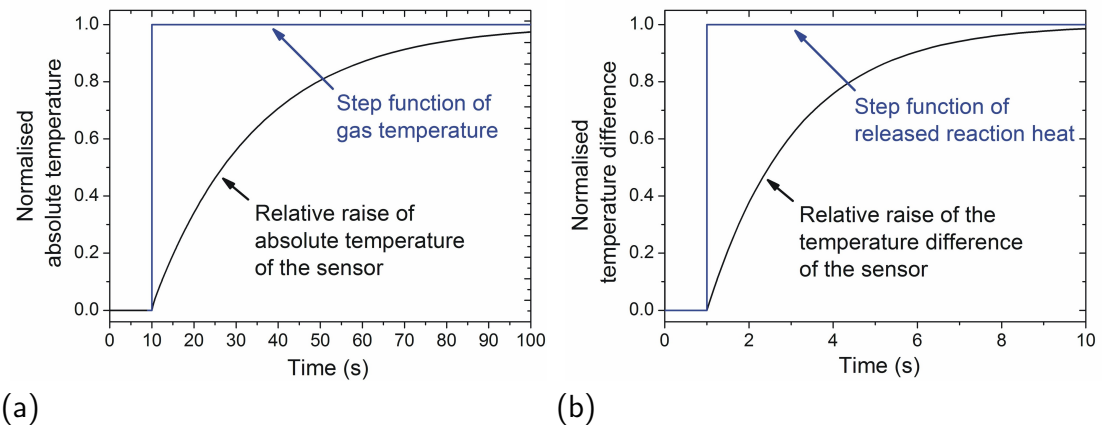

Figure 5.5: Simulated response time of the calorimetric gas sensor due to (a) an increase in gas temperature, and (b) released reaction heat resulting from the H_2O_2 decomposition.

passive sensor segment (T_{passive}) as well as the temperature difference (ΔT_{signal}) between both segments at varied H_2O_2 and water vapour concentrations are presented in Fig. 5.6. For the active sensor segment, the raise in temperature (T_{active}) at different H_2O_2 concentrations caused by the exothermic H_2O_2 decomposition can be clearly observed, whereas the passive segment was not influenced by the released reaction heat because of the low thermal conductivity of the polyimide substrate. Both sensor segments show a change in the off-set temperature from 110 °C to 135 °C during the measurement. Hence, to compensate temperature variations in the gas stream, the temperature difference between the active and passive sensor segment serves as sensor signal, which is proportional to the present H_2O_2 concentration. During the dosage of water vapour, the temperature difference slightly increases from -0.5 °C to 3.7 °C, dependent on the particular H_2O concentration.

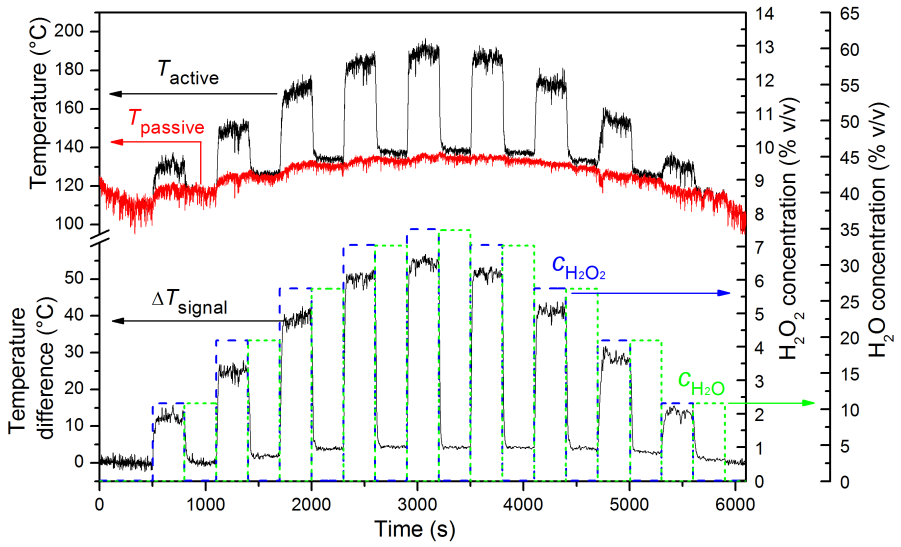

Figure 5.6: Response behaviour of the calorimetric gas sensor at various H_2O_2 concentrations (0 to 8% v/v) and H_2O concentrations (0 to 35% v/v) with constant evaporation temperature of 270 °C and flow rate of 10 m^3/h.

From the measurement curve in Fig. 5.6, the calibration plot of the calorimetric gas sensor was established (s. Fig. 5.7). Here, a sensitivity of 7.15 °C/(% v/v) and an off-set of -0.52 °C, resulting from the inhomogeneous temperature distribution in the measuring chamber of the experimental set-up, were determined. In comparison to silicon-based sensors presented in [5], the sensitivity of the polyimide-based sensor device is 12.5 times higher. This relies on the avoidance of an undesired heat transfer between the active and passive sensor segment due to the low thermal conductivity of polyimide during the exothermic H_2O_2 decomposition. In addition, a maximum hysteresis of 2.41 °C at a

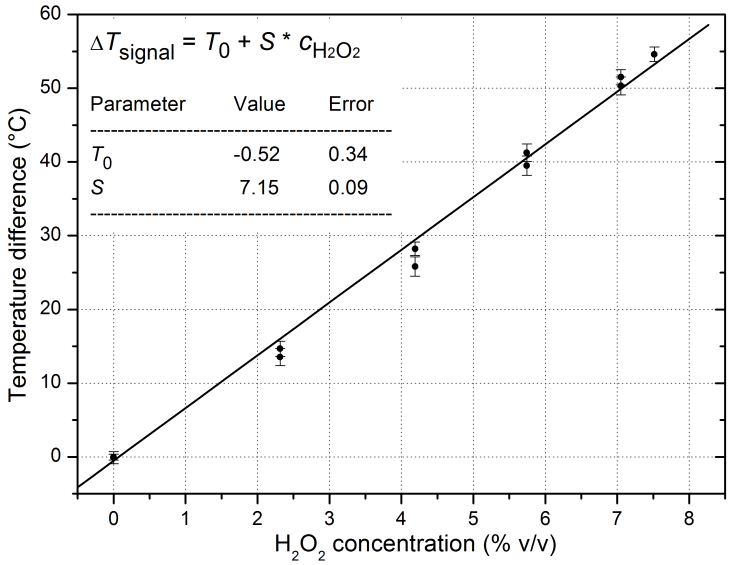

Figure 5.7: Calibration plot of the calorimetric gas sensor.

H_2O_2 concentration of 4.2% v/v could be observed, leading to a maximum deviation of 0.32% v/v for the measured H_2O_2 concentration.

Furthermore, the temporal response behaviour of the calorimetric gas sensor, presented in Fig. 5.8, has been investigated. Therefore, a constant H_2O_2 concentration of 5.7% v/v was adjusted after 100 s and by opening a cover slide, which shields the sensor from the H_2O_2 vapour, after 150 s (for a time period of 300 s), the response time of the sensor was determined.

From Fig. 5.8(a), the slow increase of T_{active} and T_{passive} can be observed, whereas the ΔT_{signal} rises rapidly. The response time for T_{active} and T_{passive} is 51.7 s and for ΔT_{signal} the response time amounts to 5.9 s until 90% of the final value was achieved (s. Fig. 5.8(b)). Both of them are comparable to their theoretical response time (57.5 s for T_{active} and T_{passive} as well as 4.7 s for ΔT_{signal}).

Finally, the impact of the evaporation temperature on the sensor signal was investigated (s. Fig. 5.9). Here, a constant H_2O_2 concentration of 2.3% v/v was adjusted and the evaporation temperature was gradually reduced from 270 °C to 150 °C in steps of 30 °C and back to 270 °C. Each temperature step was maintained for 300 s. During variation of the evaporation temperature, no change in the sensor signal (ΔT_{signal}) was observed, even though the temperature on the sensor surface (T_{passive}) varied between 85 °C and 125 °C.

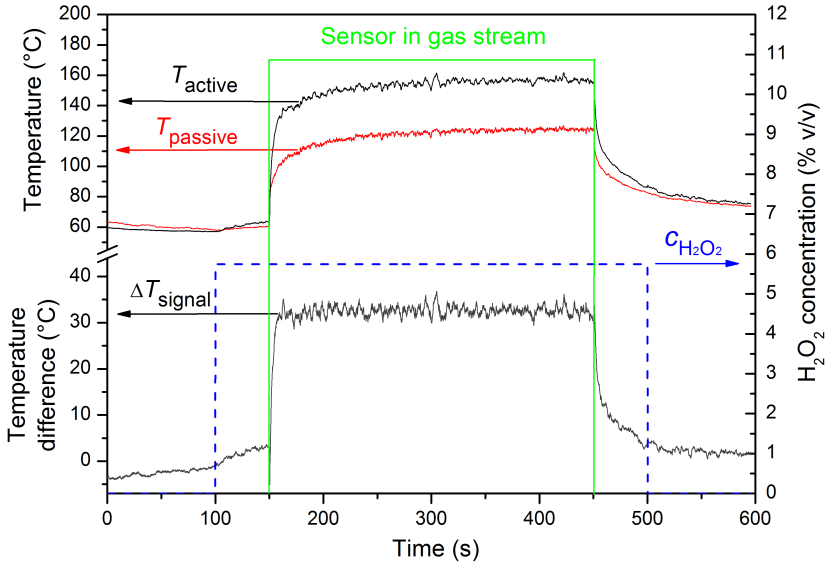

(a)

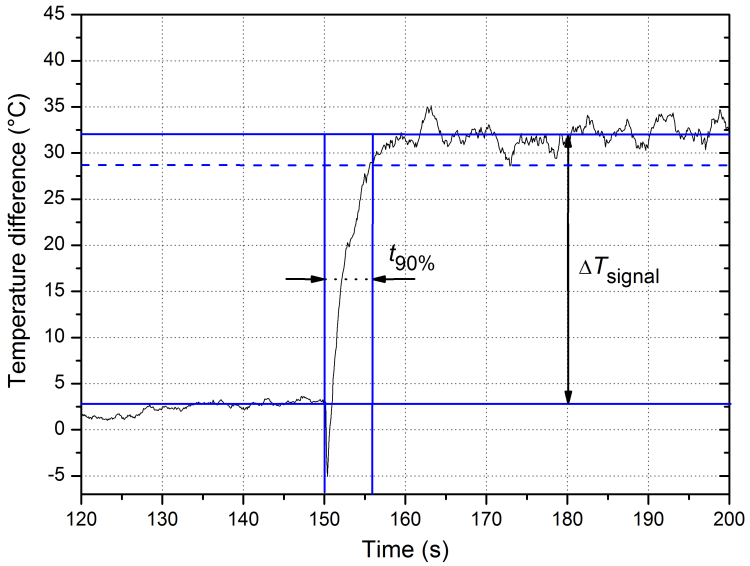

(b)

Figure 5.8: (a) Temporal response behaviour of the calorimetric gas sensor at constant H_2O_2 concentration of 5.7% v/v, and (b) response time of the temperature difference (ΔT_{signal}).

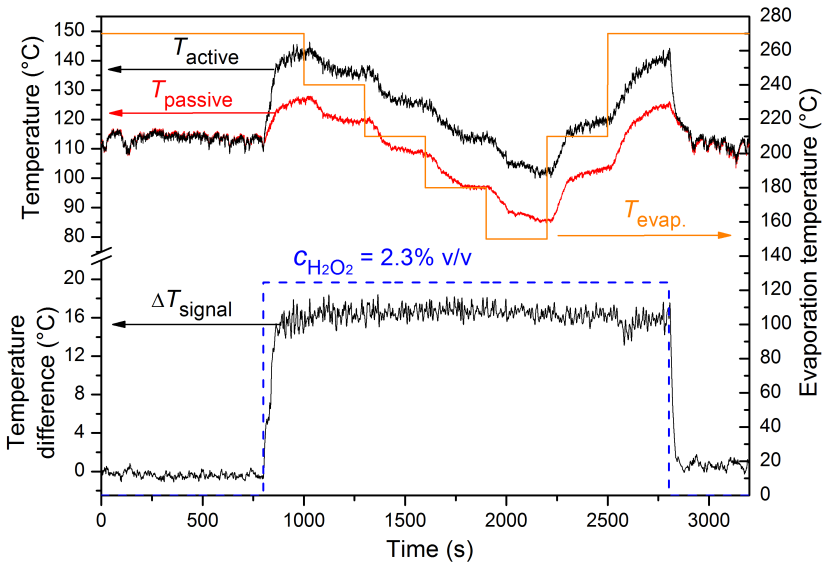

Figure 5.9: Influence of evaporation temperature (varied between 150 and 270 °C) on the polyimide-based sensor device at a constant H_2O_2 concentration of 2.3% v/v and flow rate of 10 m^3/h.

5.5 Conclusions

In the present work, a calorimetric gas sensor was successfully fabricated in form of an "on chip" differential set-up of a catalytically activated and a passivated platinum thin-film resistance on a polyimide foil (Kapton® HN from DuPont) for monitoring vapour-phase hydrogen peroxide in sterilisation processes of aseptic filling machineries. In this sensor set-up, a dispersion of manganese(IV) oxide serves as catalyst for hydrogen peroxide. A reaction mechanism has been proposed, wherein hydrogen peroxide is decomposed into hydroxyl radicals by cleavage of the O-O binding in an initial step followed by a chain reaction between surface-near radicals and hydrogen peroxide. During the H_2O_2 decomposition, reaction enthalpy is released, which causes a temperature increase on the active sensor segment depending on the present H_2O_2 concentration. In a H_2O_2 concentration range of 0-8% v/v, the calorimetric sensor device has shown a linear response behaviour with a sensitivity of 7.15 °C/(% v/v) and a response time ($t_{90\%}$) of 5.7 s that is comparable to the theoretical value (4.7 s) determined by a thermal equivalent circuit. In addition, by varying the evaporation temperature no change in the sensor signal could be observed. This demonstrates the suitability of the calorimetric gas sensor for monitoring the H_2O_2 concentration in sterilisation processes of aseptic filling machineries.

Acknowledgements

The authors thank the Bundesministerium für Bildung und Forschung and VDI/VDE for financial support of this work, project "Intellipack".

References

[1] Moruzzi, G., Garthright, W. E., and Floros, J. D. Aseptic packaging machine pre-sterilisation and package sterilisation: statistical aspects of microbiological validation. *Food Control 11*, 1 (2000), 57–66.

[2] Gould, G. W. Methods for preservation and extension of shelf life. *International Journal of Food Microbiology 33*, 1 (1996), 51–64.

[3] Cerny, G. Testing of aseptic machines for efficiency of sterilization of packaging materials by means of hydrogen peroxide. *Packaging Technology and Science 5*, 2 (1992), 77–81.

[4] Kirchner, P., Ng, Y. A., Spelthahn, H., Schneider, A., Henkel, H., Friedrich, P., Kolstad, J., Berger, J., Keusgen, M., and Schöning, M. J. Gas sensor investigation based on a catalytically activated thin-film thermopile for H_2O_2 detection. *Physica Status Solidi A 207*, 4 (2010), 787–792.

[5] Kirchner, P., Li, B., Spelthahn, H., Henkel, H., Schneider, A., Friedrich, P., Kolstad, J., Keusgen, M., and Schöning, M. J. Thin-film calorimetric H_2O_2 gas sensor for the validation of germicidal effectivity in aseptic filling processes. *Sensors and Actuators B: Chemical 154*, 2 (2011), 257–263.

[6] Glassbrenner, C. J., and Slack, G. A. Thermal conductivity of silicon and germanium from 3 K to the melting point. *Physical Review 134*, 4A (1964), A1058–A1069.

[7] Morf, T., Biber, C., and Bachtold, W. Effects of epitaxial lift-off on the DC, RF, and thermal properties of MESFET's on various host materials. *IEEE Transactions on Electron Devices 45*, 7 (1998), 1407–1413.

[8] Ralston, A. R., Klein, C. F., Thoma, P. E., and Denton, D. D. A model for the relative environmental stability of a series of polyimide capacitance humidity sensors. *Sensors and Actuators B: Chemical 34*, 1–3 (1996), 343–348.

[9] Lee, C.-Y., Wu, G.-W., and Hsieh, W.-J. Fabrication of micro sensors on a flexible substrate. *Sensors and Actuators A: Physical 147*, 1 (2008), 173–176.

[10] Oprea, A., Barsan, N., Weimar, U., Bauersfeld, M.-L., Ebling, D., and Wöllenstein, J. Capacitive humidity sensors on flexible RFID labels. *Sensors and Actuators B: Chemical 132*, 2 (2008), 404–410.

[11] Wessa, T., Barié, N., Rapp, M., and Ache, H. J. Polyimide, a new shielding layer for sensor applications. *Sensors and Actuators B: Chemical 53*, 1–2 (1998), 63–68.

[12] Mahmood, A., Butler, D. P., and Celik-Butler, Z. Micromachined bolometers on polyimide. *Sensors and Actuators A: Physical 132*, 2 (2006), 452–459.

[13] Dayeh, S. A., Butler, D. P., and Celik-Butler, Z. Micromachined infrared bolometers on flexible polyimide substrates. *Sensors and Actuators A: Physical 118*, 1 (2005), 49–56.

[14] Xiao, S. Y., Che, L. F., Li, X. X., and Wang, Y. L. A novel fabrication process of MEMS devices on polyimide flexible substrates. *Microelectronic Engineering 85*, 2 (2008), 452–457.

[15] Lichtenwalner, D. J., Hydrick, A. E., and Kingon, A. I. Flexible thin film temperature and strain sensor array utilizing a novel sensing concept. *Sensors and Actuators A: Physical 135*, 2 (2007), 593–597.

[16] Kim, Y. S. Microheater-integrated single gas sensor array chip fabricated on flexible polyimide substrate. *Sensors and Actuators B: Chemical 114*, 1 (2006), 410–417.

[17] Aslam, M., Gregory, C., and Hatfield, J. V. Polyimide membrane for micro-heated gas sensor array. *Sensors and Actuators B: Chemical 103*, 1–2 (2004), 153–157.

[18] Briand, D., Colin, S., Courbat, J., Raible, S., Kappler, J., and de Rooij, N. Integration of MOX gas sensors on polyimide hotplates. *Sensors and Actuators B: Chemical 130*, 1 (2008), 430–435.

[19] Näther, N., Juárez, L. M., Emmerich, R., Berger, J., Friedrich, P., and Schöning, M. J. Detection of hydrogen peroxide (H_2O_2) at exposed temperatures for industrial processes. *Sensors 6*, 4 (2006), 308–317.

[20] Näther, N., Henkel, H., Schneider, A., and Schöning, M. J. Investigation of different catalytically active and passive materials for realising a hydrogen peroxide gas sensor. *Physica Status Solidi A 206*, 3 (2009), 449–454.

[21] Hart, A. B., McFadyen, J., and Ross, R. A. Solid-oxide-catalyzed decomposition of hydrogen peroxide vapour. *Transactions of the Faraday Society 59* (1963), 1458–1469.

[22] Salem, I. A., El-Maazawi, M., and Zaki, A. B. Kinetics and mechanisms of decomposition reaction of hydrogen peroxide in presence of metal complexes. *International Journal of Chemical Kinetics 32*, 11 (2000), 643–666.

[23] Ono, Y., Matsumura, T., Kitajima, N., and Fukuzumi, S. Formation of superoxide ion during the decomposition of hydrogen peroxide on supported metals. *The Journal of Physical Chemistry 81*, 13 (1977), 1307–1311.

[24] Giamello, E., Rumori, P., Geobaldo, F., Fubini, B., and Paganini, M. The interaction between hydrogen peroxide and metal oxides: EPR investigations. *Applied Magnetic Resonance 10*, 1 (1996), 173–192.

[25] Anpo, M., Che, M., Fubini, B., Garrone, E., Giamello, E., and Paganini, M. Generation of superoxide ions at oxide surfaces. *Topics in Catalysis 8*, 3 (1999), 189–198.

[26] Salem, I. A., Elhag, R. I., and Khalil, K. M. S. Catalytic activity of a zirconium(IV) oxide surface supported with transition metal ions. *Transition Metal Chemistry 25*, 3 (2000), 260–264.

[27] Do, S.-H., Batchelor, B., Lee, H.-K., and Kong, S.-H. Hydrogen peroxide decomposition on manganese oxide (pyrolusite): kinetics, intermediates, and mechanism. *Chemosphere 75*, 1 (2009), 8–12.

[28] Hasan, M. A., Zaki, M. I., Pasupulety, L., and Kumari, K. Promotion of the hydrogen peroxide decomposition activity of manganese oxide catalysts. *Applied Catalysis A: General 181*, 1 (1999), 171–179.

[29] Lee, Y. N., Lago, R. M., Fierro, J. L. G., and González, J. Hydrogen peroxide decomposition over $Ln_{1-x}a_xMnO_3$ (Ln = La or Nd and A = K or Sr) perovskites. *Applied Catalysis A: General 215*, 1–2 (2001), 245–256.

[30] Kanungo, S. B., Parida, K. M., and Sant, B. R. Studies on MnO_2-III. the kinetics and the mechanism for the catalytic decomposition of H_2O_2 over different crystalline modifications of MnO_2. *Electrochimica Acta 26*, 8 (1981), 1157–1167.

[31] Haber, F., and Weiss, J. The catalytic decomposition of hydrogen peroxide by iron salts. *Proceedings of the Royal Society of London. Series A - Mathematical and Physical Sciences 147*, 861 (1934), 332–351.

[32] Hiroki, A., and LaVerne, J. A. Decomposition of hydrogen peroxide at water-ceramic oxide interfaces. *The Journal of Physical Chemistry 109*, 8 (2005), 3364–3370.

[33] Auerbach, F. J., Meiendres, G., Müller, R., and Scheller, G. J. E. Simulation of the thermal behaviour of thermal flow sensors by equivalent electrical circuits. *Sensors and Actuators A: Physical 41*, 1–3 (1994), 275–278.

[34] Kolev, S. D., Ádám, M., Bársony, I., van den Berg, A., Cobianu, C., and Kulinyi, S. Mathematical modelling of a porous silicon-based pellistor-type catalytic flammable gas sensor. *Microelectronics Journal 29*, 4–5 (1998), 235–239.

[35] van der Heide, P., Ed. *X-ray photoelectron spectroscopy: an introduction to principles and practices.* John Wiley & Sons, Hoboken, 2011.

[36] Chen, H., Dong, X., Shi, J., Zhao, J., Hua, Z., Gao, J., Ruan, M., and Yan, D. Templated synthesis of hierarchically porous manganese oxide with a crystalline nanorod framework and its high electrochemical performance. *Journal of Materials Chemistry 17*, 9 (2007), 855–860.

[37] Nesbitt, H. W., and Banerjee, D. Interpretation of XPS Mn(2p) spectra of Mn oxyhydroxides and constraints on the mechanism of MnO_2 precipitation. *American Mineralogist 83*, 3–4 (1998), 305–315.

[38] Rao, C. N. R., Sarma, D. D., Vasudevan, S., and Hegde, M. S. Study of transition metal oxides by photoelectron spectroscopy. *Proceedings of the Royal Society of London. A. Mathematical and Physical Sciences 367*, 1729 (1979), 239–252.

[39] Oku, M., Hirokawa, K., and Ikeda, S. X-ray photoelectron spectroscopy of manganese-oxygen systems. *Journal of Electron Spectroscopy and Related Phenomena 7*, 5 (1975), 465–473.

[40] Oku, M., and Hirokawa, K. X-ray photoelectron spectroscopy of Co_3O_4, Fe_3O_4, Mn_3O_4, and related compounds. *Journal of Electron Spectroscopy and Related Phenomena 8*, 5 (1976), 475–481.

[41] Foord, J. S., Jackman, R. B., and Allen, G. C. An X-ray photoelectron spectroscopic investigation of the oxidation of manganese. *Philosophical Magazine A 49*, 5 (1984), 657–663.

[42] McBride, J. R., Nietering, K. E., and Ellwood, K. R. Design considerations for optimizing the sensitivity of catalytic calorimetric gas sensors: modeling and experimental results. *Sensors and Actuators B: Chemical 73*, 2–3 (2001), 163–173.

[43] Welty, J., Wicks, C., Rorrer, G., and Wilson, R. *Fundamentals of momentum, heat and mass transfer*, 5 ed. John Wiley & Sons Inc., 2007.

[44] Reid, R., Prausnitz, J., and Poling, B. *The properties of gases and liquids*, 4 ed. McGraw-Hill series in chemical engineering. McGraw-Hill Book Company, 1987.

[45] Glenn Research Center, NASA. Database of thermodynamic properties, `http://www.grc.nasa.gov`, date: 21 July 2010.

5.6 Supporting information[2]

5.6.1 X-ray photoelectron spectroscopy

The mangenese oxide catalyst has further been investigated by X-ray photoelectron spectroscopy (XPS). XPS is a surface analysis technique. The basic mechanism of XPS relies on the photoelectric effect. If a material probe is irradiated by a beam of X-ray, electrons eject from the probe surface with a characteristical kinetic energy, once the photonic energy is higher than the quantified binding energy of the electron. The kinetic energy and the number of electrons that ejects from the probe surface generates an energy peak with specific intensity on a detector, whereby the binding energy of the electron can be determined. Thus, XPS can be used for studying the electronic state of elements within a material surface as well as the oxidation states of its chemical compounds. A detailed description of XPS technique is given in [35].

In the present work, the XPS analysis has at first been conducted in order to observe any changes in the elemental composition of the pure manganese oxide particles, before and after they were exposed to H_2O_2. In Fig. 5.10(a), the XPS spectra of the manganese oxide, before and once they were exposed to H_2O_2 are shown. Therein, the typical binding energies of Mn ($2p_{1/2}$) and ($2p_{3/2}$) as well as of O (1s) can be clearly identified in both spectra [36]. However, by taking a closer look to the Mn ($2p_{3/2}$) peak (s. Fig. 5.10(b)), a difference of both spectra can be seen resulting from a change in the oxidation state of manganese. The initial manganese oxide particles show an almost sharp peak at a binding energy of 641.9 eV resulting from the oxidation state of Mn^{4+} in manganese(IV) oxide (MnO_2). The particles after H_2O_2 treatment have a small plateau around 642.1 and 640.9 eV, indicating further oxidation states of mangenese (Mn^{3+} in manganese(III) oxide (Mn_2O_3), $Mn^{2+/3+}$ in manganese(II/III) oxide (Mn_3O_4) as well as Mn^{2+} in manganese(II) oxide (MnO)) according to Tab. 5.1. Thus, the XPS analysis demonstrates that the mangenese gets reduced in H_2O_2 resulting in a phase change on the surface of the manganese oxide particles due to an electron exchange of the initial reaction step (s. section 5.3.2). However, it seems that the catalytical activity is not influenced from this phenomenon because the sensor's sensitivity does not alter during measurements in H_2O_2 atmosphere.

In a further XPS analysis, the prepared catalytically active dispersion of manganese oxide with SU-8 photoresist as adhesive component was studied by means of XPS to find out, how the mangenese oxide particles are embedded inside the SU-8 photoresist. Therefore, the XPS analysis of the dispersion was conducted, directly after it was drop-coated on the sensor surface and once, the sensor was situated in the H_2O_2 flow for a short

[2]Note: Results of section 5.6.1 and section 5.6.2 are not part of the present article and will be published separately.

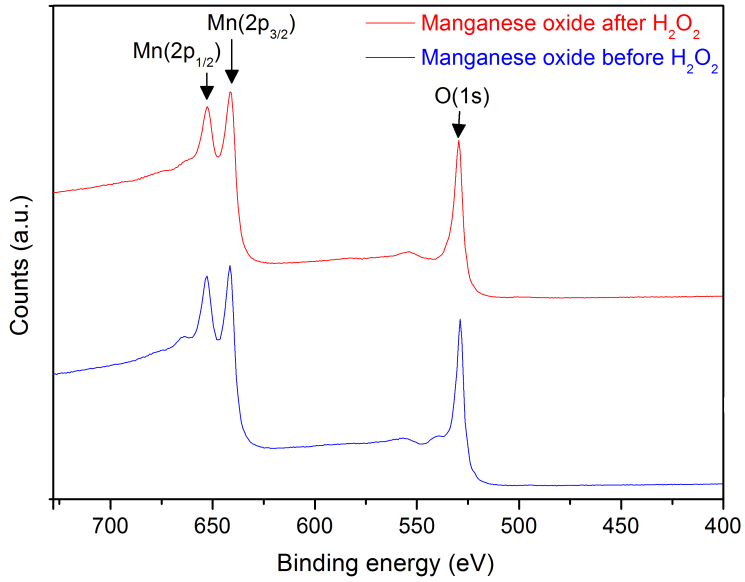

(a)

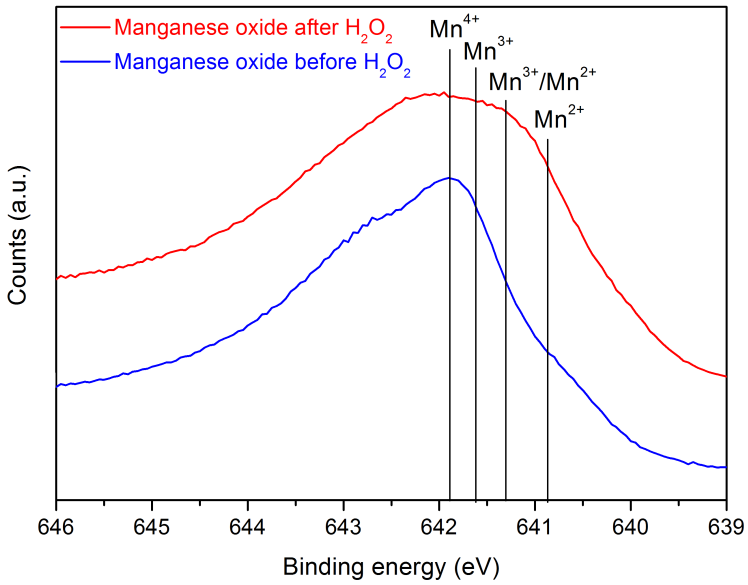

(b)

Figure 5.10: (a) XPS spectra of the pure manganese oxide particles, before (lower curves) and after (upper curves) they were exposed to H_2O_2 atmosphere. (b) Difference in the intensity of the Mn ($2p_{3/2}$) peak, before and after the manganese oxide was exposed to H_2O_2.

Table 5.1: Phase of manganese oxide, binding energy maxima of Mn ($2p_{3/2}$) and oxidation states of manganese (adopted from [37]).

Phase	Binding energy (eV)	Oxidation state	Ref.
MnO_2	641.9	4+	[38]
Mn_2O_3	641.7	3+	[39]
Mn_3O_4	641.4	2+/3+	[39, 40]
MnO	640.9	2+	[41]

exposure time (conditioning phase). In Fig. 5.11, the XPS spectra of the drop-coated dispersion, before and once, it was exposed to H_2O_2, are shown. From the spectrum of the dispersion before H_2O_2 exposition, a strong peak can be identified at 284 eV resulting from the carbon fraction (C (1s)) of the SU-8 photoresist, whereas the characteristical binding energies of manganese oxide (Mn ($2p_{1/2}$) and ($2p_{3/2}$) as well as of O (1s)) are rather low. This indicates that the manganese oxide particles are strongly covered by the SU-8 photoresist after the dispersion was deposited via drop-coating on the sensor surface. However, after a conditioning phase in H_2O_2, the C (1s) peak of the carbon fraction of SU-8 photoresist is sharply shrunk and at the same moment, the binding

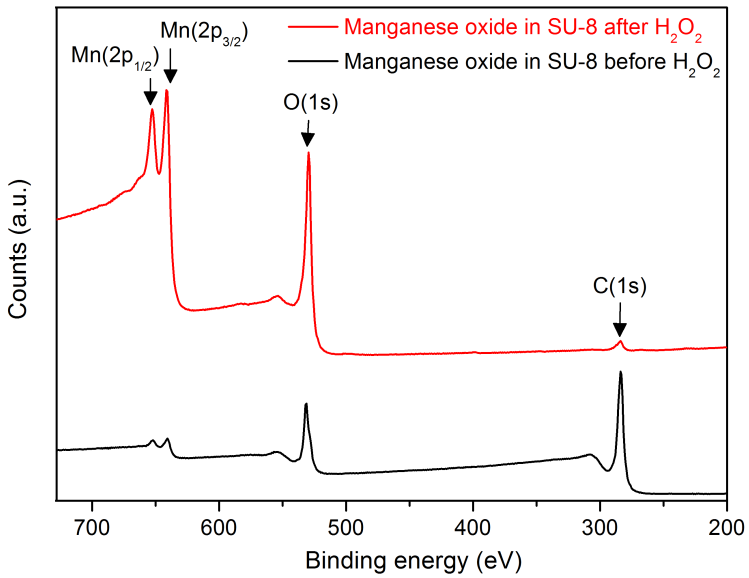

Figure 5.11: XPS spectra of manganese oxide particles embedded in SU-8 photoresist (drop-coated dispersion), before (lower curve) and after (upper curve) it was exposed to H_2O_2 atmosphere.

energies resulting from the manganese oxide are strongly increased. This indicates that the manganese oxide particles are almost completely bared after a short conditioning phase in H_2O_2.

5.6.2 Theoretical consideration of the sensor's sensitivity

In the following, a theoretical consideration of the sensor response in terms of the concentration-dependent temperature rise is given, wherein an overall H_2O_2 decomposition on the sensor surface is presupposed. Therein, the temperature rise is at first, merely calculated in case of an exothermic surface reaction for a stationary H_2O_2 atmosphere (without convection) and without any diffusion effects. In a following model, diffusion effects are also comprised into the calculation, and in a final step, the forced gas flow is introduced as well. The developed calculation models are derived from the eminent work of McBride et *al.* [42].

Temperature rise caused by exothermic surface reaction alone (stationary condition)

First of all, the maximum temperature rise is simply calculated by taking the change of the reaction enthalpy into account and ignoring the influence of the gas flow as well as of diffusion effects. Assuming that the decomposition occurs at constant pressure, the total heat released from the exothermic surface reaction can be described by Eq. 5.11:

$$\Delta Q = n_\mathrm{v} \cdot \Delta_\mathrm{R} H = \rho_\mathrm{c} \cdot c_\mathrm{c} \cdot \Delta T_\infty \tag{5.11}$$

where n_v is the number density of H_2O_2, ρ_c and c_c are the density and specific heat of the carrier gas stream, respectively, and ΔT_∞ is the resulting, maximum temperature rise.

The number density can be described by Eq. 5.12:

$$n_\mathrm{v} = \frac{\dot{n}_{\mathrm{H_2O_2}}}{\dot{V}_\mathrm{c}} \tag{5.12}$$

Here, $\dot{n}_{\mathrm{H_2O_2}}$ is the molar flow of H_2O_2 and $\dot{V}_\mathrm{c}$ is the volume flow rate of the carrier gas stream.

For a considered H_2O_2 concentration range up to 7.5% v/v and a volume flow of 10 m^3/h, values for molar flow as well as the number density of H_2O_2 are presented in Tab. 5.2.

The resulting temperature rise (ΔT_∞) defines the upper limit of the sensor response. For a reaction enthalpy of -105.3 kJ/mol and the values for ρ_c and c_c given in Tab. 5.3,

a maximum sensor response can be calculated according to Eq. 5.13:

$$\Delta T_\infty = c_{\mathrm{H_2O_2}} \cdot 24.1\ ^\circ\mathrm{C}/(\%\ \mathrm{v/v}) \tag{5.13}$$

with $c_{\mathrm{H_2O_2}}$ as H_2O_2 concentration.

However, this upper limit of temperature rise can only be attained for low gas flows and when diffusion effects are neglected.

Table 5.2: Relation between concentration, molar flow and number density of H_2O_2 for a considered volume flow of 10 m^3/h.

$c_{\mathrm{H_2O_2}}$ (% v/v)	$\dot{n}_{\mathrm{H_2O_2}}$ (mmol/s)	n_v (mol/m^3)
0	0	0
2.3	28.9	0.30
4.2	57.9	0.60
5.7	86.8	0.90
7.1	116	1.20
7.5	127	1.32

Temperature rise calculation involving gas diffusion

For a more precise description of the temperature rise, heat and mass transport merely induced by diffusion effects are introduced into the calculation. The temperature rise can then be described as:

$$\Delta T_\mathrm{d} = \frac{D_{\mathrm{H_2O_2}} \cdot n_\mathrm{v} \cdot \Delta_\mathrm{R} H}{k_\mathrm{c}} \tag{5.14}$$

Here, $D_{\mathrm{H_2O_2}}$ is the diffusion coefficient of H_2O_2 in air and k_c is the thermal conductivity of the carrier gas stream.

The temperature-dependent diffusion coefficient can be determined with the Chapman-Enskog theory according to Eq. 5.15 [43]:

$$D_{\mathrm{H_2O_2}} = \frac{1.858 \cdot 10^{-3} \cdot T^{3/2} \sqrt{1/M_{\mathrm{H_2O_2}} + 1/M_\mathrm{air}}}{p \cdot \sigma^2_{\mathrm{H_2O_2}/air} \cdot \Omega} \tag{5.15}$$

where T is the gas temperature, $M_{\mathrm{H_2O_2}}$ and M_air are the molar mass of H_2O_2 and air, respectively, p is the absolute pressure, $\sigma_{\mathrm{H_2O_2}/air}$ is the collision diameter and Ω is the collision integral both given in [44].

For a calculated diffusion coefficient of $3.06 \cdot 10^{-5}$ m^2/s and the thermal conductivity of the carrier gas stream given in Tab. 5.3, the diffusion-limited temperature rise of the

sensor results in:

$$\Delta T_{\mathrm{d}} = c_{\mathrm{H_2O_2}} \cdot 14.4\,^{\circ}\mathrm{C}/(\%\ \mathrm{v/v}) \tag{5.16}$$

At this point, it is important to note that in case of mass and heat transport accompanied by diffusion alone, the calculated temperature rise is excluded from the impact of a forced gas flow. Furthermore, geometrical aspects of the sensor's catalytic surface area are neglected in this calculation.

Temperature rise calculation comprising forced gas convection and gas diffusion

In a final consideration, the sensor response is determined by including the impact of a forced gas flow besides diffusion effects into the calculation. Starting from the energy balance equation (s. Eq. 5.11), wherein the transfer coefficients for mass (h_{mass}) and heat (h_{heat}) are additionally introduced,

$$\Delta Q = h_{\mathrm{mass}} \cdot n_{\mathrm{v}} \cdot \Delta_{\mathrm{R}} H = h_{\mathrm{heat}} \cdot \rho_{\mathrm{c}} \cdot c_{\mathrm{c}} \cdot \Delta T_{\mathrm{f}} \tag{5.17}$$

These coefficients comprise the characteristics of the forced gas flow and the gas diffusion as well as the sensor's geometry. In this case, the sensor is simply considered as a sphere situated in the gas flow. According to the description given by McBride et *al.* [42], the transfer coefficients can be expressed as:

$$h_{\mathrm{mass}} = \frac{D_{\mathrm{H_2O_2}}}{r_{\mathrm{s}} \cdot (1 + 0.3 \cdot N_{\mathrm{Re}}^{1/2} \cdot N_{\mathrm{Sc}}^{1/3})} \tag{5.18}$$

$$h_{\mathrm{heat}} = \frac{k_{\mathrm{c}}}{r_{\mathrm{s}} \cdot (1 + 0.3 \cdot N_{\mathrm{Re}}^{1/2} \cdot N_{\mathrm{Pr}}^{1/3})} \tag{5.19}$$

Here, N_{Re}, N_{Sc}, N_{Pr} are the Reynolds, Schmitd and Prandtl number and r_{s} is the radius of the sensor's geometry simplified as sphere.

The temperature rise depending on the forced gas flow can then be expressed by:

$$\Delta T_{\mathrm{f}} = \frac{n_{\mathrm{v}} \cdot D_{\mathrm{H_2O_2}} \cdot \Delta_{\mathrm{R}} H}{k_{\mathrm{c}}} \cdot \frac{(1 + 0.3 \cdot N_{\mathrm{Re}}^{1/2} \cdot N_{\mathrm{Sc}}^{1/3})}{(1 + 0.3 \cdot N_{\mathrm{Re}}^{1/2} \cdot N_{\mathrm{Pr}}^{1/3})} \tag{5.20}$$

The Reynolds number is described by Eq. 5.21:

$$N_{\mathrm{Re}} = \frac{2 \cdot r_{\mathrm{s}} \cdot \rho_{\mathrm{c}} \cdot v_{\mathrm{c}}}{\mu_{\mathrm{c}}} \tag{5.21}$$

where v_{c} is the gas velocity and μ_{c} is the viscosity of the carrier gas stream.

The Schmidt number can be expressed by Eq. 5.22:

$$N_{\mathrm{Sc}} = \frac{\mu_{\mathrm{c}}}{\rho_{\mathrm{c}} \cdot D_{\mathrm{H_2O_2}}} \tag{5.22}$$

and the Prandtl number can be calculated by Eq. 5.23:

$$N_{\mathrm{Pr}} = \frac{c_{\mathrm{p}} \cdot \mu_{\mathrm{c}}}{k_{\mathrm{c}}} \tag{5.23}$$

According to the given process conditions and the values presented in Tab. 5.3, the maximum temperature rise on the sensor surface for a forced gas flow could be calculated as:

$$\Delta T_{\mathrm{f}} = c_{\mathrm{H_2O_2}} \cdot 15.9\,^{\circ}\mathrm{C}/(\%\ \mathrm{v/v}) \tag{5.24}$$

Table 5.3: Density, specific heat, thermal conductivity, gas velocity and viscosity of the carrier gas stream at elevated gas temperature of 270 °C and a volume flow of 10 m^3/h (adapted from [43, 45]).

ρ_{c} ($\mathrm{kg/m^3}$)	c_{c} ($\mathrm{J/(kg \cdot K)}$)	k_{c} ($\mathrm{W/(m \cdot K)}$)	v_{c} (m/s)	μ_{c} ($\mathrm{Pa \cdot s}$)
0.693	1034	0.0404	6.22	$27.6 \cdot 10^{-6}$

The results of the three different calculation models of the sensor's sensitivity as well as the actual sensitivity ($\Delta T_{\mathrm{signal}}$) are listed in Tab. 5.4. The resulting difference between the actual sensitivity of the sensor (7.15°C/(% v/v)) and the calculated sensitivity for a forced gas flow (15.9°C/(% v/v)), wherein the actual sensitivity is quite lower than the calulated one, could result from a heat loss by radiation as well as from an incomplete decomposition of the H_2O_2 on the catalytic surface of the sensor.

Table 5.4: Comparison of the sensitivity determined by the calculation models as well as the actual sensor's sensitivity.

ΔT_{∞} (°C/(% v/v))	ΔT_{d} (°C/(% v/v))	ΔT_{f} (°C/(% v/v))	$\Delta T_{\mathrm{signal}}$ (°C/(% v/v))	$\Delta T_{\mathrm{signal}}/\Delta T_{\mathrm{f}}$ (%)
24.1	14.4	15.9	7.15	45

6 Realisation of a calorimetric gas sensor on polyimide foil for applications in aseptic food industry

KIRCHNER, P., Oberländer, J., Friedrich, P., Berger, J., Rysstad, G., Keusgen, M., and Schöning, M. J.

Sensors and Actuators B 170 (2012), 60–66.

6.1 Abstract

A calorimetric gas sensor is presented for the monitoring of vapour-phase H_2O_2 at elevated temperature during sterilisation processes in aseptic food industry. The sensor was built up on a flexible polyimide foil (thickness: 25 μm) that has been chosen due to its thermal stability and low thermal conductivity. The sensor set-up consists of two temperature-sensitive platinum thin-film resistances passivated by a layer of SU-8 photo resist and catalytically activated by manganese(IV) oxide. Instead of an active heating structure, the calorimetric sensor utilises the elevated temperature of the evaporated H_2O_2 aerosol. In an experimental test rig, the sensor has shown a sensitivity of 4.78 °C/(% v/v) in a H_2O_2 concentration range of 0% v/v to 8% v/v. Furthermore, the sensor possesses the same, unchanged sensor signal even at varied medium temperatures between 210 °C and 270 °C of the gas stream. At flow rates of the gas stream from 8 m^3/h to 12 m^3/h, the sensor has shown only a slightly reduced sensitivity at a low flow rate of 8 m^3/h. The sensor characterisation demonstrates the suitability of the calorimetric gas sensor for monitoring the efficiency of industrial sterilisation processes.

6.2 Introduction

Polyimide as a thermally stable polymer that features outstanding abilities, like mechanical robustness, low weight, chemical inertness as well as beneficially isolating properties, is gaining more and more interest for applications in microsystems and especially, in sensor devices. Today, its application field in sensor devices is ranging from functional layers of humidity sensors [1–3], shielding layers for SAW sensors [4] to novel platforms for tactile [5, 6] and thermal sensors (e.g., bolometers [7], temperature sensor arrays [8, 9] and micro-hotplates integrated in gas sensors [10–12]).

In this work, a calorimetric gas sensor for monitoring sterilisation processes in aseptic filling systems for food is presented, which was built up on a flexible polyimide foil. Therein, the sterilisation of packages is the essential process for achieving a long shelf life of filled products and avoiding the transmission of pathogenic microorganisms, especially for perishable food such as milk and fruit juice [13, 14]. Among the variety of physical, thermal and chemical methods, hydrogen peroxide has become the most significant sterilisation agent for carton packages within the last decades. For a sufficient sterilisation efficiency at low exposure time, the packages have to be treated by hydrogen peroxide in combination with heat. Four procedures are predominantly established [15]: (*i*) carton packages are treated by a tempered hydrogen peroxide solution (dipping path); (*ii*) hot hydrogen peroxide aerosol is sprayed on the inner surface of packages; (*iii*) cold hydrogen peroxide aerosol is sprayed into packages that have been heat-treated (>120 °C) before to gain a phase change (liquid/gaseous) on the package surfaces; (*iv*) an aerosol of hydrogen peroxide solution (35% w/w), which has been vaporised (>250 °C), is streamed into the food packages. Procedures (*iii*) and (*iv*) have the advantage that the residence time can be enormously reduced (<2 s) and gaseous H_2O_2 decomposes quickly into water vapour and oxygen, so that no residues linger in the packages and can reach the filled products. In both cases, the sterilisation effect primarily depends on the present H_2O_2 concentration at the inner surface of the packages.

For monitoring the sterilisation process with vapour-phase hydrogen peroxide in-line, silicon-based calorimetric sensor chips have been developed in former works [16, 17]. However, these sensor chips lacks from a distinct influence towards the gas flow rate and gas temperature. To increase the sensor's sensitivity and to compensate the undesired influence of the above mentioned process parameters, a novel calorimetric gas sensor based on a flexible polyimide foil has been realised, which can operate under harsh ambient conditions (H_2O_2 concentration up to 8% v/v, gas-flow rate of 10 m^3/h, medium temperature up to 250 °C and elevated humidity of the gas stream). An additional advantage of the novel sensor chip is that it can be directly applied on curved and non-rigid surfaces, the critical locations of a food package during the sterilisation process.

6.3 Experimental

6.3.1 Sensor design and fabrication

The calorimetric gas sensor consists of a chip-based differential set-up of a catalytically activated and a passivated temperature-sensitive thin-film resistance, in a similar manner as in [17]. As sensor substrate, a flexible polyimide sheet was envisaged. The reason for using polyimide instead of conventional silicon as sensor substrate relies on the low thermal conductivity of 0.147 $Wm^{-1}K^{-1}$ [18] (compared to 156 $Wm^{-1}K^{-1}$ for silicon [19]) to guarantee a high sensitivity by avoiding the heat transfer between the active and passive sensor segment. In addition, polyimide shows a chemical inertness against hydrogen peroxide and an expedient mechanical stability as well as a sufficient thermal endurance up to 400 °C.

Today, two different methods are established in chip technology, in which polyimide is used as sensor substrate [8]: (*i*) a conventional silicon wafer is used, on which a liquid polyimide layer is spin-coated together with an adhesion layer and removed at the end of the fabrication process; (*ii*) a polyimide sheet is temporarily fixed by an adhesive on a carrier wafer throughout the fabrication process and separated after finishing. In this work, the second method was applied, wherein a polyimide foil (Kapton® HN from DuPont) with a thickness of 25 μm serves as sensor substrate. The polyimide foil was punctually fixed on a 3" silicon wafer by a two-component, high-temperature epoxy (Epotek® 353ND from Polytec). At first, the two components of the epoxy were mixed and afterwards, spotted in form of small droplets on the carrier wafer by a micro-syringe dispenser. The polyimide foil was subsequently attached on the wafer and to assure a sufficient adhesion the epoxy was cured at 100 °C for 10 min on a heating plate. In a following step, the thin-film resistances were deposited on the polyimide foil. For resistance structuring standard photolithography was utilised. Platinum with a thickness of 200 nm was deposited together with an adhesion layer of 20 nm titanium by means of physical vapour deposition and patterned as meander-shaped thin-film resistances on the polyimide foil via lift off. The width of the meander-shaped paths is 40 μm and the area of each thin-film resistance amounts to be 1.0 mm^2 that results in a theoretical resistance value of about 200 Ω at room temperature. To avoid the influence of humidity on the sensor and to insulate the thin-film resistances from the gas stream, the sensor chips were passivated by SU-8 photoresist (spin-coated at 3000 rpm and heat-treated at 175 °C), which is stable up to 350 °C as well as in highly concentrated H_2O_2 atmosphere, as demonstrated in [16]. In a following step, the polyimide foil was separated into single sensor chips with a chip size of 10 mm x 10 mm via scalpel (s. Fig. 6.1(a)) and consequently removed from the carrier wafer. Each sensor chip was finally activated by a

dispersion of manganese(IV) oxide (s. Fig. 6.1(b)) that enables a high catalytic activity for vapour-phase hydrogen peroxide compared to other possible catalysts [20–22]. The total fabrication process is schematically depicted in Fig. 6.2.

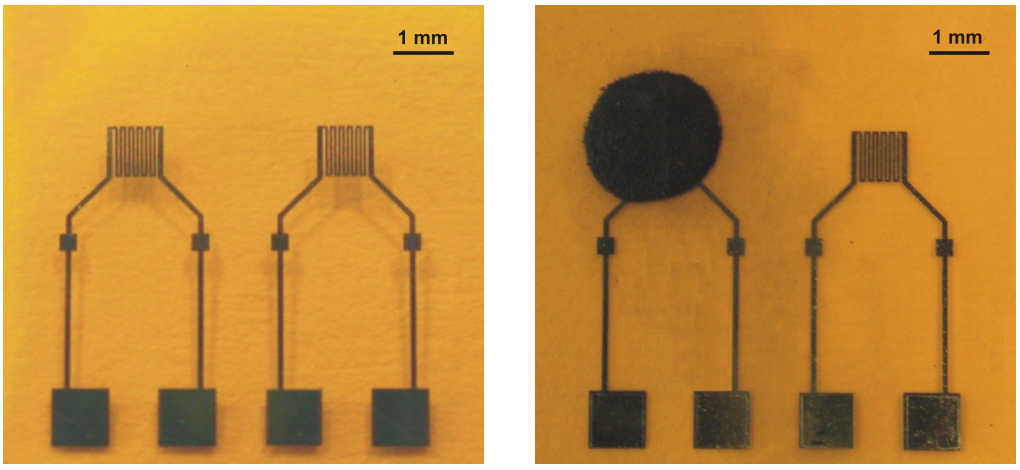

Figure 6.1: Calorimetric H_2O_2 gas sensor on polyimide foil (Kapton® HN) with a thickness of 25 μm; (a) fabricated thin-film resistances with contact pads on polyimide; (b) thin-film resistances with SU-8 photoresist as passivation and manganese(IV) oxide (left) as catalytically active layer (chip size: 10 mm x 10 mm).

After sensor fabrication, the polyimide-based sensor chip was fixed on a substrate holder by an epoxy resin (Epotek® 353ND, mentioned above) and electrically contacted to the substrate holder via silver conducting paste. Finally, the electrical contacts were encapsulated with the mentioned epoxy resin.

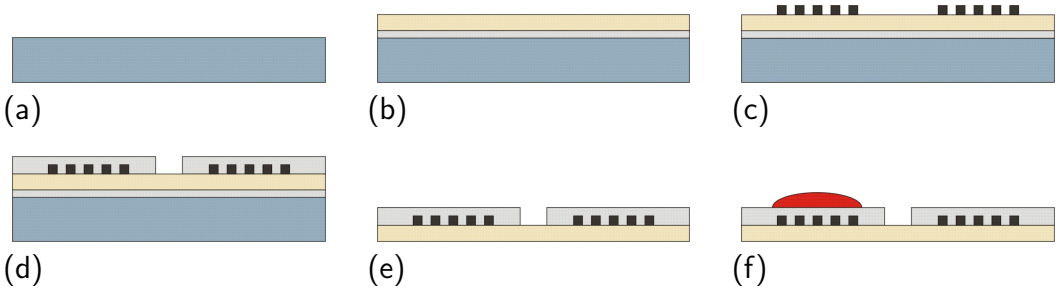

Figure 6.2: Schematic diagram of the fabrication steps of the polyimide-based sensor: (a) carrier wafer; (b) on which the polyimide foil is fixed by an adhesive layer; (c) deposition and patterning of the platinum thin-film resistances; (d) sensor passivation by spin-coated SU-8 photoresist; (e) separation of the polyimide foil from the carrier wafer by removing the adhesive layer; (f) deposition of a dispersion of manganese(IV) oxide as catalyst.

6.3.2 Sensor principle

The sensor principle is similar to that of the silicon-based sensors, introduced in [17]. If the calorimetric gas sensor is exposed to H_2O_2 atmosphere, a temperature difference between the active and passive sensor segment caused by the exothermal decomposition of hydrogen peroxide on the catalytic surface correlates with the present H_2O_2 concentration and serves as a sensor signal. Compared to conventional gas sensors, the differential set-up enables the minimisation or even the elimination of influences of temperature variations or changes in the gas flow on the sensor signal. In place of an active heating structure, the sensor utilises the elevated temperature of the sterilisation process for initialising the catalytic reaction mechanism. In the last decades, various reaction mechanisms for the decomposition of hydrogen peroxide over different metal and metal oxides have been discussed [23–27]. However, most of them are based on the classical Haber-Weiss mechanism [28], which predicts free radicals as intermediates. The total reaction mechanism of the exothermic H_2O_2 decomposition on the catalyst involves two pathways. The first relies on the initial reaction step, wherein two hydroxyl radicals are formed by cleavage of the O-O binding of a H_2O_2 molecule on the catalytic surface followed from either an electron exchange transfer between catalyst and hydrogen peroxide [24, 25] or a homolytic dissociation [26, 27]. The second pathway describes a chain reaction between the free radicals and hydrogen peroxide, wherein the final products, namely water vapour and oxygen, are formed and reaction enthalpy is released [24–27]. The stoichiometric relationship can be summarised in the following reaction:

$$2\ H_2O_2 \rightarrow 2\ H_2O + O_2 + \Delta_R H \tag{6.1}$$

where $\Delta_R H$ is the released reaction enthalpy.

The reaction kinetic follows a first-order decay and can be written as:

$$\frac{-\mathrm{d}c_{H_2O_2}}{\mathrm{d}t} = k \cdot c_{H_2O_2} \tag{6.2}$$

Therein, k is the decomposition rate coefficient, $c_{H_2O_2}$ is the H_2O_2 concentration and t is the resident time.

The resulting temperature increase on the active sensor segment arising from the released reaction enthalpy can be approximately described by the subsequent equation:

$$\Delta T_{\mathrm{reaction}} = c_{H_2O_2} \cdot \frac{\Delta_R H}{C_p} \tag{6.3}$$

Here, C_p is the heat capacity of the ambient air close to the catalyst surface of the sensor.

6.3.3 Measurement scheme

The characterisation of the calorimetric gas sensor was performed in an experimental test rig for simulating the sterilisation process with vaporised hydrogen peroxide [16, 17]. The test rig contains a dosing system with two piston pumps, one of them for H_2O_2 solution (35% w/w) and the other for deionised water, and a vaporisation unit consisting of two heater elements. For realising various H_2O_2 and water concentrations, the dosage of each liquid (H_2O_2 solution and deionised water) via piston pumps has to be adjusted. An air flow, which is controlled by a flow meter and a regulation valve, serves as carrier gas for both liquids. The heating power of the heating elements is electrically controlled by the measured medium temperature of the gas stream at the outlet nozzle of the vaporisation unit. The sensor with substrate holder is placed via mounting fixture in a distance of 5 cm beneath the outlet nozzle in a measuring chamber of the test rig and it is directly exposed to the gas flow without protecting shield, as like a mesh. The measuring chamber contains also a gas exhaust as gas outlet. For reading out the sensor signal of the calorimetric gas sensor a high-resolution data acquisition card (National Instruments, USB-9219) and a developed LabVIEW-based program was applied.

For the investigation of the calorimetric gas sensor, four different measurements were carried out in the experimental test rig. In a first measurement, the response behaviour of the calorimetric gas sensor that means its sensitivity, off-set as well as hysteresis was studied at varied H_2O_2 concentrations and at a constant gas-flow rate and medium temperature. Afterwards, the influence of humidity on the sensor signal was investigated in a second measurement. Therefore, the sensor was characterised at same H_2O_2 concentration steps with and without added water concentration (at constant gas flow and medium temperature). In a third measurement, the influence of variations in the medium temperature on the sensor signal was validated. During this test, the medium temperature was varied at same settings of H_2O_2 concentration for each temperature step and at a constant gas flow. Finally, the impact of changes in the gas flow on the sensor signal was studied. Therein, the gas flow was gradually increased at constant settings of H_2O_2 concentration and at a constant medium temperature.

6.4 Results and discussion

Before the calorimetric gas sensor was characterised in H_2O_2 atmosphere of the experimental test rig, the thin-film resistances of the active and passive sensor segment were calibrated in a temperature range between 10 °C and 85 °C in steps of 5 °C in a thermostat (RE 207 from LAUDA) (s. Fig. 6.3(a)).

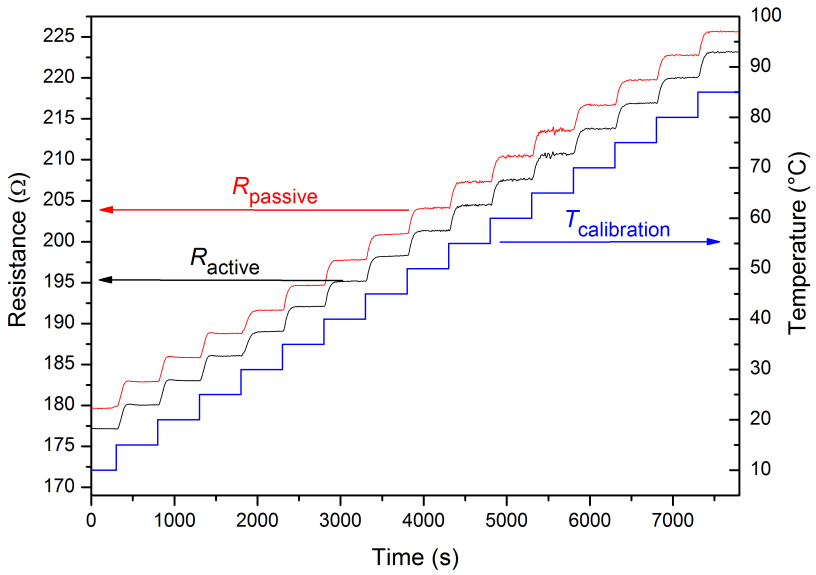

(a)

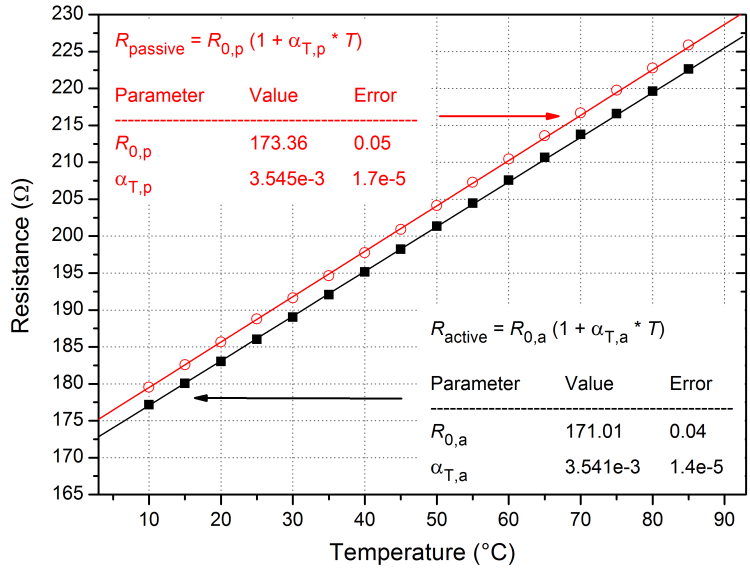

(b)

Figure 6.3: (a) Response characteristic of the thin-film resistances of active and passive sensor segment in a temperatures range between 10 °C and 8 °C, and (b) resulting temperature characteristic for each thin-film resistance of the sensor.

From the response behaviour of the thin-film resistances, the temperature characteristic for each resistance was ascertained (s. Fig. 6.3(b)). The temperature-dependent resistances of the active and passive sensor segment can be calculated by the following equations in linear approximation:

$$R_{\text{active}}(T) = 171.01\,\Omega \cdot (1 + 3.541 \cdot 10^{-3}\,^{\circ}C^{-1} \cdot T) \tag{6.4}$$

$$R_{\text{passive}}(T) = 173.36\,\Omega \cdot (1 + 3.546 \cdot 10^{-3}\,^{\circ}C^{-1} \cdot T) \tag{6.5}$$

Both resistances show almost the same temperature-dependent behaviour with a temperature coefficient of $3.54 \cdot 10^{-3}$ °C and a reference resistance of about 170 Ω.

After the temperature calibration of the thin-film resistances, the sensor-response behaviour was determined at increased H_2O_2 concentrations from 0% v/v to 8% v/v and *vice versa* in the experimental test rig (s. Fig. 6.4(a)). Each concentration step was kept for 300 s, respectively. A constant gas-flow rate of 10 m^3/h and a medium temperature of 240 °C were adjusted during this measurement. The temperature on the active sensor segment (T_{active}) has been raised from 138 °C at a H_2O_2 concentration of 0% v/v to a maximum value of 205 °C at a H_2O_2 concentration of 7.5% v/v, and on the passive sensor segment (T_{passive}) from 138 °C at 0% v/v to 171 °C at 7.5% v/v. The reason for the shift in the temperature on the passive sensor segment could rely on a heat transfer between the active and passive sensor segment during the catalytic H_2O_2 decomposition or even on a temperature change of the gas stream between different H_2O_2 concentrations because the heat capacity of the gas stream is influenced by added H_2O_2 resulting in a change of the heat transport from the vaporisation unit to the sensor. With rising H_2O_2 concentrations in the gas stream, the heat capacity increases and could generate a temperature raise on the sensor surface. To compensate variations in the temperature, the temperature difference (ΔT_{signal}) between the active and passive sensor segment served as sensor signal. From the calibration plot of the polyimide-based sensor (s. Fig. 6.4(b)), a sensitivity of 4.78 °C/(% v/v) and a low off-set of 0.35 °C can be determined. In addition, a maximum hysteresis of 1.98 °C at a H_2O_2 concentration of 4.2% v/v was observed, leading to a deviation in a measured H_2O_2 concentration of 0.4% v/v.

In a second experiment, the influence of humidity in the gas stream on the polyimide-based gas sensor was studied. Therein, the response behaviour of the sensor device was investigated at various H_2O_2 concentrations gradually changing between 0% v/v and 7% v/v without additional humidity, and in comparison to the same concentration steps with added water concentration of 25% v/v in the gas stream (s. Fig. 6.5(a)).

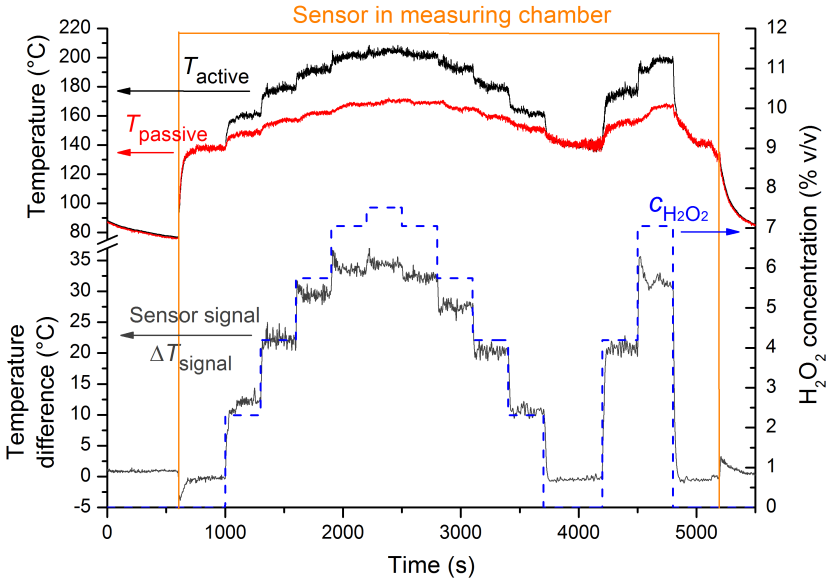

(a)

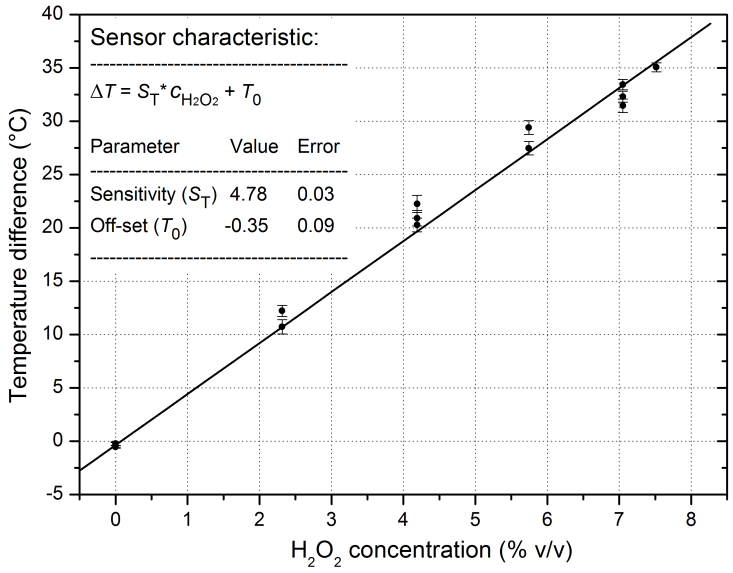

(b)

Figure 6.4: (a) Response behaviour of the calorimetric gas sensor on polyimide foil at various H_2O_2 concentrations up to 8% v/v (constant medium temperature of 240 °C and flow rate of 10 m^3/h), and (b) calibration plot of the calorimetric gas sensor.

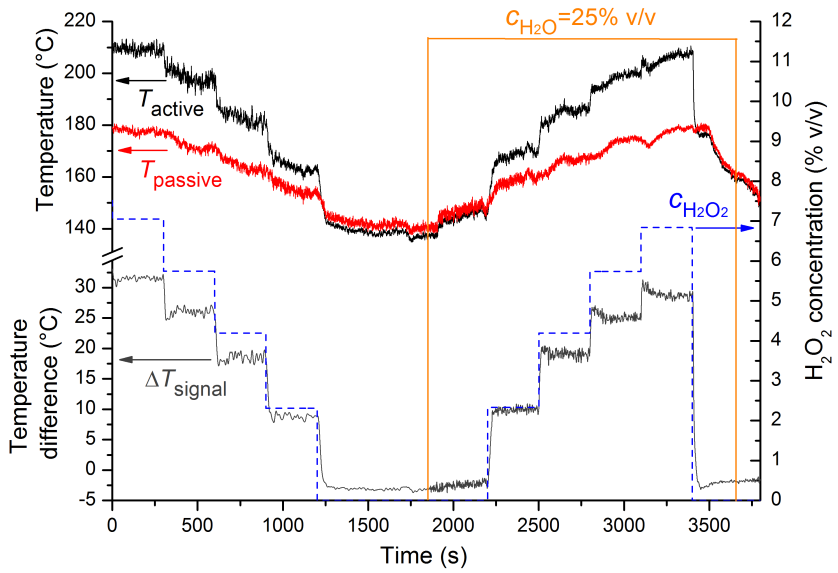

(a)

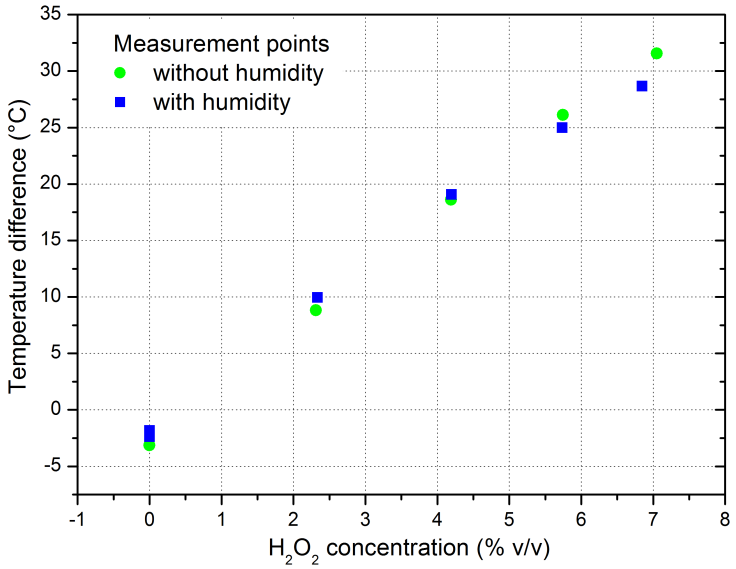

(b)

Figure 6.5: (a) Comparison between sensor-response behaviour without and with humidity of 25% v/v in gas stream (constant medium temperature of 240 °C and flow rate of 10 m^3/h), and (b) resulting temperature difference *vs.* H_2O_2 concentration with and without humidity.

Both sensor segments (T_{active} and T_{passive}) are strongly influenced by fluctuations in the gas stream during the measurement. However, the temperature difference (ΔT_{signal}) between the active and passive sensor segment at H_2O_2 concentration steps with humidity in the ambient air is in good compliance with the signal at concentration steps without humidity (s. Fig. 6.5(b)). Only at a high H_2O_2 concentration around 7.1% v/v with humidity in the ambient air a slightly lower sensor signal, compared to the signal without humidity, can be observed.

In addition, the influence of the medium temperature on the response behaviour of the calorimetric gas sensor was determined. Therefore, various H_2O_2 concentration steps between 0% v/v and 7.1% v/v were appointed for the medium temperatures of 210 °C, 240 °C and 270 °C, respectively (s. Fig. 6.6(a)). The temperature on the sensor surface (T_{active} and T_{passive} at 0% v/v) raised from 123 °C to 160 °C at increased medium temperatures from 210 °C to 270 °C. In spite of this change in the temperature on the sensor surface, the temperature difference (ΔT_{signal}) between the active and passive sensor segment is not influenced by the medium temperature itself, even by varying the H_2O_2 concentration in the investigated concentration range (s. Fig. 6.6(b)).

Finally, the impact of the gas-flow rate on the polyimide-based sensor was studied. For each gas flow rate of 8 m^3/h, 10 m^3/h and 12 m^3/h, different H_2O_2 concentrations varying from 0% v/v to 6.6% v/v were adjusted (s. Fig. 6.7(a)). Therein, the temperature on the sensor surface (T_{passive} and T_{active} at 0% v/v H_2O_2) increased from 114 °C to 149 °C with raising gas flow rate. However, concerning the temperature difference (ΔT_{signal}), only at the lowest flow rate of 8 m^3/h, a decreased sensor signal of ca. 14% compared to the signal at high flow rates of 10 m^3/h and 12 m^3/h, respectively, was detected for each H_2O_2 concentration (s. Fig. 6.7(b)). The decreased sensor signal at a flow rate of 8 m^3/h could be caused by a heat transfer between the active and passive sensor segment during the catalytic reaction at a low flow rate. Here, due to the smaller exchange rate of the gas stream in comparison to the higher flow rate, this might result in an increased temperature on the passive sensor segment and includes a decrease of the temperature difference between both sensor segments.

6.5 Conclusions

In the current work, we have presented a calorimetric gas sensor for the detection of high H_2O_2 concentrations of up to 8% v/v at elevated temperatures in sterilisation processes of packages in aseptic filling rigs. The sensor has been successfully realised as an "on-chip" differential set-up of a catalytically activated and reference thin-film resistance on a thin and flexible polyimide foil (Kapton® HN). A differential set-up was envisaged to minimise the influence of variations in the medium temperature or in the gas flow

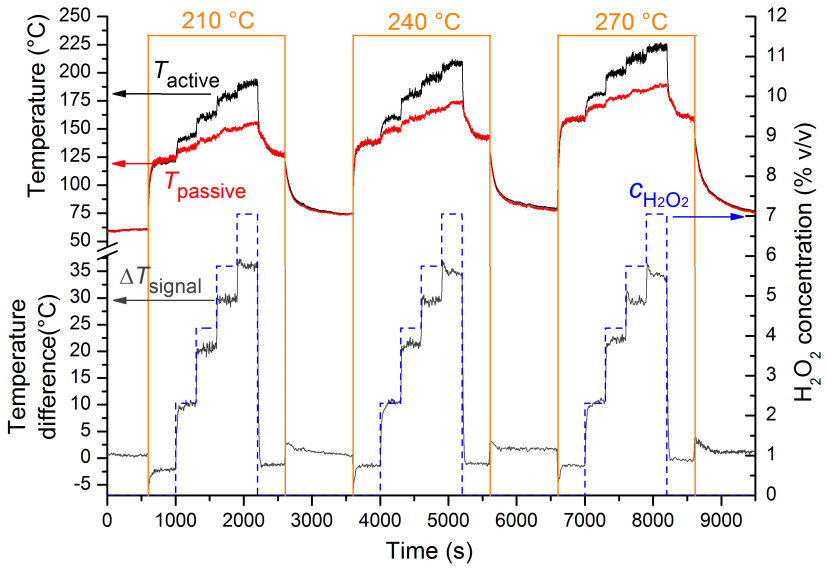

(a)

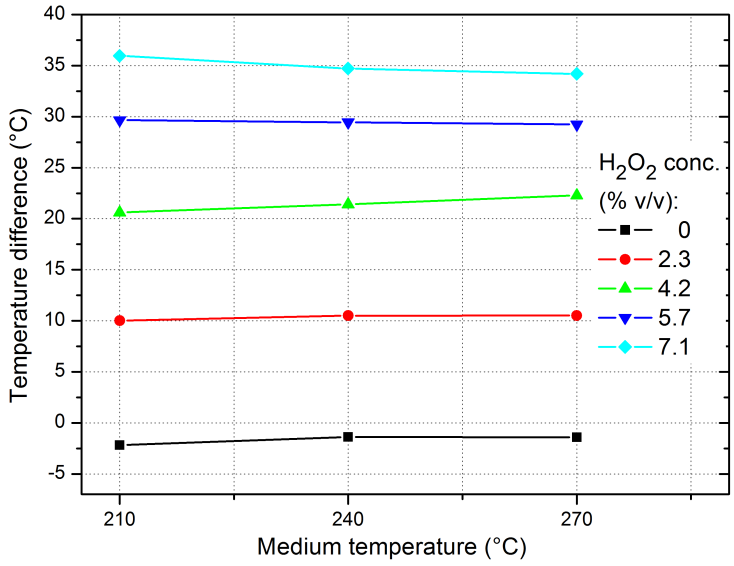

(b)

Figure 6.6: Influence of medium temperature (210 °C, 240 °C and 270 °C) on the sensor signal of the polyimide-based gas sensor (constant flow rate of 10 m^3/h), and (b) temperature difference *vs.* medium temperature plot at various H_2O_2 concentrations.

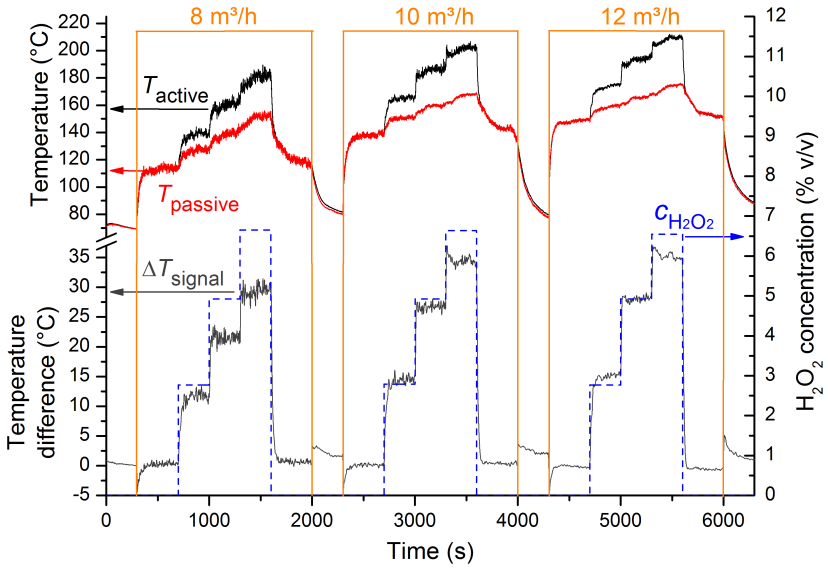

(a)

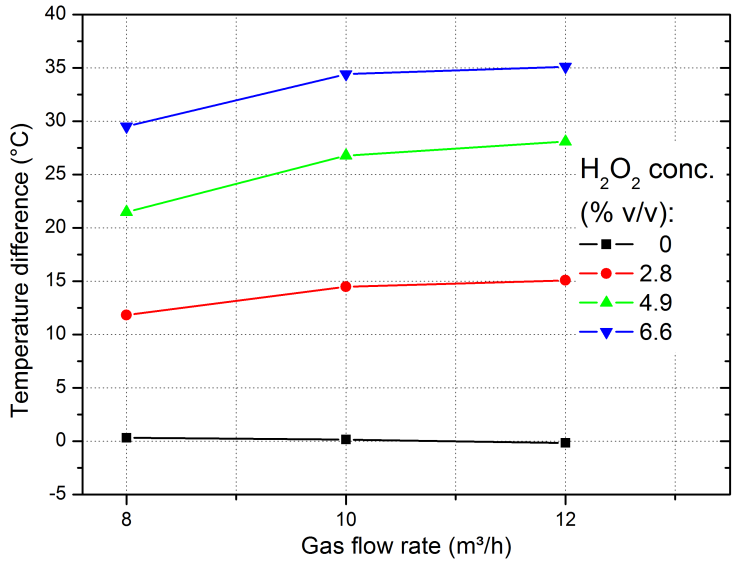

(b)

Figure 6.7: (a) Influence of gas-flow rate (8 m^3/h, 10 m^3/h and 12 m^3/h) on the sensor signal (constant medium temperature of 240 °C), and (b) temperature difference *vs.* gas flow rate plot at various H_2O_2 concentrations.

on the sensor signal. Polyimide as sensor substrate features expedient abilities, like an appropriate thermal stability and chemical inertness in H_2O_2 atmosphere as well as a low thermal conductivity in order to avoid a heat transfer from the active to the reference sensor segment during the exothermal H_2O_2 decomposition. The sensor has shown a sensitivity of 4.78 °C/(% v/v) in a H_2O_2 concentration range of 0% v/v to 8% v/v. Additionally, no impact of the medium temperature on the sensor signal was observed; at various gas flow rates, the sensor has shown only a slightly reduced sensitivity at the lowest flow rate of 8 m^3/h. The sensor characterisation demonstrates the suitability of the calorimetric gas sensor for in-line monitoring of H_2O_2 concentrations in industrial sterilisation processes. In future experiments, the flexible polyimide-based sensor shall be placed in a test package and connected to a wireless electronic board for the realisation of a so-called "intelligent" package.

Acknowledgements

The authors gratefully thank the Federal Ministry of Education and Research (Germany) and VDI/VDE (project "Intellipack") for financial support.

References

[1] Ralston, A. R., Klein, C. F., Thoma, P. E., and Denton, D. D. A model for the relative environmental stability of a series of polyimide capacitance humidity sensors. *Sensors and Actuators B: Chemical 34*, 1–3 (1996), 343–348.

[2] Lee, C.-Y., Wu, G.-W., and Hsieh, W.-J. Fabrication of micro sensors on a flexible substrate. *Sensors and Actuators A: Physical 147*, 1 (2008), 173–176.

[3] Oprea, A., Barsan, N., Weimar, U., Bauersfeld, M.-L., Ebling, D., and Wöllenstein, J. Capacitive humidity sensors on flexible RFID labels. *Sensors and Actuators B: Chemical 132*, 2 (2008), 404–410.

[4] Wessa, T., Barié, N., Rapp, M., and Ache, H. J. Polyimide, a new shielding layer for sensor applications. *Sensors and Actuators B: Chemical 53*, 1–2 (1998), 63–68.

[5] Engel, J., Chen, J., and Liu, C. Development of polyimide flexible tactile sensor skin. *Journal of Micromechanics and Microengineering 13*, 3 (2003), 359–366.

[6] Kim, K., Lee, K. R., Kim, W. H., Park, K.-B., Kim, T.-H., Kim, J.-S., and Pak, J. J. Polymer-based flexible tactile sensor up to 32 x 32 arrays integrated

with interconnection terminals. *Sensors and Actuators A: Physical 156*, 2 (2009), 284–291.

[7] Dayeh, S. A., Butler, D. P., and Celik-Butler, Z. Micromachined infrared bolometers on flexible polyimide substrates. *Sensors and Actuators A: Physical 118*, 1 (2005), 49–56.

[8] Xiao, S. Y., Che, L. F., Li, X. X., and Wang, Y. L. A novel fabrication process of MEMS devices on polyimide flexible substrates. *Microelectronic Engineering 85*, 2 (2008), 452–457.

[9] Lichtenwalner, D. J., Hydrick, A. E., and Kingon, A. I. Flexible thin film temperature and strain sensor array utilizing a novel sensing concept. *Sensors and Actuators A: Physical 135*, 2 (2007), 593–597.

[10] Kim, Y. S. Microheater-integrated single gas sensor array chip fabricated on flexible polyimide substrate. *Sensors and Actuators B: Chemical 114*, 1 (2006), 410–417.

[11] Aslam, M., Gregory, C., and Hatfield, J. V. Polyimide membrane for micro-heated gas sensor array. *Sensors and Actuators B: Chemical 103*, 1–2 (2004), 153–157.

[12] Briand, D., Colin, S., Courbat, J., Raible, S., Kappler, J., and de Rooij, N. Integration of MOX gas sensors on polyimide hotplates. *Sensors and Actuators B: Chemical 130*, 1 (2008), 430–435.

[13] Moruzzi, G., Garthright, W. E., and Floros, J. D. Aseptic packaging machine pre-sterilisation and package sterilisation: statistical aspects of microbiological validation. *Food Control 11*, 1 (2000), 57–66.

[14] Gould, G. W. Methods for preservation and extension of shelf life. *International Journal of Food Microbiology 33*, 1 (1996), 51–64.

[15] Cerny, G. Testing of aseptic machines for efficiency of sterilization of packaging materials by means of hydrogen peroxide. *Packaging Technology and Science 5*, 2 (1992), 77–81.

[16] Kirchner, P., Ng, Y. A., Spelthahn, H., Schneider, A., Henkel, H., Friedrich, P., Kolstad, J., Berger, J., Keusgen, M., and Schöning, M. J. Gas sensor investigation based on a catalytically activated thin-film thermopile for H_2O_2 detection. *Physica Status Solidi A 207*, 4 (2010), 787–792.

[17] Kirchner, P., Li, B., Spelthahn, H., Henkel, H., Schneider, A., Friedrich, P., Kolstad, J., Keusgen, M., and Schöning, M. J. Thin-film calorimetric H_2O_2 gas sensor for the validation of germicidal effectivity in aseptic filling processes. *Sensors and Actuators B: Chemical 154*, 2 (2011), 257–263.

[18] Morf, T., Biber, C., and Bachtold, W. Effects of epitaxial lift-off on the DC, RF, and thermal properties of MESFET's on various host materials. *IEEE Transactions on Electron Devices 45*, 7 (1998), 1407–1413.

[19] Glassbrenner, C. J., and Slack, G. A. Thermal conductivity of silicon and germanium from 3 K to the melting point. *Physical Review 134*, 4A (1964), A1058–A1069.

[20] Näther, N., Juárez, L. M., Emmerich, R., Berger, J., Friedrich, P., and Schöning, M. J. Detection of hydrogen peroxide (H_2O_2) at exposed temperatures for industrial processes. *Sensors 6*, 4 (2006), 308–317.

[21] Näther, N., Henkel, H., Schneider, A., and Schöning, M. J. Investigation of different catalytically active and passive materials for realising a hydrogen peroxide gas sensor. *Physica Status Solidi A 206*, 3 (2009), 449–454.

[22] Hart, A. B., McFadyen, J., and Ross, R. A. Solid-oxide-catalyzed decomposition of hydrogen peroxide vapour. *Transactions of the Faraday Society 59* (1963), 1458–1469.

[23] Salem, I. A., El-Maazawi, M., and Zaki, A. B. Kinetics and mechanisms of decomposition reaction of hydrogen peroxide in presence of metal complexes. *International Journal of Chemical Kinetics 32*, 11 (2000), 643–666.

[24] Giamello, E., Rumori, P., Geobaldo, F., Fubini, B., and Paganini, M. The interaction between hydrogen peroxide and metal oxides: EPR investigations. *Applied Magnetic Resonance 10*, 1 (1996), 173–192.

[25] Kanungo, S. B., Parida, K. M., and Sant, B. R. Studies on MnO_2–III. The kinetics and the mechanism for the catalytic decomposition of H_2O_2 over different crystalline modifications of MnO_2. *Electrochimica Acta 26*, 8 (1981), 1157–1167.

[26] Do, S.-H., Batchelor, B., Lee, H.-K., and Kong, S.-H. Hydrogen peroxide decomposition on manganese oxide (pyrolusite): kinetics, intermediates, and mechanism. *Chemosphere 75*, 1 (2009), 8–12.

[27] Hiroki, A., and LaVerne, J. A. Decomposition of hydrogen peroxide at water-ceramic oxide interfaces. *The Journal of Physical Chemistry 109*, 8 (2005), 3364–3370.

[28] Haber, F., and Weiss, J. The catalytic decomposition of hydrogen peroxide by iron salts. *Proceedings of the Royal Society of London. Series A - Mathematical and Physical Sciences 147*, 861 (1934), 332–351.

[29] Srinivasan, R. Ablation of polyimide (Kapton^{TM}) films by pulsed (ns) ultraviolet and infrared (9.17 μm) lasers. *Applied Physics A: Materials Science and Processing 56*, 5 (1993), 417–423.

[30] Feurer, T., Sauerbrey, R., Smayling, M. C., and Story, B. J. Ultraviolet-laser-induced permanent electrical conductivity in polyimide. *Applied Physics A: Materials Science & Processing 56*, 3 (1993), 275–281.

6.6 Supporting information[1]

6.6.1 Thermal characterisation

The polyimide substrate has been thermally characterised by differential scanning calorimetry (DSC) and thermogravimetric analysis (TGA) in order to study its thermal stability. A brief introduction to these thermal characterisation techniques was already given in section 4.6.1 of chapter 4. From the DSC diagram shown in Fig. 6.8(a), no melting point could be observed in the considered temperature range up to 400 °C. By means of TGA, an initial degradation temperature was observed at 562 °C (s. Fig. 6.8(b)). Thus, the thermal characterisation demonstrates the good thermal endurance of the polyimide.

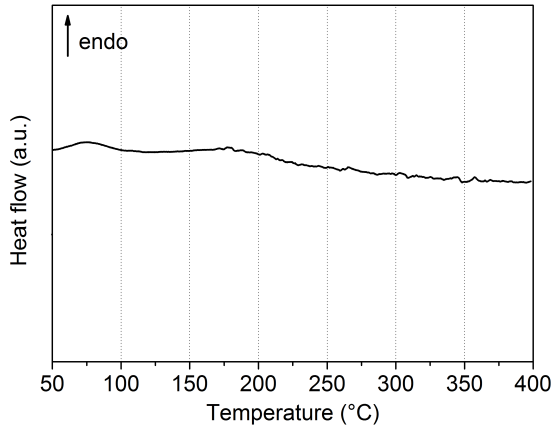

(a)

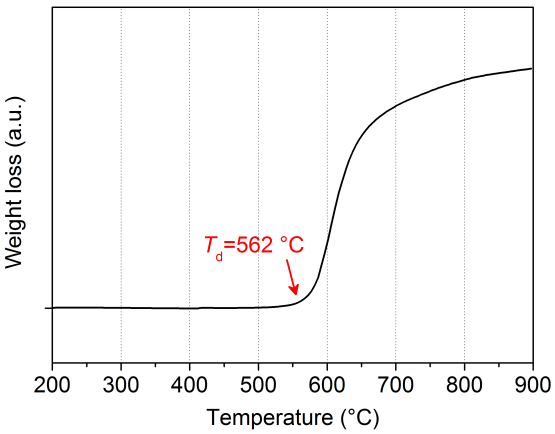

(b)

Figure 6.8: (a) DSC diagram and (b) TGA of the polyimide substrate.

[1]Note: Results of section 6.6.1 and section 6.6.2 are not part of the present article and will be published separately.

6.6.2 FTIR spectroscopy

The FTIR spectroscopy with attenuated total reflectance (ATR) has been adopted to investigate possible changes in the chemical composition of the polyimide substrate, before and after it was exposed to H_2O_2. The FTIR spectrocopic analysis was introduced in section 4.6.2 of chapter 4. For the interpretation of the ATR-FTIR spectra, the structural formula of polyimide is given in Fig. 6.9.

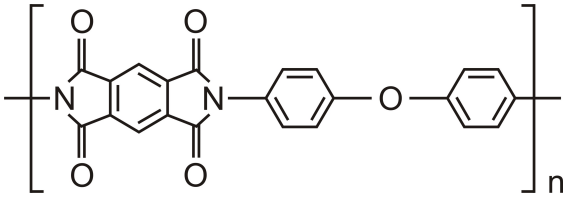

Figure 6.9: Structural formula of polyimide (modified from [29]).

The ATR-FTIR spectra of the polyimide before and after H_2O_2 treatment is shown in Fig. 6.10. Therein, no distinction can be drawn between the spectra before the polyimide substrate was treated by H_2O_2 and once, it was exposed to the H_2O_2 atmosphere. Hence, the chemical inspection of the polyimide by FTIR spectroscopy demonstrates its chemical inertness and its suitability as substrate for calorimetrc H_2O_2 gas sensors. The main absorption bands of the polyimide and their chemical assignments are finally listed in Tab. 6.1.

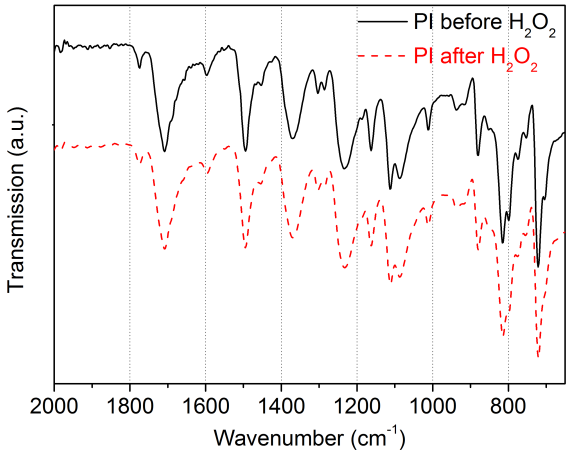

Figure 6.10: ATR-FTIR spectra of the polyimide, before (upper curve) and after (lower curve) it was exposed to H_2O_2 for several hours.

Table 6.1: Assignments of the absorption peaks (adapted from [30]).

Absorption peak (cm^{-1})	Assignment
1775, 1709	Carbonyl compounds
1605, 1501	Aromatic C-C
1369, 1115, 1088	Imide C-N
1239	C-O-C
879, 810	Aromatic C-H
721	Imide C-N-C

6.6.3 Additional measurement curve as support to results and discussion

Dynamic response behaviour of the calorimetric gas sensor based on polyimide is shown in the next diagrams as support to section 6.4.

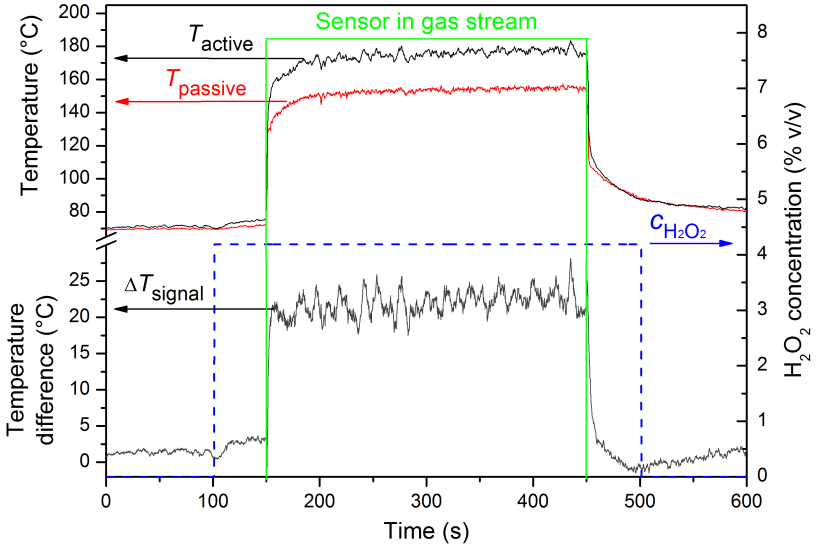

(a)

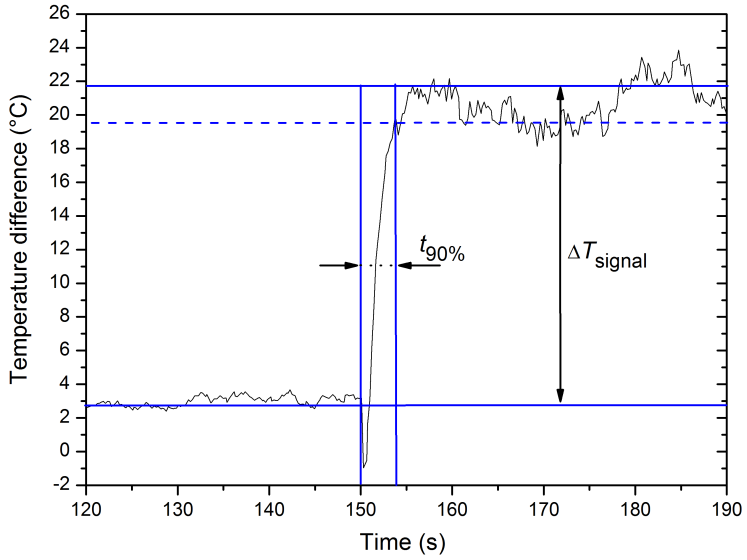

(b)

Figure 6.11: (a) Dynamic response behaviour of the calorimetric gas sensor at constant H_2O_2 concentration of 4.2% v/v, and (b) response of the temperature difference (ΔT_{signal}) with a responce time ($t_{90\%}$) of 3.8 s.

7 Monitoring the microbicidal effectiveness of gaseous hydrogen peroxide in sterilisation processes by means of a calorimetric gas sensor

KIRCHNER, P., Oberländer, J., Suso, H.-P., Rysstad, G., Keusgen, M., and Schöning, M. J.

Food Control 31, 2 (2013), 530–538.

7.1 Abstract

In the present work, a novel method for monitoring sterilisation processes with gaseous H_2O_2 in combination with heat activation by means of a specially designed calorimetric gas sensor was evaluated. Therefore, the sterilisation process was extensively studied by using test specimens inoculated with *Bacillus atrophaeus* spores in order to identify the most influencing process factors on its microbicidal effectiveness. Besides the contact time of the test specimens with gaseous H_2O_2 varied between 0.2 and 0.5 s, the present H_2O_2 concentration in a range from 0 to 8% v/v (volume percent) had a strong influence on the microbicidal effectiveness, whereas the change of the vaporiser temperature, gas flow and humidity were almost negligible. Furthermore, a calorimetric H_2O_2 gas sensor was characterised in the sterilisation process with gaseous H_2O_2 in a wide range of parameter settings, wherein the measurement signal has shown a linear response against the H_2O_2 concentration with a sensitivity of 4.75 °C/(% v/v). In a final step, a correlation model by matching the measurement signal of the gas sensor with the microbial inactivation kinetics was established that demonstrates its suitability as an efficient method for validating the microbicidal effectiveness of sterilisation processes with gaseous H_2O_2.

7.2 Introduction

The sterilisation of packaging material is an essential part of an aseptic food filling system in order to achieve an extended shelf life of packed products (especially low-acid food such as milk) on the one hand, and to obviate the transmission of pathogenic microorganisms to the consumers on the other hand [1]. In general, the process of sterilisation should possess a rapid and reliable microbicidal effectiveness so that the potential number of viable microorganisms on the package surface is entirely inactivated [2, 3]. Furthermore, it should be compatible with the packaging material, easily removable from the package surface, and the unavoidable residue of the sterilisation agent should not affect the product and should be harmless for the consumer [2].

In aseptic food technology, hydrogen peroxide (H_2O_2) is the most commonly used sterilisation agent for food-packaging material at present time. Amongst its benefits, H_2O_2 at low concentration levels of residue is not toxic and it has a highly microbicidal effectiveness against a broad spectrum of microorganisms, such as bacteria, spores, viruses, fungi and yeast [4, 5], that is enhanced by a physical process of either heat or UV radiation [6–8]. The mechanism of the microbial inactivation seems to rely on the fact that H_2O_2 serves as an oxidant by generating free hydroxyl radicals as intermediates during its physically induced decomposition [9]. These radicals damage cell components, like proteins, lipids and DNA [4, 10]. In general, the microbicidal effectiveness is significantly increased by gaseous H_2O_2 [9].

For the validation and control of the sterilisation's effectiveness, microbiological challenge tests have to be carried out. In these tests, artificially inoculated package material with bacteria spores, which are highly resistant against the sterilisation agent, are exposed to the sterilisation process, afterwards, incubated for a defined time and finally, either the number of survived spores in form of grown bacterial colonies are counted (count-reduction test) or the relation between sterile and unsterile packages is determined (end-point test) [11]. Even though, these procedures represent well-established and reliable validation methods of the sterilisation process that is indispensable for its inspections in defined intervals, they have some disadvantages: the methods are time- and labour-consuming; continuous controlling is not possible and the results are subject to statistical fluctuations. Due to these facts, there is a great demand of the aseptic food industry for a method that additionally allows the determination of the microbicidal effectiveness of the sterilisation process continuously in-line with low operational costs. Supposed that the sterilisation's effectiveness predominantly depends on the amount of gaseous H_2O_2, a sensor system is required for quantitatively measuring the gaseous H_2O_2 concentration under harsh environmental conditions of the sterilisation process and thus, this system could help to verify the sterilisation's effectiveness in-line.

The objective of this study can be divided into three steps. In a first step, the microbicidal effectiveness of gaseous hydrogen peroxide at elevated gas temperatures is evaluated for various settings of contact time, gas velocity, humidity and especially, of the gaseous H_2O_2 concentration, whereby the predominant effect of the gas concentration on the effectiveness will be demonstrated. Therein, the chosen parameter ranges correspond to real, industrial sterilisation processes. In a second step, the actual H_2O_2 concentration is quantitatively measured by a novel gas sensor at same settings of the process parameters as for the determination of the sterilisation's effectiveness. The H_2O_2 gas sensor module is based on a calorimetric differential set-up that was first introduced Näther et *al.* [12]. In a final step, a correlation model between the microbicidal effectiveness and the measurement signal of the calorimetric gas sensor is established.

As a result, the present study should demonstrate that the use of such a calorimetric H_2O_2 gas sensor and the development of a correlation model between the sensor's signal and the microbicidal effectiveness are representing a novel method to continuously monitor industrial sterilisation processes.

7.3 Materials and methods

7.3.1 Sterilisation test rig

In a developed test rig, already introduced in [13, 14], the sterilisation process with gaseous hydrogen peroxide at elevated gas temperature was reproduced. The test rig contains a dosing system with two piston pumps, where one of them serves for the H_2O_2 solution (35% w/w, from FMC Industrial Chemicals) and the other one for deionised water. A gas flow of compressed air controlled by a flow meter and a regulation valve was used as carrier gas for both liquids. Furthermore, the test rig includes a vaporisation unit built up by two heating elements in series. The heating power of the heating elements is controlled by the measured temperature of the gas stream at the outlet nozzle of the vaporisation unit. The microbiological specimens and the calorimetric gas sensor have been placed via a hydraulic slide rail in a defined distance – similar as for industrial processes with carton packages – underneath the gas-outlet nozzle in an aseptic chamber of the test rig.

7.3.2 Calorimetric gas sensor

For measuring the gaseous H_2O_2 concentration, a calorimetric gas sensor has been implemented in the aseptic chamber of the sterilisation test rig. The sensor principle is based on a calorimetric differential set-up, which consists of two temperature-sensitive thin-film resistors, wherein one of them is covered by a polymeric passivation layer (here, SU-8

photoresist) and the second one is additionally coated by a catalytically active dispersion of manganese(IV) oxide (s. Fig. 7.1).

If the calorimetric gas sensor is exposed to a H_2O_2 gas stream, a temperature difference between the catalytically activated (active sensor segment) and the passivated thin-film resistor (passive sensor segment) caused by an exothermal decomposition of hydrogen peroxide on the catalytic surface correlates with the present H_2O_2 concentration in the gas phase and yielding a measurement signal according to Eq. 7.1:

$$\Delta T_{\text{signal}} = S \cdot c_{H_2O_2} + \Delta T_0 \tag{7.1}$$

Herein, S is the sensor's sensitivity, $c_{H_2O_2}$ is the H_2O_2 concentration and ΔT_0 is the sensor's off-set.

Before the sensor was exposed to the H_2O_2 gas stream, the resistors of the sensor were calibrated in a temperature range between 10 °C and 85 °C in steps of 5 °C in a thermostat (RE 207 from LAUDA) in order to precisely detect the temperature on the active and passive sensor segment, respectively. The fabrication procedure of the thin-film sensor and its sensor-response mechanism were already presented in [15, 16] in detail.

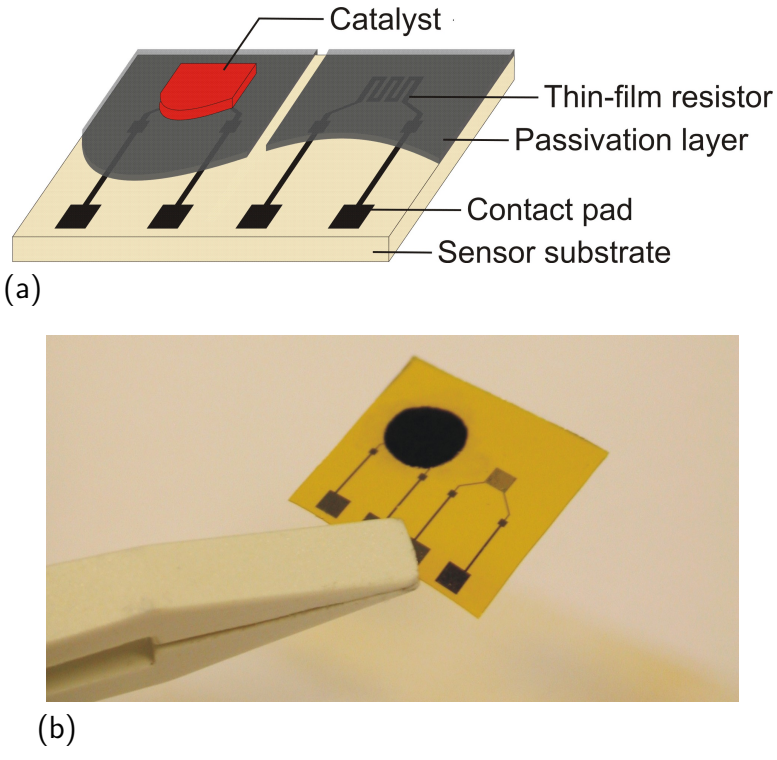

Figure 7.1: (a) Scheme of the sensor set-up with two thin-film resistors, passivation layer and catalyst and (b) calorimetric H_2O_2 gas sensor on a polyimide substrate (sensor size: 10 x 10 mm^2).

7.3.3 Microbiological test specimens

A spore suspension of *Bacillus atrophaeus* ATCC 9372 was used for the microbiological tests of the sterilisation process. Spores of *Bacillus atrophaeus* are recommended for testing H_2O_2 sterilisation processes due to their high resistance against H_2O_2 [17]. The suspension has an initial load of $8 \cdot 10^8$ cfu/ml (cfu: colony forming units) in ethanol solution (70%). The test specimens, each of them made up of a flat aluminium plate with a size of 10 x 10 mm^2, were inoculated with 10 μl of the spore suspension via a micropipette resulting in a nominal spore number of $8 \cdot 10^6$ cfu/specimen. The spore-inoculated specimens were stored for 12 h in a laminar flow hood for drying the suspension.

7.3.4 Spore quantification

In the microbiological test series, five of the microbiological test specimens were treated by the gas stream in the aseptic chamber of the test rig for each process condition (constant setting of contact time, H_2O_2 concentration, gas temperature, gas velocity and humidity), respectively. In addition, three untreated test specimens were used for the determination of the recovery rate (R) for each test series as a reference:

$$R = \frac{1}{n \cdot N_0} \cdot \sum_{i=1}^{n} N_{0,\mathrm{i}} \tag{7.2}$$

Therein, N_0 is the nominal number of spores, $N_{0,\mathrm{i}}$ is the actual number of spores for each reference specimen i, and n is the number of reference specimens.

The test specimens were put into test tubes filled with 10 ml of 1/4 Ringer's solution (38.5 mM NaCl, 1.4 mM KCl, 1.1 mM $CaCl_2$, 0.6 mM $NaHCO_3$) and 0.1% Polysorbate 80. In order to strip off the spores from the aluminium plates, the test tubes were treated by a vortex shaker for 1 min at first and afterwards, in an ultrasonic bath for 20 min. For each test specimen, a tenfold logarithmic dilution series with five dilution steps was prepared based on the initial test tube with spores stripped off from the plate. An amount of 1 ml from the spore solution of each test tube was plated on a Plate Count Agar medium and in a final step, the cultures were incubated at 30 °C for 5 days, the formed bacterial colonies counted according to Farmiloe's formula [18] and the logarithmic cycle reduction (LCR) – a measure of the microbicidal effectiveness of a sterilisation process – for a constant parameter setting calculated:

$$LCR = \lg \frac{N_{0,\mathrm{i}}}{N_{\mathrm{S}}} \tag{7.3}$$

Here, N_{S} is the total number of survived spores after the sterilisation process.

7.3.5 Experimental scheme

A sequence of four microbiological test series was carried out, wherein the influence of the main process factors (contact time, H_2O_2 concentration, gas temperature, gas velocity and humidity) on the microbicidal effectiveness of gaseous H_2O_2 was ascertained. In the first test series, the contact time was varied between 0.2 and 0.5 s in a specified H_2O_2 concentration range from 0 to 8% v/v for a gas velocity of 20 m/s and at a constant temperature of 240 °C of the vaporisation unit measured directly on the gas-outlet nozzle. In the following series, the gas temperature of the vaporisation unit was incrementally changed from 210 to 270 °C, again in a H_2O_2 concentration range of 0 to 8% v/v for a gas velocity of 20 m/s as well as for a fixed contact time of 0.2 s. For the evaluation of the influencing factor of the gas velocity on the sterilisation's effectiveness, the flow of the H_2O_2 gas stream was varied so that the resulting gas velocity could be adjusted gradually from 16 to 20 and 24 m/s in the mentioned H_2O_2 concentration range at a constant temperature of 240 °C and again, for a contact time of 0.2 s. In a final microbiological test series, the microbicidal effectiveness of gaseous H_2O_2 was studied with increased humidity by dosing deionised water to the H_2O_2 stream and compared to the gas stream without additional humidity, even again in a range of up to 8% v/v H_2O_2, at a vaporiser temperature of 240 °C, a gas velocity of 20 m/s and a contact time of 0.2 s.

In a further step, a sequence of four measurement series was carried out with the calorimetric H_2O_2 gas sensor similar to the microbiological test series with consistent parameter settings. In a final step, a correlation between the measurement signal of the sensor and the logarithmic cycle reduction determined at varied parameter settings for a fixed contact time of 0.2 s was established.

7.4 Results and discussion

7.4.1 Microbiological tests

Prior to each microbiological test series, the actual number of spores on three reference specimens was determined. In Fig. 7.2(a), the median and the spreading of the actual spore number ($7.8 \cdot 10^6$ $\pm 4.0 \cdot 10^6$ cfu/specimen) on a total of twelve reference specimens are shown. Compared to the nominal spore load ($8 \cdot 10^6$ cfu/specimen), the mean recovery rate according to Eq. 7.2 amounts to be 97%. Furthermore, the inoculated spores on the surface of an aluminium plate were inspected via scanning electron microscopy (SEM), wherein a homogeneous spore distribution without spore agglomerates was verified (s. Fig. 7.2(b)).

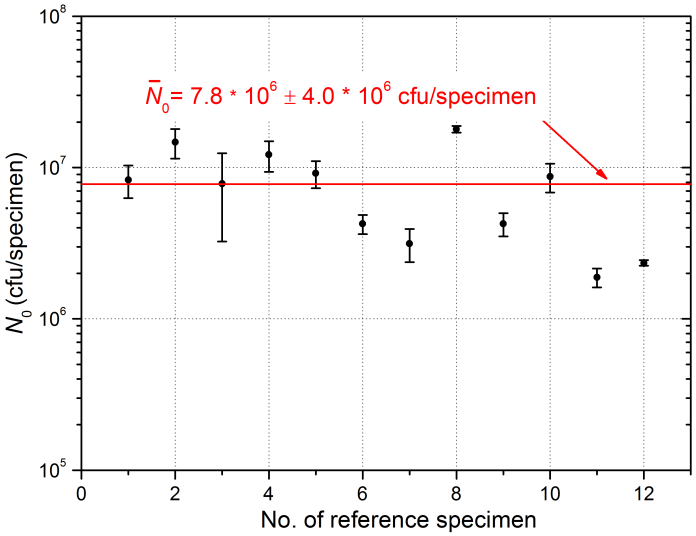

(a)

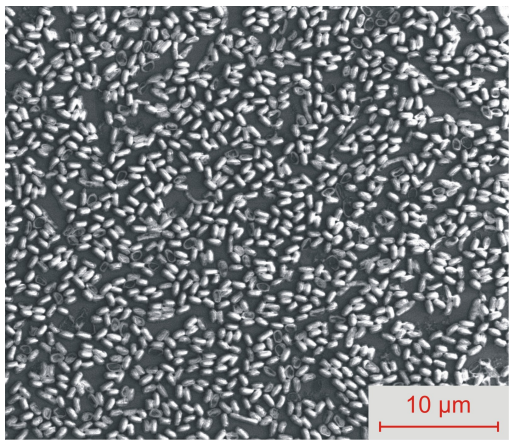

(b)

Figure 7.2: (a) Recovery of spores on reference specimens inoculated with an initial load of $8 \cdot 10^6$ cfu/specimen and (b) SEM image showing the homogenous distribution of the spores on an aluminium plate (magnification: 7,000x).

In the first microbiological test series, the influence of the contact time on the logarithmic cycle reduction (LCR) was determined in a H_2O_2 concentration range from 0 to 8% v/v (s. Fig. 7.3(a)). After the treatment of the microbiological test specimens by a hot gas stream without H_2O_2, the low LCR of about 0.5 did not reveal any distinct difference for the various contact times. In contrast, a significant difference of the LCR was observed at the lowest H_2O_2 concentration of 2.3% v/v, wherein the maximum LCR of 6.9 was already attained for the highest contact time of 0.5 s and even at the next

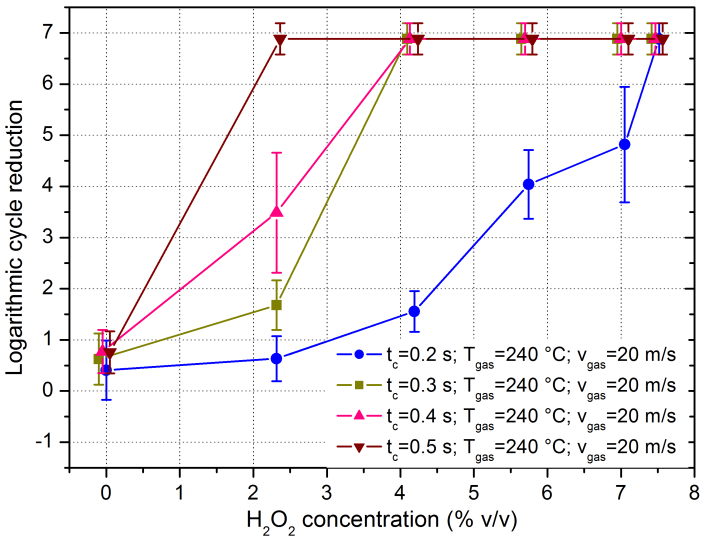

(a)

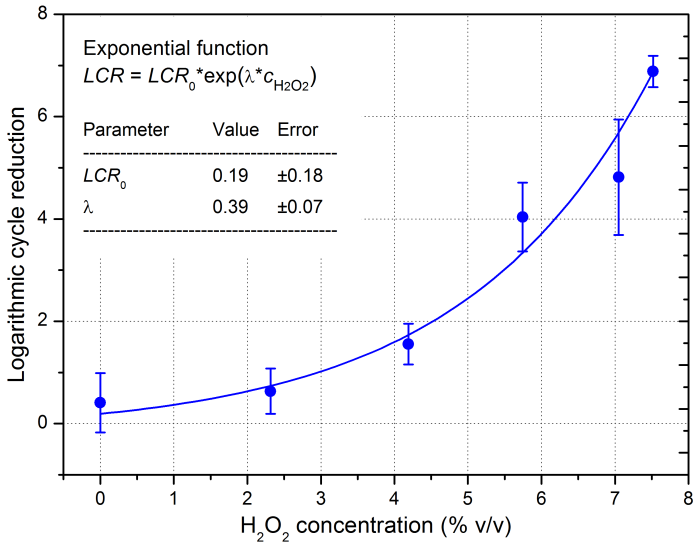

(b)

Figure 7.3: (a) Logarithmic cycle reduction (LCR) for varied contact times between 0.2 and 0.5 s and (b) interpolation of the LCR characteristic by a sigmoid function in a H_2O_2 concentration range from 0 to 8% v/v and for a contact time of 0.2 s.

concentration step of 4.2% v/v, the maximum LCR was achieved for a contact time of 0.3 and 0.4 s as well. Only for a short contact time of 0.2 s, the microbicidal effectiveness obviously depends on the H_2O_2 concentration over the whole concentration range from 0 to 8% v/v. Therein, the LCR slightly grows with low H_2O_2 concentrations and significantly increases with high H_2O_2 concentrations leading to an interpolation of the LCR against the H_2O_2 concentration by using an exponential function (s. Fig. 7.3(b)):

$$LCR = LCR_0 \cdot e^{\lambda \cdot c_{H_2O_2}} \tag{7.4}$$

Therein, LCR_0 is the logarithmic cycle reduction at 0% v/v H_2O_2 and λ is an empirical factor of the exponential function.

In addition to the evaluation of the microbicidal effectiveness by means of microbiological challenge tests, the bacterial spores inoculated on an aluminium plate were investigated via SEM after the treatment by a gas stream with a H_2O_2 concentration of 0, 4.2 and 7.6% v/v for a contact time of 0.2 s in the sterilisation test rig, respectively (s. Fig. 7.4). After treating the spores by a hot gas stream without H_2O_2, the mostly intact spores were homogenously distributed on the aluminium plate demonstrating their good adhesion on the plate surface even at a forced gas flow and moreover, they showed a uniform, ellipsoidal shape without markable deformations (s. Fig. 7.4(a)). In contrast to that, the bacterial spores were strongly deformed or even disrupted by gaseous H_2O_2 and due to their formation, most of them did not adhere to the plate surface leading to spore agglomerates that increase with rising H_2O_2 concentration (s. Fig. 7.4(b),(c)).

In further microbiological test series, the influence of the gas temperature, gas velocity and humidity on the microbicidal effectiveness of gaseous H_2O_2 was evaluated. In Fig. 7.5(a), the dependence of the LCR on gas temperature of the vaporisation unit is shown. Therein, the gas temperature measured directly below the vaporisation unit was changed in three temperature steps of 210, 240 and 270 °C and the LCR was determined against the H_2O_2 concentration, respectively. The variation of the gas temperature at the vaporisation unit led to a difference in the surface temperature at the placement of the test specimens from 120 to 140 and 160 °C measured by a temperature sensor in the gas flow without H_2O_2 dosage. It can be clearly observed that the progressions of the LCR in the considered H_2O_2 concentration range are in good compliance for the three different gas temperatures. This test series demonstrates that the gas temperature in an adjusted range highly above the dew point of H_2O_2 did not markedly influence the microbicidal effectiveness. In the third microbiological test series, wherein the microbicidal effectiveness was detected for varied gas velocities of 16, 20 and 24 m/s, no significant distinctions of the LCR progressions between the gas velocities could be drawn (s. Fig. 7.5(b)). Only a slightly decreased LCR was achieved for the lowest gas velocity

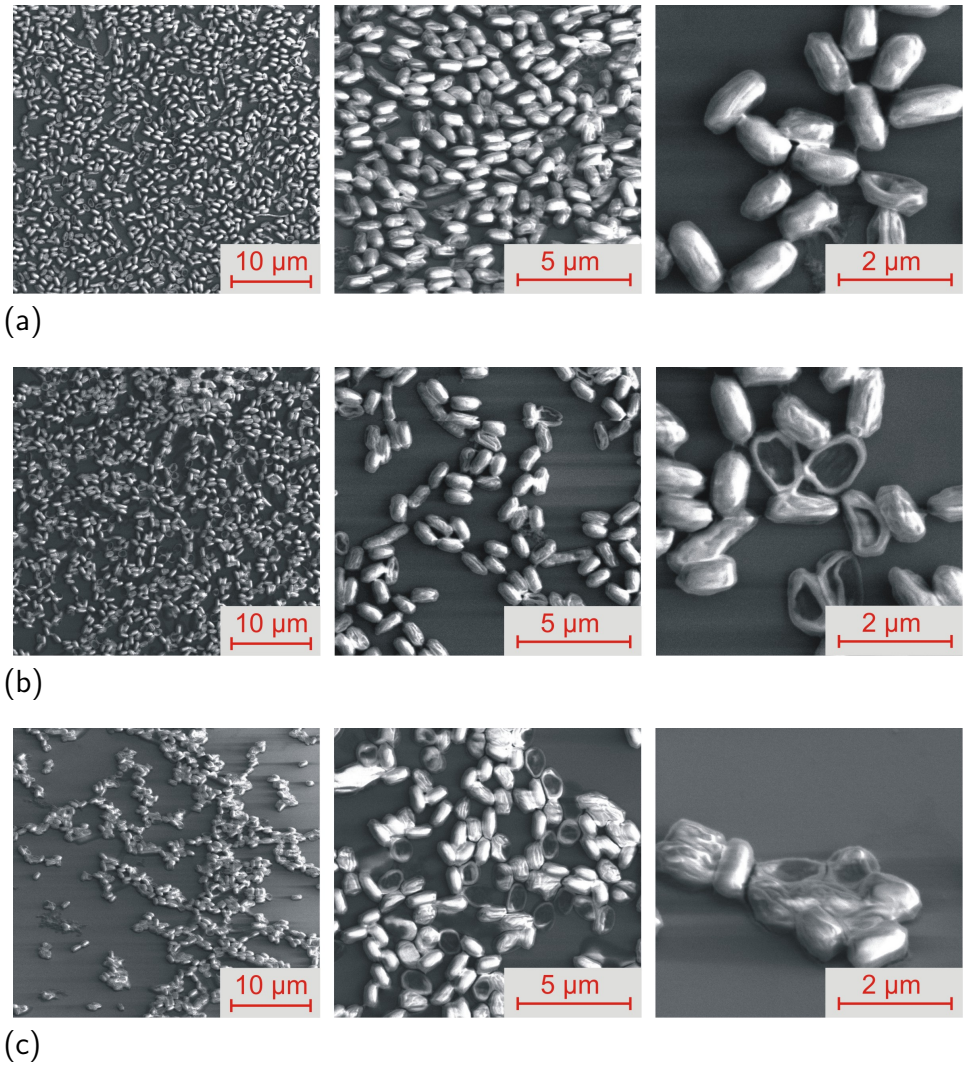

Figure 7.4: SEM images of spores on aluminium plates treated by (a) a hot air stream, (b) a H_2O_2 gas stream with a H_2O_2 concentration of 4.2% v/v and (c) by a gas stream of 7.5% v/v H_2O_2, each of them at a gas temperature of 240 °C, a gas velocity of 20 m/s and for a contact time of 0.2 s (magnifications: 7,000x, 20,000x and 50,000x).

of 16 m/s at the highest H_2O_2 concentration of 6.7% v/v. In the final test series, the effect of additionally dosed, deionised water on the LCR was inspected and compared to the LCR determined in the same H_2O_2 concentration range without elevated humidity (s. Fig. 7.6). Therein, the LCR showed the same characteristic behaviour for gaseous H_2O_2 both with and without elevated humidity, except to the highest H_2O_2 concentration of 6.7% v/v, wherein the LCR was slightly decreased for a H_2O_2 gas stream with additionally dosed water. During the test series, it could be observed that the dosage of high amounts of water vapour to the H_2O_2 gas stream led to condensation droplets of

water and H_2O_2 in the aseptic chamber, resulting in a lower LCR according to a lower amount of H_2O_2 in the gas stream.

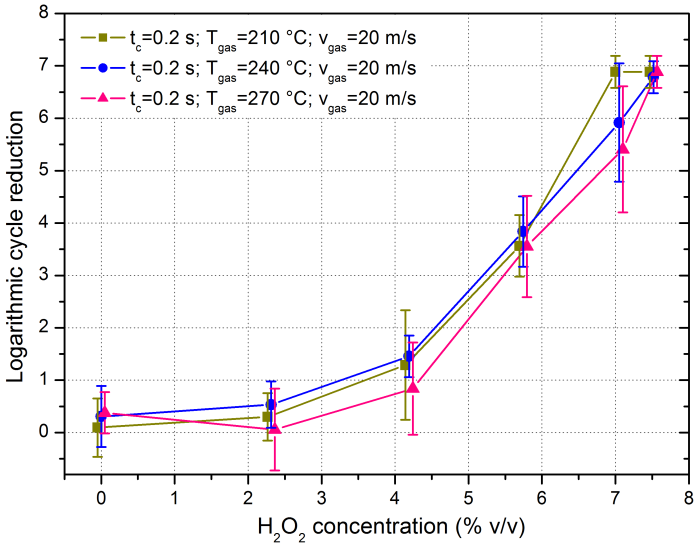

(a)

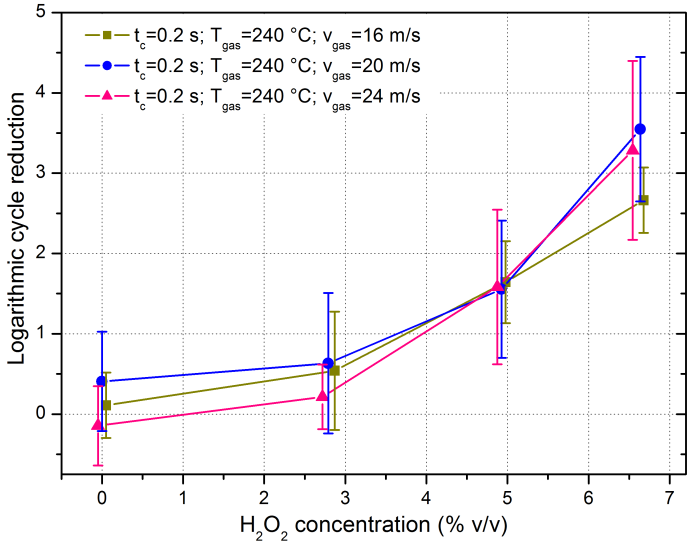

(b)

Figure 7.5: Influence of (a) gas temperature (setting range: 210 to 270 °C) and (b) gas velocity (16 to 24 m/s) on the logarithmic cycle reduction (LCR).

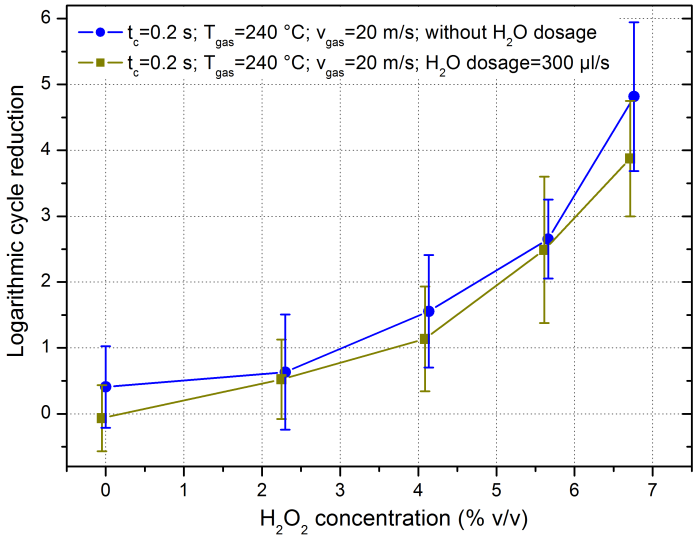

Figure 7.6: Influence of humidity (additional dosage of 300 μl/s deionised water) on the logarithmic cycle reduction (LCR).

In summary, the inactivation kinetics demonstrated that both, H_2O_2 concentration and contact time, have a strong influence on the microbicidal effectiveness of gaseous H_2O_2. As a result, the LCR was additionally plotted against the dose ($D_{H_2O_2}$), wherein a clear dependence of the LCR on the dose of gaseous H_2O_2 in form of an exponential function similar to Eq. 7.4 can be identified (s. Fig. 7.7). Therein, the dose of gaseous H_2O_2 was calculated according to Eq. 7.5:

$$D_{H_2O_2} = c_{H_2O_2} \cdot t_c \tag{7.5}$$

Here, t_c is the contact time of the test specimens with gaseous H_2O_2.

7.4.2 Sensor measurements

In addition to the microbiological tests, the calorimetric H_2O_2 gas sensor was characterised in the aseptic chamber of the sterilisation test rig. First of all, a sensor calibration procedure was carried out. Therefore, the temperatures on the active (T_{active}) and the passive sensor segment ($T_{passive}$) were detected at defined H_2O_2 concentration steps between 0 and 8% v/v, at a constant gas temperature of 240 °C and a gas velocity of 20 m/s (s. Fig. 7.8). The temperatures on both sensor segments are always below the gas temperature of the vaporizer. The sensor was situated in a defined distance below the gas-outlet nozzle of the "cold" aseptic chamber so that the H_2O_2 gas stream is cooled

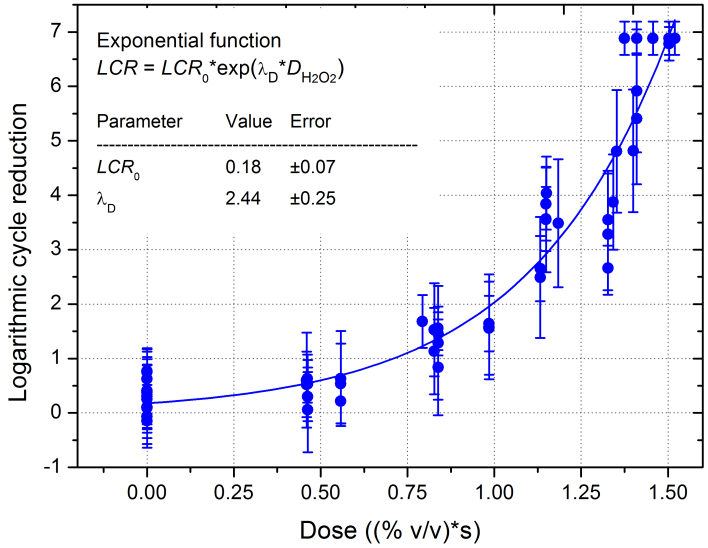

Figure 7.7: Logarithmic cycle reduction (LCR) plotted against the dose of H_2O_2 until the maximum LCR of 6.9 was obtained.

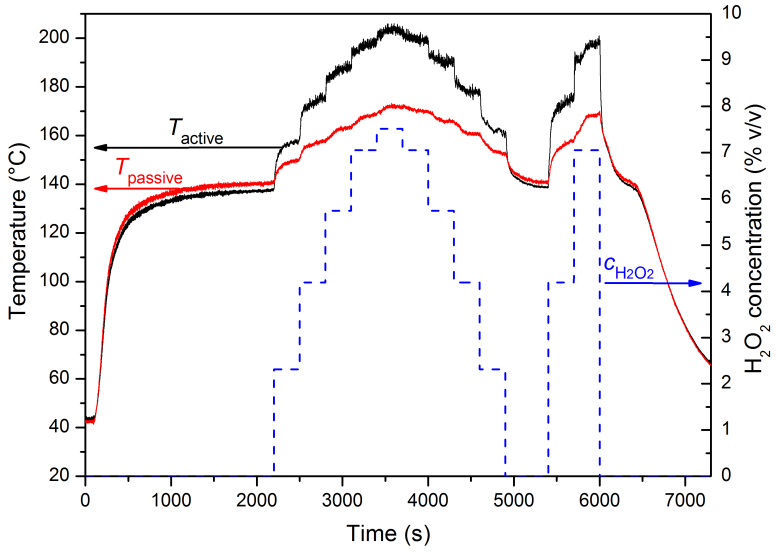

Figure 7.8: (a) Temperature-response behaviour of the calorimetric gas sensor (active and passive sensor segment) at varied H_2O_2 concentrations up to 8% v/v (gas temperature: 240 °C, gas velocity: 20 m/s).

down to temperatures below 200 °C until the stream attained to the sensor. The temperature on the active sensor segment T_{active} increased from 136 °C at 0% v/v H_2O_2 to a maximum of 205 °C at a H_2O_2 concentration of 7.6% v/v. $T_{passive}$, which should not be affected by the decomposition effect of H_2O_2, showed also a temperature rise from 140 °C at 0% v/v H_2O_2 to 172 °C at 7.6% v/v H_2O_2. The temperature shift on the passive sensor segment could depend on the heat transfer between the active and passive sensor segment during the decomposition of H_2O_2 on the active sensor segment as well as on a possible temperature change of the gas stream between different H_2O_2 concentrations caused by a change of the heat capacity of the gas stream that depends on the present H_2O_2 concentration. As measurement signal, the temperature difference (ΔT_{signal}) between the active and passive sensor segment was calculated (s. Fig. 7.9(a)) and a calibration plot with a good linear correlation between ΔT_{signal} and the particular H_2O_2 concentration was generated (s. Fig. 7.9(b)). The characterised sensor had a sensitivity (S) of 4.75 °C/(% v/v) and a low temperature off-set (ΔT_0) of -2.25 °C in the considered H_2O_2 concentration range.

In a second measurement series, the influence of gas temperature on the sensor signal was investigated. From the diagram depicted in Fig. 7.10(a), it can be clearly seen that a change of the gas temperature in temperature steps of 210, 240 and 270 °C had no effect on ΔT_{signal} in a H_2O_2 concentration range from 0 to 8% v/v.

However, by changing the gas velocity in steps of 16, 20 and 24 m/s, a slight difference in the sensor-response behaviour can be noticed (s. Fig. 7.10(b)). The measurement signal was approximately 15% lower at a gas velocity of 16 m/s compared to the signal at 20 and 24 m/s, caused by an increase of the heat transfer between the active and passive sensor segment during the catalytic H_2O_2 decomposition at a reduced gas velocity.

In the final sensor-measurement series, the sensor signal was detected for various H_2O_2 concentrations with and without additionally dosed deionised water (s. Fig. 7.11). Here, the sensor signal at elevated humidity is in good compliance to the signal without humidity. Only a slightly smaller sensor signal was observed at the highest H_2O_2 concentration step of 6.7% v/v with additionally dosed water. The reason for the lower signal relies on the fact that condensation droplets appeared during the dosage yielding a decrease of the gaseous H_2O_2 concentration as observed in the final microbiological test series.

7.4.3 Correlation model

For developing a correlation model between the measurement signal of the calorimetric H_2O_2 gas sensor and the microbicidal effectiveness of gaseous H_2O_2, all measurement data of the sensor were matched with the logarithmic cycle reductions determined at a fixed contact time of 0.2 s for the various setting points of H_2O_2 concentration, gas

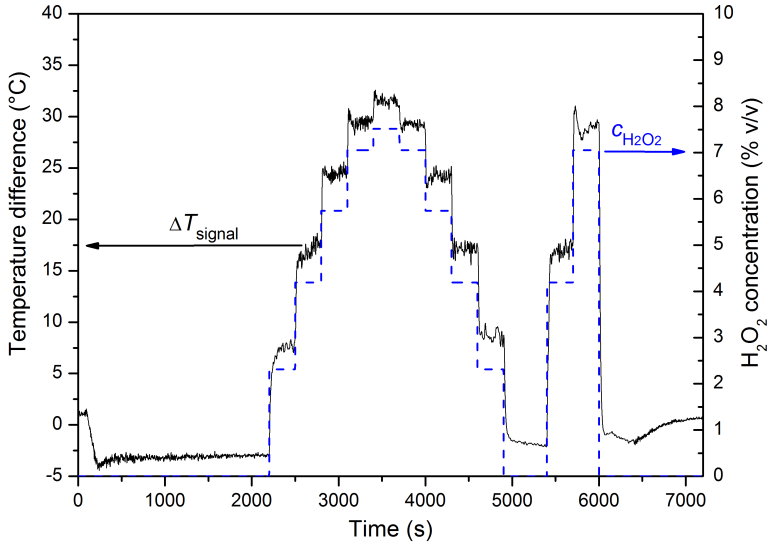

(a)

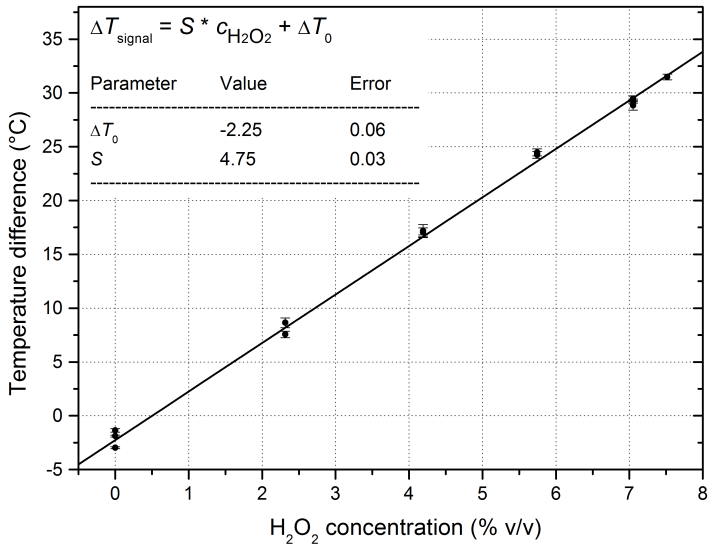

(b)

Figure 7.9: (a) Temperature difference at varied H_2O_2 concentrations up to 8% v/v (gas temperature: 240 °C, gas velocity: 20 m/s), and (b) calibration plot of the gas sensor.

temperature, gas velocity and humidity. In a first step, the logarithmic cycle reductions detected at higher contact times were disregarded in the correlation model. In

Fig. 7.12(a), a diagram is shown, wherein the correlation of the sensor signal with the logarithmic cycle reduction could almost be interpolated by a logarithmic function.

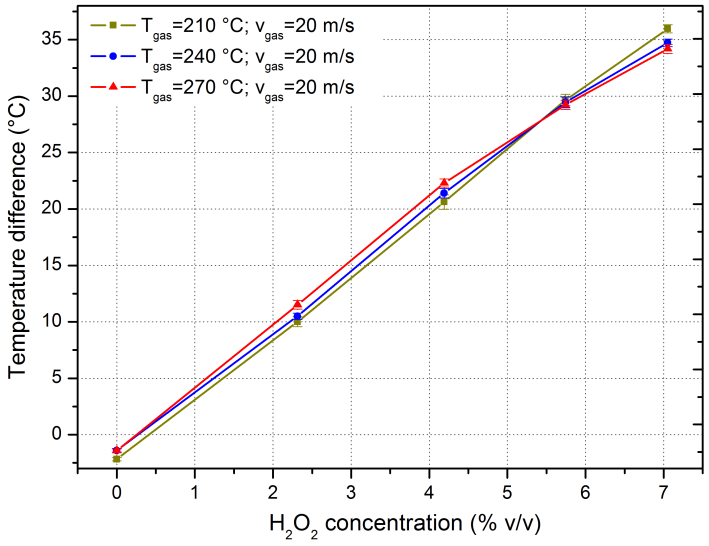

(a)

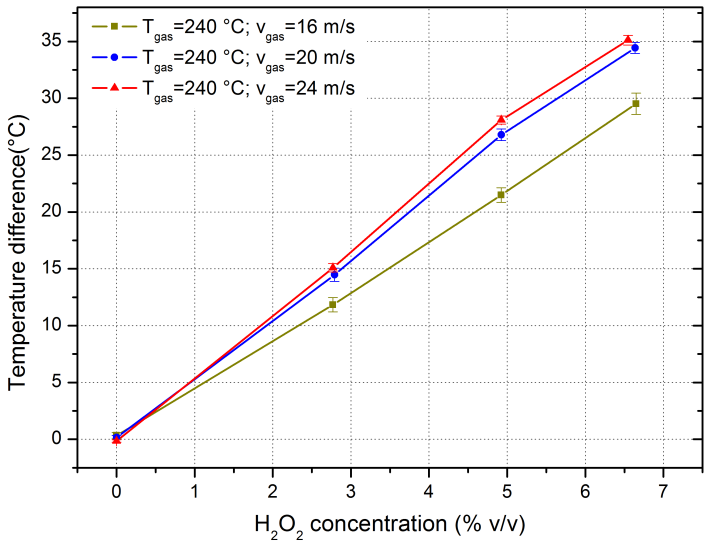

(b)

Figure 7.10: Influence of a) gas temperature (setting range: 210 to 270 °C) and b) gas velocity (16 to 24 m/s) on the sensor signal (ΔT_{signal}).

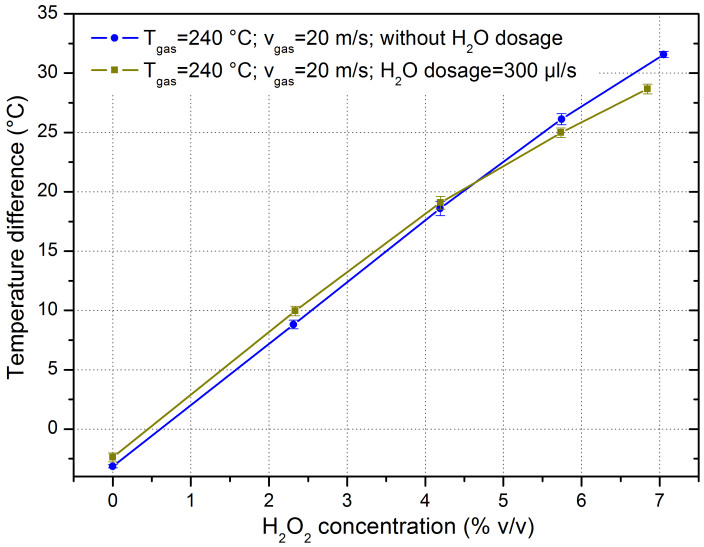

Figure 7.11: Influence of humidity (additional dosage of 300 μl/s deionised water) on the sensor's signal (ΔT_{signal}).

The measurement signal increases rapidly to a temperature difference of up to 20 °C for low logarithmic cycle reductions. This sharp rise of the measurement signal against the logarithmic cycle reduction matches with a slight effect of low H_2O_2 concentrations on the microbicidal effectiveness, whereas the measurement signal correlates linearly with further raising H_2O_2 concentrations. Above a measurement signal of 20 °C, a linear approximation was drawn between the measurement signal and logarithmic cycle reduction (s. Fig. 7.12(b)) according to Eq. 7.6:

$$\Delta T_{\text{signal}} = S_{\text{LCR}} \cdot LCR + \Delta T_{0,\text{LCR}} \tag{7.6}$$

Herein, the sensor's sensitivity (S_{LCR}) amounts to be 2.16 °C per logarithmic cycle reduction and its off-set ($\Delta T_{0,\text{LCR}}$) to be 20.92 °C. This linear correlation results from both an approximately linear relationship between the logarithmic cycle reduction and the H_2O_2 concentration between 4 and 8% v/v (s. section 7.4.1), as well as a linear dependency of the measurement signal and the H_2O_2 concentration in the considered concentration range (s. section 7.4.2).

In addition to the relationship between the measurement signal and the LCR specified for a defined contact time, a correlation model can be established, wherein the relevant contact time over all inactivation kinetics to the maximum LCR of 6.9 is implicated. Therefore, the measurement signal of the sensor was multiplied by the contact time and

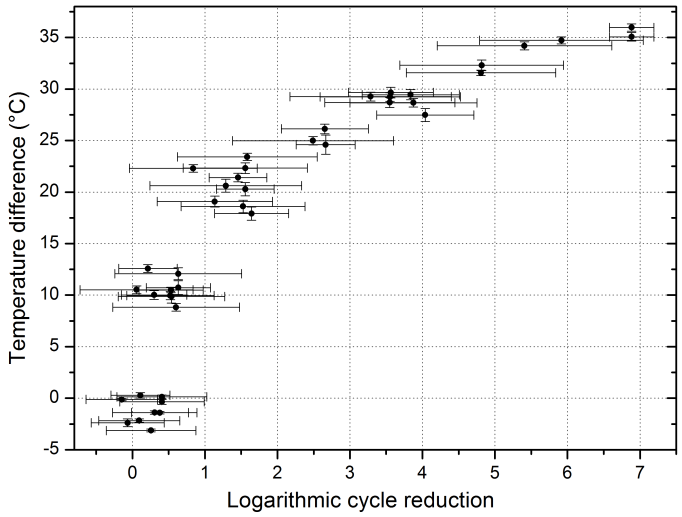

(a)

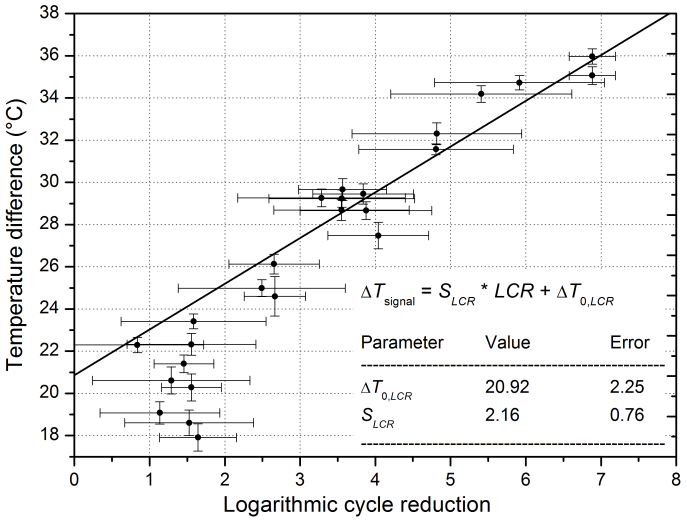

(b)

Figure 7.12: (a) Correlation between measurement signal (ΔT_{signal}) and logarithmic cycle reduction (LCR) determined for a contact time of 0.2 s of the considered setting points, and (b) linear approximation at increased $\Delta T_{0,\text{LCR}}$ (between 21 and 36 °C temperature difference) for the relevant LCR range at elevated H_2O_2 concentrations.

related to the LCR (s. Fig. 7.13). The resulting progression can also be interpolated by a logarithmic function with a similar behaviour to the correlation model for a fixed

contact time of 0.2 s shown in Fig. 7.12(a). Such correlation models could be used for the indirect determination of the microbicidal effectiveness in sterilisation processes of gaseous H_2O_2 in combination with elevated gas temperatures.

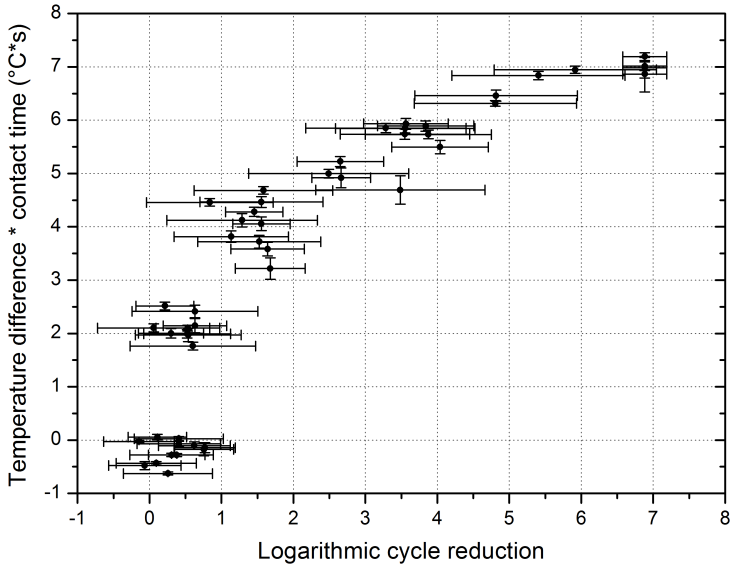

Figure 7.13: Logarithmic cycle reduction (LCR) plotted against measurement signal multiplied by the contact time until the maximum LCR of 6.9 was attained.

7.5 Conclusions

The evaluation of the microbicidal effectiveness of gaseous H_2O_2 in combination with heat by using microbiological specimens inoculated with *Bacillus atrophaeus* spores showed that the most influencing factors of the sterilisation process are the contact time varied between 0.2 and 0.5 s, on the one hand, and the H_2O_2 concentration inspected in a range of 0 to 8% v/v, on the other hand, whereas the effect of changing the gas temperature highly above the dew point of H_2O_2, the gas velocity and the humidity in the considered ranges is negligible. In addition to the microbiological tests, a novel H_2O_2 gas sensor module arranged as calorimetric differential set-up was extensively characterised at various parameter settings of the sterilisation process, and the measurement signal was successfully correlated with the logarithmic cycle reduction of *Bacillus atrophaeus* spores. The use of the calorimetric H_2O_2 gas sensor and the establishment of a correlation model between the sensor's signal and the microbial inactivation kinetics specific to the sterilisation process of gaseous H_2O_2 feature a reliable and time-consuming method

to determine the sterilisation's microbicidal effectiveness. In contrast to microbiological challenge tests, the calorimetric sensor set-up might enable a quantitative in-line monitoring for sterilisation processes for future applications.

Acknowledgements

The authors gratefully thank H. P. Bochem, S. Groebel and V. Thönnessen for technical support.

References

[1] Gould, G. W. Methods for preservation and extension of shelf life. *International Journal of Food Microbiology 33*, 1 (1996), 51–64.

[2] Ansari, I., and Datta, A. An overview of sterilization methods for packaging materials used in aseptic packaging systems. *Food and Bioproducts Processing 81*, 1 (2003), 57–65.

[3] Moruzzi, G., Garthright, W. E., and Floros, J. D. Aseptic packaging machine pre-sterilisation and package sterilisation: statistical aspects of microbiological validation. *Food Control 11*, 1 (2000), 57–66.

[4] Block, S. S., Ed. *Desinfection, sterilization and preservation.* Lea & Febiger, Philadelphia, 1991.

[5] Heckert, R. A., Best, M., Jordan, L. T., Dulac, G. C., Eddington, D. L., and Sterritt, W. G. Efficacy of vaporized hydrogen peroxide against exotic animal viruses. *Applied And Environmental Microbiology 63*, 10 (1997), 3916–3918.

[6] Bayliss, C. E., and Waites, W. M. Effect of simultaneous high intensity ultraviolet irradiation and hydrogen peroxide on bacterial spores. *International Journal of Food Science & Technology 17*, 4 (1982), 467–470.

[7] Smith, Q. J., and Brown, K. L. The resistance of dry spores of *Bacillus subtilis* var. *globigii* (NCIB 8058) to solutions of hydrogen peroxide in relation to aseptic packaging. *International Journal of Food Science & Technology 15*, 2 (1980), 169–179.

[8] Toledo, R. T., Escher, F. E., and Ayres, J. C. Sporicidal properties of hydrogen peroxide against food spoilage organisms. *Appl. Environ. Microbiol. 26*, 4 (1973), 592–597.

[9] McDonnell, G., and Russell, A. D. Antiseptics and disinfectants: activity, action, and resistance. *Clinical Microbiology Reviews 12*, 1 (1999), 147–179.

[10] Russell, A. D. Bacterial spores and chemical sporicidal agents. *Clinical Microbiology Reviews 3*, 2 (1990), 99–119.

[11] Cerny, G. Testing of aseptic machines for efficiency of sterilization of packaging materials by means of hydrogen peroxide. *Packaging Technology and Science 5*, 2 (1992), 77–81.

[12] Näther, N., Henkel, H., Schneider, A., and Schöning, M. J. Investigation of different catalytically active and passive materials for realising a hydrogen peroxide gas sensor. *Physica Status Solidi A 206*, 3 (2009), 449–454.

[13] Näther, N., Juárez, L. M., Emmerich, R., Berger, J., Friedrich, P., and Schöning, M. J. Detection of hydrogen peroxide (H_2O_2) at exposed temperatures for industrial processes. *Sensors 6*, 4 (2006), 308–317.

[14] Kirchner, P., Ng, Y. A., Spelthahn, H., Schneider, A., Henkel, H., Friedrich, P., Kolstad, J., Berger, J., Keusgen, M., and Schöning, M. J. Gas sensor investigation based on a catalytically activated thin-film thermopile for H_2O_2 detection. *Physica Status Solidi A 207*, 4 (2010), 787–792.

[15] Kirchner, P., Oberländer, J., Friedrich, P., Berger, J., Suso, H.-P., Kupyna, A., Keusgen, M., and Schöning, M. J. Optimisation and fabrication of a calorimetric gas sensor built up on a polyimide substrate for H_2O_2 monitoring. *Physica Status Solidi A 208*, 6 (2011), 1235–1240.

[16] Kirchner, P., Oberländer, J., Friedrich, P., Berger, J., Rysstad, G., Keusgen, M., and Schöning, M. J. Realisation of a calorimetric gas sensor on polyimide foil for applications in aseptic food industry. *Sensors and Actuators B: Chemical 170* (2012), 60–66.

[17] Verband Deutscher Maschinen- und Anlagenbauer (VDMA). Filling machines of VDMA hygiene class V: testing the effectiveness of packaging sterilization devices. Code of practice 6, 2008.

[18] Farmiloe, F. J., Cornford, S. J., Coppock, J. B. M., and Ingram, M. The survival of *Bacillus subtilis* spores in the baking of bread. *Journal of the Science of Food and Agriculture 5*, 6 (1954), 292–304.

8 Towards a wireless sensor system for real-time H_2O_2 monitoring in aseptic food processes

KIRCHNER, P., Oberländer, J., Suso, H.-P., Rysstad, G., Keusgen, M., and Schöning, M. J.

Physica Status Solidi A (2013), in press.

8.1 Abstract

A wireless sensor system based on the industrial ZigBee standard for low-rate wireless networking was developed that enables real-time monitoring of gaseous H_2O_2 during the package sterilisation in aseptic food processes. The sensor system consists of a remote unit connected to a calorimetric gas sensor, which was already established in former works, and an external base unit connected to a laptop computer. The remote unit was built up by an XBee radio frequency module for data communication and a programmable system-on-chip controller to read out the sensor signal and process the sensor data, whereas the base unit is a second XBee radio frequency module. For the rapid H_2O_2 detection on various locations inside the package that has to be sterilised, a novel read-out strategy of the calorimetric gas sensor was established, wherein the sensor response is measured within the short sterilisation time and correlated with the present H_2O_2 concentration. In an exemplary measurement application in an aseptic filling machinery, the suitability of the new, wireless sensor system was demonstrated, wherein the influence of the gas velocity on the H_2O_2 distribution inside a package was determined and verified with microbiological tests.

8.2 Introduction

Aseptic packaging is defined as the filling of a microbiologically stable product into sterilised packages under aseptic conditions that prevent microbial recontamination. Therein, the sterilisation of packaging material is the essential process prior to the food filling in order to inactivate microorganisms, which could contain in packages during their transport and forming [1]. The result is a safe, packed product with long shelf-life that does not require preservatives or refrigeration during storage.

Since more than a half century, hydrogen peroxide (H_2O_2) is used for the sterilisation of packaging material started with the first aseptic filling system for carton packages from Tetra Pak in 1961 [2]. Even today, hydrogen peroxide is the most significant sterilisation agent in aseptic food processes among a variety of other physical and chemical methods (e.g., UV radiation, ionisation, ethylene oxide, peracetic acid) [3]. The wide-spread usage of H_2O_2 in sterilisation processes relies on its strong microbicidal effectiveness, especially in combination with heat [4, 5], and on its non-hazardous effect on the package surface, product or consumer at a low concentration level of residue [1]. Due to the fact that the microbicidal effectiveness is additionally enhanced by gaseous H_2O_2 [6, 7], the aseptic food industry has been enlarged its focus on using H_2O_2 in gas phase as sterilisation agent within the last few decades in order to improve the efficiency of the sterilisation process. In this process, it is indispensable that the package surface is uniformly treated by gaseous H_2O_2 during a short sterilisation time, wherein the microbicidal effectiveness predominantly depends on the local H_2O_2 concentration. Due to this fact, there is a great demand in the aseptic food industry for a monitoring device that enables the measurement of the H_2O_2 distribution on the inner surface of a package within this short sterilisation time.

In previous works, gas sensors for measuring the H_2O_2 concentration were introduced, which are based on a calorimetric differential set-up of a catalytically activated and passivated temperature-sensitive segment. If the sensor is exposed to gaseous H_2O_2, it detects the reaction enthalpy of H_2O_2 decomposition on the catalyst in form of an increased temperature difference between the catalytically activated and passivated temperature-sensitive segment. Starting from a macroscopic sensor set-up introduced by Näther et *al.* [8, 9] that was designed for on-line monitoring of H_2O_2, thin-film gas sensors with different layouts and material compositions have been developed in ongoing research activities, which can be mounted on the package's inner surface and detect the local H_2O_2 concentration. First, thin-film gas sensors were successfully built up on conventional silicon substrates with thin-film resistances or even thin-film thermopiles as temperature-sensitive segments, which have been passivated by perfluoralcoxy, fluorinated ethylene propylene or SU-8 photoresist and catalytically activated by platinum black, palladium

or manganese oxide [10–12]. Furthermore, sensors on a polyimide substrate have been additionally realised and extensively characterised in order to optimise their response behaviour in terms of sensitivity and response time in comparison to silicon-based sensors [13, 14]. The characteristics of the different thin-film gas sensors are overviewed in Tab. 8.1.

Table 8.1: Characteristics (sensitivity, off-set and response time) of the different thin-film gas sensors for H_2O_2 detection (adapted from [10–14]).

Sensor concept	Sensitivity (°C/(% v/v))	Off-set (°C)	Response time, $t_{90\%}$ (s)
Silicon-based sensor (thin-film resistance)	0.57	0.12	6.7
Silicon-based sensor (thin-film thermopile)	0.84*	0.61*	2.5
Polyimide-based sensor (large contact area)	7.15	-0.52	5.9
Polyimide-based sensor (small contact area)	4.78	-0.35	3.8

* *Calculated sensitivity and off-set from specified signal in mV.*

Even though, various sensors have been successfully established, a sensor electronic is required for measuring the H_2O_2 concentration inside of a moving package with one of the mentioned gas sensors during the rapid and dynamic sterilisation process in an aseptic filling machinery. Therefore, the open standard ZigBee for short-range wireless connections between miniaturised electronic modules was envisaged. This standard is built on top of the physical layer (PHY) and medium-access control sublayer (MAC) in the network-protocol stack defined in the IEEE standard 802.15.4 for low-rate wireless networking [15, 16]. ZigBee specifies the network layer (NWK) that is responsible for the organisation of data forwarding and routing in a network and the application layer (APL) providing a framework for communication and application programming [16, 17]. Its architecture provides cost-effective, low-power and reliable wireless networking with convenience of installation that can also be applied in dynamic industrial processes. Thus, ZigBee has gained huge attractiveness in the development of wireless sensor networks, since the standard was released in 2004. Today, the application field of wireless sensor networks based on the ZigBee standard varies in a wide range: for instance, in civil engineering such as for measuring the mechanical stress of bridges [18, 19]; to determine

the climatic conditions in crop fields [20, 21]; for detecting forest fires [22]; for monitoring the ambient conditions in food logistics [23] and in the medical field, e.g., to control the physiological state of patients by measuring the heartbeat (ECG) or blood pressure [24–26].

In the present work, a ZigBee-based wireless sensor system has been designed, which enables the monitoring of the local H_2O_2 concentration on the inner surface of a package in a dynamic sterilisation process. Furthermore, a novel read-out strategy for the investigated thin-film gas sensors has been established that is necessary for measuring the local H_2O_2 concentration in real-time during the short sterilisation time in the order of 1.9 s.

8.3 Experimental

8.3.1 Wireless sensor system

The wireless sensor system consists of three main components: (*i*) a remote unit, which is directly connected to (*ii*) the calorimetric gas sensor - in this case, a sensor with thin-film resistances as temperature-sensitive segments, and (*iii*) an external base unit connected to a laptop computer.

The remote unit comprises a low-power XBee radio frequency (RF) module (model series 1 from Digi International) with a pre-assembled XBee circuit board and a programmable system-on-chip (PSoC) controller (PSoC 3 from Cypress Semiconductor) connected to a sensor interface (s. Fig. 8.1(a)). The PSoC controller is applied for reading out the sensor signal over the sensor interface, processing the sensor data and providing them to the XBee RF module. The XBee RF module with integrated antenna is based on the ZigBee standard using the industrial, scientific and medical (ISM) frequency band at 2.4 GHz. It has an effective radio range of 30 m (indoor). The XBee RF module of the remote unit was configured as an end-point device that only allows it to communicate with the base unit. Both, PSoC controller and XBee RF module, are supplied by a 9 V battery.

The base unit is merely another XBee RF module fixed on a pre-assembled XBee circuit board with USB connection (s. Fig. 8.1(b)). The XBee RF module of the base unit was configured as coordinator that serves as central node of the wireless network with the envisaged star topology. This network architecture enables the operator to simply include additional remote units as end devices connected to further gas sensors for simultaneous read-out of H_2O_2 concentrations even for different food-processing lines in an aseptic filling machinery. The base unit is directly connected to a laptop computer via USB port. To initialise the remote unit as well as to read out and store the sensor data, which

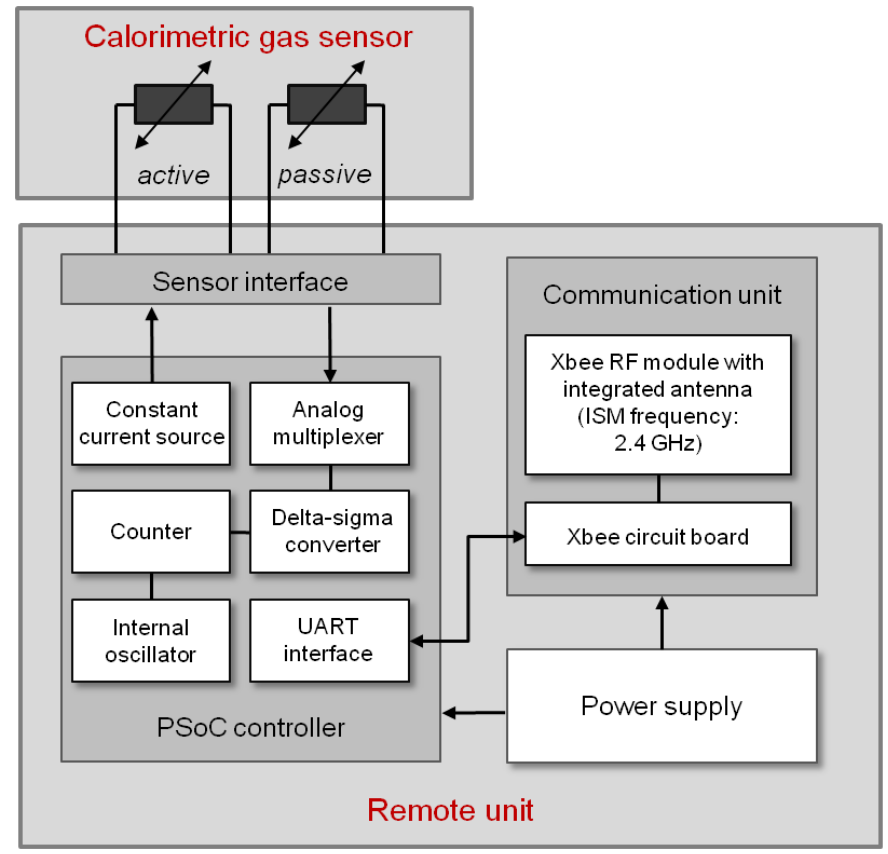

Figure 8.1: (a) Block diagram of the remote unit comprising an XBee RF module with circuit board, a PSoC controller with sensor interface connected to the calorimetric gas sensor and a power supply. (b) Block diagram of the base unit built up by an XBee RF module with circuit board and the user interface made up of a laptop with a developed LabVIEW program.

are transmitted by the remote unit and received by the base unit, a LabVIEW program was developed as graphical user interface.

The constructed wireless sensor electronic, which consists of a remote unit with sensor interface and a base unit with USB connection, is depicted in Fig. 8.2.

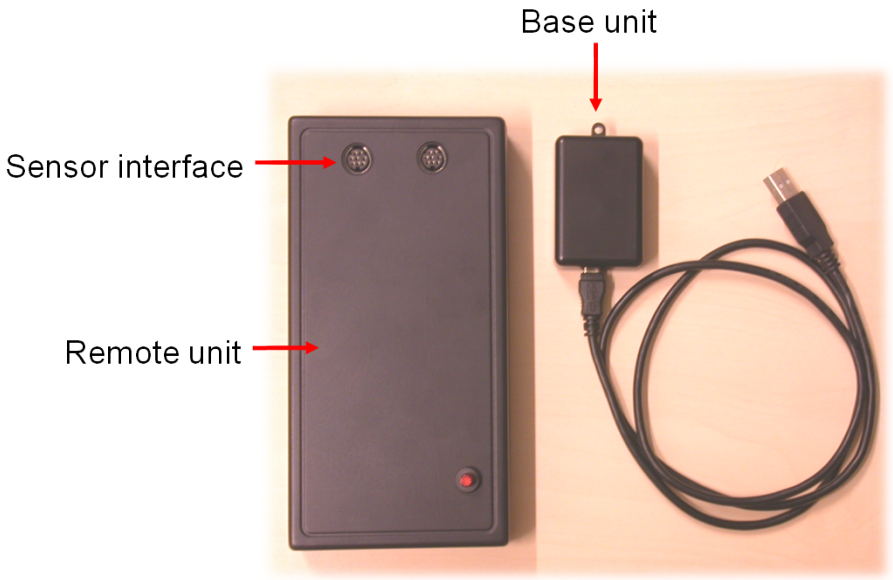

Figure 8.2: Wireless sensor electronic consisting of the remote unit with sensor interface and the base unit with USB connection.

8.3.2 Configuration of the PSoC controller

The programmable system-on-chip (PSoC) controller includes an embedded microcontroller unit (MCU) together with mixed-signal integrated circuits of configurable analog and digital peripheral blocks and functions (e.g., analog-to-digital converter, signal amplifier, filter, serial data transmission, timer, counter, pulse width modulator) and general purpose input/output (GPIO) pins on a single chip platform. Its architecture offers the possibility to create application-specific configurations just by selecting the desired embedded peripheral blocks or functions that reduce the number of electronic components in an external electronic circuitry and thus, affords a high degree of flexibility in programming [27, 28].

In this work, a PSoC 3 controller has been used that contains an 8-Bit MCU based on 8051 architecture. Two current digital-to-analog converters have been implemented in the controller configuration as constant current sources for the thin-film resistances of the calorimetric gas sensor, wherein each of them providing an output current of 1 mA. A delta-sigma analog-to-digital converter with a resolution of 20 Bit and an analog mul-

tiplexer with two input channels were configured to read out the voltage drops on the thin-film resistances and to digitise the voltage signals. A sampling rate of 1 kHz was ascertained by a counter linked to an internal oscillator (IMO: internal main oscillator). By means of a developed subroutine, the temperatures of the catalytically activated and passivated thin-film resistances of the calorimetric gas sensor as well as the H_2O_2 concentration resulting from the temperature difference is calculated from the temperature drops on both thin-film resistances.

For serial communication between the PSoC controller and the XBee RF module, a UART (universal asynchronous receiver transmitter) component was implemented in the controller configuration.

8.3.3 Sensor read-out strategy

Due to the fact that the different thin-film gas sensors based on a calorimetric differential set-up offer response times above the contact time of the sterilisation process that amounts to be 1.9 s (s. Tab. 8.1), a novel read-out strategy has been established for real-time monitoring. In the present work, the calorimetric gas sensor built-up on a polyimide substrate with small catalytic contact area, which was already introduced in [14], was used due to its high sensitivity by a low response time (s. Tab. 8.1). The temperature difference ($\Delta T_{\mathrm{signal}}$) between the catalytically active (T_{active}) and passive sensor segment (T_{passive}) serves as sensor signal. Instead of waiting until the sensor signal has reached a steady state condition, the signal peak after a contact time of 1.9 s with gaseous H_2O_2 has been correlated with the present H_2O_2 concentration. For calibrating the sensor signal in a developed sterilisation test rig, which was already presented in [8, 10] in detail, the sensor was mounted on a hydraulic slide rail and exposed to gaseous H_2O_2 for a contact time of 1.9 s at varied H_2O_2 concentration steps between 0 and 8% v/v, at a constant outlet-gas temperature of 240 °C and a gas flow of 10 m^3/h. Three signal peaks were detected for each concentration step, respectively, which have been correlated with the particular H_2O_2 concentration.

8.3.4 Application of the wireless sensor system

In an exemplary application of the wireless sensor system in an aseptic filling machinery, its suitability for measuring the distribution of the H_2O_2 concentration on the inside of a package in real-time during the sterilisation process should be demonstrated. Two measurement series were conducted, wherein the influence of the gas flow on the homogeneity of the H_2O_2 distribution on the package's inner surface has been investigated during the sterilisation process. Therefore, a constant, initial H_2O_2 concentration of 3.7% v/v at the gas-outlet nozzle was adjusted for two different gas velocities of 40 and 100 m/s,

respectively. The local H_2O_2 concentration was consecutively measured by the calorimetric gas sensor at five different positions (upper and middle position of side panel as well as middle position and at two corners of the package bottom) on the inner surface of a package, respectively (s. Fig. 8.3(a)). The sensor signal was read out by the remote unit of the wireless sensor electronic mounted on the outer side of the test package (s. Fig. 8.3(b)) and transmitted to the external base unit.

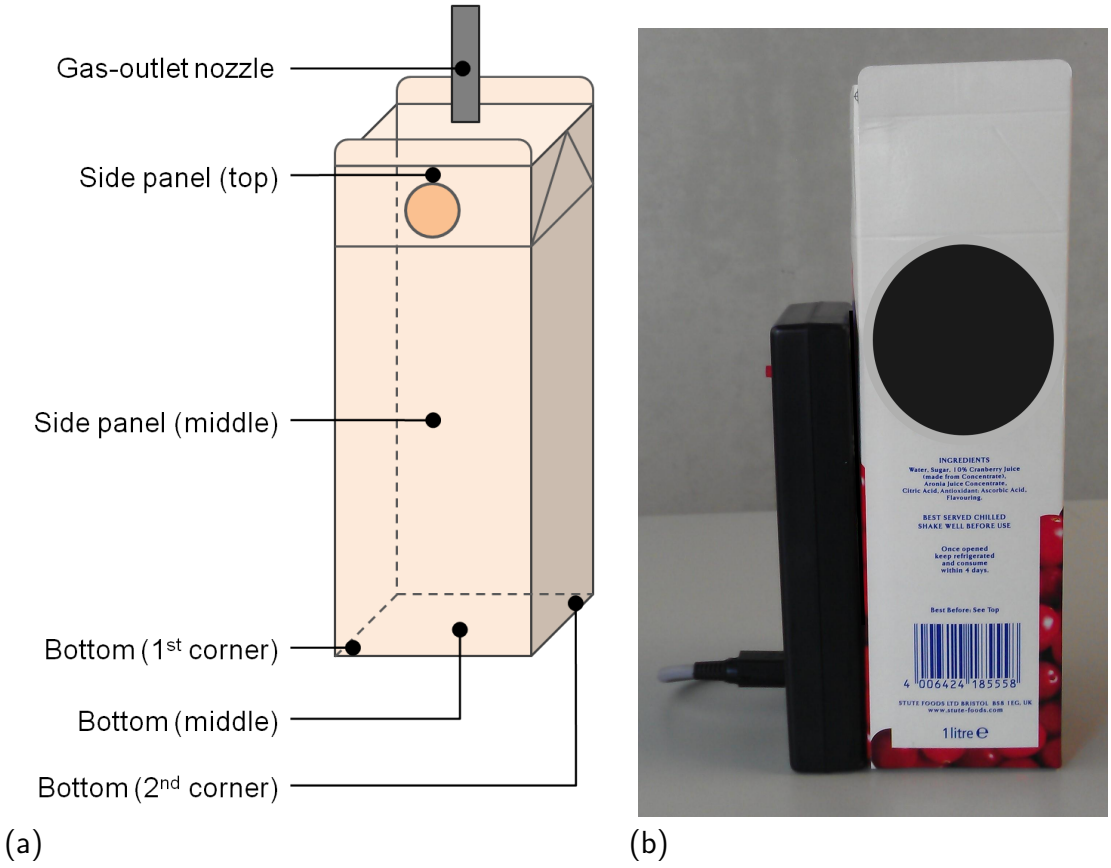

Figure 8.3: (a) Schematic picture of a test package with marked sensor positions and (b) test package with mounted remote unit.

In addition to the sensor measurements, the logarithmic cycle reduction (LCR) – a measure of the microbicidal effectiveness of a sterilisation process by using bacterial spores of *Bacillus atrophaeus* – was determined for the two varied gas velocities in a corner of the package bottom according to Eq. 8.1 and compared to the concentration measurement results:

$$LCR = \lg \frac{N_0}{N_S} \tag{8.1}$$

Here, N_0 is the initial spore load of the package surface located on a corner of the

bottom, and N_S is the total number of survived spores after the sterilisation process.

8.4 Results and discussion

8.4.1 Sensor calibration

After transmission tests of the wireless sensor electronic were successfully carried out and the functionality of the PSoC controller was verified, the electronic was connected to the calorimetric gas sensor and a calibration protocol has been conducted. Therein, the sensor was calibrated in a H_2O_2 concentration range between 0 and 8% v/v according to the novel read-out strategy introduced in section 8.3.3. During the measurement a constant gas temperature of 240 °C and a gas flow of 10 m^3/h were adjusted in the sterilisation test rig. In Fig. 8.4(a), the response behaviour of the temperatures on the active (T_{active}) and passive sensor segment ($T_{passive}$) as well as the temperature difference (ΔT_{signal}) are depicted. During the measurement, a rapid rise of T_{active} and $T_{passive}$ was noticed after the sensor was exposed to the gas stream for a short contact time of 1.9 s. Even in a gas stream without H_2O_2, both T_{active} and $T_{passive}$ increased from 75 °C to 125 °C resulting from the elevated gas temperature, whereas the temperature difference (ΔT_{signal}) did not change significantly demonstrating an equal temperature-response behaviour of the active and passive sensor segment.

A growth in ΔT_{signal} was observed with rising H_2O_2 concentrations caused by a fast H_2O_2 decomposition effect on the sensor surface during the contact time. After the sensor was exposed again to the same H_2O_2 concentration, even no distinction between the peaks of ΔT_{signal} could be drawn (s. Fig. 8.4(b)) that points out a high repeatability of the novel read-out strategy.

The resulting calibration plot from the measurement curve shows a linear correlation between the signal peaks of ΔT_{signal} and the applied H_2O_2 concentration (s. Fig. 8.5). Therein, a sensitivity of 2.06 °C/(% v/v) was determined that amounts to be 43% of the sensor's sensitivity as steady-state signal (s. Tab. 8.1). Furthermore, the sensor showed a low off-set of 0.60 °C.

8.4.2 Application of the wireless sensor system

In an exemplary measurement application of the wireless sensor system, the impact of the gas flow on the H_2O_2 distribution on the package's inner surface has been studied at a H_2O_2 concentration of 3.7% v/v on the gas-outlet nozzle of the sterilisation process. Therein, the local H_2O_2 concentration was determined by the sensor system at five different locations inside the package at an adjusted gas velocity of 40 and 100 m/s,

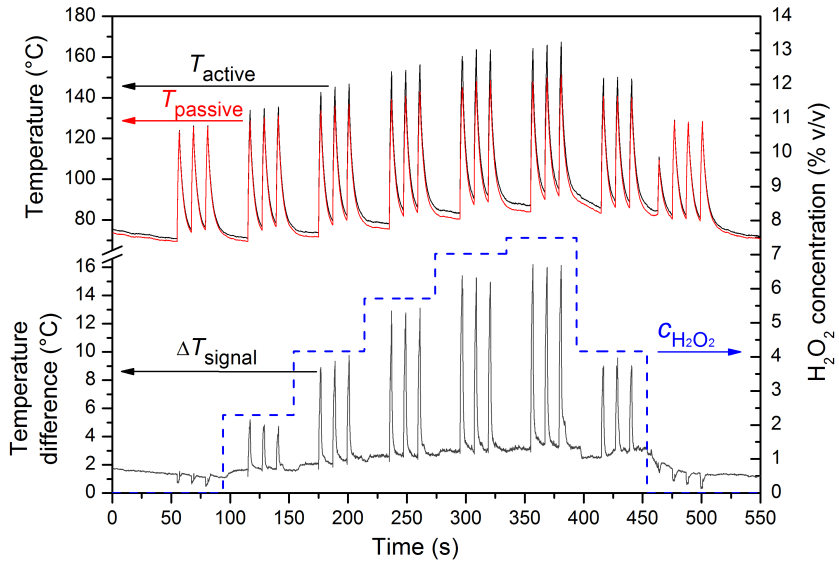

(a)

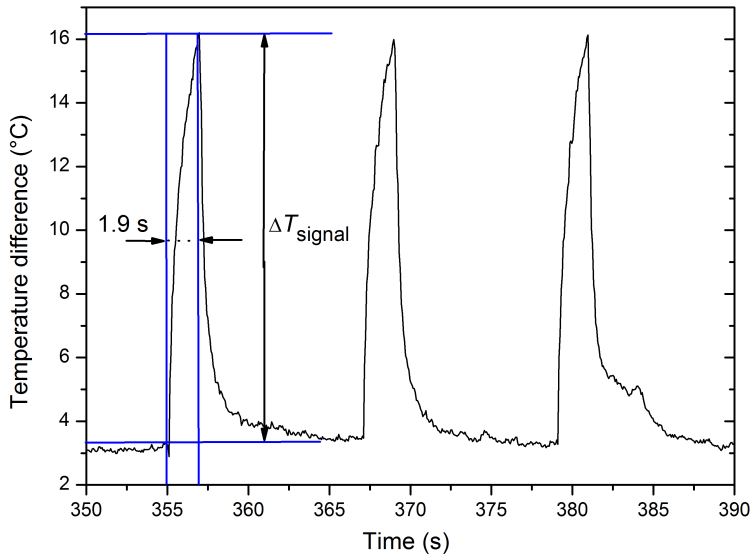

(b)

Figure 8.4: (a) Measurement curve of the calorimetric gas sensor exposed for a contact time of 1.9 s with the gas stream in a H_2O_2 concentration range from 0 to 8% v/v (gas temperature: 240 °C, gas flow: 10 m^3/h); and (b) signal peaks for a H_2O_2 concentration of 7.6% v/v demonstrating the repeatability of the novel read-out strategy.

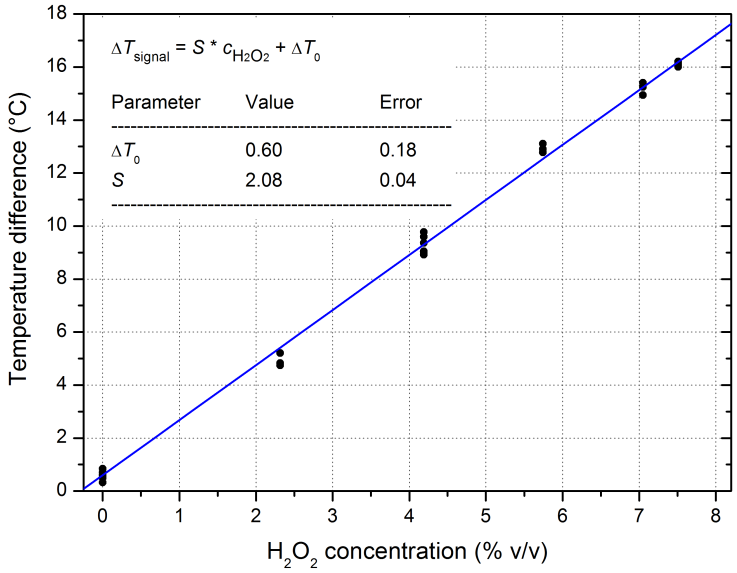

Figure 8.5: Calibration plot of the calorimetric gas sensor for the considered H_2O_2 concentration range from 0 to 8% v/v.

respectively (s. Fig. 8.6(a)). A strong influence of the velocity on the distribution of the H_2O_2 concentration inside the package was observed.

At a low gas velocity a decreased H_2O_2 concentration with a minimum of 1.6% v/v on the bottom of the package compared to the upper region of the side panel with a maximum concentration of up to 2.8% v/v was identified. This effect could rely on the low gas flow resulting in a non-uniform dilution of the H_2O_2 gas stream with ambient air, which increases with longer distances from the gas-outlet nozzle leading to a reduced H_2O_2 concentration on the package bottom. In contrast, an almost equal H_2O_2 concentration level of around 2.5% v/v was achieved at the different measurement points inside the package for an increased gas velocity of 100 m/s, presenting a homogenous H_2O_2 distribution on the package's inner surface. Both measurement series implicate a strong influence of the H_2O_2 gas distribution inside the package. Moreover, a maximum H_2O_2 concentration of 2.8% v/v was detected that is 25% lower compared to the H_2O_2 concentration of 3.7% v/v at the gas-outlet nozzle. The reason for decreased H_2O_2 concentrations inside the package results from an unavoidable dilution of the H_2O_2 gas stream with the ambient air during the short sterilisation period.

An exemplary, real-time measurement curve with two measurement cycles for each gas velocity (100 and 40 m/s) in a bottom corner of a moving package is depicted in Fig. 8.6(b). The diagram demonstrates a good reproducibility in measuring the local

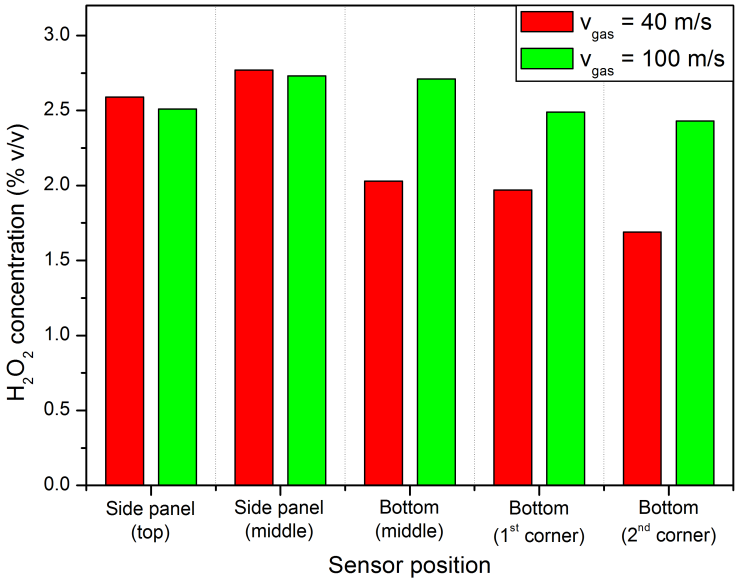

(a)

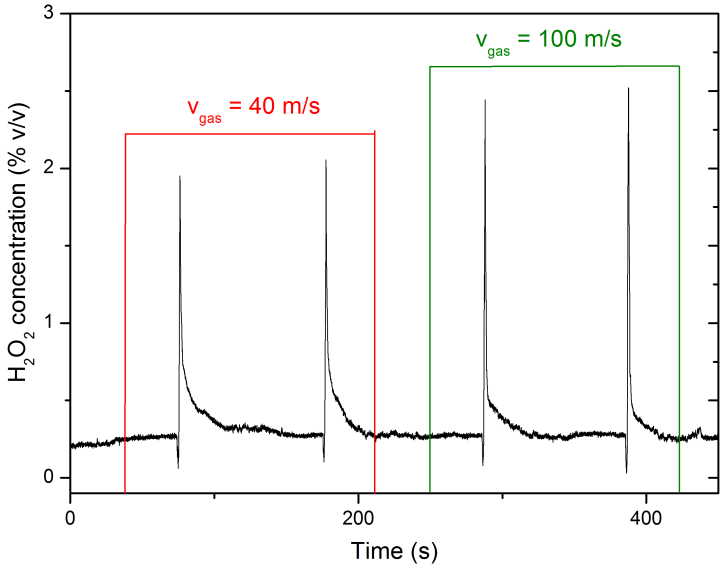

(b)

Figure 8.6: (a) Distribution of the H_2O_2 concentration on five different positions at the package's inner surface measured by the wireless sensor system for a gas velocity of 40 and 100 m/s, respectively, during the sterilisation process; and (b) real-time measurement curve for the two gas velocities detected in the 1st corner on the bottom of a moving package.

H_2O_2 concentration by means of the wireless sensor system and presents the distinct difference in the measured H_2O_2 concentration of the two different gas velocities.

To confirm the measurement results obtained by means of the wireless sensor system, the logarithmic cycle reduction of bacterial spores as test microorganisms was determined in one of the corners of the package bottom for each H_2O_2-gas stream (gas velocity of 40 and 100 m/s) and for a gas stream without H_2O_2, respectively. Afterwards, the LCR was matched with the local H_2O_2 concentration measured by the wireless sensor system. From the diagram depicted in Fig. 8.7, an obvious dependency of the LCR on the local H_2O_2 concentration was figured out.

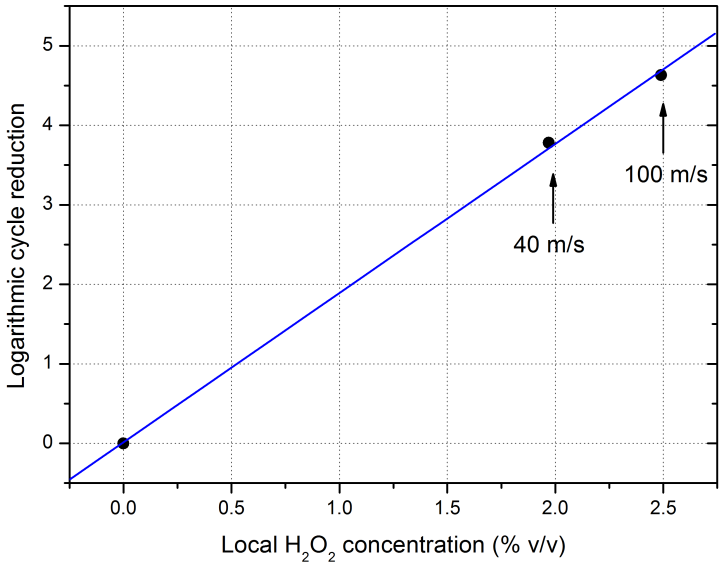

Figure 8.7: Logarithmic cycle reduction determined in the 1st corner of the package bottom for a gas velocity of 40 and 100 m/s, respectively, as well as for a gas stream without H_2O_2 and matched with the local H_2O_2 concentration.

Thus, this experiment the wireless sensor system highlights its suitability to monitor local H_2O_2 concentrations inside of packages in real-time during their sterilisation in aseptic food processes.

8.5 Conclusions

In the present work, a wireless sensor system was developed for monitoring the distribution of H_2O_2 concentrations inside of food packages in real-time, when they are sterilised by gaseous H_2O_2. The wireless sensor system contains a remote unit connected to one of

the calorimetric gas sensors, which have been realised in former works, and an external base unit with USB interface. The remote unit is built up by an XBee RF module for wireless data communication based on the ZigBee standard and a PSoC controller with sensor interface for reading out the sensor signal and providing the sensor data. The base unit only consists of another XBee RF module serving as coordinator of the ZigBee network. The sensor system allows the monitoring of gaseous H_2O_2 inside of packages in a dynamic sterilisation process. Furthermore, a novel read-out strategy for real-time detection of the H_2O_2 concentration within the sterilisation period was established. Instead of correlating the steady-state sensor signal with the H_2O_2 concentration, the signal peak attained within the sterilisation was matched with the present gas concentration. In an exemplary measurement, the functionality of the wireless sensor system was demonstrated, wherein the influence of the gas flow on the H_2O_2 distribution on the package's inner surface was investigated. The obtained measurement results were additionally confirmed by microbiological inspections with bacterial spores as test microorganisms.

Thus, the novel sensor system could be a supporting monitoring device for the control and the optimisation of sterilisation processes in aseptic filling systems.

Acknowledgements

The authors gratefully thank Prof. Dr. H.-J. Ackermann and Dipl.-Ing. H.-G. Römer for technical support.

References

[1] Ansari, I., and Datta, A. An overview of sterilization methods for packaging materials used in aseptic packaging systems. *Food and Bioproducts Processing 81*, 1 (2003), 57–65.

[2] Burton, H., Ed. *Ultra high temperature processing of milk and milk products.* Elsevier Applied Science, London, 1988.

[3] Cerny, G. Testing of aseptic machines for efficiency of sterilization of packaging materials by means of hydrogen peroxide. *Packaging Technology and Science 5*, 2 (1992), 77–81.

[4] Block, S. S., Ed. *Desinfection, sterilization and preservation.* Lea & Febiger, Philadelphia, 1991.

[5] Heckert, R. A., Best, M., Jordan, L. T., Dulac, G. C., Eddington, D. L., and Sterritt, W. G. Efficacy of vaporized hydrogen peroxide against exotic animal viruses. *Applied And Environmental Microbiology 63*, 10 (1997), 3916–3918.

[6] McDonnell, G., and Russell, A. D. Antiseptics and disinfectants: activity, action, and resistance. *Clinical Microbiology Reviews 12*, 1 (1999), 147–179.

[7] Unger-Bimczok, B., Kottke, V., Hertel, C., and Rauschnabel, J. The influence of humidity, hydrogen peroxide concentration, and condensation on the inactivation of *Geobacillus stearothermophilus* spores with hydrogen peroxide vapor. *Journal of Pharmaceutical Innovation 3*, 2 (2008), 123–133.

[8] Näther, N., Juárez, L. M., Emmerich, R., Berger, J., Friedrich, P., and Schöning, M. J. Detection of hydrogen peroxide (H_2O_2) at exposed temperatures for industrial processes. *Sensors 6*, 4 (2006), 308–317.

[9] Näther, N., Henkel, H., Schneider, A., and Schöning, M. J. Investigation of different catalytically active and passive materials for realising a hydrogen peroxide gas sensor. *Physica Status Solidi A 206*, 3 (2009), 449–454.

[10] Kirchner, P., Ng, Y. A., Spelthahn, H., Schneider, A., Henkel, H., Friedrich, P., Kolstad, J., Berger, J., Keusgen, M., and Schöning, M. J. Gas sensor investigation based on a catalytically activated thin-film thermopile for H_2O_2 detection. *Physica Status Solidi A 207*, 4 (2010), 787–792.

[11] Kirchner, P., Li, B., Spelthahn, H., Henkel, H., Schneider, A., Friedrich, P., Kolstad, J., Keusgen, M., and Schöning, M. J. Thin-film calorimetric H_2O_2 gas sensor for the validation of germicidal effectivity in aseptic filling processes. *Sensors and Actuators B: Chemical 154*, 2 (2011), 257–263.

[12] Kirchner, P., Reisert, S., Pütz, P., Keusgen, M., and Schöning, M. J. Characterisation of polymeric materials as passivation layer for calorimetric H_2O_2 gas sensors. *Physica Status Solidi A 209*, 5 (2012), 859–863.

[13] Kirchner, P., Oberländer, J., Friedrich, P., Berger, J., Suso, H.-P., Kupyna, A., Keusgen, M., and Schöning, M. J. Optimisation and fabrication of a calorimetric gas sensor built up on a polyimide substrate for H_2O_2 monitoring. *Physica Status Solidi A 208*, 6 (2011), 1235–1240.

[14] Kirchner, P., Oberländer, J., Friedrich, P., Berger, J., Rysstad, G., Keusgen, M., and Schöning, M. J. Realisation of a calorimetric gas sensor on polyimide foil for applications in aseptic food industry. *Sensors and Actuators B: Chemical 170* (2012), 60–66.

[15] IEEE Standard 802.15.4, Part 15.4: Wireless medium access control (MAC) and physical layer (PHY) specifications for low-rate wireless personal area networks (LR-WPAN). Technical report, 2003.

[16] ZigBee Alliance `http://www.zigbee.org`, date: 20 September 2012.

[17] Baronti, P., Pillai, P., Chook, V. W., Chessa, S., Gotta, A., and Hu, Y. F. Wireless sensor networks: a survey on the state of the art and the 802.15.4 and ZigBee standards. *Computer Communications 30*, 7 (2007), 1655–1695.

[18] Mascarenas, D. L., Todd, M. D., Park, G., and Farrar, C. R. Development of an impedance-based wireless sensor node for structural health monitoring. *Smart Materials and Structures 16*, 6 (2007), 2137–2145.

[19] Lynch, J. P., and Loh, K. J. A summary review of wireless sensors and sensor networks for structural health monitoring. *Shock and Vibration Digest 38*, 2 (2006), 91–128.

[20] Liu, H., Meng, Z., and Cui, S. A wireless sensor network prototype for environmental monitoring in greenhouses. In *International Conference on Wireless Communications, Networking and Mobile Computing, 2007. WiCom 2007* (2007), pp. 2344–2347.

[21] Verma, S., Chug, N., and Gadre, D. Wireless sensor network for crop field monitoring. In *International Conference on Recent Trends in Information, Telecommunication and Computing (ITC)* (2010), pp. 207–211.

[22] Garcia-Sanchez, A.-J., Garcia-Sanchez, F., and Garcia-Haro, J. Wireless sensor network deployment for integrating video-surveillance and data-monitoring in precision agriculture over distributed crops. *Computers and Electronics in Agriculture 75*, 2 (2011), 288–303.

[23] Ruiz-Garcia, L., Barreiro, P., and Robla, J. Performance of ZigBee-based wireless sensor nodes for real-time monitoring of fruit logistics. *Journal of Food Engineering 87*, 3 (2008), 405–415.

[24] Hu, F., Jiang, M., Celentano, L., and Xiao, Y. Robust medical ad hoc sensor networks (MASN) with wavelet-based ECG data mining. *Ad Hoc Networks 6*, 7 (2008), 986–1012.

[25] Boquete, L., Ascariz, J. M. R., Cantos, J., Barea, R., Miguel, J. M., Ortega, S., and Peixoto, N. A portable wireless biometric multi-channel system. *Measurement 45*, 6 (2012), 1587–1598.

[26] Du, Y.-C., Lee, Y.-Y., Lu, Y.-Y., Lin, C.-H., Wu, M.-J., Chen, C.-L., and Chen, T. Development of a telecare system based on ZigBee mesh network for monitoring blood pressure of patients with hemodialysis in health care centers. *Journal of Medical Systems 35*, 5 (2011), 877–883.

[27] Ashby, R., Ed. *Designer's guide to the cypress PSoC*. Elsevier-Newnes, Oxford, 2005.

[28] Seguine, D. Just add sensor - integrating analog and digital signal conditioning in a programmable system on chip. In *Proceedings of IEEE Sensors* (2002), vol. 1, pp. 665–668.

8.6 Appendix

8.6.1 Additional information of the wireless sensor system

In Fig. 8.8, the interior part of the remote unit of the wireless sensor system is depicted as support to section 8.3.1.

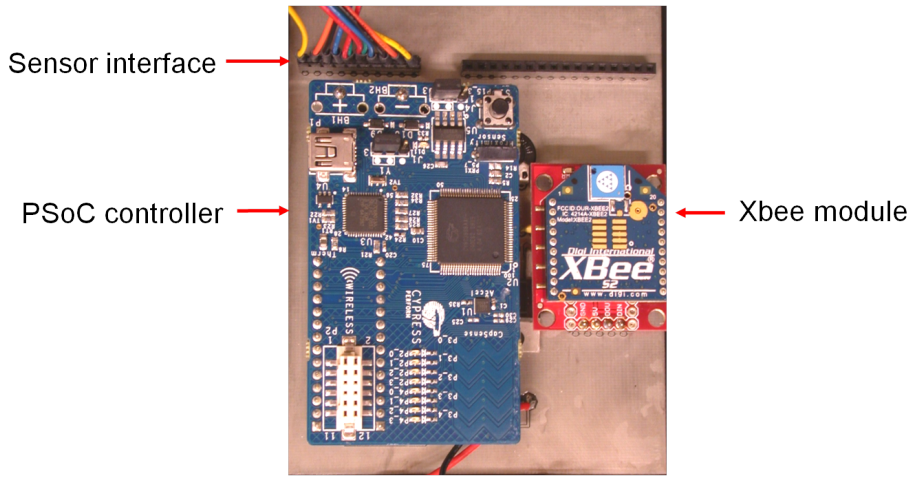

Figure 8.8: Interior part of the remote unit of the wireless sensor system.

9 Summary and perspectives

In aseptic food processes, the sterilisation of the packaging material is the decisive step in order to avoid that the product subsequently filled into the package stays in contact with food-spoilage microorganisms or even pathogenic organisms. Today, the packaging material is progressively treated by gaseous H_2O_2 at elevated temperatures due to its strong microbicidal effectiveness and its environment-friendly decomposition products. In this process, the H_2O_2 concentration ranging up to several volume percent must be high enough in order to ensure a required degree of sterility of the packaging material. Furthermore, the gaseous H_2O_2 must be uniformly distributed on the package's inner surface during the rapid sterilisation process. This is leading to the huge demand of the aseptic food industry for a gas-sensor system to monitor quantitatively the H_2O_2 concentration during the sterilisation of food packages under real-time conditions.

The initial situation led to the realisation of thin-film gas sensors based on a calorimetric differential set-up, which is suitable for the measurement of H_2O_2 gas concentrations up to the percentage range under harsh environmental conditions. The sensors consist of a catalytically active sensing segment, where H_2O_2 decomposes at elevated gas temperature in an exothermic reaction, and a passive sensing segment, where decomposition is avoided. The temperature difference between the active and passive segment serves as a measure of the gaseous H_2O_2 concentration and can be detected by an implemented temperature transducer. The results obtained in each chapter of this thesis have conduced to achieve this overall principal outcome and consequently, they demonstrate the feasibility of the thin-film calorimetric gas sensors as a novel, potential method for monitoring the gaseous H_2O_2 concentration within the package sterilisation carried out by gaseous H_2O_2 as sterilant in aseptic food processes.

Chapter 1 gives an introduction to calorimetric gas sensors, in general, and to hydrogen peroxide and in particular, to its usage in aseptic food processes. Furthermore, the state of the art of measurement systems for gaseous H_2O_2 and the initial situation as motivation for this work is presented in **chapter** 1.

In **chapter** 2, thin-film calorimetric gas sensors with silicon-based, monolithic thermopiles have been fabricated and their response behaviour for the detection of H_2O_2 under altered atmospheric conditions – changed gas concentration, temperature and gas flow – has been investigated. The thermopiles are made up of gold/nickel and tung-

sten/nickel and they have been designed in form of circular and linear arrangements. In a first comparative study, the response behaviour of the sensors with different thermopile layouts and material compositions activated by the same catalyst of MnO_2, have been characterised in H_2O_2 atmosphere. Therein, the sensors with linear thermopile exhibit an enlarged sensitivity in comparison to the sensors with circular thermopile. This phenomenon can be derived from the different distances of the "hot" and "cold" junctions of the thermopiles leading to a change in the heat transfer from the "hot" to the "cold" junctions of the thermopiles. Moreover, the sensors with thermopiles made up of gold/nickel showed always a slightly higher sensitivity than the sensors of tungsten/nickel. Even though, the theoretical Seebeck coefficient of tungsten/nickel is greater than the coefficient of gold/nickel, the elevated resistance of the tungsten layer is effecting a voltage drop that results in a lower sensor sensitivity. A further study was conducted in order to determine the response characteristics of sensors activated by manganese(IV) oxide particles in the range of several micrometres and nanometre-sized palladium, respectively. The sensors with palladium as catalyst possessed the largest sensitivity of 166 μV/(% v/v), which is adequate to a maximum temperature rise of 0.84 °C/(% v/v) and results from the enlarged surface-to-volume ratio of the particles in the nanometre range compared to the lower ratio of the manganese(IV) oxide particles. In final measurements at altered gas temperatures and gas-flow rates, the sensor signal was hardly influenced from the changed process conditions. The obtained results of **chapter** 2 highlight the stable response characteristic of the sensors made up of thin-film thermopiles and their suitability as monitoring device for gaseous H_2O_2 concentrations even at harsh conditions. However, drawbacks of the sensors represent their low voltage rise in H_2O_2 atmosphere of several microvolts and that the thermopile layouts could act as antenna leading to an increased noise behaviour in industrial food processes.

Consequently, **chapter** 3 was focusing on the realisation of calorimetric gas sensors made up of thin-film resistances as temperature transducer, where each sensor was also built up on a single silicon chip. In this study, the sensors were coated by three different catalytically active dispersions of platinum black, palladium or manganese(IV) oxide particles, respectively, and they have been characterised under gaseous H_2O_2 atmosphere. The particle size of each dispersion was in an equal range of up to 10 μm in order to enable a comparability of the chosen catalytically active materials. In this study, the sensor activated by a dispersion of manganese(IV) oxide showed the largest sensitivity of 0.565 °C/(% v/v), which could rely on its reactive properties allowing a strong surface interaction with the H_2O_2 molecules. The oxidised manganese as transition metal with partially filled *d*-orbitals and its diversified oxidation states seem to effectively promote the cyclic transfer of electrons between H_2O_2 as strong oxidant and the catalyst surface, and thus, it yields a high surface reactivity for the exothermic H_2O_2 decomposition. In

a further intensified study of the sensor response at varied process conditions, a strong impact of gas temperature and gas flow on the sensor signal was recognised. During this measuement series, the sensor was situated very close to the gas-outlet nozzle of the vaporizer, where the elevated gas temperature on the sensor surface seems to affect strongly the sensor's sensitivity. Nevertheless, the sensor chips with thin-film resistances built up on a silicon substrate represent an alternative H_2O_2 gas-sensing device, where potential improvements could help to enforce an increase in sensitivity and its response characteristic under changed process conditions.

In the following chapter, the encapsulation of the thin-film gas sensors with passive, polymeric materials has been investigated in detail. As potential passive materials, fluorinated ethylene propylene, perfluoralkoxy and epoxy-based SU-8 photoresist have been tested due to their well-known temperature stability and chemical inertness. In order to create thin, homogeneous layers, the polymers have been deposited as liquid films via spin-coating with specific fabrication protocols and cured by defined heat-treatment profiles. The morphological characteristics of the polymeric layers have been studied by scanning electron microscopy, wherein agglomerates have been recognised at the layers of the fluorpolymers, and by profilometry, where is to be seen that the polymeric surfaces are enclosed and the layer thicknesses amount to be in the lower micrometre range, but can be distinguished from each other. From contact angle measurements, the fluorpolymers exhibit pronounced hydrophobic surfaces, whereas the SU-8 photoresist has a more hydrophilic surface, which might have an effect on the encapsulation properties in extremely humid surroundings. Nevertheless, as a result of the characterisation in H_2O_2 atmosphere, the sensors covered by the different polymeric materials beared equal response behaviour towards gaseous H_2O_2 with slight differences in the sensors' sensitivities. In additionally conducted studies, the polymeric layers' stability in H_2O_2 under harsh environmental conditions have been approved by FTIR spectroscopy, where no changes of their chemical structure were observed after H_2O_2 treatment. Their elevated thermal endurance was further confirmed by differential scanning calorimetry and thermogravimetric analysis. To summarise **chapter** 4, all of the tested polymeric materials are suitable as thin passivation layers for calorimetric gas sensors to detect gaseous H_2O_2 concentrations.

Chapter 5 deals with the optimisation of the calorimetric gas sensors with regard to the response behaviour, concerning the sensitivity in particular. In former works, silicon was used as sensor substrate. Even though, silicon as conventional substrate in thin-film technology implicates a well-known fabrication procedure, it has also a drawback for the use in single chip, calorimetric gas sensors. Silicon holds a large thermal conductivity that does not allow to thermally isolate the active from the passive sensing segment on a single chip leading to a drop in the sensor signal – the temperature difference between the

two sensor segments. As a consequence, a new substrate was needed, which offers a low thermal conductivity, and hence, it should acting as thermal barrier between the active and passive sensor part. Therefore, a thin polyimide foil with low thermal conductivity has been chosen as novel substrate for the calorimetric gas sensor. For comparison with the sensors developed in the previous works, thin-film resistances were chosen as temperature transducers, which are passivated by SU-8 photoresist and activated by mangenese(IV) oxide catalyst.

In order to gain a better understanding how the surface reaction takes place, a review of the literature on H_2O_2 decomposition processes, in particular on manganese(IV) oxide, has been done. The initial step of the surface reaction is the cleavage of the O-O binding of the H_2O_2 molecule inducing the formation of hydroxyl radicals as intermediated products, which react with H_2O_2 in further steps of the reaction pathway, whereby H_2O_2 decomposes to water vapour and oxygen in a summarised stoichiometric reaction. From an additionally taken XPS analysis, it can be observed that the manganese becomes reduced in H_2O_2 atmosphere causing a phase change on the surface of the manganese oxide particles due to an electron exchange of the initial reaction step – the formation of radicals. However, the phase change seems to do not have any effect on the sensor-response behaviour. Before the sensor was tested in H_2O_2 atmosphere, a theoretical approach of the released temperature from the catalytic reaction was developed, to determine what is the maximum (theoretical) temperature increase arising from the catalytic H_2O_2 decomposition. Therein, the temperature rise was at first calculated in case of an exothermic surface reaction for a stationary H_2O_2 atmosphere without convection and diffusion effects, and in following models, diffusion effects were also comprised into the calculation, as well as the forced gas flow was introduced in the theoretical consideration. For the latter calculation model, the maximum temperature rise amounts to be 15.9 °C/(% v/v).

In an subsequent step, the novel calorimetric gas sensor based on a polyimide foil was then characterised in H_2O_2 atmosphere, wherein a sensitivity of 7.15 °C/(% v/v) was achieved, which is 45% of the calculated maximum temperature rise, but even 12.5 times higher than for the silicon-based sensor of **chapter** 3. The difference between calculated and measured temperature rise could rely on a heat loss by radiation and thermal dissipation due to the gas flow as well as on an incomplete decomposition of the H_2O_2 on the catalytic surface of the sensor. As a result of **chapter** 5, the developed calorimetric gas sensor built up on a thin polyimide foil showed a distinctly improved response behaviour and moreover, this chapter gives also a deep insight into the sensor-response mechanism with regard to the catalytic surface reaction and the resulting temperature rise.

In **chapter** 6, the sensor design was slightly modified, wherein the active and passive sensing areas were reduced compared to the sensor introduced in the chapter before. Moreover, a detailed description is given about how exactly the polyimide-based sensor

was fabricated and how the sensor responds to altered process conditions in a wide range of parameter settings (H_2O_2 concentration with and without additional water dosage, gas temperature and gas flow). In an initial step of the sensor fabrication, a polyimide sheet was temporarily fixed by an adhesive on a conventional silicon wafer as carrier platform throughout the fabrication process. The thin-film resistances were deposited via physical vapour deposition and structured by conventional photolithography. The thin-film resistances have been passivated by spin-coated SU-8 photoresist and the single sensor chips separated via scalpel and thereby, removed from the carrier platform. In a final process step, a dispersion consisting of manganese(IV) oxide particles have been drop-coated on one of the passivated thin-film resistances acting as active sensing element. The response behaviour of the sensor was further on intensively studied in H_2O_2 atmosphere, wherein over the whole measurement sequences a stable sensor response could be observed without strong influence from changed process conditions in form of varied gas temperature and gas flow as well as added humidity. In an additionally conducted characterisation of the polyimide foil by differential scanning calorimetry and thermogravimetric analysis as well as by FTIR spectroscopy, its outstanding thermal stability and chemical inertness was verified.

A summary of the response characteristics in form of sensitivity, off-set, hysteresis and response time of the different thin-film gas sensors based on a calorimetric differential set-up is given in the following table (s. Tab. 9.1). The sensor built up on polyimide foil with large contact area possesses the highest sensitivity. However, it offers a response time of 5.9 s, which relies on the large surface area that has to be heated during H_2O_2 decomposition, whereas the polyimide-based sensor with small contact area delivers a shorter response time of 3.8 s and an adequate sensitivity of 4.78 °C/(% v/v).

Furthermore, a comparative study of the developed thin-film gas sensors with regard to the effort of the fabrication process (the number of process steps, the degree of complexity and the time- as well as cost-consumption), their response behaviour (sensitivity and response time), the long-term stability in H_2O_2 atmosphere and their suitability for monitoring the H_2O_2 concentration in packages during their sterilisation is given in Tab. 9.2. The fabrication of the sensor with thin-film thermopile as temperature transducer needs more process steps, whereas the sensors with thin-film resistances are quiet faster to realise. The response behaviour are in general improved by using polyimide as sensor substrate, but the silicon-based sensors showed a slightly higher long-term stability. For the sensor implementation on the package surface for detecting the H_2O_2 concentration spatially resolved, the flexible polyimide foils are more suitable than the silicon-based sensors due to the possibility to fix the sensor also on rugged and curved surfaces. Furthermore, a sensor with small contact area enables the detection of H_2O_2 concentration even of tiny spots on the package's inner surface. As a result of the sensor comparison, it

Table 9.1: Summary of the response characteristics (sensitivity, off-set, hysteresis and response time) of the different thin-film gas sensors for H_2O_2 detection.

Thin-film gas sensor	Temperature transducer	Sensitivity (°C/(% v/v))	Off-set (°C)	Hysteresis (°C)	Response time, $t_{90\%}$ (s)
Sensor on silicon	Thin-film thermopile	0.84*	0.61*	0.34*	2.5
Sensor on silicon	Thin-film resistances	0.57	0.12	0.18	6.7
Sensor on polyimide (large size)	Thin-film resistances	7.15	-0.52	2.41	5.9
Sensor on polyimide (small size)	Thin-film resistances	4.78	-0.35	1.98	3.8

*Calculated sensitivity and off-set from specified signal in mV.

can be emphasised that the calorimetric gas sensor with thin-film resistances and small contact area seems to possess the most appropriate attributes for monitoring the H_2O_2 concentration during the package sterilisation in aseptic food processes.

In **chapter** 7, the microbicidal effectiveness of gaseous H_2O_2 has been extensively studied in order to find out the most influencing process factors on the degree of sterility corresponding to the sterilisation of food-packaging materials. Furthermore, measurements have been carried out with the calorimetric gas sensor that was developed in the previous **chapter** 6, and the sensor response has been correlated with the microbiological results. For the investigation of the microbicidal effectiveness of gaseous H_2O_2, test specimens inoculated with *Bacillus atrophaeus* spores have been used. Besides the contact time of the test specimens with gaseous H_2O_2, the present H_2O_2 gas concentration is the most influencing process factor on the microbial inactivation, whereas the change of the gas temperature, gas flow and humidity could be almost neglected in the considered setting ranges. The resulting inactivation kinetics follow an exponential function against the H_2O_2 concentration. From studies conducted with scanning electron microscopy, a strong morphological deformation of the bacterial spores after H_2O_2 treatment was observed, where some spores seemed even to be burst. Therein, the degree of deformation depended on the present H_2O_2 concentration. The inactivation kinetics have then been matched with measurements done with the gas sensor, and a correlation model in form of a linear approximation was developed for a considered concentration range, which is applied at package sterilisation in aseptic food processes. The correlation model, wherein the sensor-response signal was directly related to the microbial inactivation kinetics,

Table 9.2: Comparison of the thin-film gas sensors with regard to fabrication process, response behaviour, long-term stability and suitability for detecting H_2O_2 concentrations inside of packages during their sterilisation.

Thin-film gas sensor	Temperature transducer	Fabrication process	Response behaviour	Long-term stability	Suitability
Sensor on silicon	Thin-film thermopile	–	–	+	∘
Sensor on silicon	Thin-film resistances	+	–	++	∘
Sensor on polyimide (large size)	Thin-film resistances	∘	+	∘	+
Sensor on polyimide (small size)	Thin-film resistances	∘	+	∘	++

Here, ++ is excellent, + is good, ∘ is satisfactory and – is poor.

demonstrated that the calorimetric gas sensor can also be used for the validation of the microbicidal effectiveness of sterilisation processes with gaseous H_2O_2, and consequently, provide information about the sterility of the packaging material that has to be sterilised in aseptic food processes.

For monitoring the H_2O_2 concentration during the package sterilisation in aseptic food processes under real-time conditions, a specially designed wireless sensor system including one of the thin-film calorimetric gas sensors is introduced in **chapter** 8. The sensor system, which is based on the industrial ZigBee standard, comprises a remote unit connected to the calorimetric gas sensor on polyimide foil that was presented in **chapter** 6 and an external base unit. The remote unit was built up by an XBee radio frequency module and a programmable system-on-chip controller. The base unit consists of a second XBee radio frequency module, which is connected to a laptop computer. The sensor system can be used for measuring the H_2O_2 concentration on various locations inside of packages, in particular on critical locations, during the sterilisation process. However, for detecting the gas concentration within the extremely short sterilisation time of almost two seconds, a novel read-out strategy needed to be established. Instead of reading out the steady-state signal of the sensor response, the maximum signal peak within the short sterilisation time has been considered as measure for the local H_2O_2 concentration. In order to verify the wireless sensor system and the accuracy of the read-out strategy, an exemplary measurement has been conducted, wherein the influence of the gas flow on the distributed H_2O_2 concentration on the inner surface of a package has been determined during the sterilisation process. To demonstrate that the sensor signal is acting also as

a measure for the microbicidal effectiveness, the spatially resolved H_2O_2 concentration detected by the sensor system was then correlated with the microbial inactivation of inoculated *Bacillus atrophaeus* spores on spots of the package's surface, wherein a proper compliance of detected H_2O_2 concentration and microbicidal effectiveness can be drawn. As a result, the novel wireless sensor system and the specified read-out strategy represent a promising method for measuring the H_2O_2 gas concentration in real-time and thus, enabling the monitoring of the microbicidal effectiveness of the sterilisation process – the sterility of the package that is to be treated by gaseous H_2O_2 – under industrial production conditions.

In summary, the ultimate result of this thesis was the establishment of novel thin-film gas sensors based on a calorimetric sensing principle in various arrangements and with different material compositions, which have been extensively investigated. The sensors are suitable for detecting H_2O_2 gas concentrations up to the percentage range under harsh environmental conditions as predominantly occurs during the sterilisation of packaging material in aseptic food processes. For the sensor application in industrial, aseptic food processes a wireless sensor system and a novel sensor read-out strategy have been developed, which can be used to built up "intelligent" packages for the validation and control of the package sterilisation in aseptic food processes under real-time conditions. In ongoing studies, the application of the novel thin-film calorimetric gas sensors and the whole sensor system could be broadened to monitor the sterilisation or disinfection of medical equipment and operating rooms as well. Therein, H_2O_2 even in the gas phase or in form of condensation is increasingly used due to its strong microbicidal properties.

In order to gain a better understanding about the microbicidal action of gaseous H_2O_2 on bacterial spores, the microbial inactivation kinetics have been studied in the present work as well. Furthermore, they have been correlated with the sensor-response behaviour. The results provides a lot of valuable information for the design and interpretation of sterilisation processes. However, as already mentioned in **chapter** 1, the inactivation mechanism of H_2O_2 in particular on bacterial spores is not yet fully understood in detail. In prospective works, a deeper look onto the microbicidal properties of gaseous H_2O_2 should be envisaged, wherein more information about the inactivation effect, especially on resistant bacterial spores should be gained.

10 Zusammenfassung und Ausblick

In der aseptischen Lebensmittelindustrie stellt die Entkeimung von Packstoffen einen Schlüsselprozess dar, um eine möglichst lange Haltbarkeit des abgefüllten Lebensmittels zu gewährleisten und um eine Übertragung von pathogenen Mikroorgansimen auf den Endverbraucher zu verhindern. Zur Inaktivierung lebensfähiger Mikroorganismen auf dem Packstoff wird zunehmend gasförmiges Wasserstoffperoxid bei erhöhten Prozesstemperaturen aufgrund der hohen, keimreduzierenden Wirkung und des Zerfalls in umweltfreundliche Abbauprodukte – Wasserdampf und Sauerstoff – als Entkeimungsmittel eingesetzt. Dabei muss eine ausreichend hohe H_2O_2-Konzentration sowie eine gleichmäßige Gasverteilung an den Packstoffinnenflächen während der meist kurzen Einwirkzeit erlangt werden, um eine vollständige Keimfreiheit der Verpackung garantieren zu können.

In der vorliegenden Arbeit wurden Dünnschicht-Gassensoren in Form einer kalorimetrischen Differenzanordnung realisiert, die quantitativ die H_2O_2-Konzentration während der Packstoffentkeimung erfassen können, um somit den sensiblen Schlüsselprozess des aseptischen Abfüllvorgangs besser kontrollieren zu können. Die Sensoren bestehen dabei aus einem katalytisch aktivierten und einem passivierten Sensorsegment. Am aktiven Segment zerfällt H_2O_2 unter den erhöhten Prozesstemperaturen exotherm, woraufhin ein lokaler Temperaturanstieg entsteht, der als Temperaturdifferenz zwischen aktivem und passivem Sensorsegment über Temperaturtransducer erfasst werden kann. Die Temperaturdifferenz dient somit als Maß für die vorliegende H_2O_2-Konzentration.

In einem ersten Sensorlayout wurden Chip-basierte Dünnschicht-Thermosäulen auf einem Siliziumsubstrat als Temperaturtransducer zur Erfassung der konzentrationsabhängigen Temperaturdifferenz ausgelegt. Die Temperaturdifferenz wurde dabei direkt als Thermospannung erfasst, wodurch keine zusätzliche Hilfsenergie zur Versorgung des Sensors benötigt worden ist. In einem weiteren Sensoraufbau wurden Dünnschicht-Widerstände als Temerpaturtransducer zunächst ebenfalls auf einem Siliziumsubstrat prozessiert und verschiedene Katalysatormaterialien – Mangan(IV)-oxid, Palladium und Platinschwarz – auf ihre Empfindlichkeit hin untersucht. Generell konnte mit allen Katalysatoren eine lineare Abhängigkeit des entstehenden Temperaturanstiegs von der vorliegenden H_2O_2-Konzentration erreicht werden. In einer direkten Gegenüberstellung der Ansprechverhalten zeigte Mangan(IV)-oxid jedoch die höchste Empfindlichkeit. Darüber hinaus wurden verschiedene Passivierungsmaterialien aus Perfluorethylenpropy-

len, Perfluoralkoxylalkan und SU-8 Photoresist mittels Spin-Coating auf die Sensorchip-Oberflächen abgeschieden und mit Hilfe von oberflächenanalytischen Methoden sowie thermischen Analyseverfahren charakterisiert. Trotz erkennbarer Unterschiede in der Oberflächenbeschaffenheit – Hydrophobizität und Schichthomogenität – eignen sich alle drei Materialien zur Sensorpassivierung, insbesondere unter den harschen Prozessbedingungen.

Auch wenn mit den oben genannten Sensoraufbauten bereits eine lineare Abhängigkeit zwischen Temperaturdifferenz und H_2O_2-Konzentration erzielt und die Funktionalität der Sensoren nachgewiesen werden konnte, so hat sich gezeigt, dass durch die Wahl von Silizium als Grundsubstrat mit seiner hohen thermischen Leitfähigkeit das Sensorsignal stark verringert wird, da der Temperaturanstieg am aktiven Sensorsegment über das Substrat auch eine Temperaturerhöhung am passiven Sensorsegment erzeugt. Deshalb wurde anschließend der Sensoraufbau auf einer dünnen Polyimidfolie aufgrund der niedrigen thermischen Leitfähgkeit realisiert, wodurch die Sensorempfindlichkeit deutlich gesteigert werden konnte.

Im weiteren Verlauf der vorliegenden Arbeit wurde die keimreduzierende Wirkung von gasförmigen H_2O_2 auf *Bacillus atrophaeus*-Sporen unter veränderten Prozessparametern eruiert. Es konnte gezeigt werden, dass in erster Linie die Keimreduktion von der vorliegenden H_2O_2-Konzentration und von der Einwirkzeit des H_2O_2 auf die Baktierensporen abhängt. Die resultierenden Inaktivierungskinetiken wurden anschließend mit simultan durchgeführten Messungen des Poylimid-basierten Sensors in Relation gebracht und ein Korrelationsmodell aufgestellt. Somit können die Sensoren auch direkt zur Bestimmung der keimreduzierenden Wirkung des gasförmigen H_2O_2 während der Packstoffentkeimung herangezogen werden.

Um mit den Dünnschicht-Gassensoren die lokale H_2O_2-Konzentration an der zu entkeimenden Packstoffoberfläche unter Echtzeitbedingungen messen und somit die örtliche Keimreduktion während des Entkeimungsvorgangs bestimmen zu können, wurde eine berührungslose Sensorelektronik basierend auf dem ZigBee-Standard realisiert und eine neue Auslesestrategie der Sensoren etabliert. Diese Art "intelligenter Verpackung" dient der aseptischen Lebensmittelindustrie als eine neuartige Messmethode, insbesondere zur Validierung und zur Inline-Kontrolle der Packstoffentkeimung mit gasförmigem H_2O_2.

In weiterführenden Arbeiten könnte die Anwendung der kalorimetrischen Gassensoren auf die Überwachung von Sterilisations- und Desinfektionsprozessen von medizinischem Equipment und von Operationssälen ausgeweitet werden, worin ebenfalls zunehmend gasförmiges H_2O_2 zur Keimreduktion Einsatz findet. Schließlich wäre eine intensivere Betrachtung des Inaktivierungsmechanismus insbesondere auf Bakteriensporen durch gasförmiges H_2O_2 ratsam, um den Entkeimungsprozess besser verstehen und den Schlüsselmechanismus der Keimreduktion durch H_2O_2 eindeutig identifizieren zu können.

List of publications

Book article

- Kirchner, P., Reisert, S., and Schöning, M. J. Hydrogen peroxide monitoring in aseptic food processes by means of calorimetric gas sensors. In *Springer series on chemical sensors and biosensors: Gas sensing fundamentals*, C.-D. Kohl and T. Wagner, Eds. Springer, Berlin, 2013, *submitted*.

Publications in peer-reviewed journals

- Kirchner, P., Ng, Y. A., Spelthahn, H., Schneider, A., Henkel, H., Friedrich, P., Kolstad, J., Berger, J., Keusgen, M., Schöning, M. J. Gas sensor investigation based on a catalytically activated thin-film thermopile for H_2O_2 detection. *Physica Status Solidi A 207*, 4 (2010), 787–792.

- Kirchner, P., Li, B., Spelthahn, H., Henkel, H., Schneider, A., Friedrich, P., Kolstad, J., Keusgen, M., Schöning, M. J. Thin-film calorimetric H_2O_2 gas sensor for the validation of germicidal effectivity in aseptic filling processes. *Sensors and Actuators B: Chemical 154*, 2 (2011), 257–263.

- Kirchner, P., Oberländer, J., Friedrich, P., Berger, J., Suso, H.-P., Kupyna, A., Keusgen, M., Schöning, M. J. Optimisation and fabrication of a calorimetric gas sensor built up on a polyimide substrate for H_2O_2 monitoring. *Physica Status Solidi A 208*, 6 (2011), 1235–1240.

- Kirchner, P., Reisert, S., Pütz, P., Keusgen, M., Schöning, M. J. Characterisation of polymeric materials as passivation layer for calorimetric H_2O_2 gas sensors. *Physica Status Solidi A 209*, 5 (2012), 859–863.

- Kirchner, P., Oberländer, J., Friedrich, P., Berger, J., Rysstad, G., Keusgen, M., Schöning, M. J. Realisation of a calorimetric gas sensor on polyimide foil for applications in aseptic food industry. *Sensors and Actuators B: Chemical 170* (2012), 60–66.

- Kirchner, P., Oberländer, J., Suso, H.-P., Rysstad, G., Keusgen, M., Schöning, M. J. Monitoring the microbicidal effectiveness of gaseous hydrogen peroxide in sterilisation processes by means of a calorimetric gas sensor. *Food Control 31*, 2 (2013), 530–538.
- Hennemann, J., Kohl, C.-D., Reisert, S., Kirchner, P., Schöning, M. J. Copper oxide (CuO) nanofibers for detection of hydrogen peroxide (H_2O_2) vapour at high concentrations. *Physica Status Solidi A* (2013), in press.
- Kirchner, P., Oberländer, J., Suso, H.-P., Rysstad, G., Keusgen, M., Schöning, M. J. Towards a wireless sensor system for real-time H_2O_2 monitoring in aseptic food processes. *Physica Status Solidi A* (2013), in press.

Patent application

- Kirchner, P., Oberländer, J., Schöning, M. J. (Erfinder) Verfahren für einen Gassensor oder Sensor in der Gasphase. *DE 10 2012 221 436.4.*

Other publications

- Kirchner, P., Li, B., Spelthahn, H., Henkel, H., Schneider, A., Kolstad, J., Friedrich, P., Schöning, M. J. Realisierung eines miniaturisierten Gassensors in Chiptechnologie basierend auf einer Dünnschicht-Thermosäule zur H_2O_2-Detektion in aseptischen Abfüllsystemen. *Dresdner Beiträge zur Sensorik 39* (2009), 293–296.
- Kirchner, P., Li, B., Spelthahn, H., Henkel, H., Schneider, A., Friedrich, P., Kolstad, J., Keusgen, M., Schöning, M. J. Thin-film calorimetric H_2O_2 gas sensor for the validation of germicidal effectivity in aseptic filling processes. *Procedia Chemistry 1* (2009), 983–986.
- Kirchner, P., Spelthahn, H., Henkel, H., Schneider, A., Friedrich, P., Kolstad, J., Berger, J., Schöning, M. J. Realisierung eines Polyimid-basierten kalorimetrischen Gassensors zur Inline-Überwachung der H_2O_2-Konzentration in aseptischen Abfüllsystemen. *Sensoren und Messsysteme* (2010), *VDE-Verlag* Berlin, 607–612.
- Kirchner, P., Oberländer, J., Friedrich, P., Berger, J., Rysstad, G., Keusgen, M., Schöning, M. J. Realization of a calorimetric gas sensor on polyimide foil for applications in aseptic food industry. *Procedia Engineering 5* (2010), 264–267.

Interview

- Kirchner, P. Verpackungen intelligent überwacht. *RFID im Blick 9* (2011), 43.

Oral and poster presentations

- Kirchner, P., Henkel, H., Näther, N., Spelthahn, H., Schneider, A., Berger, J., Kolstad, J., Friedrich, P., Schöning, M. J. RFID-basiertes Sensorsystem zur Realisierung intelligenter Verpackungen für die Nahrungsmittelindustrie. *Statustagung KMU-innovativ: IKT*, 17.-18.11.2008, Darmstadt.

- Kirchner, P., Näther, N., Spelthahn, H., Henkel, H., Schneider, A., Schöning, M. J. RFID-based sensor system for the realisation of intelligent packages for food industry. *Joint General Meeting of the Belgian Physical Society*, 01.04.2009, Hasselt (Belgien).

- Kirchner, P., Näther, N., Spelthahn, H., Schneider, A., Henkel, H., Friedrich, P., Berger, J., Kolstad, J., Schöning, M. J. Gas sensor investigation based on a thin-film thermopile for H_2O_2 detection activated by MnO_2 particles. *Engineering of Functional Interfaces*, 18.-19.06.2009, Hasselt (Belgien).

- Kirchner, P., Näther, N., Henkel, H., Spelthahn, H., Schneider, A., Friedrich, P., Berger, J., Kolstad, J., Schöning, M. J. Thin-film calorimetric H_2O_2 gas sensor for the validation of germicidal effectivity in aseptic filling processes. *Eurosensors XXIII*, 06.-09.09.2009, Lausanne (Schweiz).

- Kirchner, Henkel, H., Schneider, A., Friedrich, P., Keusgen, M., Schöning, M. J. Calorimetric sensor system based on RFID for H_2O_2 monitoring in aseptic filling processes. *2. Graduiertentagung*, 05.11.2009, Aachen.

- Kirchner, Spelthahn, H., Schneider, A., Henkel, H., Friedrich, P., Kolstad, J., Schöning, M. J. Investigation of a thin-film calorimetric gas sensor for H_2O_2 detection in industrial processes. *Advancements in Nanotechnology and Microelectronics*, 13.-14.11.2009, Gammarth (Tunesien).

- Kirchner, Li, B., Spelthahn, H., Henkel, H., Schneider, A., Kolstad, J., Friedrich, P., Schöning, M. J. Realisierung eines miniaturisierten Gassensors in Chiptechnologie basierend auf einer Dünnschicht-Thermosäule zur H_2O_2-Detektion in aseptischen Abfüllsystemen. *9. Dresdner Sensor-Symposium*, 07.-09.12.2009, Dresden.

- Kirchner, Spelthahn, H., Henkel, H., Schneider, A., Friedrich, P., Kolstad, J., Berger, J., Schöning, M. J. Realisierung eines Polyimid-basierten kalorimetrischen Gassensors zur Inline-Überwachung der H_2O_2-Konzentration in aseptischen Abfüllsystemen. *Sensoren und Messsysteme*, 18.-19.05.2010, Nürnberg.

- Kirchner, P., Oberländer, J., Pütz, P., Friedrich, P., Berger, J., Rysstad, G., Keusgen, M., Schöning, M. J. Optimisation and fabrication of a calorimetric gas sensor built up on a polyimide substrate for H_2O_2 monitoring. *Engineering of Functional Interfaces*, 15.-16.06.2010, Marburg.

- Kirchner, P., Oberländer, J., Friedrich, P., Berger, J., Rysstad, G., Keusgen, M., Schöning, M. J. Realization of a calorimetric gas sensor on polyimide foil for applications in aseptic food industry. *Eurosensors XXIV*, 05.-08.09.2010, Linz (Österreich).

- Kirchner, P., Oberländer, J., Pütz, P., Friedrich, P., Berger, J., Rysstad, G., Keusgen, M., Schöning, M. J. Thin-film gas sensor with flexible polyimide foil for the detection of gaseous H_2O_2. *3. Graduiertentagung*, 04.11.2010, Jülich.

- Kirchner, P., Friedrich, P., Berger, J., Keusgen, M., Schöning, M. J. Kalorimetrische Sensoranordnung zur Echtzeit-Erfassung von H_2O_2-Konzentrationen in Sterilisationsprozessen von Lebensmittelverpackungen. *7. Deutsches Biosensor Symposium*, 03.-06.04.2011, Heiligenstadt.

- Kirchner, P. Schöning, M. J. Intellipack – intelligente Verpackungen zur Qualitätskontrolle bei Lebensmittelverpackungen. *Branchendialog Nanopackaging*, 16.05.2011, Düsseldorf.

- Kirchner, P., Pütz, P., Berger, J., Suso, H.-P., Keusgen, M., Schöning, M. J. Characterization of polymeric materials as passivation layers for calorimetric H_2O_2 gas sensors. *Engineering of Functional Interfaces*, 19.-20.07.2011, Linz (Österreich).

- Kirchner, P., Oberländer, J., Pütz, P., Suso, H.-P., Keusgen, M., Schöning, M. J. Calorimetric gas sensor on micro-plates for inline monitoring of H_2O_2 concentrations. *4. Graduiertentagung*, 24.11.2011, Aachen.

- Kirchner, P., Oberländer, J., Suso, H.-P., Rysstad, G., Keusgen, M., Schöning, M. J. Towards a wireless sensor system for real-time H_2O_2 monitoring

in aseptic food processes. *Engineering of Functional Interfaces*, 16.-17.07.2012, Zweibrücken.

Acknowledgements

This dissertation would not have been possible unless the assistance of many people, who give me invaluable support at various moments and in different ways during the time working on it. I am whole-heartedly indebted to all these people.

Above all, I would like to express my sincere gratitude to Prof. Dr. Michael J. Schöning. It was a pleasure for me to be a part of your team at the Institute of Nano- and Biotechnologies. Thank you for the support, the vast amount of discussions and the guidance throughout the scientific work, the freedom and creative leeway for own ideas as well as for the opportunity to constantly improve my non-scientific skills as well. I hope that my sense of orientation is now trained enough also to find the right way in hotel corridors during conferences.

In the same way, I would like to thank Prof. Dr. Michael Keusgen for the supervision of my thesis. Thank you for your advice, the uncomplicated and open manner, whenever questions or issues have been arisen, as well as for the great support throughout the time working on this thesis.

My special thanks belong to Dr. Jörg Berger for his introduction in the world of aseptic food processing and his technical support, in particular for all mechanical constructions. It was a pleasure for me to work with you and to learn how to solve problems in a calm way while enjoying a cup of coffee, even if something seems to be impossible.

I want to thank also Dr. Peter Friedrich for his introduction in the field of sterilisation. Thank you for your support and your never-ending interest in this work. It was exciting for me to conduct chemical experiments with an expert in the field of hydrogen peroxide.

I am very grateful to Dr. Gunnar Rysstad and Henri-Pierre Suso, PhD, for the opportunity to conduct sensor experiments under real industrial conditions and the possibility to stay several times in Norway. Thank you for your support and your interest in this work.

I would like to thank Hans Peter Bochem for taking so many SEM images as well as to Alfred Steffen and the whole clean-room team of the Peter Grünberg Institute (PGI-8) at Forschungszentrum Jülich.

I am very grateful to Markus Raue for his instructive explanation about polymeric materials and his willingness (after bribery with coffee) to conduct a lot of FTIR, TGA

and DSC measurements together, even for times outside the regular working hours.

I would like to thank also Simone Gröbel and Vera Thönnessen for providing the technical support and the required material to conduct all the microbiological studies.

Many thanks belong to Prof. Dr. Hans-Gerd Boyen from Hasselt University for the support and the realisation of the XPS analysis.

I would like to thank Prof. Dr. Hans-Josef Ackermann, Heinrich-Gerd Römer and Dr. Józef Wiora for their contribution to build up a microelectronic platform.

I would like to express my deepest thanks to all of my colleagues at the Institute of Nano- and Biotechnologies for the friendly atmosphere and the solidarity during the daily work. In particular, I want to thank Prof. Dr. Arshak Poghossian, David Rolka, Heiko Spelthahn, Marcel Leinhos and Shoko Takenaga, PhD. My special thanks go also to my "officemates", Steffen Reisert, thank you for the fruitful discussions and to be not only a companion during the working hours but also in the evenings, and Carl Frederik Werner, thank you for your support in the field of software and electronics, and the late tea breaks after work. I would like to thank also all other, former and present fellow PhD students, Dr. Matthias Bäcker, thank you also for the squash matches on almost every Saturday morning, Christina Huck, Sebastian Schusser, Dr. Monika Turek and Dr. Maryam Abouzar.

I would like to gratefully thank all the students for their individual contributions in different manners and at various stages of this thesis. Thank you, Yue Ann Ng, Bin Li, Patrick Pütz and Jan Oberländer, for your great help, the many diversified, scientific discussions and for the friendly working atmosphere that we could enjoy during the time working together.

I need also to thank all the further students and colleagues, who contributed to such a good atmosphere in the lab. Thank you, Benno, for the vast amount of ice cream, and thank you, Christoph, for the frequent replenishment of coffee.

My family receives my deepest gratitude for allowing me to realise my own potential and to do, whatever I want to do. Thank you for your whole-hearted support in my life, which is one of the greatest gift anyone has ever given to me.

Finally, I would like to address my warmest appreciation to Kristina Kaufmann, my girlfriend. It is difficult to find words for expressing my gratitude to you, but I know that this dissertation would not have been possible without your tireless support and encouragement throughout the years.

Thank you all for your help!

Curriculum vitae

Patrick Kirchner

geboren am 29.08.1983 in Bad Neustadt a.d. Saale

Ausbildung

09/1990–07/1999	Besuch der Volksschule Bischofsheim a.d. Rhön Abschluss: Qualifizierender Hauptschulabschluss
09/1999–07/2002	Ausbildung zum IT-Systemelektroniker, Elektro Müller GmbH, Salz
09/2002–07/2004	Besuch der Berufsoberschule Bad Neustadt a.d. Saale Abschluss: Fachhochschulreife
09/2004–09/2008	Studium der Physikalischen Technik an der FH Aachen, Campus Jülich Abschluss: Diplom-Ingenieur (FH)
10/2008–jetzt	Kooperative Promotion zwischen der FH Aachen und der Philipps-Universität Marburg Thema der Dissertation: Thin-film calorimetric gas sensors for hydrogen peroxide monitoring in aseptic food processes

Beruflicher Werdegang

07/2006–09/2006	Praktikum am Institut für Kernphysik, Forschungszentrum Jülich GmbH
12/2006–03/2007	Praktikum am Institut für Chemie und Dynamik der Geosphäre, Forschungszentrum Jülich GmbH
04/2007–03/2008	Praxissemester am Fraunhofer Institut für Lasertechnik, Aachen

04/2008–09/2008	Diplomarbeit am Institut für Nano- und Biotechnologien der FH Aachen, Campus Jülich
10/2008–09/2012	Wissenschaftlicher Mitarbeiter am Institut für Nano- und Biotechnologien der FH Aachen, Campus Jülich
10/2012–01/2013	Mitarbeiter der Elopak EQS GmbH, Mönchengladbach-Güdderath
seit 02/2013	Mitarbeiter der Imagine Gesellschaft für interaktive Medien mbH, Brühl